THERMO- AND ELECTRO-MODULATION SPECTROSCOPY OF THIN EVAPORATED FILMS

A thesis submitted to the Faculty of Science of the University of London for The Degree of Doctor of Philosophy.

by

Margaret Syms B.Sc. (Lond.)

Abstract

Thin evaporated films have been used to study the effects on reflection and transmission of visible and near visible light through solids by modulating the temperature of the specimen and the electric field in which it is situated. The principal aims of the studies were:

(a) to obtain reliable data for comparison with electronic band structure calculations

(b) to investigate a possible device application.

Thermally modulated reflectance measurements have been performed on thick absorbing films of gold and copper and on the heavy rare earth metals, gadolinium, terbium, dysprosium and erbium. The modulated reflectance results have been transformed to $\Delta\varepsilon_2$, the change in the imaginary part of the dielectric constant, by the Kramers-Kronig method of analysis. The $\Delta\varepsilon_2$ spectra have been correlated with electronic band structure calculations. Shifts in the principal absorption edges of gold and copper with temperature (shifts of -2.3×10^{-4} eV/k and -1.2×10^{-4} eV/K respectively), not previously observed in thermal modulation experiments although theoretically predicted by expanded lattice band structure calculations, have been detected. The technique has been found to be capable of locating weak structure in the $\Delta\varepsilon_2$ dispersion curve.

New thermal modulation experiments on the heavy rare earth metals have enabled changes in the $\Delta R_p/R_p$ spectra to be observed as the temperature of the sample is decreased. These changes occur at the magnetic ordering temperatures and have not previously been observed using conventional static reflectance.

By using electro-modulation, an integrated thin film optical modulator has been produced. The device has been constructed from thermally evaporated thin films of aluminium, silicon monoxide and cadmium sulphide, the latter being the active medium. Modulation degrees of between 10 and 15% have been observed for very low modulating voltages $\sim$ 15 volts. However the

device is limited by the very large insertion loss at the centre of the cadmium sulphide absorption edge.

Some studies have been made on the electro-modulation of metals using a "dry-package" configuration. No electro-modulation response of the metal was observed. This null result is in contradiction to electrolytic measurements. Computational analysis has been performed to demonstrate that the electroreflectance spectra observed using the electrolytic technique may hot be an electro-modulation of the optical constants of the metal but an absorption induced by the modulating electric field in the Gouy region of the electrolyte.

CONTENTS

LIST OF FIGURES AND PLATES

FIGURES

PLATES

ACKNOWLEDGEMENTS

I should like to thank my supervisor, Dr. R.F. Miller, for his encouragement and advice during the course of this work. I am also greatly indebted to Dr. L.S. Julien with whom I have had many stimulating discussions on optical properties and band structure calculations. My thanks are also expressed to the technical staff of the Physics Department, Royal Holloway College, in particular: Mr. L. Ellinson, Mr. R.P. May and Mr. M.E. Thyer.

I also wish to acknowledge the Scientific Research Council for their patronage in the form of a postgraduate studentship. Finally my thanks are expressed to Mrs. B. Rutherford who has patiently typed this thesis and to my husband, Robert, for his tolerance and help during the course of this work.

CHAPTER I

Modulation Spectroscopy

(1.1) Introduction

In this thesis we are concerned primarily with the use of modulation spectroscopy as a solid state diagnostic. In recent years optical modulation spectroscopy has emerged as a powerful technique for examining optical transitions in solids. Modulation, or differential, techniques as they are sometimes known, are techniques whereby the material under investigation is perturbed by some periodic external parameter. The perturbation modulates the band structure and thereby the dielectric constant of the material. Thus, the observables in a modulation experiment are the changes in the optical properties i.e. the changes in reflectance, transmittance, absorption or phase, with respect to the modulating parameter. In this chapter we discuss the role of optical measurements in solid state physics and also discuss the advantages of modulation measurements over conventional "static" optical measurements where the unmodulated reflectance, transmittance or absorption of a material are measured. Each of the modulation techniques is described in detail and its merits discussed. In the present work we have chosen one of the modulation techniques as a solid state diagnostic and the reasons governing this choice are given.

In all branches of physics there is a dichotomy as to whether a particular technique should be used as a pure diagnostic or should be exploited to produce a practical device. In view of this we discuss the use of modulation techniques in various fields including solid state physics and show how in the present work one of the modulation techniques has been used to produce an integrated optical modulator.

(1.2) The role of optical measurements in solid state physics

The study of the optical properties of solids has proved to be a powerful tool in the understanding of the atomic and electronic structure of materials. Optical techniques have provided much information about the position of energy bands and the symmetry of their associated wave functions in a large number of materials. We see in (2.2) that one of the most important quantities derived from optical measurements is the optical conductivity $\sigma(\nu)$ which is related to the optical constants n and k of a material by

$$\sigma(\nu) = nk\nu = \varepsilon_2\nu/2 \qquad (1.1)$$

where n is the real part of the refractive index

k is the extinction coefficient

ε_2 is the imaginary part of the dielectric constant

ν is the frequency of the incident radiation

The optical conductivity is a measure of absorption in the system and the variation of $\sigma(\nu)$ with photon energy gives information about the optically induced electron transitions. Clearly, from equation (1.1) we see that to calculate $\sigma(\nu)$ the optical constants of the material must be found. Optical constants may be deduced from various sets of experimental observables some of which are summarized below:-

(i) The measurement of the reflectance R at near normal incidence (Bennet 1967, Lavin 1971)

The principal reason for making measurements near $\theta = 0^{\circ}$, is that for small angles the following relationship holds

$$R_s \equiv R_p \qquad (1.2)$$

where the subscripts p and s refer to the parallel and perpendicular components of polarization, and the total reflectance may be written as

$$(R_s + R_p)/2 = R_s = R_p \quad . \tag{1.3}$$

Thus, unpolarized light may be used and only one measurement is made for each determination at each photon energy. However, with only a knowledge of the reflectance at each photon energy insufficient information is available to be able to solve the Fresnel reflection equations for n and k. An extra relationship is required, an example of which is provided by the Kramers-Kronig dispersion equation (Cardona 1969) from which $\psi(w)$, the phase change of the incident light on reflection, may be calculated. The equations relating n and k to R and ψ at near normal incidence are:-

$$n = (1 - R)/(1 + R - 2R^{\frac{1}{2}}\cos\psi) \tag{1.4}$$

and

$$k = (-2R\sin\psi)/(1 + R - 2R^{\frac{1}{2}}\cos\psi) \tag{1.5}$$

Clearly, from equations (1.4) and (1.5) once R and ψ are known then n and k may be evaluated. However, the use of the Kramers-Kronig relationships requires a knowledge of the reflectance over all frequencies and numerical extrapolation techniques have to be used to extend the reflectance values. The use of reflectance values over limited frequency ranges has been shown to lead to misleading results (Bowlden 1963) and a recent analysis of the errors due to extrapolation procedures has been performed by Nilsson and Munkby (1969).

(ii) The measurement of R_s and R_p at the same angle of incidence θ_1 or the measurement of either R_s or R_p at two angles of incidence θ_1 and θ_2 (Avery 1952)

Similar measurements may be made in transmission if the sample is sufficiently thin to transmit light i.e. thin film specimens.

The advantage of using oblique incidence measurements is that the optical constants may be determined from the knowledge of two experimental observables at the same photon energy by using the Fresnel formulae. It should be noted that in this type of measurement the angle of incidence of 45° is to be avoided since

$$R_p(\theta = 45^{\circ}) = R_s^2(\theta = 45^{\circ}) \qquad (1.6)$$

and thus the measurements of R_p and R_s are not independent.

(iii) The measurement of reflectance (R_p/R_s) ratios

This method was initially used by Avery (1952) but his analysis could only be directly applied to reflection at a single interface and so the method is only useful for bulk specimens or films which are sufficiently thick for internal multiple reflections to be neglected. However, the method has been extended by Miller et al. (1974) who have used optimized reflection ratio measurements at oblique incidence to determine the optical constants of the rare earth metals, gadolinium and terbium in thin film form. Julien and Miller (1974) pointed out that a joint determination of reflectance and transmittance ratios proves satisfactory for the measurement of low n values $(n < 0.5)$ and k values in the range 1.2 to 3.0. This technique has been used to determine the optical constants of thin films of copper (Inwood, private communication).

(iv) Ellipsometric measurements

If linearly polarized light is reflected from a solid at oblique incidence the reflected light will in general be elliptically polarized. It is possible to determine the optical constants at a given photon energy by measuring the state of polarization of the reflected light (Archer 1968).

In methods (i) and (ii) above, in order to determine the reflection coefficient, a measurement of the incident light intensity at each photon energy must be made. This can be done by comparing the reflectance of the sample with that of a standard mirror, but the chemical instability and optical inhomogeneity of the mirrors makes the method inaccurate - especially in the ultra violet. The most commonly employed method involves the measurement of the incident light intensity. Thus, when measuring absolute reflection coefficients some rearrangement of the experimental system is necessary in order to measure the incident beam under near identical conditions to those for which the reflected intensity is measured. Such rearrangement is likely to introduce errors into the determination through small differences in the optical path for the two measurements. In addition, accurate rearrangement of the system is likely to take a long time. If the reflectance (or transmittance) ratio is measured, no beam normalization is required provided that the incident intensity components I_{os} and I_{op} are equal. However, even if this experimental configuration is to be used, the source and detector must remain stable and there must be no long term drift during the course of the experiment. In ellipsometry, Krizek (1973 Ph.D. thesis) has shown that measurements of the reflected intensity for at least three different azimuths of polarization are required to obtain ρ and Δ (where $r_{p,s} = \rho_{s,p} \exp i \Delta_{p,s}$ and $\rho = \rho_p/\rho_s$ and $\Delta = \Delta_p - \Delta_s$) and to exclude terms dependent on the intensity of the incident radiation. Once again, as in the reflectance ratio measurements, the source and detector must remain stable during the course of the experiment. Thus, we see that the measurement of the incident light intensity is one of the main disadvantages of these so-called "static" optical measurements and it should be noted that optical constants determined by different observers are not generally in good agreement. Figure (1.1) indicates the optical conductivity dispersion curves of gadolinium obtained by different workers.

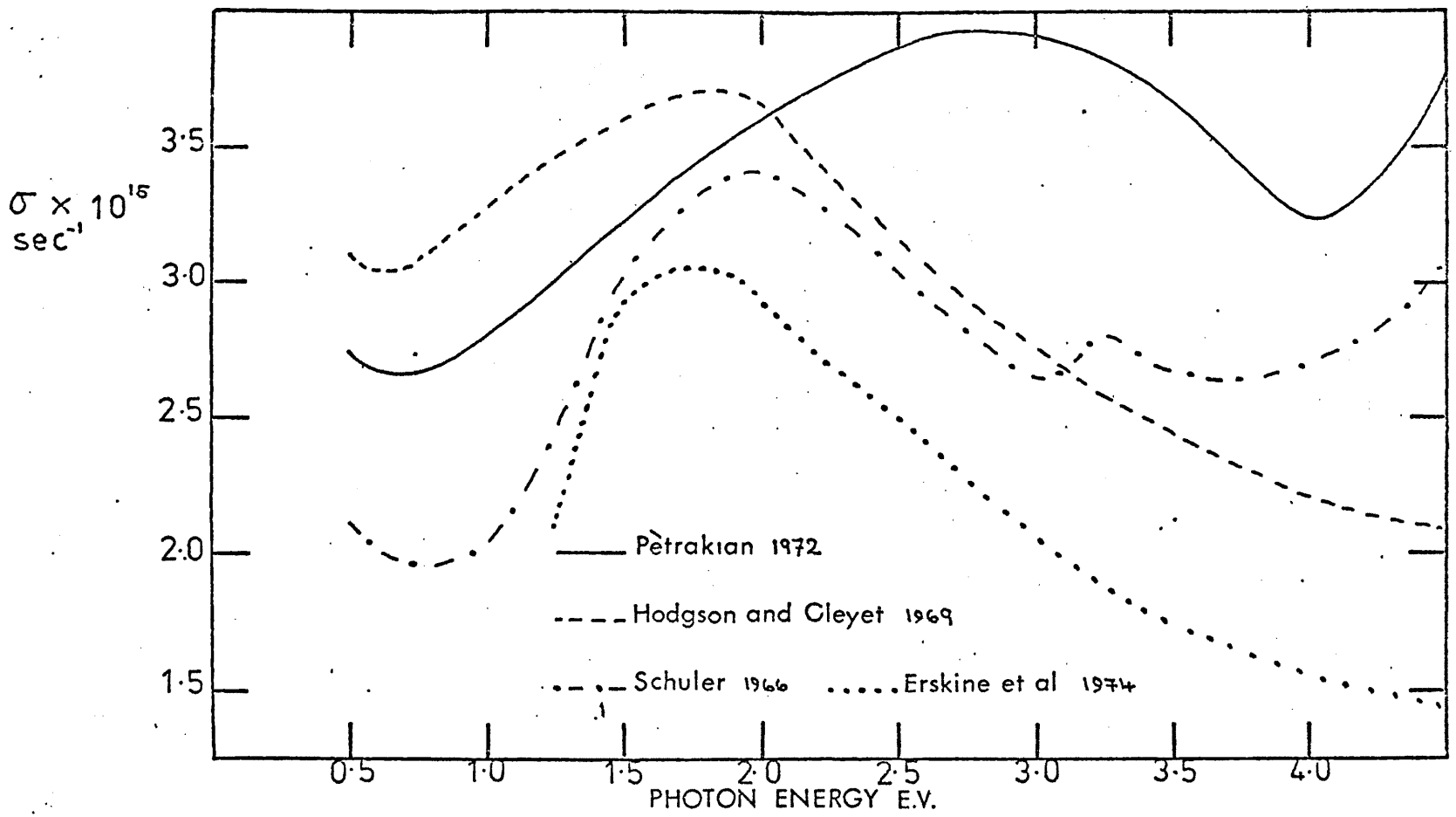

FIGURE (1·1) The variation of $\sigma(\omega)$ with photon energy for gadolinium

In (2.4) we see that the optical conductivity may be correlated with one of the band structure parameters, the joint density of states function. From this relationship we expect that sharp structure in the spectral profile of $\sigma(\nu)$ will be observed at photon energies for which there exists a high joint density of states. However sharp structure in the $\sigma(\nu)$ dispersion curve is rarely observed and this is probably due to the fact that other effects exist which are not taken into consideration in band structure calculations. For instance, the influence of non-vertical transitions, which are possible by phonon creation, are not included in the band structure calculation, nor are the effects of impurity centres and lattice faults. Also transitions may occur in regions of the Brillouin zone for which calculations have not been performed. Thus, the $\sigma(\nu)$ dispersion curve reflects the energy contour of a summation over extended, rather than localized, regions in the Brillouin zone. Clearly, the definite assignment of transitions is difficult when interpreting the weak structure in a $\sigma(\nu)$ dispersion curve. However, despite the experimental difficulties encountered in determining the optical constants and the interpretation of the $\sigma(\nu)$ dispersion curve it should be emphasized that optical measurements have yielded much data for many materials.

In 1965, work by Seraphin indicated that modulation spectroscopy was a particularly useful tool for lifting out structure due to critical point transitions from a structureless background. It became clear that sharp structure in the $\sigma(\nu)$ curve could be obtained by measuring the derivative of the reflectance with respect to some external parameter instead of the reflectance R (or the transmittance). (In Seraphin's work the change in reflectance with respect to an applied electric field of germanium was measured). This work opened a wide field of possibilities for studying optical structure and in recent years modulation techniques have been increasingly employed, yielding greater resolution and sensitivity.

The main advantages of modulation measurements over "static" optical measurements are, in summary:

(i) In a modulation experiment the observables are either the derivative (or pseudo-derivative) of the reflectance (or transmittance). Thus, any small structure in the reflectance dispersion curve is likely to be enhanced.

(ii) No measurement of the incident light intensity is required in a modulation experiment (Experimental details of a modulation technique are given in (3.3)).

(iii) There is an improved signal to noise ratio over "static" optical measurements.

The technique does however have disadvantages: we see in (2.3) that in order to correlate the modulated optical data with electronic band structure calculations it is necessary to calculate $\Delta\varepsilon_2$, the change in the imaginary part of the dielectric constant. To calculate $\Delta\varepsilon_2$ a knowledge of the optical constants of the material is still required. Also, the theory behind the various modulation techniques is complex as it involves not only the theory of the optical constants of the material but also the effect of the perturbing parameter on the optical constants.

At present, four modulation techniques are extensively used:-

(i) Modulation by an applied electric field, termed electroreflectance when taking measurements in reflection and electroabsorption when measuring the change in the transmitted light intensity.

(ii) Modulation by an applied stress: termed piezoreflectance and piezoabsorption

(iii) Modulation by an induced temperature change: thermoreflectance and thermoabsorption

(iv) Wavelength modulation.

Techniques (i) to (iii) above are generally known as internal modulation techniques, since the modulating parameter actually perturbs the energy bands of the solid. The theory of an internal modulation experiment thus involves not only the theory of the optical constants but also that of the effect of the perturbing parameter on the optical constants. Wavelength modulation is termed an external technique since only the derivative of the "static" reflectance or transmittance spectra is formed, the material under study being unaffected by the modulation. Thus, the theory of a wavelength modulation spectrum involves only the theory of the optical constants. The four modulation techniques will now be discussed in detail.

(1.3) Wavelength modulation

To obtain a wavelength derivative spectrum a wavelength modulated monochromatic light beam is required and several methods for obtaining such a beam have been reported. One method involves the mechanical vibration of an entrance or exit slit on the monochromator (Balslev 1966a) or the vibration of a mirror inside the monochromator (Balslev 1966b). The wavelength modulation technique has not however seen wide application since structure in I_o, the incident light intensity, arising from the spectral distribution of the source can be a serious problem. Although the problem may be overcome by using a double beam system (Welkowsky and Braunstein 1971), small errors in the balance of the two beams, path differences and different mirror reflectivities will still leave some residual spurious signal if I_o has strong structure. Despite the experimental difficulties, evaporated polycrystalline films of copper, gold and silver have been studied in reflection in the energy range 2.0 to 5.0 eV as a function of temperature, using wavelength modulation (Welkowsky and Braunstein 1971). In copper and gold features were observed in ε_2, whose

location in the Brillouin zone supported recent band theories.

(1.4) Modulation by an applied stress

We have seen in (1.2) that much information about interband transitions has been obtained from static optical measurements. The response of the reflectance to a static uniaxial stress has long been recognized as a powerful technique for studying band structure (Phillip et al. 1962, Gerhardt 1964). The spectral position of structure in a reflectance curve may be analysed to determine transition energies and the application of a stress adds two more sources of information: (a) Symmetry relations between the strain components and the polarization direction of the incident radiation may be evaluated in terms of thelocation of a transition and (b) the deformation potential, defined as the rate of change of the energy gap of the transition with respect to the applied stress, may be determined by observing the spectral shift of structure qualitatively as a function of the stress magnitude. However, this information can only by gained after considerable experimental difficulties have been overcome. Stress-induced changes are small and few materials withstand the strain required to observe them in a static reflectance measurement.

The initial piezomodulation measurements were made independently by Engeler et al. (1965) and Gobeli and Kane (1965) and it was found that the sensitivity of the measurement was nearly two orders of magnitude better than in a static strain experiment. Several methods have been used to apply a modulated stress to a sample. The original piezoreflectance measurements used an electromechanical transducer built with a piezoelectric material (quartz or lead zirconate). If measurements are performed on evaporated thin films, the films can be evaporated directly onto the polished surface of the transducer (Garfinkel et al. 1966). Thin single crystals prepared from the bulk can be cemented to the transducer (Engeler et al. 1965).

The theory underlying piezomodulation is very much more complicated than wavelength modulation. A knowledge of the complex dielectric constant ε is sufficient to describe the optical properties of a solid and it is possible to completely describe the piezo-optic interaction in terms of the changes induced in ε by the stress. Seraphin (1972) shows that the state of strain of a solid under stress is described by a second rank tensor $e_{k\ell}$ and the change in the dielectric tensor $\Delta\varepsilon_{ij}$ is related to $e_{k\ell}$ by

$$\Delta\varepsilon_{ij} = W_{ijk\ell} \cdot e_{k\ell} \qquad (1.7)$$

In cubic crystals $W_{ijk\ell}$ has only three components W_{11}, W_{22} and W_{44} which completely describe the piezo-optic action. Chen and Segall (1976) have obtained expressions for the components of the piezo-optical response tensor corresponding to transitions between the conduction bands around the L symmetry point in the Brillouin zone of the noble metals, and these theoretically calculated results accurately reproduce the experimentally determined W_{44} response obtained from piezoreflectance measurements of single crystals of copper, silver and gold.

Piezomodulation has seen wide application, semiconductors, insulators and metals being studied by the technique. Gerhardt et al. (1967) have measured the piezoreflectance of single crystal copper and the piezoreflectance spectra of potassium bromide and iodide have also been studied (Gerhardt and Mohler 1966). In all experiments extreme care has to be taken to avoid spurious signals due to changes in thepath of the light beam produced by the vibration of the sample. In order to reduce the signals to a minimum, a very smooth and flat reflecting surface is needed. In spite of these precautions some spurious background signal is always present.

(1.5) Modulation by an applied electric field

When an electric field is applied to a solid the translational symmetry of the material is changed along the direction of the applied field. Essentially the effect of this applied electric field is to add to the Hamiltonian of the system a potential energy of the form - eE.r (assuming a uniform electric field) which is not translationally invariant. In 1958, Franz and Keldysh independently predicted the effect of an electric field on the optical properties of a material. They predicted that in the presence of strong electric fields the absorption edges of insulators and semiconductors would be moved to longer wavelengths and the shift (for an exponential type absorption edge) would be proportional to the square of the electric field strength. (A more complete discussion of the theory underlying electromodulation will be given in Chapter VII). The effect was subsequently found in many materials (Moss 1962, Williams 1960) and was explained as being due to a photon-assisted tunneling between valence and conduction bands at photon energies smaller than the energy gap. Until 1965, all the electromodulation experiments were restricted to the study of the electric field-induced variations of the transmitted light intensity at the fundamental absorption edge. However, Seraphin (1965) studied the electroreflectance response of germanium and found a response far beyond the photon energy of the fundamental energy gap. This work led to the development of a more generalized theory of electromodulation (Aspnes 1966, 1967), taking into account the effect of an electric field on both direct and indirect transitions.

The techniques for observing electroreflectance and electroabsorption fall into two categories:

(i) Electrolytic techniques

(ii) "Dry package" techniques.

(a) Electrolytic techniques

The possibility of a space-charge layer modulation at a semiconductor-electrolyte interface has been recognised for many years (Garret 1962). In particular, it has been shown that a sizeable change in the conductivity of a thin semiconductor electrode can be obtained by changing the voltage applied to an electrolytic cell in which the semiconductor is one of the electrodes. When a semiconductor is immersed in an electrolyte electrons flow from one material to another until the electro-chemical potentials are equal and the space-charge layer at the surface is established. A surface charge layer is also present at the electrolyte side of the interface and is known as the Gouy layer. The ions in the electrolyte cannot get any closer to the surface of the semiconductor than their radius, this layer being called the Helmoltz layer. In high conductivity electrolytes the Gouy layer is typically 5Å thick and the potential drop across it may be disregarded; non aqueous electrolytes usually have lower ion densities and the Gouy layer may produce a drop in the modulating voltage. The Helmoltz layer is typically 1Å thick and therefore simulates a field electrode of extreme proximity to the semiconductor and has a very high breakdown strength. Large electric field strengths and large reflectance changes caused by small modulation voltages are therefore a characteristic advantage of the electrolytic technique. Cardona (1965) has investigated the electroreflectance spectra of a wide variety of semiconductors using this method. However, the technique does suffer from several limitations: the use of the electrolytic method at low temperatures is limited since aqueous electrolytes freeze near 278K although non-aqueous electrolytes e.g. methyl alcohol, permit operation to approximately 150 K. However, we have mentioned above that organic electrolytes usually have low ion densities and the influence of the Gouy layer on the modulating voltage cannot be generally disregarded. Aspnes and Cardona (1968) have found that slow adjustment processes across this layer can lead to a drift of the point of operation. The choice of electrolyte is also influenced by the spectral range of interest.

Although water transmits into the ultra-violet, its transmission region in the infra red is limited to 0.6 eV. Electrolytes must also be chosen that do not react with the material under investigation.

Perhaps the most surprising result from the use of an electrolytic technique came in 1966 when Feinleib reported the electric field modulation of the reflectance from metal-electrolyte interfaces. In the case of metals, screening of an electric field occurs within atomic dimensions of the surface leaving the bulk of the metal as a field-free region. The actual modulation mechanism in metals is not clear and the final explanation will probably require a better understanding of electroreflectance at an electrolyte interface (this topic is discussed further in Chapter VII).

(b) "Dry package" techniques

In the case of dry package techniques uniform electric fields may be applied to materials with a high resistivity using a capacitor configuration, and electroabsorption measurements may be made with the material under investigation as the dielectric and thin metal films as the electrodes. For electroreflectance measurements two techniques have been developed: transverse electroreflectance (TER) and surface barrier electroreflectance (SBER) and the sample configurations for these technqiues are shown in Figure (1.2a) and (1.2b) respectively. Both of these techniques have been extensively used (Ludeke and Paul 1967, Groves et al. 1966, Pidgeon et al. 1967, Gähwiller 1966, 1967). Transverse electroreflectance is perhaps the more versatile technique, since in this configuration the polarization vector of the incident light can be oriented parallel or perpendicular to the modulating field. In surface barrier electroreflectance the modulating field is necessarily oriented normal to the reflecting surface. Also the TER technique does not require a front electrode, which often limits the spectral range of investigation. However, Rehn (1968) has shown that materials having a resistivity greater than 10^8 Ωcm must be used to limit heating effects.

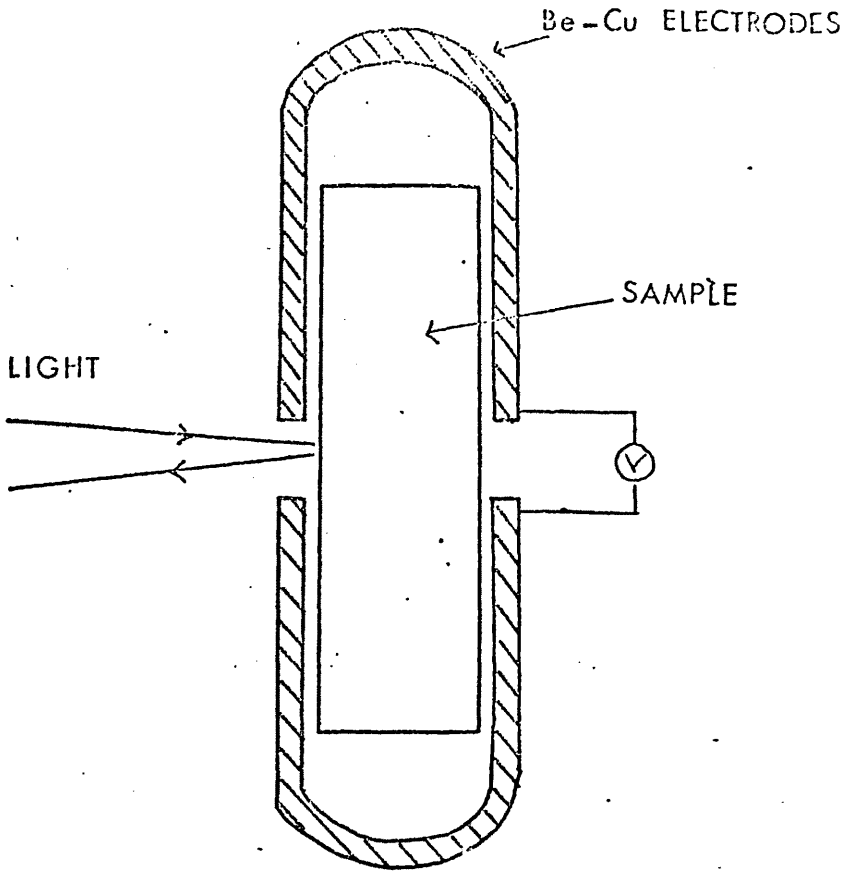

Figure (1.2a) Transverse electroreflectance configuration

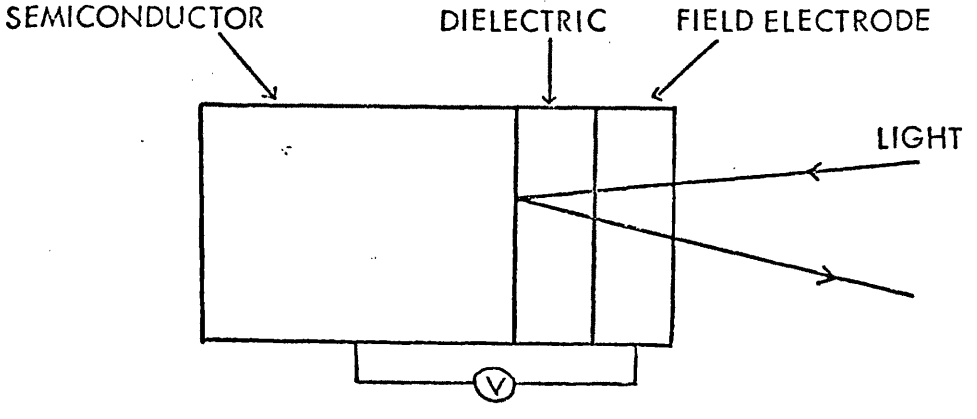

Figure (1.2b) Surface barrier electroreflectance configuration.

(1.6) Thermal modulation

A temperature modulation usually produces two effects on an absorption edge: a change in the energy gap arising directly from dilation of the lattice, and a change in the broadening parameter which is associated with the change in the number of permitted indirect transitions. However, the optical modulation caused by the shift of the energy gap is usually larger than the modulation caused by broadening.

The scalar character of temperature modulation gives it a special position among the other modulation techniques. Both electro-and piezomodulation accomplish modulation by the periodic change of a vectorial quantity. Depending on the orientation of this vector with respect to the material under investigation, or the polarization vector of the incident light, anisotropies may be observed that lead to the identification of a particular transition. However, thermal modulation lacks this potential, but the simplicity of the basic mechanism seems to compensate for this.

Batz (1966) and Berglund (1966) independently introduced temperature as a modulation parameter. Both workers used current pulses to produce a periodic temperature rise in the sample. The current was either sent through the sample directly or through a heater operating through a thermally conducting but electrically insulating medium. The sample was glued to a heat sink to dissipate the heat generated. Batz investigated the thermoreflectance of a 150 μm platelet of germanium whilst Berglund's (1966) studies were restricted to the thermoabsorption of thin platelets of silicon, cadmium sulphide and gallium arsenide. As with the other modulation techniques, thermal modulation improves on the resolution and sensitivity of "static" optical measurements. In a thermoreflectance study of graphite (Balzarotti and Grandolfo (1968)) the broad peak at 5.0 eV previously observed in static reflectance measurements was resolved into two separate peaks.

Thermal modulation has perhaps seen the widest application on metal samples and the initial experiment on a metallic element was performed by Scouler (1967) who studied the thermoreflectance response of polycrystalline thin films of gold. The measurements were made at 120K and covered an extensive spectral range. Additional structure to that previously observed was found at high photon energies but no analysis of the thermoreflectance data was undertaken by Scouler. However, in 1969 Cardona analyzed the data in terms of $\Delta\varepsilon_2$, the change in the imaginary part of the dielectric constant, and correlated this with existing band structure calculations. He was then able to compile for the structure a list of tentative assignments in terms of interband transitions. Much of the early thermoreflectance studies were restricted to gold, copper and silver (Rosei and Lynch 1972, Baldini and Nobile 1970 and Cheyssac and Penavaire 1974). However, the technique has recently been extended to the transition elements. Weaver et al. (1976) have studied the thermoreflectance response of polycrystalline thin films of vanadium, molybdenum, niobium and paramagnetic chromium. These workers found that the thermoreflectance response of these transition metals did not possess the sharp and distinctive features observed when dealing with semiconductors. The latter authors state that the cause of this was that critical point transitions are minimized in the transition metals and the broad structure arose from large volumes of k space. Perhaps the most remarkable data obtained by thermal modulation studies was that found by Hanus et al. (1967) who reported thermoreflectance measurements for nickel. A rather featureless response was observed in the visible part of the spectrum but extremely sharp structure was observed at low photon energies at 0.25, 0.4 and 1.3 eV. In order to interpret the observed thermoreflectance spectrum, the authors proposed a new band structure of nickel near the Fermi surface, based on the majority spin-minority spin band model proposed by Ehrenreich et al. (1963). It was found that the structure at 0.25 and 1.3 eV could then be understood as due to an

increase in the Fermi energy with respect to the initial states for the spin up band. However, the structure at 0.4 eV could not be described by this mechanism.

Thermal modulation experiments have now been extended to photon energies as high as 30 eV. Olson et al. (1974) using synchrotron radiation as the source have measured the thermoreflectance of gold up to 30 eV. From the foregoing we see that thermal modulation is perhaps the modulation technique with the widest range of application. It is not restricted to certain groups of materials and is superior to many forms of electromodulation because a spectrally limiting electrode is not required. Although thermoreflectance shares this advantage with piezomodulation the latter has been found by many workers to be hampered by the presence of parasitic vibrational signals. In view of this, thermal modulation has been chosen as the solid state diagnostic in the present work.

(1.7) Application of modulation techniques in other fields

In the preceding sections we have seen that modulation spectroscopy is a powerful tool in solid state physics. However, modulation techniques are gaining increasing importance in other fields: modulation spectroscopy has found a use in biological applications. Tada et al. (1974) report the use of thermoreflectance to study the optical properties of organo-metallic complexes. The work was undertaken because of the difficulty in obtaining sharp discrete spectra from solutions of the biologically significant compounds spermine and spermidine. These compounds have been postulated to have an important role in the control of cellular growth. The authors found that the thermoreflectance studies provided much needed information for studying organo-metallic complexes and proposed that the method should accelerate the development of cancer tests.

Electroreflectance has been used by Masawa et al. (1976) to determine the surface properties of thermally oxidised silicon in MOS (metal-oxide-semiconductor) capacitors. The authors show that from a plot of the electroreflectance signal against the gate voltage of the device, the flat band voltage, V_{FB}, of the device may be obtained. The V_{FB} value derived in this manner was found to agree with that derived by conventional conductance measurements.

With the advancement of the use of integrated components in the electronics industry, interest has also centred on producing components for integrated optical circuits. Eden and Coleman (1964) proposed a system whereby the microwave modulation of light could be accomplished by employing the shift of an absorption edge with an applied electric field (the Franz-Keldysh effect). The authors theoretically examined the case of cadmium selenide and showed that for a crystal with an electrode separation of 1.5mm a 1kV d.c. bias and 275 volts of a.c. signal would be required to produce an 85% transmitted light intensity modulation at 77K at the fundamental frequency. It was found that modulation at room temperature because of the reduced steepness of the absorption edge would require about eight times the field strength. A modification of this theoretical proposal was experimentally undertaken by Frova and Handler (1964). They showed that the influence of an electric field on the direct interband optical absorption edge in a germanium p-n junction may be used to produce modulation of a monochromatic beam of light. The sample was an arsenic diffused p-n junction on a 7Ωcm, 100μm thick p type base. The greatest effect was observed at a photon energy of 0.795 eV with 150V reverse bias applied. Clearly then, one of the limitations of bulk specimens is that high voltages are required to generate the high field strengths to produce the modulation. Although Eden and Coleman (1964) and Frova and Handler (1964) showed both theoretically and experimentally that optical modulators could be designed based on the Franz-Keldysh effect the designs were very far from integrated.

In 1972, Honda et al. reported light intensity modulation in a cadmium sulphide film. An investigation was made of the influence of an electric field on the transmission of light through a multilayer structure consisting of cadmium sulphide and glass films. Between 10% and 36% modulations of the transmitted light intensity were found for applied voltages of between 10 and 50 volts. However, although only low voltages were required to operate the modulator the system was not completely integrated, essentially comprising two separate structures having an air gap between them. In the present work a totally integrated thin film optical modulator has been designed based on the Franz-Keldysh effect, and in Chapter IV we present the configuration of such a modulator together with its advantages over conventional electro-opic modulators. Although overcoming these disadvantages, this results in a reduced performance in terms of modulation efficiency and in Chapter VII we see how this may be partially overcome by suitable filter design.

CHAPTER II

The analysis and interpretation of the thermoreflectance data

2.1 Introduction

In this chapter we deal with the effects of a modulating parameter on the fundamental optical properties of a material. The discussion is centred on the effects of modulating the temperature of the sample, effects of modulating an applied electric field being considered in more detail in Chapter VII. For completeness, definitions of the fundamental optical properties are given together with a general discussion of the interpretation of both static and modulated optical data in terms of electronic band structure calculations. To correlate the modulated optical data with band structure calculations, it is necessary to calculate $\Delta\varepsilon_2$ - the change in the imaginary part of the dielectric constant. The method by which this has been performed is described and computational details given. The effects of experimental errors on the $\Delta\varepsilon_2$ dispersion curve are also discussed.

2.2 The fundamental optical properties of a medium

The linear response of a non magnetic (permeability $\mu = 1$) medium to transverse electromagnetic radiation is completely described by the frequency-dependent dielectric tensor ε or by the conductivity tensor $\sigma = (-iw/4\pi)(\varepsilon - 1)$ where w is the angular frequency of the electromagnetic radiation. For isotropic materials, ε and σ reduce to scalars and throughout the following analysis are treated as such, since the structures of all the specimens used in the experimental work were either cubic and polycrystalline, or hexagonal close packed and polycrystalline, with no strong fibre axes or evidence of strains, and could therefore be assumed homogeneous and isotropic. The quantities ε and σ are therefore assumed constant for a given material. From Maxwell's theory we have the

relationship

$$n = \varepsilon^{\frac{1}{2}} \tag{2.1}$$

where n is known as the refractive index of the material and is defined as the ratio of the velocity of light in the vacuum to the velocity of light in the medium. Equation (2.1) provides a relationship between the behaviour of light in a medium and a property of that medium.

Application of Maxwell's equations to conducting media shows that, in general, n is a complex quantity. A plane polarized wave incident on a vacuum-metal interface may be represented by

$$E = E_o \exp iw(t - x/c) \tag{2.2}$$

where E_o = the amplitude of the electric vector of the incident wave

c = the velocity of light.

The transmitted wave can be completely described by

$$E = E_o \exp i\left(wt - \frac{wx\underline{n}}{c}\right) \tag{2.3}$$

$\underline{n}$, known as the complex refractive index, may be written as:-

$$\underline{n} = (n - ik) \tag{2.4}$$

n, the real part of the refractive index, determines the wave velocity in the medium and k, the extinction coefficient, determines the rate at which the amplitude of the wave decays. n and k are known collectively as the optical constants of the medium. From equation (2.1), n and k are related to ε by

$$n^2 - k^2 = \varepsilon_1 \tag{2.5}$$

$$2nk = \varepsilon_2 \tag{2.6}$$

where ε_1 = the real part of the dielectric constant

ε_2 = the imaginary part of the dielectric constant.

From electromagnetic theory it can be shown (Mott and Jones 1936) that the ratio

$$\frac{\text{rate of loss of energy/unit volume}}{\text{square of the electric vector}} = nk\nu \qquad (2.7)$$

By analogy with the flow of direct electric current

$$nk\nu = \sigma(\nu) \qquad (2.8)$$

where $\sigma(\nu)$ is known as the optical conductivity. The absorption coefficient K of the medium can be shown to be:-

$$K = 2nk/\lambda \qquad (2.9)$$

The optical conductivity is thus directly proportional to the absorption coefficient, both quantities giving a measure of the capacity of a metal to absorb energy at a frequency ν.

2.3 The effect of a modulating parameter on the optical properties

Clearly the effect of a modulating parameter on the optical properties of a material must appear as a change in the real and imaginary parts of the dielectric constant. In a typical modulation experiment the measurable quantities are either $\Delta R/R$ or $\Delta T/T$ (see Chapter III),

where R, T = the reflectance and transmittance of the material respectively,

and ΔR, ΔT = the amplitude of the modulation in the reflectance and transmittance.

The relationship of the reflectance and transmittance of a material to the angle of incidence θ_o and the dielectric constant is given by the Fresnel equations (Born and Wolf 1965) which are listed below

$$r_p = \frac{(\varepsilon_o)^{\frac{1}{2}}\cos\theta_1 - (\varepsilon_1')^{\frac{1}{2}}\cos\theta_o}{(\varepsilon_o)^{\frac{1}{2}}\cos\theta_1 + (\varepsilon_1')^{\frac{1}{2}}\cos\theta_o} \qquad (2.10)$$

$$r_s = \frac{(\varepsilon_o)^{\frac{1}{2}}\cos\theta_o - (\varepsilon_1')^{\frac{1}{2}}\cos\theta_1}{(\varepsilon_o)^{\frac{1}{2}}\cos\theta_o + (\varepsilon_1')^{\frac{1}{2}}\cos\theta_1} \tag{2.11}$$

$$t_p = \frac{2(\varepsilon_o)^{\frac{1}{2}}\cos\theta_o}{(\varepsilon_o)^{\frac{1}{2}}\cos\theta_1 + (\varepsilon_1')^{\frac{1}{2}}\cos\theta_o} \tag{2.12}$$

$$t_s = \frac{2(\varepsilon_o)^{\frac{1}{2}}\cos\theta_o}{(\varepsilon_o)^{\frac{1}{2}}\cos\theta_o + (\varepsilon_1')^{\frac{1}{2}}\cos\theta_1} \tag{2.13}$$

where $r_{p,s}$ and $t_{p,s}$ are known as the Fresnel amplitude reflection and transmission coefficients respectively and the subscripts p and s refer to the parallel and perpendicular components of polarization

ε_o is the complex dielectric constant of the medium in which the light is incident

ε_1' is the complex dielectric constant of the medium in which the light is transmitted

θ_o is the angle of incidence and

θ_1 is the angle of refraction.

The reflectance R and the transmittance T are related to the Fresnel amplitude reflection and transmission coefficients by

$$R_{s,p} = |r_{s,p}|^2, \quad T_{s,p} = |t_{s,p}|^2 \tag{2.14}$$

The total differentials of the reflectance equations may be written as

$$\Delta R_{p,s} = (\partial R_{p,s}/\partial \varepsilon_1)\Delta\varepsilon_1 + (\partial R_{p,s}/\partial \varepsilon_2)\Delta\varepsilon_2 \tag{2.15}$$

and give a phenomenological description of the reflectance modulation. The analysis will be centred on reflectance modulation since, for reasons discussed in Chapter III, all the thermal modulation experiments in the present work were performed on thick (>100 n.m) absorbing films. For such

films the effects of multiple reflections may be ignored in the analysis. The following assumptions are made in taking the derivatives of the Fresnel equations:-

(i) the amplitude of the optical perturbation is small.

(ii) the changes induced in the optical constants by the modulating parameter are spatially invariant. Although this is a legitimate assumption for piezo and thermal modulation it is not necessarily so for modulation by an electric field. Aspnes and Frova (1969) have pointed out that it is necessary to use a W.K.B. approximation to deal with the resulting spatial dependence of the optical constants in the Fresnel equations

From equation (2.15) we see that the differentials may be expressed in the form:-

$$\Delta R_{p,s}/R_{p,s} = \alpha_{p,s}(\varepsilon_1,\varepsilon_2,\theta_o)\Delta\varepsilon_1 + \beta_{p,s}(\varepsilon_1,\varepsilon_2,\theta_o)\Delta\varepsilon_2 \qquad (2.16)$$

where

$$\alpha_{p,s} = \frac{1}{R_{p,s}} (\partial R_{p,s}/\partial\varepsilon_1)$$

$$\beta_{p,s} = \frac{1}{R_{p,s}} (\partial R_{p,s}/\partial\varepsilon_2)$$

The coefficients $\alpha_{p,s}$ and $\beta_{p,s}$ are common to all modulated reflectance experiments irrespective of the modulating parameter used. However the shapes of the $\Delta\varepsilon_1$ and $\Delta\varepsilon_2$ dispersion curves vary with the modulation parameter. This point is illustrated by comparing the work of Cardona (1969), based on the results obtained by Scouler (1967), with Garfinkel (1966) and Garrigos (1971) who studied the thermally modulated reflectance, piezo-reflectance and electro-reflectance responses respectively of thin films of gold. In the thermal and piezo-modulation experiments a sharp peak in the $\Delta\varepsilon_2$ dispersion curve is observed near to 2.4 eV while weaker structure is seen in the $\Delta\varepsilon_2$ spectra derived from the electroreflectance data.

The structure at 2.4 eV has been attributed (Christensen 1971) to an optical transition from the d band to the Fermi surface. The similarity between the thermally and piezo-modulated responses is due to dilation since the sample is constrained to the substrate in the thermal modulation experiment. The electroreflectance mechanism in gold is not clearly understood but Prostak and Hansen (1967) attribute the effect to modulation of the free carrier concentration which will change the Fermi level and hence all interband transitions involving the Fermi level.

We see that the analysis of the shapes of the $\Delta\varepsilon_1$ and $\Delta\varepsilon_2$ dispersion curves is complex, however Batz (1967) has computed the $\Delta\varepsilon_1$ and $\Delta\varepsilon_2$ dispersion curves for the effect of thermal modulation on M_o, M_1, M_2, M_3 type critical points. The theory has been found to be in good agreement with experiment. A similar calculation has been made by Rosei et al. (1973) for transitions from d bands to the Fermi surface.

The general form for the coefficients $\alpha_{p,s}$ and $\beta_{p,s}$ has been given by Fischer and Seraphin (1967) who find

$$\alpha_s = \frac{2us}{(u^2+v^2)} \frac{(u^2-3v^2-s^2)}{\left[(u-s)^2+v^2\right]\left[(u+s)^2+v^2\right]} \qquad (2.17)$$

$$\beta_s = \frac{-2vs}{(u^2+v^2)} \frac{(3u^2-v^2-s^2)}{\left[(u-s)^2+v^2\right]\left[(u+s)^2+v^2\right]} \qquad (2.18)$$

$$\alpha_p = \alpha_s + \frac{2ut}{(u^2+v^2)} \frac{(u^2-3v^2-t^2)}{\left[(u-t)^2+v^2\right]\left[(u+t)^2+v^2\right]} \qquad (2.19)$$

$$\beta_p = \beta_s - \frac{2vt}{(u^2+v^2)} \frac{(3u^2-v^2-t^2)}{\left[(u-t)^2+v^2\right]\left[(u+t)^2+v^2\right]} \qquad (2.20)$$

where $s = n_o\cos\theta_o$

$t = n_o\sin\theta_o\tan\theta_o$

$u^2-v^2 = \varepsilon_1 - n_o{}^2\sin^2\theta_o$

$uv = -\varepsilon_2/2$

The medium in which the light is incident has a refractive index n_o and is considered to be non-absorbing. The medium under study is described by $\varepsilon = \varepsilon_1 - i\varepsilon_2$. In solving explicitly for u and v, the signs of the square roots are determined by requiring $\varepsilon_2 \geq 0$ and $R_s, R_p \leq 1$. This gives $u \geq 0$ and $v \leq 0$.

The modulation will also produce a change $\Delta\psi$ in the phase shift ψ of the incident radiation on reflection. The reflectance R of the material is related to ψ by

$$r_{p,s} = |r|_{p,s} \exp i\psi_{p,s} \tag{2.21}$$

The effect of the modulation on ψ is given by

$$\Delta\psi_{p,s} = \gamma_{p,s}(\varepsilon_1,\varepsilon_2,\theta_o)\Delta\varepsilon_1 + \delta_{p,s}(\varepsilon_1,\varepsilon_2,\theta_o)\Delta\varepsilon_2 \tag{2.22}$$

where the coefficients $\gamma_{p,s}$ and $\delta_{p,s}$ are given below: (the derivation is given in Appendix 1)

$$\gamma_p = \frac{ab-cd}{a^2+c^2} \tag{2.23}$$

$$\delta_p = \frac{ae-cf}{a^2+c^2} \tag{2.24}$$

$$\gamma_s = \frac{gh-k\ell}{g^2+k^2} \tag{2.25}$$

$$\delta_s = \frac{gm-kn}{g^2+k^2} \tag{2.26}$$

where

$$a = n_o^2(\varepsilon_2^2+q^2) - 2\cos^2\theta_o(\varepsilon_1^2+\varepsilon_2^2)q \tag{2.27}$$

$$b = \frac{\sqrt{2}n_o\cos\theta_o}{r}(q^{3/2}(3\varepsilon_1-r) - \varepsilon_2^2 q^{1/2}) \tag{2.28}$$

$$c = -2\sqrt{2}n_o q^{1/2}(\cos\theta_o(\varepsilon_1 q-\varepsilon_2^2)) \tag{2.29}$$

$$d = 2q/r(\cos^2\theta_o(\varepsilon_1^2+\varepsilon_2^2-2\varepsilon_1 r)-n_o^2 q) \tag{2.30}$$

$$e = \frac{\sqrt{2}n_o\cos\theta_o}{r}\left(\varepsilon_2 q^{1/2}(4r-3\varepsilon_1) + \varepsilon_2^{\,3} q^{-1/2}\right) \qquad (2.31)$$

$$f = 2/r\left(n_o^{\,2} q\varepsilon_2 - \varepsilon_2\cos^2\theta_o(\varepsilon_1^{\,2}-\varepsilon_2^{\,2})\right) + 4\varepsilon_2\cos^2\theta_o(\varepsilon_1 - n_o^{\,2}\sin^2\theta_o - r) + 2\varepsilon_2 n_o^{\,2} \qquad (2.32)$$

$$g = q(2n_o^{\,2}\cos^2\theta_o - q) - \varepsilon_2^{\,2} \qquad (2.33)$$

$$h = \frac{-3\sqrt{2}n_o\cos\theta_o q^{3/2}}{r} \qquad (2.34)$$

$$k = 2\sqrt{2}n_o\cos\theta_o q^{3/2} \qquad (2.35)$$

$$\ell = 2q/r(q - n_o^{\,2}\cos^2\theta_o) \qquad (2.36)$$

$$m = \frac{2\sqrt{2}\cos\theta_o q^{1/2}\varepsilon_2}{r} \qquad (2.37)$$

$$n = 2\varepsilon_2/r(n_o^{\,2}\cos^2\theta_o - q - r) \qquad (2.38)$$

with

$$r = \left((\varepsilon_1 - n_o^{\,2}\sin^2\theta_o)^2 + \varepsilon_2^{\,2}\right)^{\frac{1}{2}} \qquad (2.39)$$

$$q = \left(r - (\varepsilon_1 - n_o^{\,2}\sin^2\theta_o)\right) \qquad (2.40)$$

The coefficients $\alpha_{p,s}$, $\beta_{p,s}$, $\gamma_{p,s}$ and $\delta_{p,s}$ are functions of ε_1 and ε_2 and are therefore dispersive. In the analysis of a modulated reflectance spectrum the coefficients $\alpha_{p,s}$ and $\beta_{p,s}$ must be considered since from equation (2.16) we see that structure in the $\Delta R/R$ responses may be due to structure in the coefficients as well as structure in $\Delta\varepsilon_1$ and $\Delta\varepsilon_2$. An illustration of this point is given in Figures (2.1 a,b) where the spectral dependences of α and β (at normal incidence) are plotted. For both metals the coefficient α is always negative but not monotonically so. For copper β is always negative, but for gold it goes through zero near to 2.6 eV and then remains positive up to 5 eV, although again not monotonically. Interpretation of structure in $\Delta R/R$ at a particular photon energy directly in terms of transitions between electronic states with the corresponding

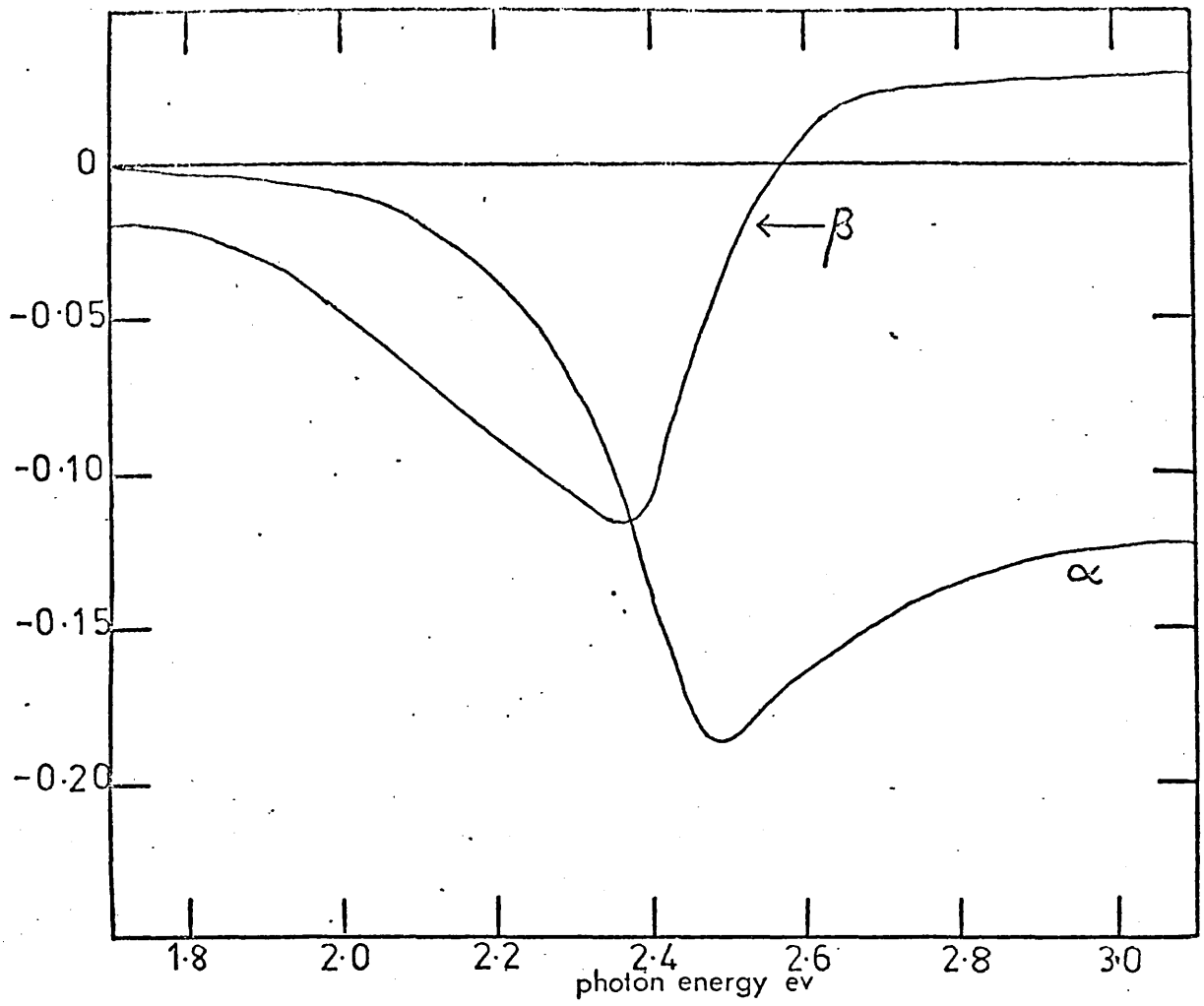

FIGURE (2·1a) The variation of α and β with photon energy for gold

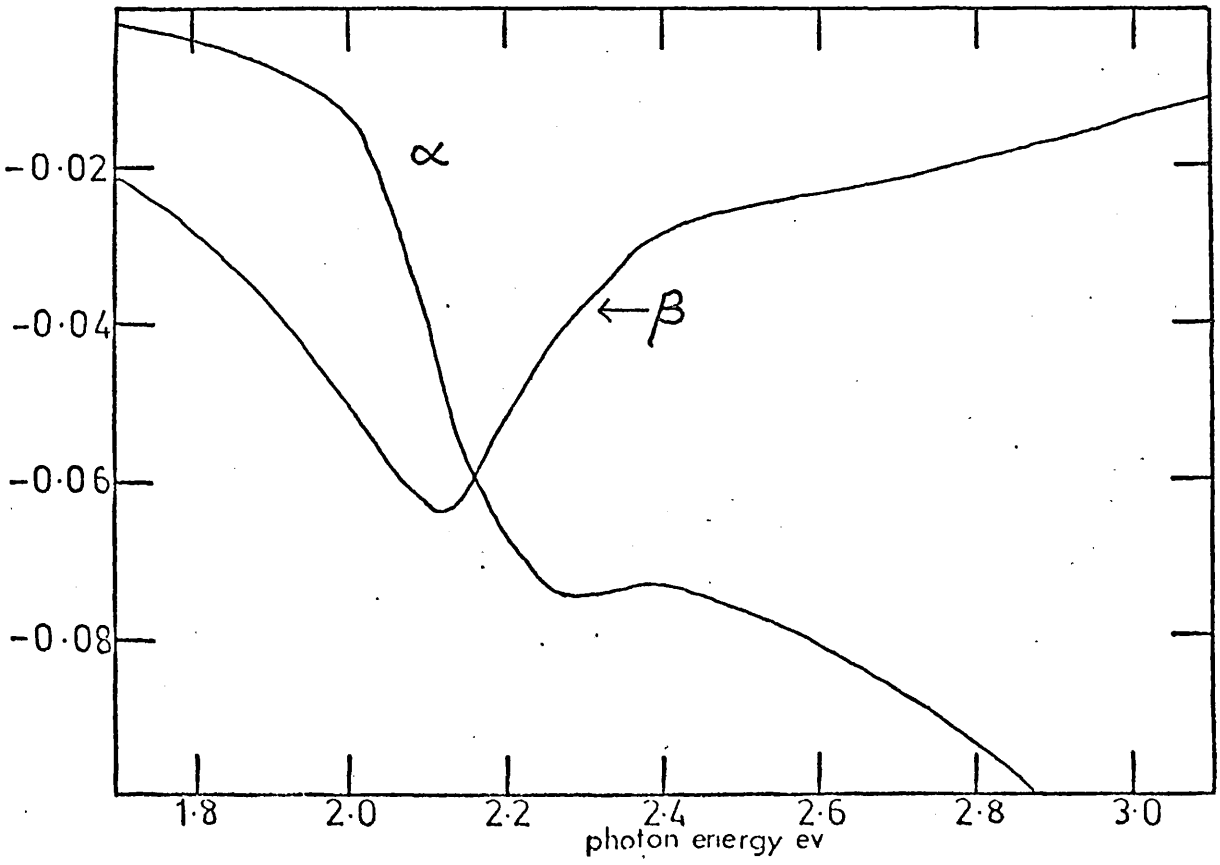

FIGURE (2·1b) The variation of α and β with photon energy for copper

energy difference may thus lead to misleading results. For this reason the experimentally measured values of $\Delta R/R$ are reduced to the more meaningful quantities $\Delta\varepsilon_1$ and $\Delta\varepsilon_2$, the latter being correlated with band structure calculations.

Miller et al. (1971, 1972) have determined the optimum ranges of angles of incidence for the determination of optical constants of a material from static reflectance measurements. The application of a similar technique was considered for modulated reflectance measurements to determine whether $\Delta R/R$ was highly sensitive to angle of incidence θ_o. From equation (2.16) we see that the coefficients $\alpha_{s,p}$ and $\beta_{s,p}$ are functions of θ_o ($\Delta\varepsilon_1$ and $\Delta\varepsilon_2$ do not depend on θ_o; $\Delta\varepsilon_2$ follows changes in the joint density of states function). Fischer and Seraphin (1967) have found that for a variety of semiconductors (Ge, Si, GaAS) that if $\alpha_{s,p}$ and $\beta_{s,p}$ are plotted against θ_o, the parallel coefficients α_p and β_p considerably amplify (in some cases by two orders of magnitude) the reflectance modulation in comparison with the normal incidence values. Preliminary electro-reflectance experiments (Schmidt and Knausenberger 1969) on germanium confirmed this response. Observation at oblique incidence may thus be applicable to the study of weak modulation signals. $\alpha_{s,p}$ and $\beta_{s,p}$ have been plotted against θ_o for both gold and copper in figures (2.2a,b) and (2.3a,b) for two photon energies. The coefficients α_s and β_s for both metals decrease monotonically with increasing θ_o, indicating that $(\Delta R_s/R_s)$ also decreases. The coefficients α_p and β_p exhibit extrema in a small angular range 65° to 75° about the pseudo-Brewster angle. The amplification factor of α_p and β_p varies in the different spectral regions but at its maximum does not exceed a value of two. Thus a preliminary investigation indicated that the modulated reflectance response for the metals gold and copper is not strongly dependent on the angle of incidence in the visible and near visible.

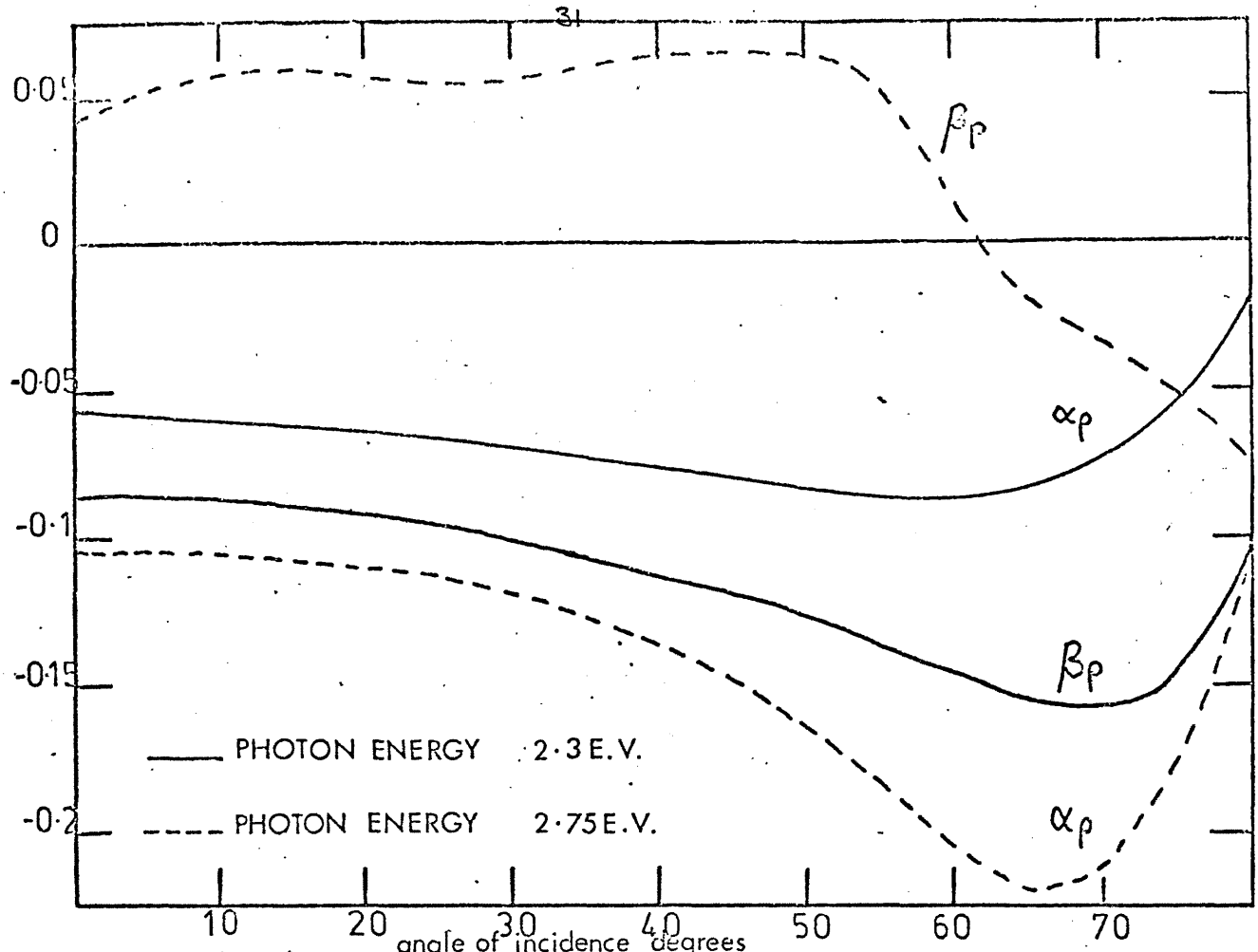

FIGURE (2·2a) The angular dependence α_p and β_p for gold

FIGURE (2·2b) The angular dependence of α_s and β_s for gold

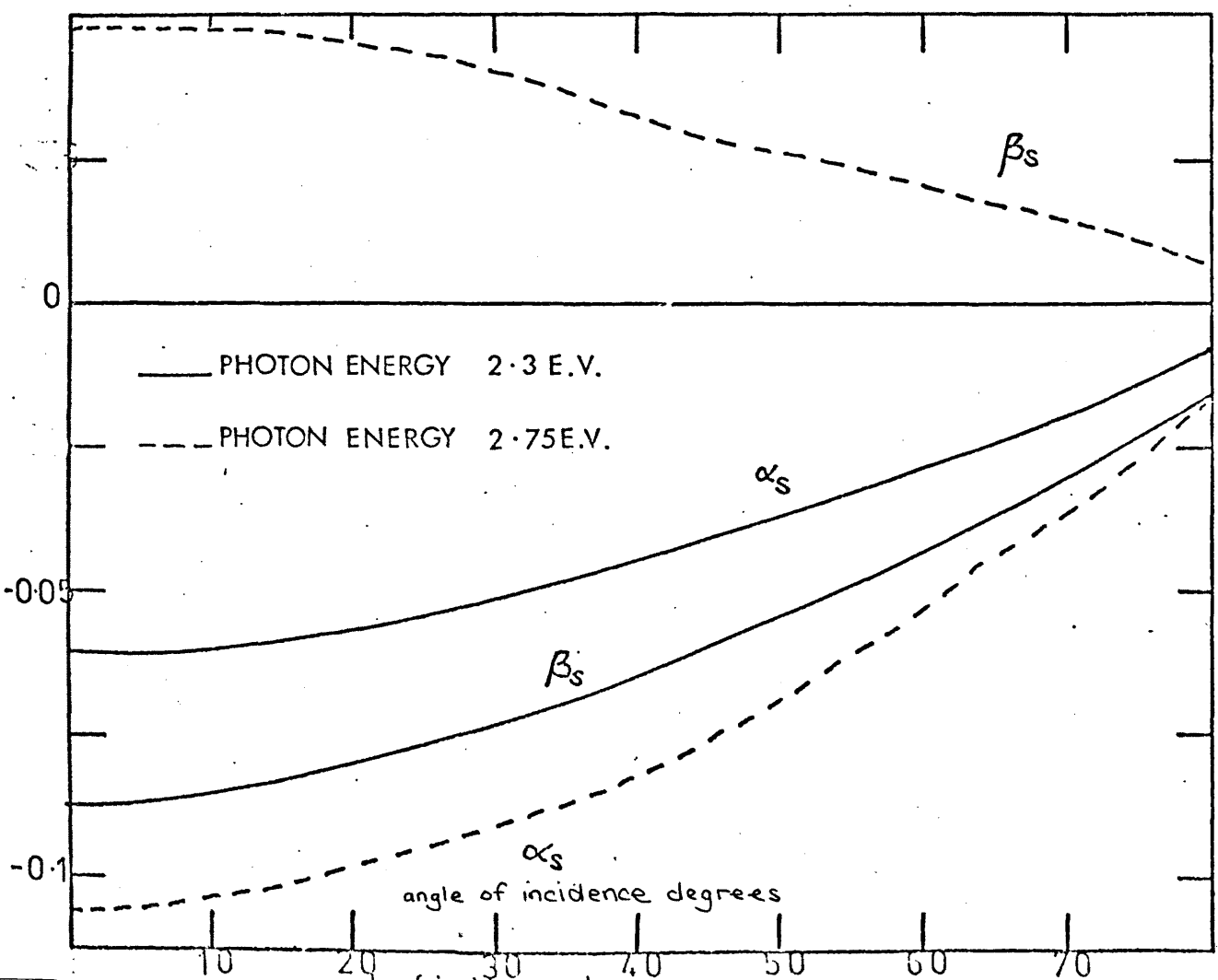

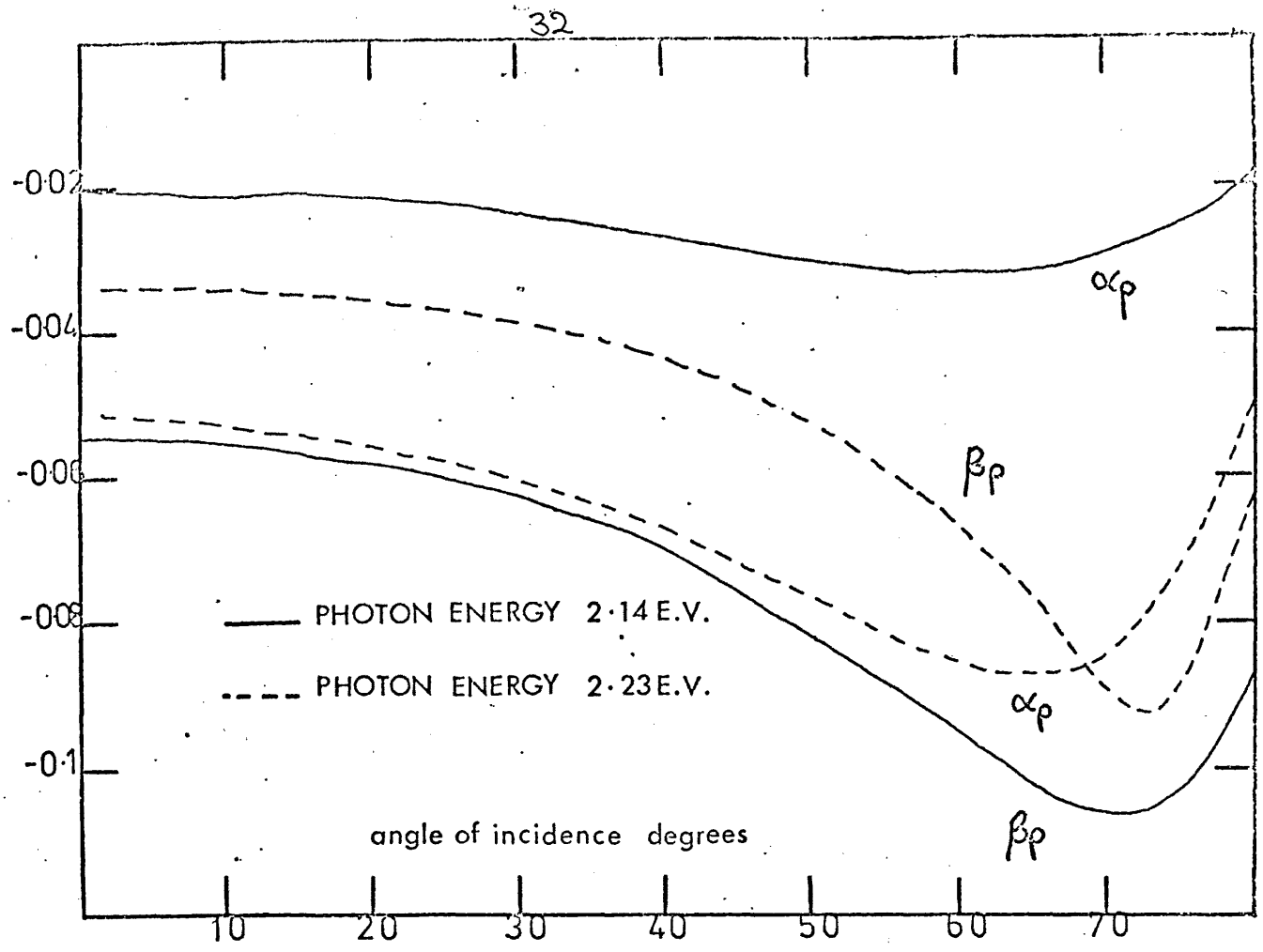

FIGURE (2·3a) The angular dependence of α_p and β_p for copper

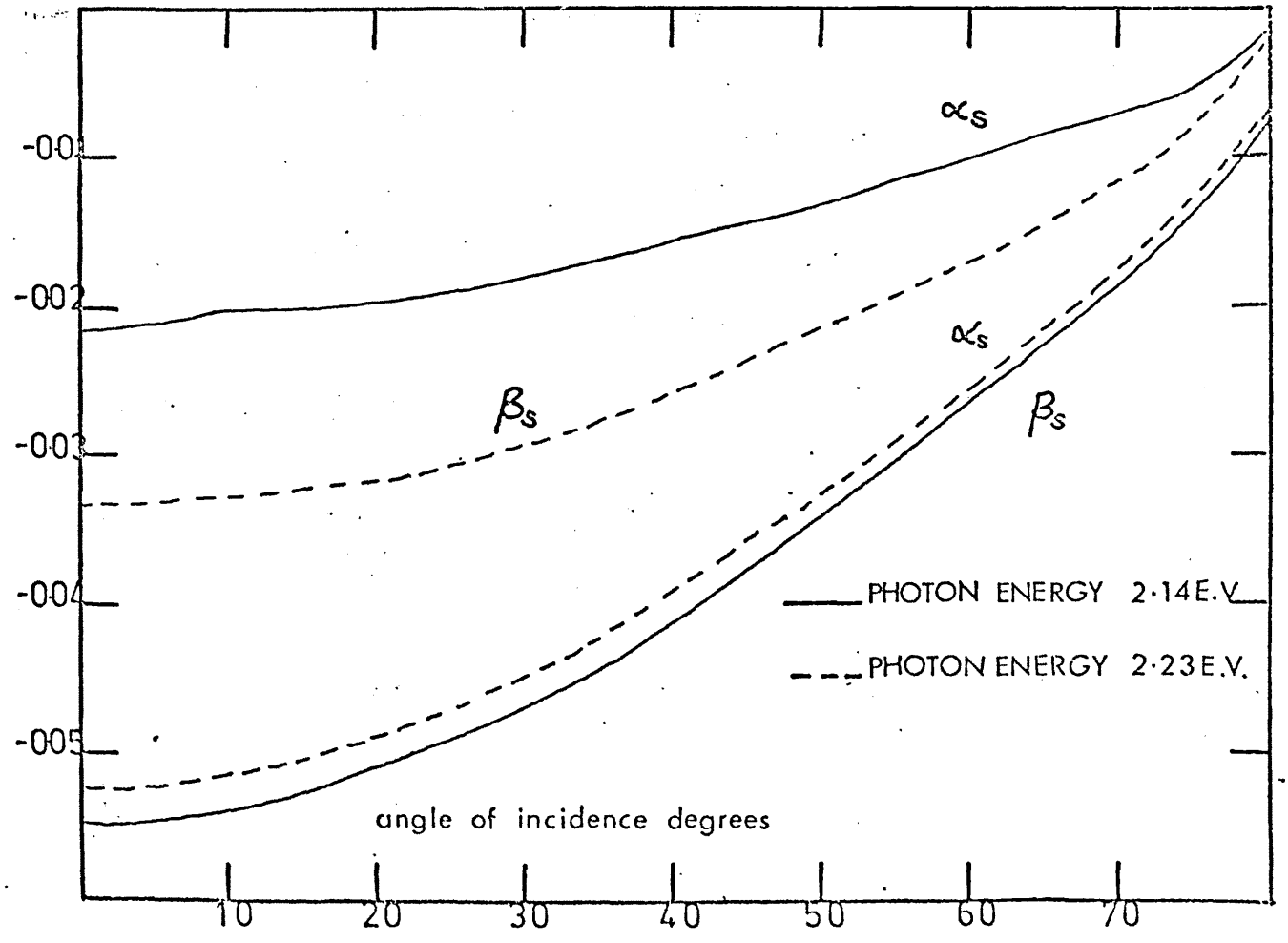

FIGURE (2·3b) The angular dependence of α_s and β_s for copper

2.4 The correlation of the experimental data with band structure calculations

The fundamentals of electronic band structure calculations have been extensively reviewed (Callaway 1964, Loucks 1967, Altmann 1970). A general expression given by Kubo (1957) and Greenwood (1958) relates the optical conductivity, $\sigma(\nu)$, to the electron states in the Brillouin zone. However, in general, all the states are not known, moreover, experimental results depend strongly on the properties of the surface and these are not accounted for in the Kubo-Greenwood equation. The correlation between ε_2 and band structure parameters is established by assuming that the absorption is the sum of transitions between electron states of the same wave vector $\underline{k}$ and separated by an energy difference $E_f - E_i = \Delta E = h\omega$. then

$$\varepsilon_2(w) \sim \int_{B.Z} 2/(2\pi)^3 \; |e.M_{if}|^2 \; \delta(\Delta E - h\omega) d^3k \qquad (2.41)$$

where B.Z refers to the Brillouin zone.

If it is assumed that the optical matrix element M_{if} is the same for all pairs of states located vertically above each other regardless of their location in the Brillouin zone, then the joint density of states function $J(\Delta E)$ may be defined as

$$J(\Delta E) = \int_{B.Z} 2d^3k/(2\pi)^3 \; \delta(\Delta E - \hbar\omega) \qquad (2.42)$$

$J(\Delta E)$ represents the simple counting of states in the Brillouin zone. The spectral profile of an experimentally determined $\varepsilon_2(w)$ curve is expected to reflect features of this summation, and pronounced structure is expected to occur at energies for which there exists a high joint density of states between bands. A transformation of the volume integral in equation (2.42) into a surface integral over the surface ΔE = constant gives

$$J(\Delta E) = 2/(2\pi)^3 \int \frac{ds}{\nabla_k (E_f(\underline{k}) - E_i(\underline{k}))} \qquad (2.43)$$

Equation (2.43) predicts striking features in ε_2 (and hence in $\sigma(w)$ the optical conductivity) when

$$\nabla_K(E_f(\underline{k}) - E_i(\underline{k})) = 0 \qquad (2.44)$$

i.e. the denominator in equation (2.43) is equal to zero and the integrand has a singularity. Such points are known as Van Hove critical points (Callaway 1964). The critical points correspond to the direct optical interband transitions at those points in the Brillouin zone given by the wave vector $\underline{k}$ for which the bands i and f are parallel i.e. symmetry interband points. However attempts by Pells and Shiga (1969) to interpret their static reflectance measurements of gold in terms of critical point transitions were unsuccessful. A relativistic augmented plane wave (R.A.P.W) band calculation for gold by Christensen and Seraphin (1971) indicated that some of Pells' and Shiga's assignments were erroneous. They concluded that in static reflectance measurements critical points are masked by the large background of transitions from extended regions in the Brillouin zone. The general view that has been adopted for interpreting the structure in the optical conductivity curve is to assume that the general shape of the curve is determined by non $\underline{k}$ conserving processes (i.e phonon creation). Any structure superimposed on this background is likely to be due to transitions at symmetry interband points.

Seraphin (1972) indicates that modulation spectroscopy is a particularly useful tool in lifting out structure due to critical point transitions from a structureless background. He shows that modulation of the spectral position E_g of a critical point affects ε_2 through the joint density of states function $J(\Delta E)$ and gives the relationship

$$\Delta\varepsilon_2/\Delta E_g = C/w^2 \, \Delta J/\Delta E_g \qquad (2.45)$$

where C contains the optical matrix element and effective mass parameters. For all four types of critical point (M_o, M_1, M_2, M_3) the joint density

of states function varies as the square root of the spectral distance from E_g. Hence the derivative of $J(\Delta E)$ with respect to E_g has a singularity of the type $(E_g-hw)^{-\frac{1}{2}}$ at the critical point. Thus the response of the modulated reflectance disappears as the spectral distance from E_g increases and non critical areas with a smooth $J(\Delta E)$ contribute very little to the modulation spectrum. However in the case of metals, particularly gold, much of the structure in $\epsilon_2(w)$ and $J(\Delta E)$ is probably due to transitions involving the Fermi surface (Winsemius 1973). Equally sharp structure in $\Delta\epsilon_2(w)$ may thus be observed for transitions other than critical point transitions, this is the view adopted in the present work for the interpretation of the experimental results.

2.5 The method of reducing $\Delta R/R$ to $\Delta\epsilon_1$ and $\Delta\epsilon_2$

As already discussed in section (2.3), since the experimental read-out $\Delta R/R$ from a thermally modulated reflectance experiment does not directly yield the changes in $\Delta\epsilon_1$ and $\Delta\epsilon_2$, the measurements must be interpreted before they yield information about band structures. If equations (2.16) and (2.22) are solved simultaneously then $\Delta\epsilon_1$ and $\Delta\epsilon_2$ may be found, the latter being correlated with band structure calculations. To solve the equations for $\Delta\epsilon_1$ and $\Delta\epsilon_2$, the change in the phase shift, $\Delta\psi_{p,s}$, of the light on reflection must be known. The phase shift $\psi_{p,s}(w)$ is related to the reflectance $R(w)$ by the Kramers Kronig dispersion relationship (Cardona 1969)

$$\psi(w) = \frac{w}{\pi}\rho\int_0^\infty \frac{\log R(w') - \log R(w)}{w'^2 - w^2}\,dw' \qquad (2.46)$$

where ρ designates the Cauchy principal part of the integral and w is the angular frequency.

The change in $\psi(w)$ brought about by the effect of the modulating parameter is given by (Cardona 1969)

$$\Delta\psi(w) = \frac{w}{\pi}\rho\int_0^\infty \frac{\frac{\Delta R(w')}{R(w')} - \frac{\Delta R(w)}{R(w)}}{(w'^2 - w^2)}\,dw' \qquad (2.47)$$

where $\Delta R(w)/R(w)$ is the modulation measured. The evaluation of $\Delta\varepsilon_1$ and $\Delta\varepsilon_2$ was carried out using a C.D.C. 6600 computer, the program being written in Fortran IV language. A schematic diagram of the program is shown in Figure (2.4) and a complete listing is given in Appendix 2. Optical constants derived by other workers were read into the program and a linear interpolation scheme was used to associate optical constants with the photon energy of each $\Delta R/R$ data point from the thermoreflectance experiment. To perform the integral in equation (2.47) a library subroutine Q.S.F. was called. This routine performs the integration of an equidistantly tabulated function using Simpson's Rule and Newton's 3/8th rule. Clearly, difficulties arise in evaluating equation (2.47) since the integral extends over all frequencies and because we only have an incomplete knowledge of the modulated reflectance spectrum, $\Delta R/R$ has to be extrapolated. However, Cardona (1969) has pointed out that due to the sharpness of the $\Delta R/R$ lines found in modulated reflectance spectra, contributions of the extrapolated region to $\Delta\psi$ are non-singular. To evaluate equation (2.47) a constant extrapolation was used beyond the end points of the experimental data. The program then calculated the coefficients α,β,γ and δ in equations (2.16) and (2.22) and finally $\Delta\varepsilon_1$ and $\Delta\varepsilon_2$.

As discussed above, to extract $\Delta\varepsilon_1$ and $\Delta\varepsilon_2$ from $\Delta R/R$ a knowledge of the optical constants of the material is required. At this point it should be mentioned that optical constants determined by different workers are not generally in good agreement. Figure (2.5a) gives an indication of the effects of different optical constants on $\Delta\varepsilon_2$. The experimental data were those for the thermally modulated reflectance spectra of a gold film at 107K, the measurements being taken at an angle of incidence $\theta_o = 45^\circ$ with light polarized parallel to the plane of incidence. The optical constants used were those of Pells and Shiga (1969) and Johnson and Christy (1972). We see that the positions of structure in the $\Delta\varepsilon_2$ spectra are unchanged, the only difference being that the use of Pells and Shiga's optical constants result in slightly larger $\Delta\varepsilon_2$ values than those using Johnson and Christy's constants. Similarly, 10% errors in $\Delta R_p/R_p$ and θ_o (see Figure 2.5b) do not affect the spectral positions of structure in $\Delta\varepsilon_2$.

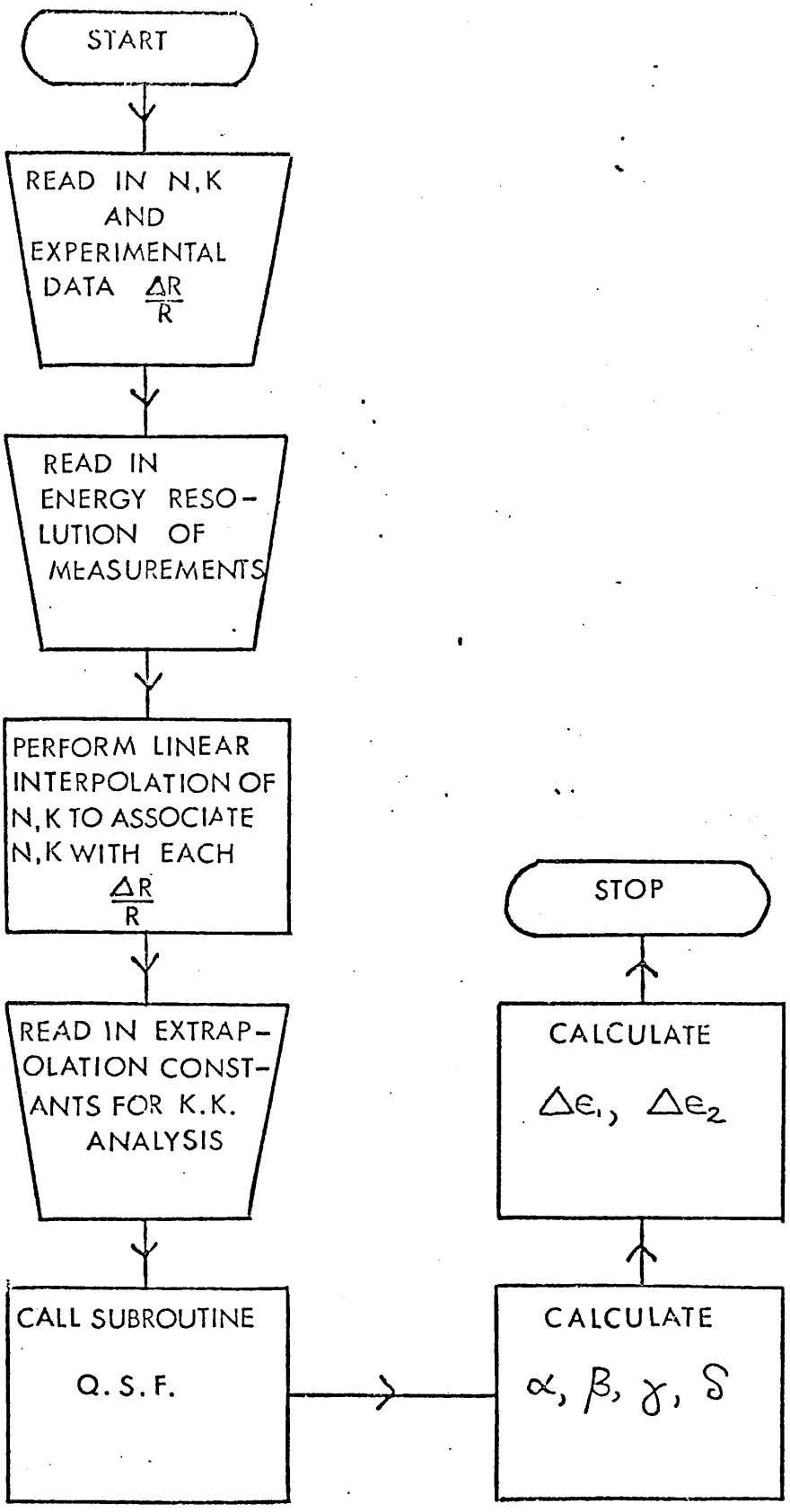

Figure (2.4) Flow diagram of the computer program used in the Kramers Kronig analysis.

Figure (2.5a) The $\Delta\varepsilon_2$ spectra of gold computed using different n and k data.

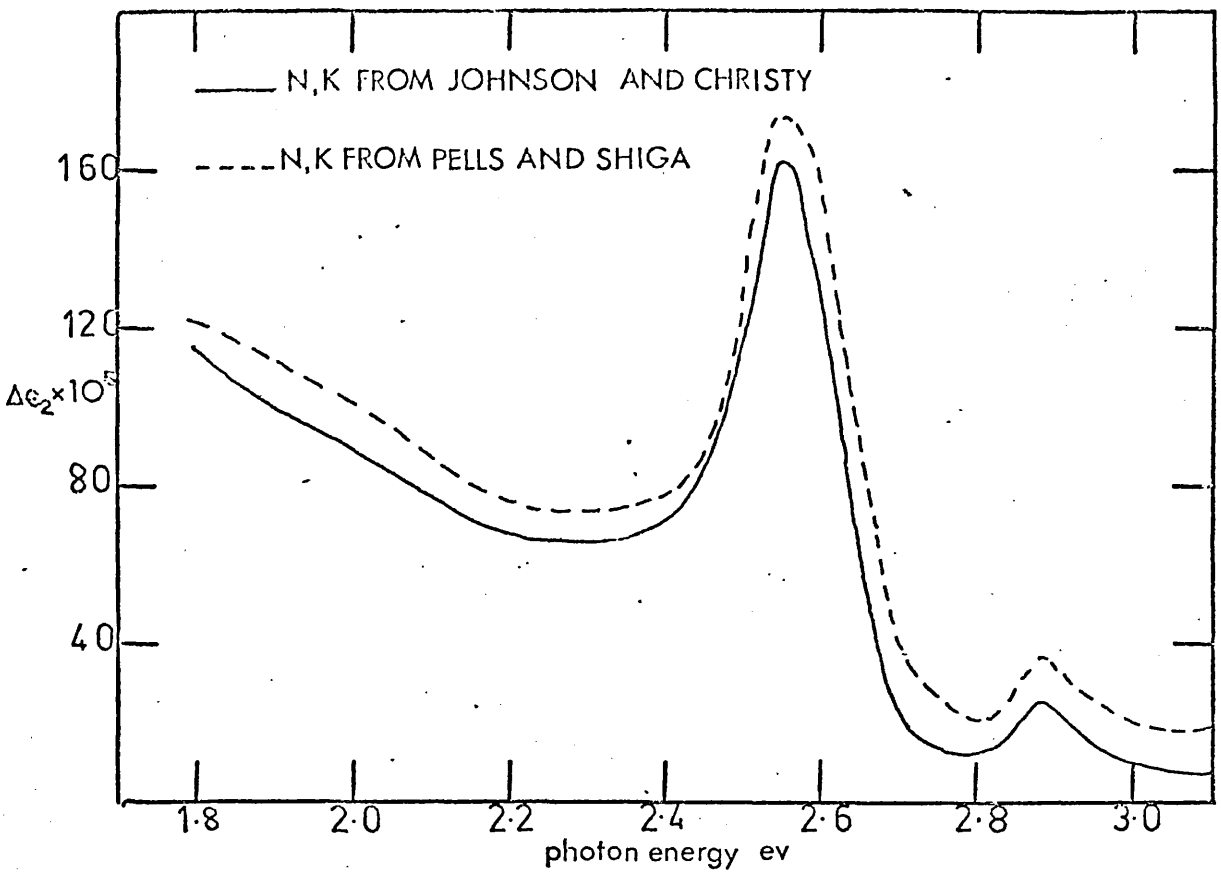

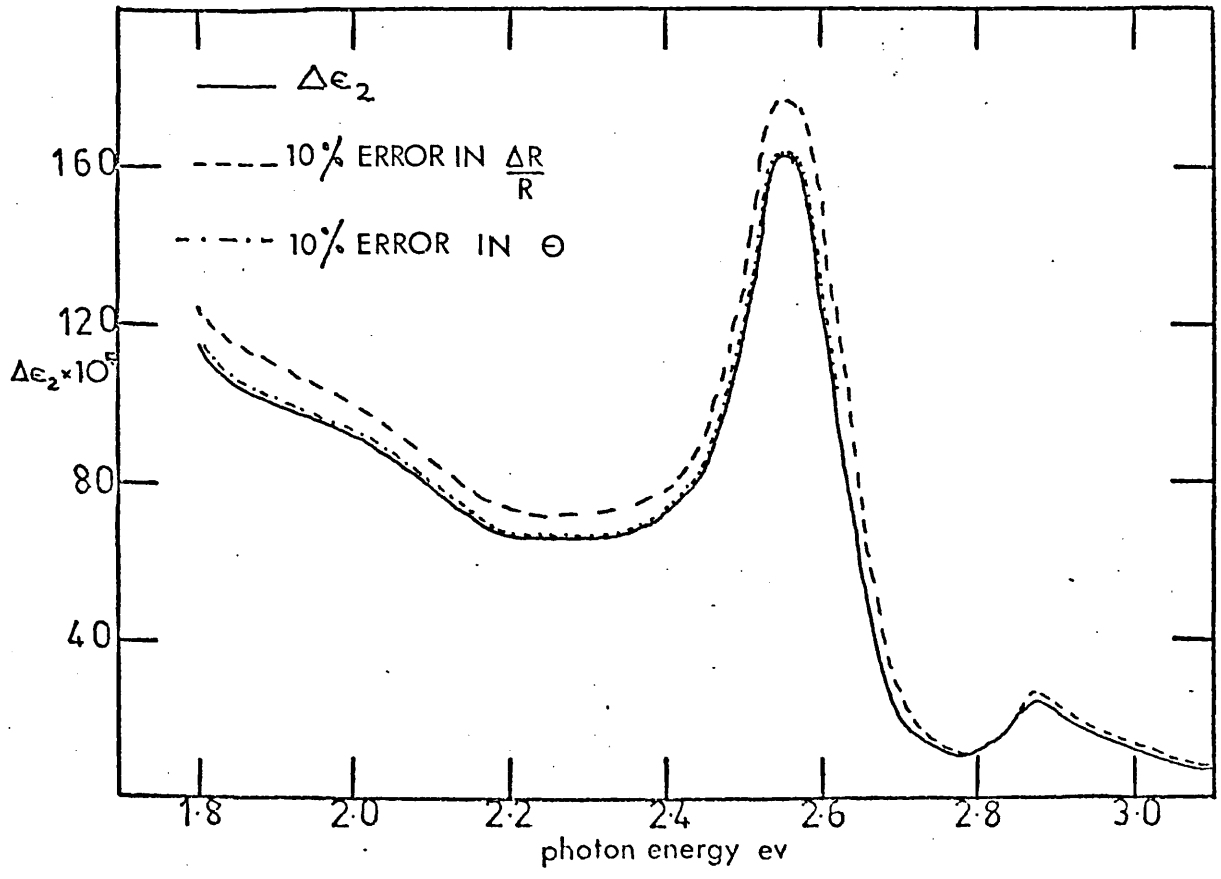

Figure (2.5b) The effect of errors in $(\Delta R/R)$ and θ on the $\Delta\varepsilon_2$ response.

An attempt was made to analyse the thermally modulated reflectance data other than by the Kramers-Kronig method. Measurements were taken at two angles of incidence $\theta_o = 0^o$ and 45^o and $\Delta R_p/R_p$ measured at both angles. Equation (2.16) was then solved for $\Delta\varepsilon_1$ and $\Delta\varepsilon_2$. This method has the advantage that no extrapolation procedures are required as in the Kramers-Kronig method. However the resulting $\Delta\varepsilon_2$ analysis indicated that the two equations were probably ill conditioned at these two angles. A computer simulation of errors in $(\Delta R_p/R_p)$ showed that only a 1% error in the magnitude of $(\Delta R_p/R_p)$ would result in a 30% error in $\Delta\varepsilon_2$. This is to be compared with a 1% error in $\Delta\varepsilon_2$ using the Kramers-Kronig method of analysis. For this reason all the thermally modulated reflectance analysis was undertaken using the Kramers-Kronig method.

CHAPTER III

The experimental system for the study of the thermally modulated reflectance of thick absorbing films

(3.1) Introduction

The principles and advantages of thermal modulation spectroscopy have been described in detail in Chapter I. Thermal modulation is usually achieved by passing a modulating electric current along a relatively thin sample which is mounted on a heat sink (Batz 1966, Scouler 1967). A periodic fluctuation in temperature is induced in the sample and the resultant changes in the reflectance ΔR (thermoreflectance) or the transmittance ΔT (thermoabsorption) are measured. In the present work thermoreflectance was chosen as the basis of study in preference to thermoabsorption for two reasons:-

(i) Thermoabsorption measurements require a semi-transparent film. This has the disadvantage of introducing an additional error of measurement, that of the film thickness, into the calculation of $\Delta\varepsilon_1$ and $\Delta\varepsilon_2$. The effect of multiple reflections needs to be taken into account in the analysis. Moreover, thinner films ($\sim$ 400 Å) are required whose properties are more likely to deviate from those of the bulk material.

(ii) One group of materials to be studied using this system was the heavy rare earth metals (gadolinium terbium, dysprosium, holmium and erbium). Rahman-Khan (private communication) has indicated that in both ordinary high vacuum (O.H.V.$\sim 10^{-6}$ torr) and ultra high vacuum (U.H.V.$\sim 10^{-10}$ torr) environments, thin evaporated films of these metals nucleate initially as the dihydride. It is not until a film reaches a thickness of > 1000 Å that its composition is predominantly that of the metal.

(3.2) Modulation efficiency

Cardona (1969) has indicated that a greater thermal modulation efficiency may be obtained if a square wave current is pulsed to the sample rather than a sine wave. Assuming that the temperature of the sample is uniform and that the increase in the average temperature of the sample $\langle T \rangle$ above that of the heat sink T_o is much larger than the amplitude ΔT of the temperature modulation, the modulation efficiency γ may be defined as the ratio

$$\Delta T/(\langle T \rangle - T_o) = \gamma \qquad (3.1)$$

then it may be shown (Cardona 1969 p.123)

$$\gamma(\Omega)_{\text{square wave}} = 4Q\tau/\pi^2 C = 0.405Q\tau/C \qquad (3.2)$$

$$\gamma(\Omega)_{\text{sine wave}} = Q\tau/2^{\frac{1}{2}}\pi C = 0.22Q\tau/C \qquad (3.3)$$

$$\gamma(2\Omega)_{\text{sine wave}} = 0.08Q\tau/C \qquad (3.4)$$

where C = the heat capacity of the sample

Q = the heat loss from sample to the sink per unit time and unit temperature difference $(T-T_o)$ between sample and sink

τ = the periodicity of the current, and $\Omega = 2\pi/\tau$

From equations (3.2) and (3.3) we see that the efficiency of the modulation is almost a factor of two higher for square waves than for sine waves. Moreover the modulation efficiency is higher when working at the fundamental frequency rather than the 2nd harmonic. The efficiency also decreases as the frequency of the modulation increases. For large γ the heat capacity C of the sample must be kept small and the heat leak Q large. However Cardona (1969) has shown that the maximum permissible value of Q in equation (3.3) is given by:

$$Q_{max} = K/d \qquad (3.5)$$

where K = the thermal conductivity of the sample

d = the thickness of the sample.

Clearly, to obtain as large an efficiency as possible a thin sample is required. This is therefore one of the techniques for which a thin film specimen configuration is highly suitable (we take films of thickness $< 1\ \mu m$ as a working definition of "thin film" in this case).

(3.3) Detection System

Although in any modulation experiment the modulating parameter induces changes in the optical constants of the specimen which in principle may be detected in a variety of ways e.g. changes in absorption or transmittance, the most commonly measured experimental quantities are the change in transmittance ΔT (if the sample is transparent) or the reflectance ΔR. Modulated ellipsometric experiments have been undertaken (Buckman and Bashara 1968) where $\Delta\psi$ and $\Delta\chi$ are measured (ψ and χ relate the state of polarization of an obliquely reflected light beam to that of the incident beam). One of the main advantages of static ellipsometric experiments over static reflectance experiments is that ε_1 and ε_2, the real and imaginary parts of the dielectric constant respectively, may be derived from measurements of ψ and χ at one angle of incidence at one photon energy. Modulated ellipsometric measurements share this advantage with static measurements. However it has been shown (Roberts 1963) that static ellipsometric measurements are extremely sensitive to variations in the surface condition of the sample. It is to be expected that modulated ellipsometry measurements will hardly be less sensitive to surface conditions. Great accuracy and sensitivity may be achieved if ΔR (or ΔT) are measured by means of phase sensitive detection (the modulation must be synchronous with its cause). High sensitivity is desirable since an accurate measurement

of the derivative requires a modulation amplitude as small as possible (Cardona 1969). Cardona also shows that the amplitude of the reflectance modulation at the fundamental frequency equals (dR/dw) only for small modulation amplitudes, a correction proportional to the third derivative of R appearing for higher amplitudes.

A schematic diagram of the detection system used in the present experiment is shown in Figure (3.1). An E.M.I. 9659 QB (extended S20 photocathode) photomultiplier was used to detect the reflected light intensity. The specified quantum efficiency of this tube is 19% at 4000 Å, falling to 1% at 9000 Å. The dynode chain was designed to give a linear high gain in accordance with recommendations in the E.M.I. handbook. The tube was electrically and magnetically shielded by two coaxial mu-metal shields. The output of the tube was split into two channels: a d.c. channel with a signal proportional to I_oR (the reflected light intensity) and an a.c. channel proportional to $I_o\Delta R$ (the change in the reflected light intensity induced by the modulating parameter). These two channels were separated: the d.c. channel was monitored by a Dymar voltmeter and the a.c. channel was sent to a lock-in amplifier (Ortec Brookdeal 9501). The d.c. output of the lock-in amplifier was monitored by a chart recorder (Type Panax Servoscribe SPEC-2p). If the d.c. output of the lock-in amplifier is divided by the d.c. channel of the photomultiplier tube we have

$$I_o\Delta R/I_oR = \Delta R/R \qquad (3.6)$$

and thus the incident light intensity, one of the main sources of error in conventional static reflectance experiments, is eliminated from the measurement and problems of light source instability are largely avoided. The ratio $\Delta R/R$ may be obtained in several ways: one method is to run the photomultiplier at constant gain and obtain the ratio $\Delta R/R$ electronically. However, this mode of operation requires that the spectral response of the detector be linear over the range of experimental interest - which was not

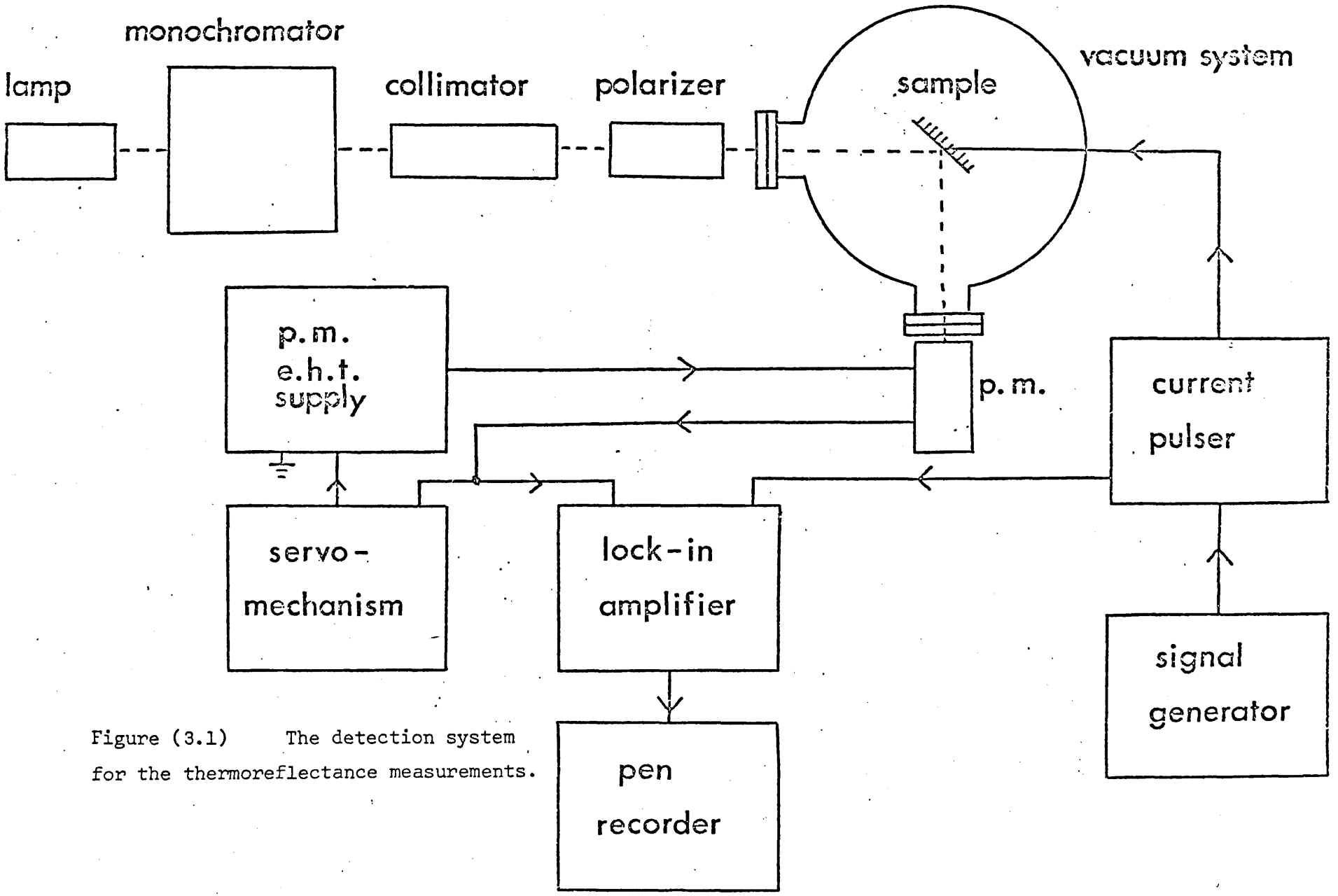

Figure (3.1) The detection system for the thermoreflectance measurements.

possible in this case. The actual method used was to keep the d.c. component of the photomultiplier signal (which corresponds to $I_o R$) constant at 1 volt over the spectral range scanned, (1.5 to 3.2 eV), by controlling the gain of the photomultiplier. This was achieved by means of a servo-mechanism which varied the voltage on the photomultiplier e.h.t. supply. As the d.c. component is constrained to be constant then the a.c. component is directly proportional to $\Delta R/R$. A safety trip was built into the servo-mechanism unit so that if the lamp failed or the specimen was broken, deflecting the reflected beam away from the photomultiplier, during the course of the experiment, the servo would not increase the e.h.t. voltage above the photomultiplier tube's specified maximum operating voltage. An upper limit of 750 volts was fixed for the e.h.t. supply well within the photomultiplier tube's specifications. Voltages greater than 750 volts increased the noise in the detection system to such an extent that repeatable results could not be obtained. A schematic diagram of the various components of the servo-mechanism is shown in Figure (3.2) and the circuits for the servo-amplifier and the e.h.t. monitor (trip mechanism) are given in Figure (3.3). The servo-amplifier comprised of a buffer stage which matched the high output impedance of the photomultiplier with the low input impedance of the voltage amplifier. The voltage amplifier increased the 1 volt output of the photomultiplier to 83 volts, the line voltage of the e.h.t. supply. The e.h.t. monitor utilized a Schmidt trigger which operated a relay inside the e.h.t. supply such that when 750 volts was reached the e.h.t. supply was cut off.

(3.4) Source Optics

The light source was a 100 watt quartz halogen lamp, housed in a water cooled holder and was powered by a stabilized d.c. supply (Farnell type B30/20). The intensity drift of the lamp was found to be less than 1% per hour. The light was condensed and then passed through a grating monochromator

Figure (3.2) Schematic diagram of the servomechanism.

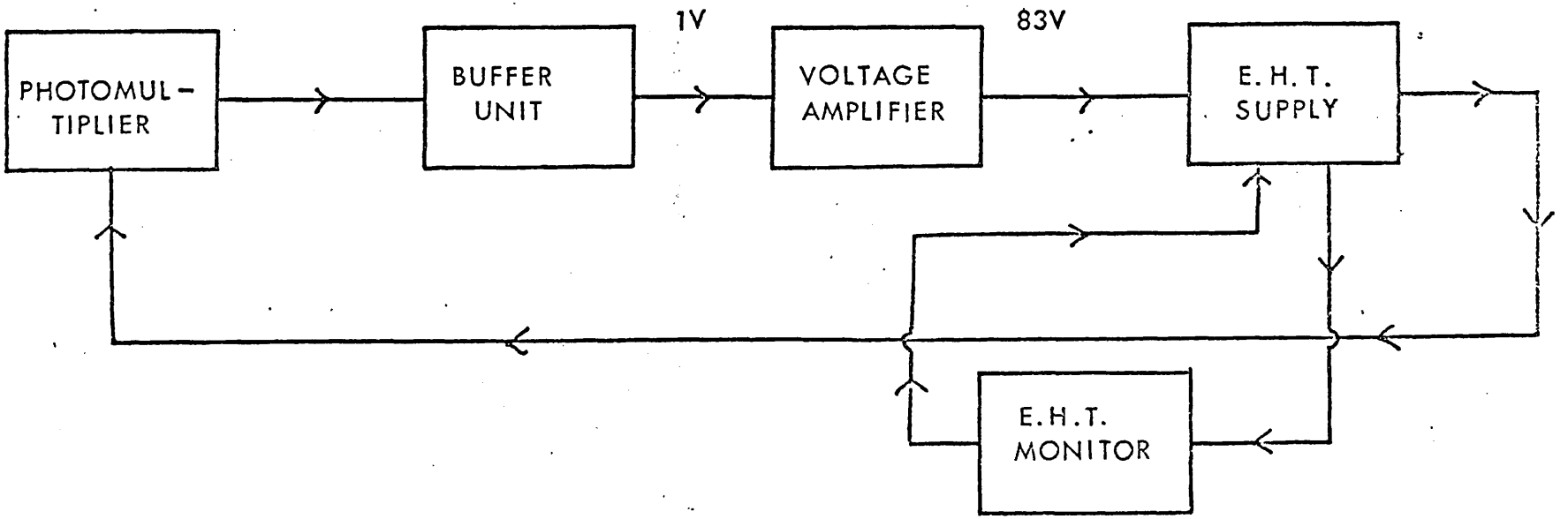

the servo amplifer circuit

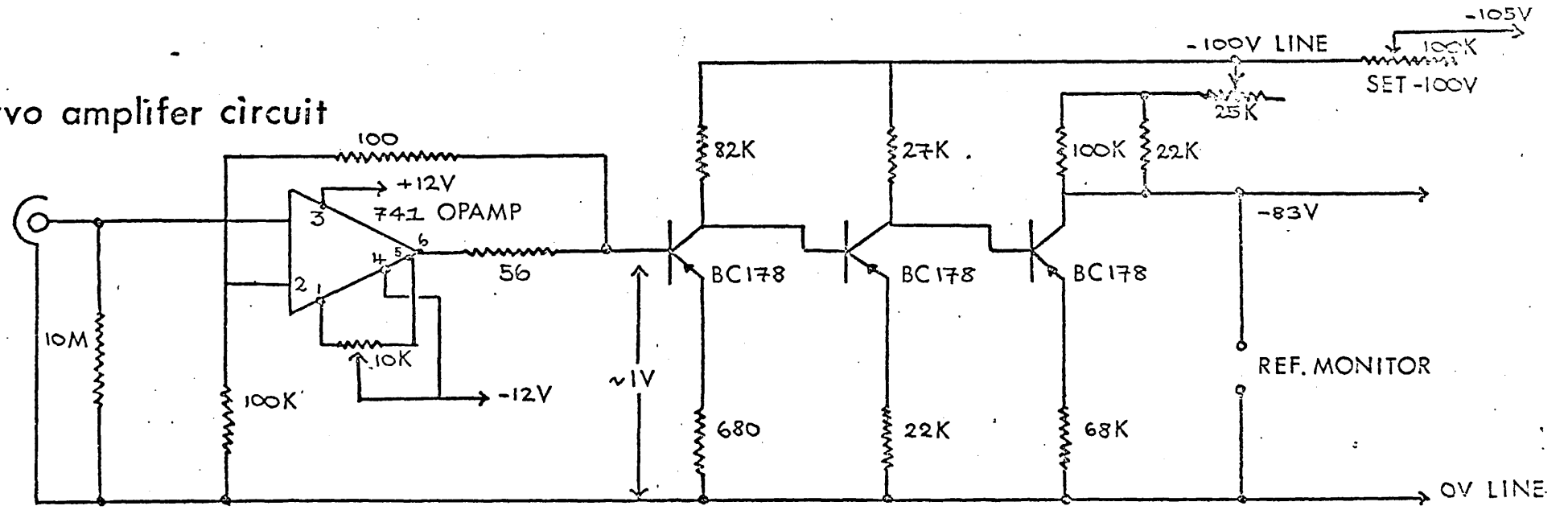

circuit for the e.h.t. monitor

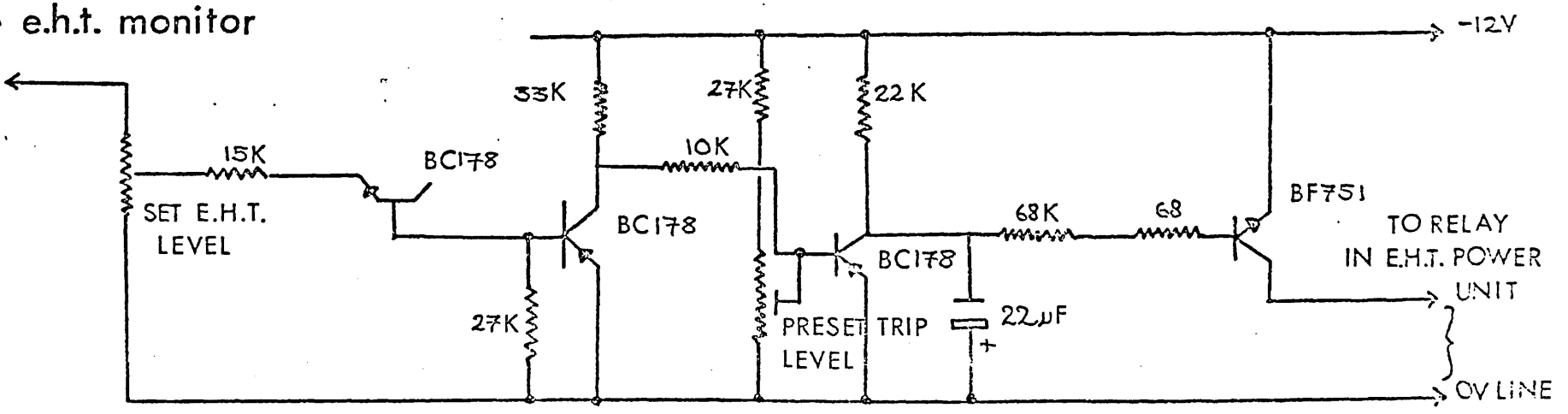

Figure (3.3) The servo-amplifier.

(Spex minimate) which, with slit widths of 0.5 mm gave a mean resolution of 0.004 eV over the spectral range 1.5 to 3.2 eV. The emergent monochromatic light was then collimated by means of an achromatic doublet of focal length 17 cm. For convenience of experimental layout, the light was reflected from the sample at an angle of incidence of 45°. A preliminary investigation had indicated that the sensitivity of the system was not strongly dependent on angle of incidence (see (2.3)). For measurements taken at oblique incidence the light was plane polarized using a Glan Thompson prism fitted with a small circular aperture of diameter 5mm. For reasons discussed in (2.3), measurements at oblique incidence were taken with light polarized parallel to the plane of incidence. Some initial measurements were taken with polaroid sheet as the polarizer, but the absorption edge for this material, starting at 4100 Å, caused the signal to noise ratio of the system to deteriorate rapidly, and repeatable results could not be achieved below this wavelength. All measurements were therefore taken with the Glan Thompson polarizer which allowed measurements to be taken down to λ = 3500 Å. The lower limit of detection was determined by the quartz halogen lamp which has a cut off at $\sim$ 3500 Å and the upper limit of the detection was determined by the response of the photomultiplier. Some measurements were taken at near normal incidence: to achieve this, two plane aluminium mirrors were mounted in the vacuum system in the configuration shown in Figure (3.4).

The monochromator wavelength scan was driven by a bi-directional electric motor, the speed of which was fixed at 1 rev/6 mins. The time taken for a typical experiment to be performed, scanning from 8500 to 3500 Å was $2\frac{1}{2}$ hours. All the optical components were mounted on an optical bench which was itself bolted to a wooden bench supported by two concrete pillars. The position of the optical bench could be adjusted in any direction. A light-tight tube enclosed all the optical components, one end being bolted to the input port of the stainless steel bell jar on the vacuum system, the other being fixed at the exit of the monochromator.

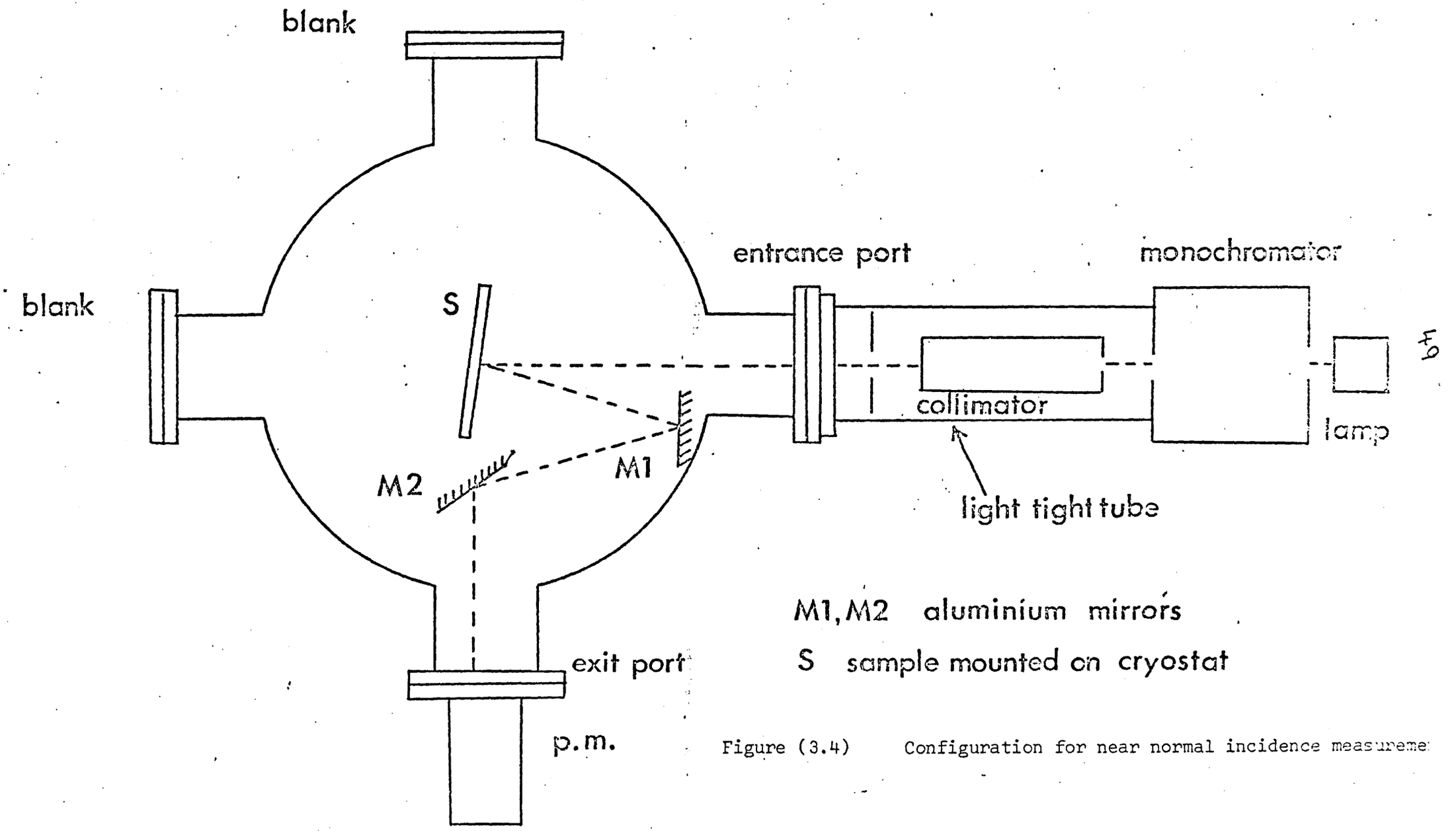

Figure (3.4) Configuration for near normal incidence measureme

(3.5) The Vacuum system

Most of the thermoreflectance experiments were performed in an ordinary high vacuum environment ($\sim 10^{-7}$ torr). Initial experiments were conducted in an optical cell arrangement previously used for static reflectance measurements and described in detail by Hasan (Ph.D thesis 1975). The system consisted of a 10 cm high 11 cm diameter cylinder of Spectrosil A of wall thickness 2mm coaxially positioned on a 15 cm diameter dural plate. The plate was inset with an 11 cm diameter "O" ring seal. A 12 cm diameter dural plate inset with an "O" ring seal rested on the top of the quartz cylinder. The unit was fixed to the centre of a spectrometer table and could be rotated through 360 degrees. The spectrometer telescope was removed and replaced by a photomultiplier (9659 QB). The system thus allowed modulated reflectance measurements to be made at oblique incidence. The sample was positioned on a cryostat, of similar design to that shown in Plate (3.2) and was fixed to the top dural plate. A 4-way low current feedthrough was inserted into the top dural plate so that power could be fed to the sample and its temperature monitored. The whole unit could be evacuated to a pressure of $\sim$ 0.005 torr by a rotary pump. However, it was found that low temperature measurements ($\sim$ 77K) could not be made using this arrangement because, on lowering the temperature of the sample, the residual water vapour present in the system condensed onto the surface of the sample. This caused rapid deterioriation in the detected signal, and eventual loss of electrical contact to the film, resulting in total loss of signal. Drying agents such as phosphorus pentoxide and silica gel failed to trap the excess water vapour satisfactorily at low temperatures. Preliminary measurements were however, made on gold films in this system at room temperature wherethe condensation of water vapour was not a problem. We were able to experimentally confirm the theoretical prediction (see (2.3)) that the modulation response was not strongly dependent on angle of incidence, and also that the thermally modulated reflectance data ($\Delta R_p/R_p$) obtained

using light polarized parallel to the plane of incidence became larger than the data ($\Delta R_s/R_s$) obtained with light polarized perpendicular to the plane of incidence as the angle of incidence was increased. This behaviour is shown in Figure (3.5).

The high vacuum system employed an Edwards E04 600 litres/sec. diffusion pump with Edwards Santo-vac 5 (polyphenyl ether) in place of a conventional silicone oil. This oil has less tendency to creep and hence hydrocarbon contamination in the main chamber is reduced. The diffusion pump was backed by an Edwards ED200 rotary pump. The ultimate vacuum achieved by this pump alone was 0.001 torr, measured by a Pirani gauge (Edwards Model). The diffusion pump backed by the rotary pump reduced the pressure in the chamber to 10^{-6} torr as measured by a Penning ionization gauge. A stainless steel cold trap situated above the diffusion pump and below the flap value to the main service chamber further reduced the pressure to an ultimate of 4×10^{-7} torr.

The chamber consisted of a 12" stainless steel bell jar sealed to the base plate by an L shaped viton gasket. Although the chamber had 5 viewing ports only two of these were used, the rest being blanked off. Windows made of Spectrosil B were sealed to the two operational ports with "O" ring seals. One of the windows acted as the entrance port for the light beam and the other the exit port, the photomultiplier being mounted on the latter. The vacuum system together with the source optics are shown in Plate (3.1).

(3.6) The Cryostat

A cryostat was constructed to allow low temperature ($\sim$ 77K) measurements, and also to act as a heat sink for the sample. The cryostat, with a sample in place, is shown in Plate (3.2). The unit was manufactured entirely from stainless steel and consisted of a cylindrical tube 17 cm long and 2cm in diameter, welded to a cylindrical reservoir 5 cm long and 4.5 cm in diameter.

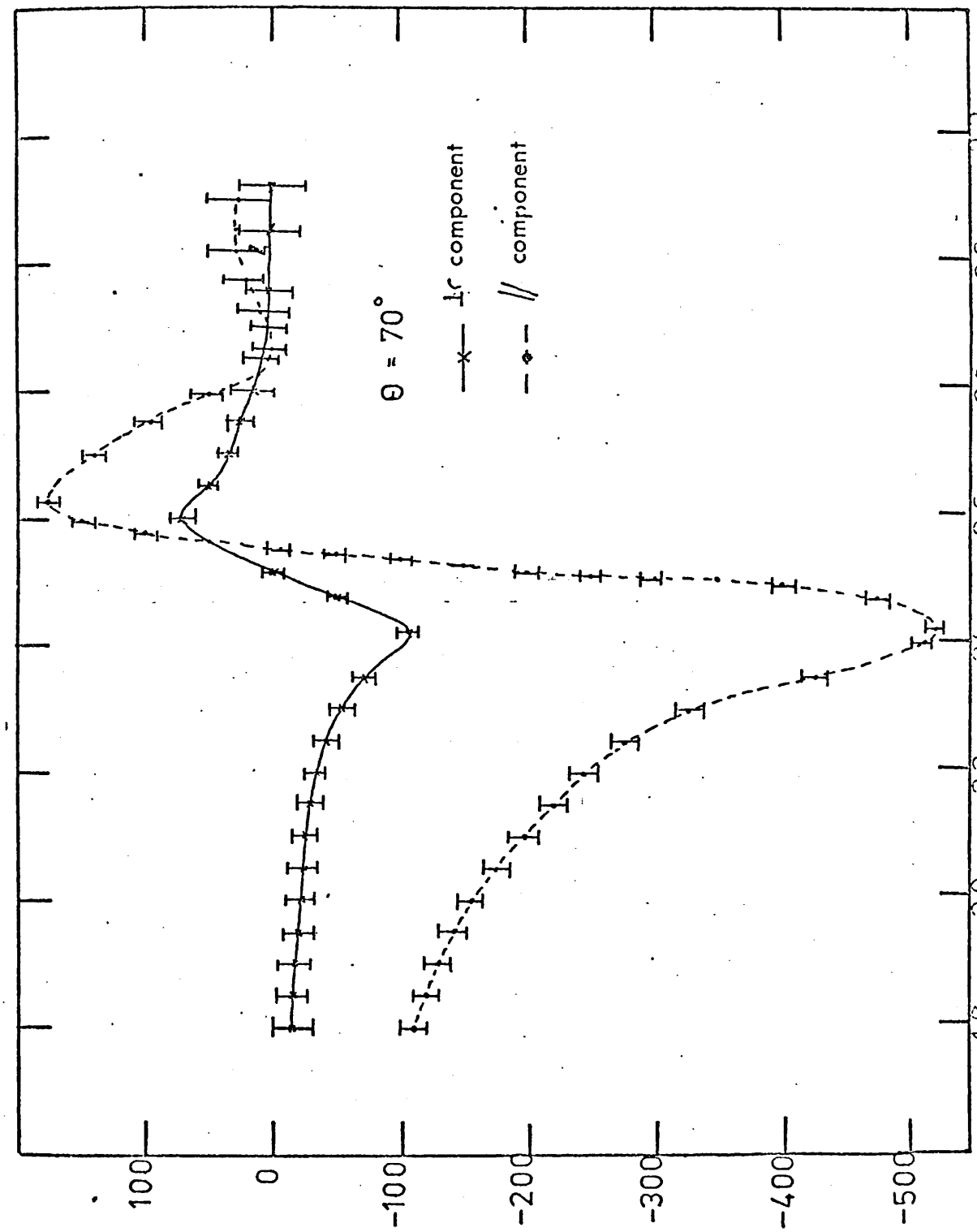

FIGURE (3·5) The thermally modulated reflectance responses of a gold film at Θ = 70°

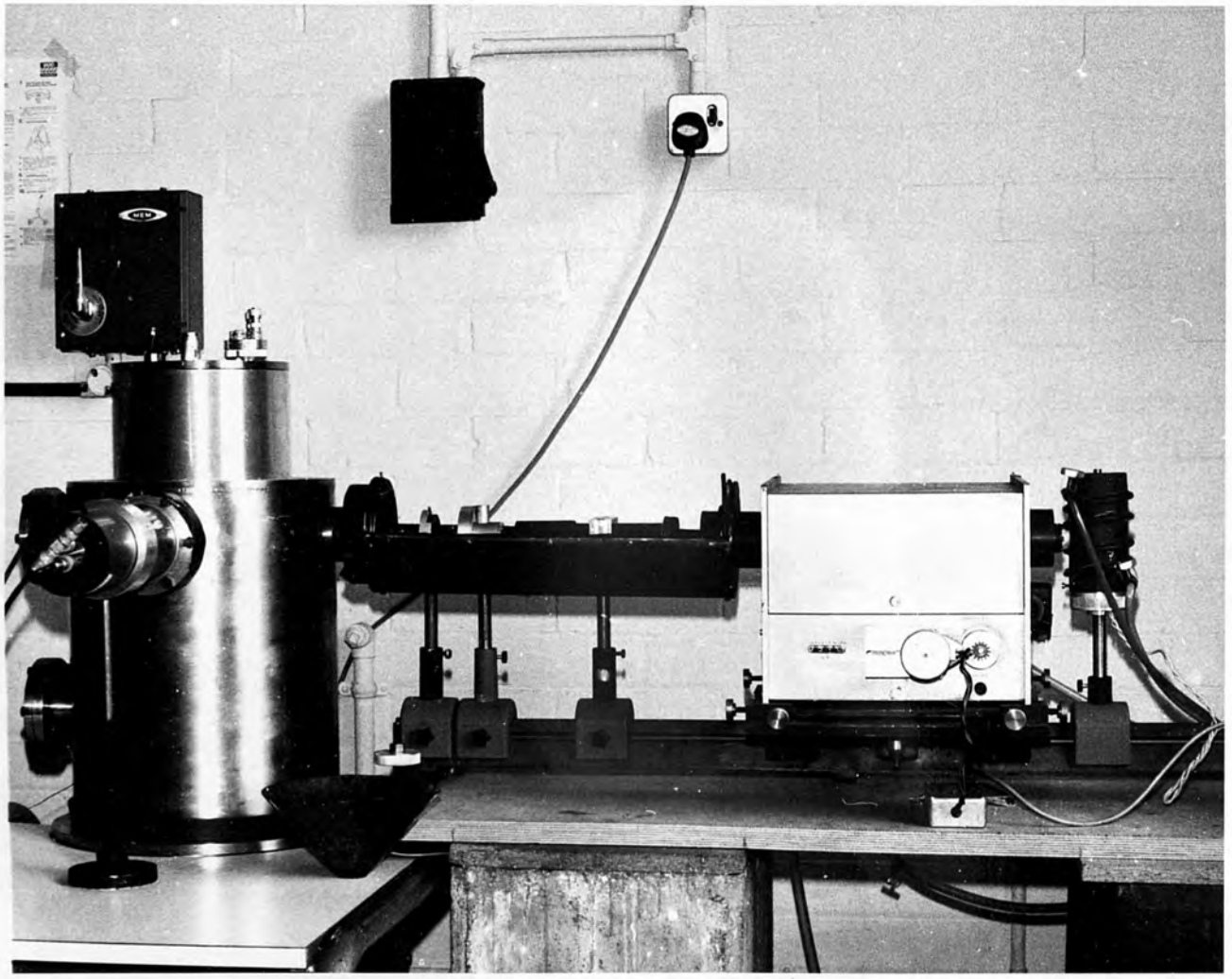

RS
RS

The front face of the reservoir was inset by 2mm to allow a glass microscope slide to rest on it. The slide was held in place by two nylon screws which were set into a copper ring fixed to the front face of the reservoir. To ensure good thermal contact between specimen and cryostat, the front face of the unit was highly polished. Thermal contact was further improved by an intervening layer of vacuum grease between sample and cryostat. The whole unit was positioned onto a 20 cm diameter x 0.8 cm thick stainless steel plate with a gold wire seal. A high current feedthrough and a 4-way low current feedthrough were inserted into the top of the plate so that power could be fed to the sample and the specimen temperature could be monitored. The plate plus cryostat could then be positioned on top of the stainless steel chamber where it was sealed with an "O" ring. For measurements at room temperature, cold water was pumped through the cryostat to dissipate the heat generated by the passage of current through the sample.

(3.7) Specimen geometry and electrical connections

Initially, experiments were undertaken with films deposited on glass cover slips of thickness 0.02 cm. Glass substrates were chosen because of their surface smoothness and because films deposited thereon are specularly reflective. To compensate for the effects of the low thermal conductivity of glass, thin substrates were required. However it was found to be extremely difficult to hold the cover slips on the cryostat. If the nylon screws were screwed too tightly the sample cracked as soon as the current was pulsed through the film. Releasing the screw pressure reduced the thermal contact between sample and heat sink, but nevertheless a thermal modulation response was detected. However, on the majority of specimens the response was masked by a constant signal which was wavelength independent and was above 5 times the magnitude of $(\Delta R/R)$. Close inspection of the system revealed that the spurious signal was caused by the substrate flexing when the current was pulsed through the film. Although the thermal modulation signal could be recovered by using the zero offset of the lock-in

amplifier, it was better to avoid these difficulties by using films grown on thicker substrates i.e. float glass microscope slides 0.2 cm thick. The films were rectangular, 7.5 cm x 0.5 cm, and were typically between 1000 and 2000 Å thick. Growth conditions are fully described in Chapter IV.

Electrical power was passed into the sample in the form of a square wave at 15 Hz. This signal was used also as a reference for the lock-in amplifier which detected variations, ΔR, in the reflectance, at the reference frequency. The resulting thermally modulated reflectance was detected at the fundamental frequency by adding a d.c. bias to the square wave. Currents of 1 to 6 amps were passed into the sample from a power amplifier driven by an audio frequency signal generator (Advance type H1B). Two such power amplifiers were used in the course of the experiment, one having an output impedance of $\sim 2\Omega$, for use with films of the noble metals, and the other having an impedance of $\sim 100\Omega$, for use with films of the heavy rare earth metals. Whenever possible, electrical leads were indium soldered to the films. However, with the rare earth films the solder would not take and it was thought probable that an oxide coating was formed due to the heat of the soldering iron. Contact was made to these films by applying a layer of high conductivity silver paint (Acheson Dag 1950) to the ends of the film and then clipping a piece of copper shim to the substrate.

(3.8) Modification of the detection system for the study of the characteristics of the integrated thin film optical modulator

The detection system described above for the measurement of the thermally modulated reflectance spectra of thick absorbing films was used, with a few minor modifications, to study the characteristics of the integrated thin film optical modulator. The collimator was removed and replaced by a + 25D lens which focussed the monochromatic light onto the sample. The device was held in a jig designed to allow good electrical contact to be made to the specimen and also to allow light to be transmitted through the

system. The sample configuration is fully described in Chapter IV. All devices were deposited on float glass substrates 2.5 x 2.5 x 0.3 cm. The sample holder shown in Plate (3.3) consisted of a 7.5 cm diameter and 1.5 cm thick perspex disc. Inset into the surface of the disc were four brass studs (A,B,C,D) to which electrical contact was made by means of screws passing through the disc to the studs. The sample rested electrode side onto the studs. A dural disc of the same diameter as the perspex disc was located onto the perspex base by four brass pillars. Four wing nuts held the dural down, pressing the specimen against the brass studs and an "O" ring seal inset into the face of the dural cushioned the sample. Electrical contact could be made to the specimen by points E,F,G,H. A 2mm diameter aperture was drilled through the dural and perspex discs, allowing light to be transmitted through the specimen.

The photomultiplier was located directly behind the specimen holder. All measurments were made in transmission at normal incidence and in air at room temperature. The current pulser used in the thermoreflectance experiments was removed and the signal generator (Advance type H1B) produced the electric field across the specimen. In some of the work the lock-in amplifier was bypassed and the modulated signal ($\Delta T/T$) was monitored directly across the anode load resistor of the photomultiplier and displayed on a Tetronix 454 oscilloscope.

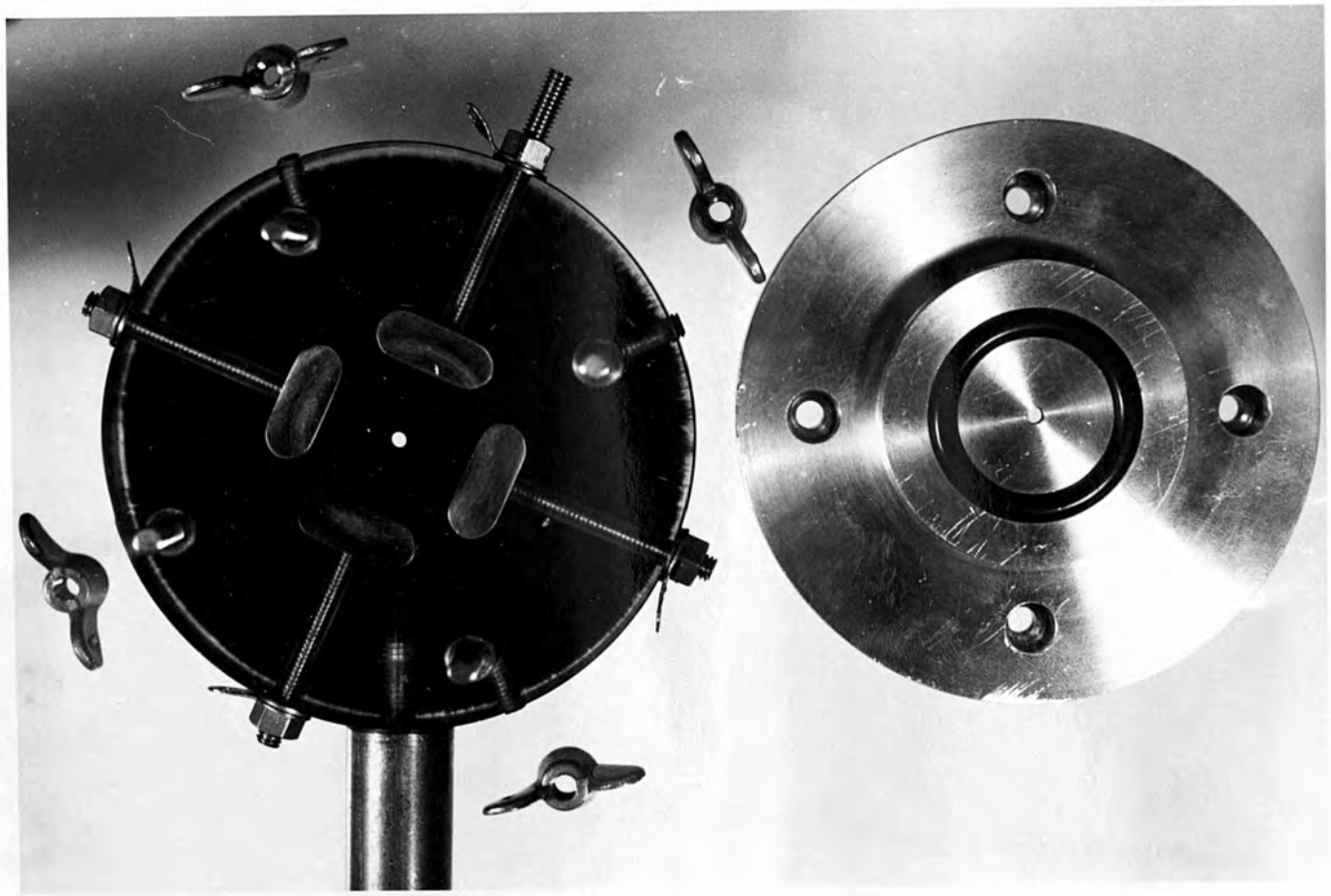

CHAPTER IV

Sample preparation in ordinary high vacuum and ultra high vacuum

4.1 Introduction

In the present work metal, dielectric and semiconducting films have been grown. Opaque metal films were required for the thermoreflectance measurements and a combination of dielectric, semiconducting and semi-transparent metal films were needed in the integrated thin film optical modulator. Extensive reviews of the methods of deposition of thin solid films have been given by Holland (1966), Chopra (1969) and Campbell (1976). All the films used in the present work were prepared by thermal evaporation in either ordinary high vacuum (O.H.V. $\sim 10^{-6} \rightarrow 10^{-7}$ torr) or ultra high vacuum (U.H.V. $\sim 10^{-10}$ torr). Any study of the optical properties of a material requires the preparation of a surface free from contamination, and in particular, the high reactivity of some of the materials studied in this work made the method of thermal evaporation in a U.H.V. environment the most suitable. The structure and properties exhibited by materials in thin film form depends on an array of factors. Heavens (1970) has discussed the more important factors for films deposited by thermal evaporation and these are summarized below:

(i) Pressure and nature of the residual gas in the deposition chamber.

(ii) Temperature of the evaporation source.

(iii) Rate of deposition of the condensing atoms.

(iv) Temperature of the substrate.

(v) Nature of the substrate.

(vi) Contamination of evaporated materials by the supporting material of the source.

In the present work particular attention was paid to the following:

(a) Evaporation of reactive materials such as the heavy rare earths was carried out in ultra high vacuum in which the residual gas composition was monitored with a mass spectrometer.

(b) In the deposition of the semiconducting and dielectric films careful control was kept on the temperature of the evaporation source, the temperature of the substrate and the rate of deposition of the condensing atoms. All these factors were found to have a profound effect on the structure and stoichiometry of the films.

(c) Rigorous cleaning procedures were adopted for the float glass substrates used. It was found particularly important, when depositing films of the rare earths, that the substrate was perfectly clean; otherwise a specularly reflective film was not produced.

4.2 The ultra high vacuum system

Films for the thermoreflectance study were prepared in both ordinary high vacuum and ultra high vacuum environments. A description of U.H.V. system together with details of its operation are now given. A schematic diagram of the pumping group is shown in Figure (4.1). The system comprised a 12" diameter stainless steel chamber which could be rough pumped by either an Edwards alumina-trapped rotary pump or by two sorption pumps. The latter did not ulitize silicone oils and if hydrocarbon contamination in the chamber was to be further minimized they were used. A Varian 140 litres/sec diode ion pump further reduced the pressure in the main chamber. A 4,000 litres/sec four element titanium sublimation pump situated below the stainless steel baffle further reduced the pressure in the system. Pumping action was achieved by sublimating titanium from the heated filaments onto the chamber walls and the liquid nitrogen-cooled reservoir base thus providing a film of titanium metal which was then available to getter gas molecules. The liquid nitrogen reservoir provided an appreciable extra

FIGURE (4·1) The U.H.V. pumping group

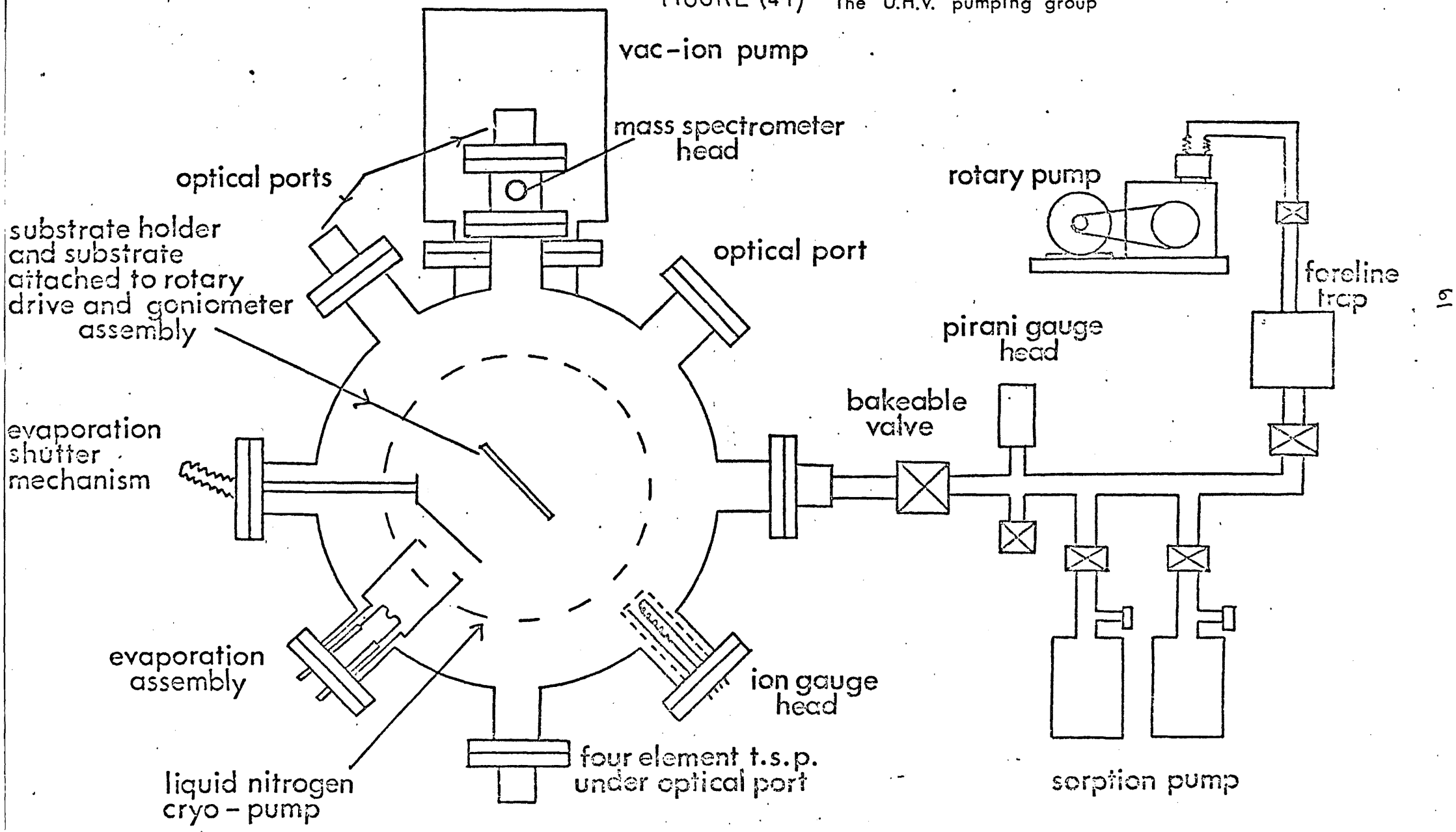

(cryogenic) pumping capacity for vapours which condense at liquid nitrogen temperature. The entire system could be baked at 250°C. Low pressure measurements in the system were made with a Bayard-Alpert gauge and residual gas analysis was made with a Spectramass 80 mass spectrometer.

The main service chamber had various optical ports used by other workers. Either copper con-flat gaskets or gold wire seals were used on all the ports. All flanges in contact with the gold wire seals were cleaned with fine grade emery cloth wetted with isopropyl alchol and distilled water. All tools used in the assembly of experiments to go in the chamber were ultrasonically cleaned with a degreasing agent (Decon 90) diluted with distilled water and then rinsed in distilled water. The materials used for structures in the chamber were made from stainless steel. All stainless steel components were first degreased by ultrasonic agitation in the degreasing agent and then a smooth surface produced by electropolishing in orthophosphoric acid. The components were then washed in distilled water.

Ultra high vacuum was achieved in the following manner: initially, the backing line, with the bakeable valve closed, was rough pumped by the rotary pump. The sorption pumps were then started, the rotary pump being isolated from them, and the bakeable valve to the main service chamber opened. The chamber was pumped by the sorption pumps until a pressure of 10^{-3} torr had been reached: at this stage the ion pump was started. A pressure of 10^{-6} torr was quickly attained with the main chamber isolated from the sorption pumps by the bakeable valve. The sorption pumps were then isolated from the backing line, which was pumped throughout the pumping cycle by the rotary pump. Once a pressure of 10^{-6} torr (indicated by the ion pump current) had been reached in the chamber the Bayard-Alpert gauge was outgassed by electron bombardment. The titanium sublimation pump filaments were also outgassed at this stage. The system was then baked at 250°C until a pressure of 5×10^{-8} torr was attained. The time needed to achieve the pressure depended critically on the cleanliness of the system and

how long the system had been up to atmospheric pressure before restarting. The system was always let up to atmospheric pressure with dry nitorgen and pumping was usually restarted within 2 hours. A 12- to 18- hour bake was usually required, but if the system was left at atmospheric pressure for longer than 3 hours it was found necessary to bake for longer periods ∿ 36 to 48 hours. After baking, the system was allowed to cool and the Bayard-Alpert gauge was again outgassed. The pressure after cooling was ∿ 5×10^{-9} torr. The titanium sublimation pump was then used for 12 hours in conjunction with the ion pump to reduce the pressure to 10^{-10} torr. At this stage liquid nitrogen was fed to the stainless steel baffle. Condensation of gases onto this baffle further reduced the pressure to 6×10^{-11} torr. Low pressure measurements ($< 10^{-10}$ torr) were made using the modulation facility on the Bayard-Alpert gauge.

4.3 The ordinary high vacuum systems

Thin films were produced in two O.H.V. systems, a Birvac T4150 and an Edwards 12EA/424. The basic features of these systems were similar to those of the system described in (3.5). The pumping chambers consisted of 12" diameter pyrex bell jars sealed to the stainless steel base plates of the systems by L shaped neoprene gaskets. The main service chambers could be initially evacuated by a rotary pump to a pressure of < C.005 torr. A water cooled diffusion pump backed by the rotary pump evacuated the Birvac T4150 plant to a pressure of 10^{-6} torr and the Edwards 12EA/424 to 2×10^{-5} torr. Both the systems had stainless steel cold traps situated below the flap valve of the main service chamber and above the diffusion pumps. With the cold traps in operation the ultimate pressure achieved by the Birvac system was ∿ 3×10^{-7} torr and by the Edwards system ∿ 7×10^{-6} torr. A Birvac Pirani and Penning gauge measured the pressure in the Birvac system. Pressures in the Edwards plant was measured by a philani gauge which combined a Pirani type gauge and a Philips type cold cathode ionization gauge.

Electrical feedthroughs passing through the base plates of the system provided electrical access to the apparatus. The filament holders were designed so that evaporations could take place using either boats or tungsten helical coil filaments. The evaporation filaments could be shielded from the substrate by means of a shutter activated from outside the chamber by a rotary shaft mechanism. All components in the main service chambers were manufactured from stainless steel. Three 15cm long stainless steel pillars screwed to the base plates of the system supported a circular gantry. Two adjustable rods were placed across a diameter of the gantry and the substrate could be positioned on these rods so as to be directly above the source.

Some of the dielectric films were deposited by electron bombardment, which used a Birvac RG2 ring gun. Material was evaporated using either carbon or cermet crucibles. The carbon crucible is particularly useful for evaporation of insulators because of its high thermal conductivity, which allows a uniform crucible temperature to be attained.

4.4 Filament preparation

The rare earth metals were evaporated from a tungsten filament.or, most often in the U.H.V. chamber, from a tantalum boat. The tantalum boat together with the filament holders is shown in Plate (4.1). It was found that a more easily controlled rate of evaporation, and better outgassing, could be accomplished with such a boat rather than a tungsten filament. The tungsten filaments were used for fast evaporations ($\sim$ 60 $\mathring{A}$ sec^{-1}) of the rare earths in O.H.V. The tungsten filament had an internal diameter of $\sim$ 2 mm and a length of 2.25 cm. The filament, without any charge material in place, was first outgassed at a pressure of better than 10^{-5} torr. The filament was held at red heat for approximately 10 minutes (the same procedure was adopted for outgassing the tantalum boat). A rod of material to be evaporated was inserted into the filament which was heated to high

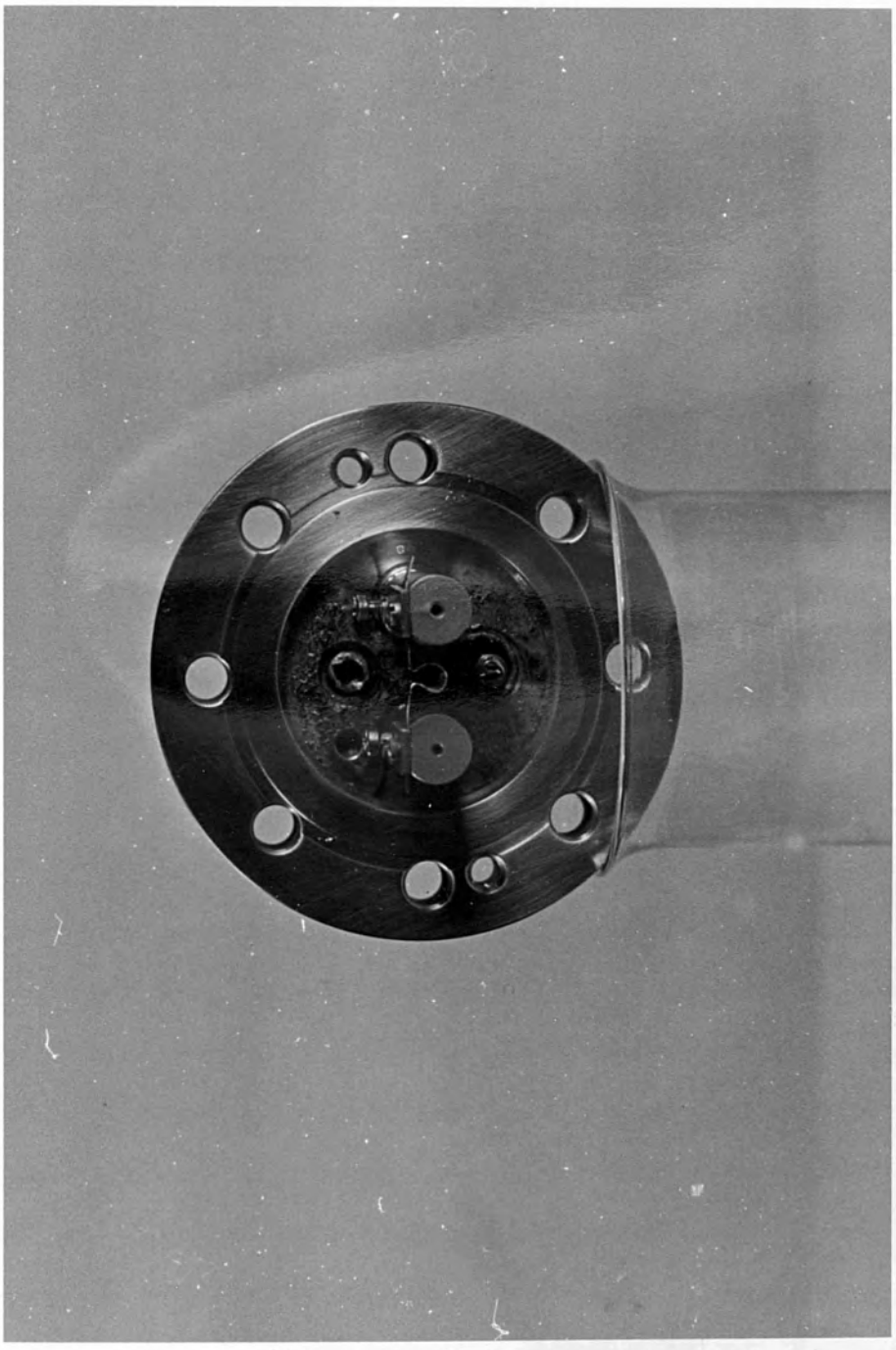

temperatures by Joule heating until the rod melted. The system was then let up to atmospheric pressure and more rods were inserted into the filament until globules of the evaporant prevented further packing. This operation was repeated (usually three times) until the filament was fully loaded. The charge was then held in the molten state for approximately 30 seconds. For the rare earth metals it was necessary, for reasons discussed in (3.1), to grow films > 1000 Å thick. However it was sometimes found that although globules of material prevented further packing, there was not enough material on the filament to be able to further outgas the filament in the U.H.V. chamber and still produce a film of > 1000 Å in thickness. For this reason and also to reduce the lengthy outgassing procedures, a tantalum boat was used. Since the stream of evaporant in the U.H.V. chamber was required to be horizontal, the type of boat geometry used was that described by Tolansky (1970) for evaporating silver horizontally. Tolansky stated that contamination from boat material is less likely with this geometry than conventional vertical evaporation from a boat since in the horizontal position the substrate is "seeing" a large area of charge material and only a very thin edge of the boat material. After initially outgassing the tantalum boat, 8 rods, ∿ 1 cm long, of the material to be evaporated were placed in the trough of the boat. In the order of 60 amps a.c. were passed through the boat until the charge melted. The vacuum system was allowed to achieve its base pressure and the boat again heated until the charge melted, the material being held in this molten state for one minute to complete the outgassing. Throughout the outgassing a microscope slide was fixed near the source so that any excessive loss of evaporant during the outgassing could be observed and prevented. The boats and filaments were kept under O.H.V. until they could be mounted in the U.H.V. system. In the case of evaporations taking place in the O.H.V. environment, after the molten stage had been reached and outgassing completed, the shutter was opened and the charge material was allowed to condense onto the substrate. Details of individual evaporation parameters are given in Chapter V, VI and VII.

4.5 Substrate Preparation

All the films whether for the thermoreflectance study or the production of the integrated thin film optical modulator were deposited onto float glass substrates. For use in the thermoreflectance measurements two microscope slides (75 x 25 x 1 mm^3) were selected for their general degree of cleanliness and freedom from scratches, and were initially cleaned with a lens tissue. The substrates were then clamped vertically in a beaker of degreasing agent (Decon 90), care being taken to ensure that the slides did not touch the sides of the beaker or each other. The slides were ultrasonically cleaned for 45 minutes after which the degreasing agent was displaced with distilled water and the slides rinsed for about 5 minutes. The substrates were then ultrasonically cleaned for a further 15 minutes in distilled water. The slides were removed from the distilled water and were allowed to dry in air, covered loosely by a lens tissue: dry nitrogen was blown across the slide surface to complete the drying.

For the thermoreflectance measurements, films were deposited having dimensions 75 x 5 mm^2. The substrate holders in both the O.H.V. and U.H.V. environments were made of stainless steel and could accommodate two substrates. Samples were prepared on two slides during each evaporation:one was used to investigate the film structure "as grown", by high energy reflection electron diffraction and the other was used as the optical specimen and then examined by electron diffraction after thermomodulation. The substrate holder in the U.H.V. chamber was fixed to the rotary drive and the mounting was constructed so that the front face of the substrate passed through the axis of rotation of the drive. The source-substrate distance was fixed at 18 cm. In the O.H.V. chamber the substrates and masks were positioned 8 cm directly above the filament.

4.6 The preparation of an integrated thin film optical modulator

As discussed in Chapter 1, the possiblity exists of applying one of the modulation techniques to produce a totally integrated thin film optical modulator. The use of integrated optics has been discussed by Miller (1969) and the fundamental elements used to build optical integrated circuits, for example, planar thin film waveguides and detectors have been extensively studied (Dakss 1970, Ulrich 1971, Taylor 1974). Electro-optic crystals (i.e. $LiNbO_3$) have been used as wide band optical modulators for communication purposes. The electro-optic effect may be defined generally as the dependence of the index of refraction of a material on the applied electric field. Typrically the refractive index of an optically active material changes by 1% on the application of electric fields $\sim 10^6$ Volts/metre. In most forms of electro-optic modulators the incident light beam is coupled to a material in thin film form acting as a waveguide and multiple reflections near the critical angle serve to enhance the modulation. There are however some important constraints on the capabilities of electro-optic modulators and these are summarized below:-

(i) The incident light has to be coupled to the waveguide and this requires additional optical coupling components i.e. coupling prisms.

(ii) The electro-optic modulator is necessarily cumbersome because of the long path length required to amplify the effect.

iii) The device is limited tc small apertures. Wemple and Didomenico (1972) have shown that the required voltage V_n sufficient to turn the light on is given by

$$V_n = (\lambda/n^3 r_c)(b/\ell) \qquad (4.1)$$

where λ is the wavelength of the incident light

n is the refractive index of the active medium

r_c is the electro-optic coefficient of the active material

b is the electrode spacing

ℓ is the device length.

Clearly, to reduce V_n the electrode spacing b must be decreased and the crystal length ℓ increased.

(iv) Wemple and Didomenico (1972) have also shown that the power needed to drive the modulator increases rapidly with increasing wavelength and is in fact a function of the cube of the wavelength.

In view of these disadvantages, an alternative design for an optical modulator is presented. As with electro-optic modulators the device utlizes modulation by an applied electric field but in this case we term the type of modulation as "absorption driven". Franz (1958) and Keldysh (1958) theoretically predicted that the absorption edge of a semiconductor or insulator should be moved to longer wavelengths on application of high electric fields $\sim 10^7$ to 10^8 Volts/metre. A detailed account of the theory of electro-modulation is given in Chapter VII. We have seen in Chapter I that there are various ways of applying the modulating electric field to the sample under study. Figures (4.2a) and (4.2b) indicates the "dry package" configurations: in one case the electric field is applied using a capacitor configuration with the active medium as the dielectric and in the other a coplanar electrode system is utilized. The capacitor configuration was chosen in the present work since the coplanar electrode system restricts the aperture of the device; electrode spacings $\sim$ 100 μm are required. Also we see from Figure (4.2b) that the electric field is not uniform over the active medium in the coplanar configuration.

The important requirements for an optical modulator with a capacitor configuration are

(i) The medium producing the modulation should have a high resistivity and low photoconductivity so that power dissipation in the material is minimized.

(ii) The absorption edge of the material should be as steep as possible.

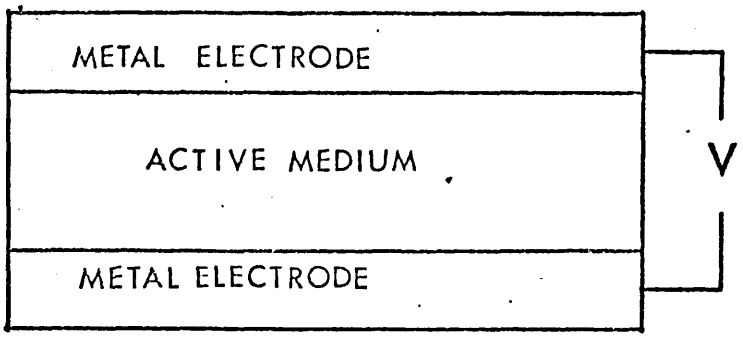

Figure (4.2a) Capacitor configuration.

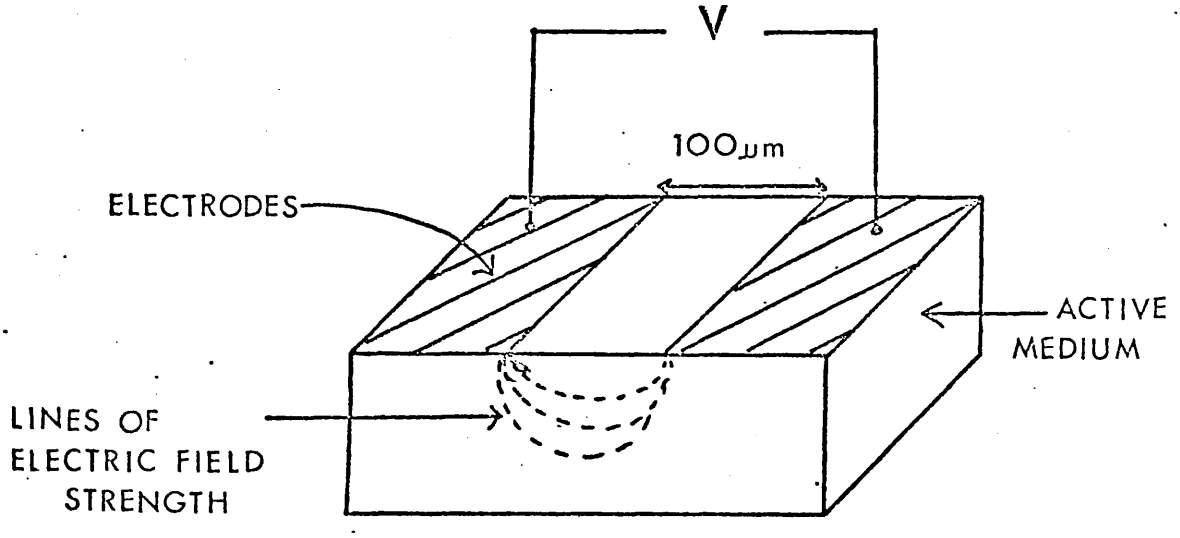

Figure (4.2b) Coplanar electrode configuration

In the present design we have used a totally integrated system, in which the device consists of a multilayer stack of thin films with no air gaps between the layers., The advantages of such a device over a system using discrete components separated by air gaps or optical cement are summarized below:-

(i) The integrated device is very compact.

(ii) Low operating voltages are required to produce the desired electric field strengths of $\sim 10^7$ Volts/metre to induce a shift in the absorption edge. In a multilayer stack of thin films having a total thickness of 10,000 Å only 30 Volts need to be applied across the device to produce an electric field strength of 3×10^7 Volts/metre. This is to be compared with the optical modulator utilizing discrete components described by French (1969). The device comprised a 12 μm platelet of gallium arsenide (the active medium) bonded to a tin oxide coated glass substrate with a 6 μm mylar spacer separating the gallium arsenide from another tin oxide electrode. It was found that 750 volts had to be applied across the device (total thickness 18 μm) to produce an electric field strength of 4×10^7 Volts/metre.

(iii) Spurious signals have been observed by workers using non-integrated devices, i.e. systems of separate components not in totally intimate contact are liable to produce misleading effects. For example, Claussin (1961) observed a 35% modulation in the reflectance of a germanium platelet. The germanium was insulated from a cadmium oxide electrode deposited on a glass plate, by means of a mylar spacer. Close inspection of the system revealed that the modulation was not due to the electromodulation of the germanium but caused by mechanical vibration of the mylar spacer.

(iv) With an integrated thin film modulator, the response may be enhanced by suitable optical design, i.e. a filter may be designed whereby the transmission of the device is peaked at a specific wavelength.

Cadmium sulphide which has a steep absorption edge centred upon 5200 Å was chosen as the active medium. The specimen configuration is shown in Figures (4.3a) and (4.3b). The capacitor-like structure has the advantage of providing substantial field strengths across the device without the joule heating which arises when the field is applied directly across the cadmium sulphide film between metallic electrodes. The choice of dielectric material is discussed in (4.8).

4.7 The preparation of the cadmium sulphide films

The cadmium sulphide films were grown by thermal evaporation in the Edwards 12EA vacuum system. The vacuum deposition of II-VI compounts is complicated by the fact that they sublime, , and eventually completely dissociate when heated (Goldfinger 1958). At a temperature of 800°C cadmium sulphide is 20% dissociated and at 1100°C it is 90% dissociated (Shalimova 1963). Thus during evaporation of cadmium sulphide there are both molecules of cadmium sulphide and free particles of atomic cadmium and diatomic sulphur in the vapour stream over the solid sulphide (Sen Gurta 1934). In the present work, preliminary evaporations of cadmium sulphide onto unheated float glass substrates did in fact reveal that there was a great deal of sublimation present and the well of the flap value of the vacuum system was quickly covered with a thick yellow deposit. A system for the vapour deposition of cadmium sulphide was designed based on the method that De Klerk and Kelly (1965) had successfully employed for the growth of high resistivity films for transducers. The cadmium sulphide, in the form of granules (B.D.H. Vactran grade 4-40 mesh), was evaporated from a molybdenum boat. Granules were used in preference to the powder form of cadmium sulphide since the latter, even with careful and slow heating of the boat, spattered violently around the vacuum chamber. The substrate and source were enclosed by a fused silica oven 15 cm long and 11 cm in diameter. Small quartz nodules $\sim$ 0.5 cm long were fused on to the outer surface of the silica tube, to

Figure (4.3a) Plan section of optical modulator

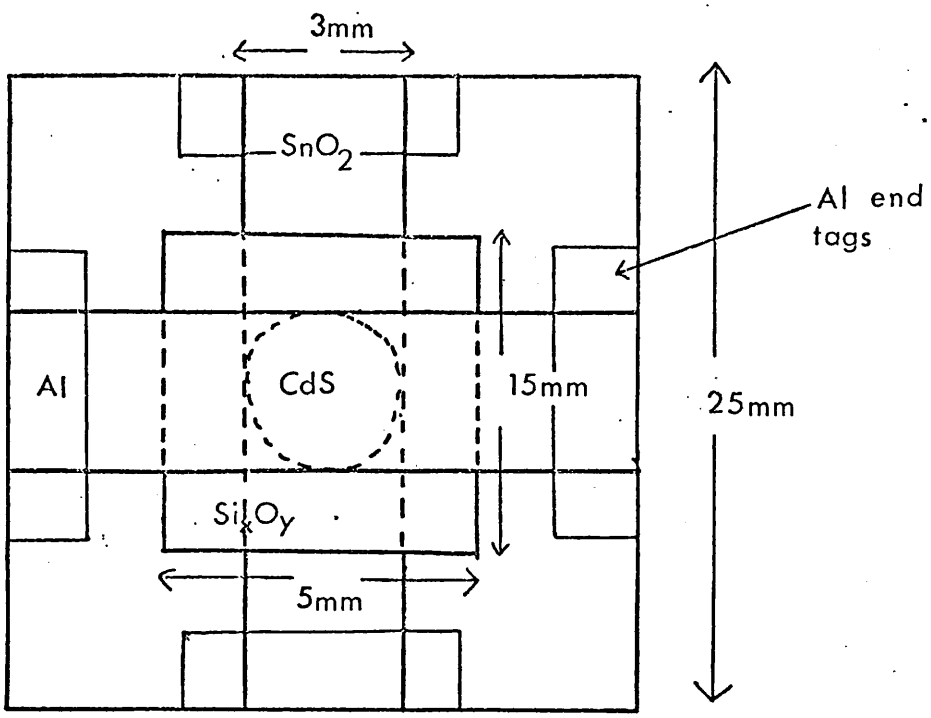

Figure (4.3b) Cross-sectional view of optical modulator.

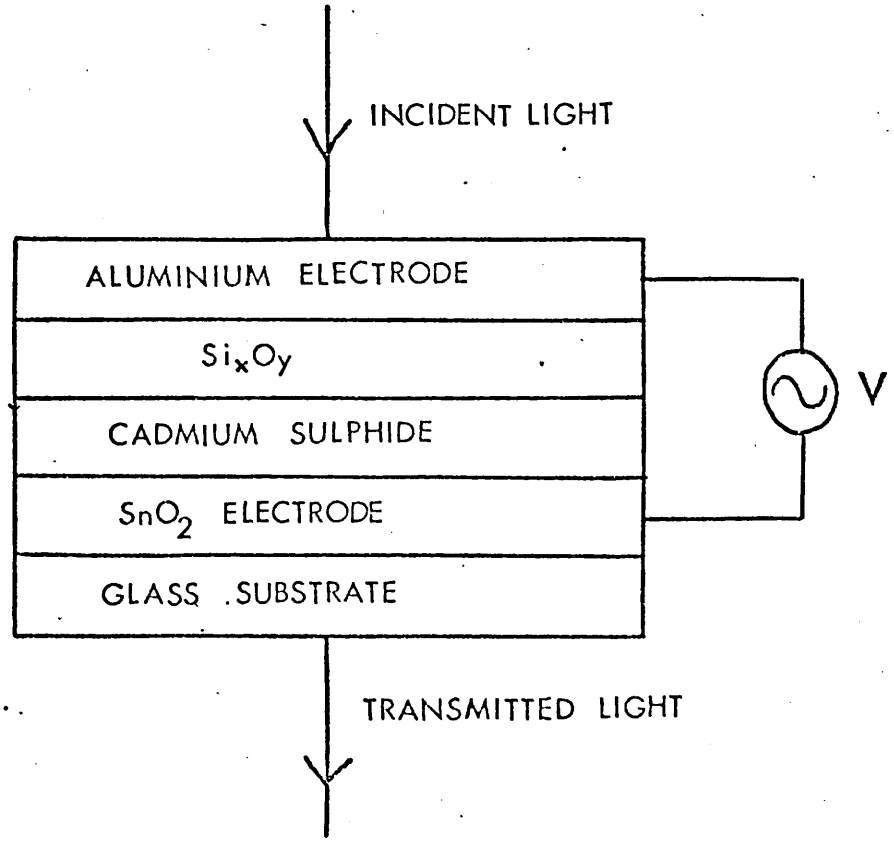

support a nichrome heating coil round the cylinder. The cylinder could thus be heated to 250°C which prevented the condensation of dissociated sulphur onto the walls. A stainless steel circular cap rested on the top of the oven and four pillars were fixed into the cap so as to support two stainless steel bars. The substrate could be clamped to the bars and thus held directly above the source. The source-substrate distance could be varied from 5 cm to 13 cm. The majority of the cadmium sulphide evaporations were carried out at a source-substrate distance of 8 cm. The walls of the silica oven were maintained at a temperature of 150°C, and a wire wound mica strip or a tin oxide coated microscope slide acted as the local substrate heater. The stainless steel cap had three feedthroughs inserted into the top in order that electrical connections could be made to the substrate heater, and also a chrome-alumel thermocouple could be attached to the substrate to monitor the temperature of the sample. Plate (4.2) shows the silica oven in the vacuum system.

Initially, cadmium sulphide films were deposited on unheated float glass substrates: these films were highly conducting, the majority having a resistivity $\sim 0.1\ \Omega$cm. Resistivity measurements were made by a four point probe technique, the electrode configuration being shown in Figure (4.4). Thermally evaporated gold films ~ 2000 Å thick served as the electrodes, gold being used in preference to other materials as it has been shown that cadmium sulphide films make an ohmic contact when deposited onto this element. Cadmium sulphide films > 1000 Å thick tended to be dark brown in colour. Both transmission and reflection high energy electron diffraction analyses were undertaken on the films, which could easily be stripped from the glass substrates. The film was scored into $3mm^2$ squares, and the whole slide was then held, partially immersed at an oblique angle in a dish of distilled water. After about five minutes, the squares of film floated free from the slide and could be picked up on copper specimen grids for e.m. analysis in transmission. The electron microscope used was an A.E.I. EM6 having a maximum accelerating voltage of 100KV and a maximum usable magnification of 60K. A transmission diffraction pattern and an electron micrograph of a

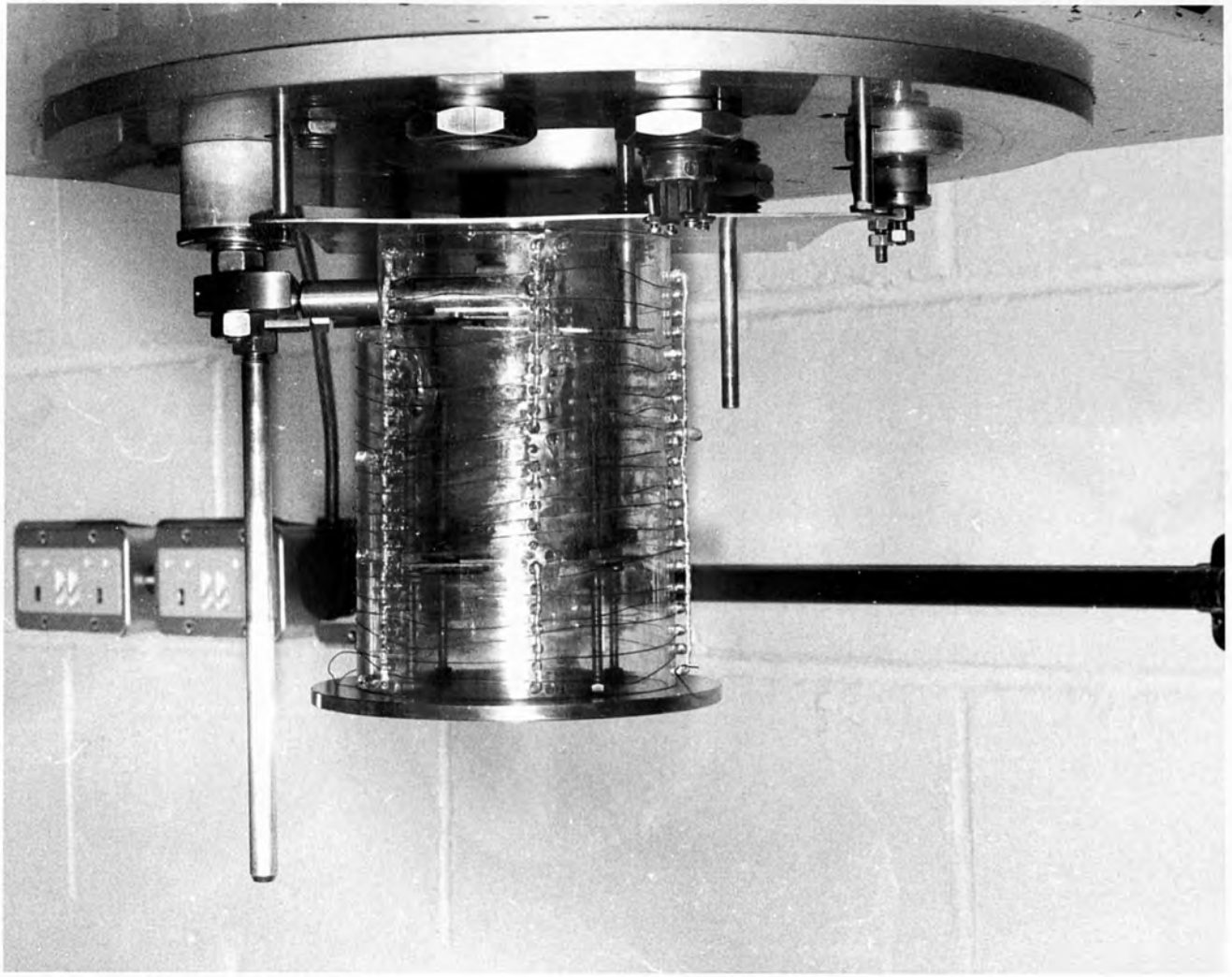

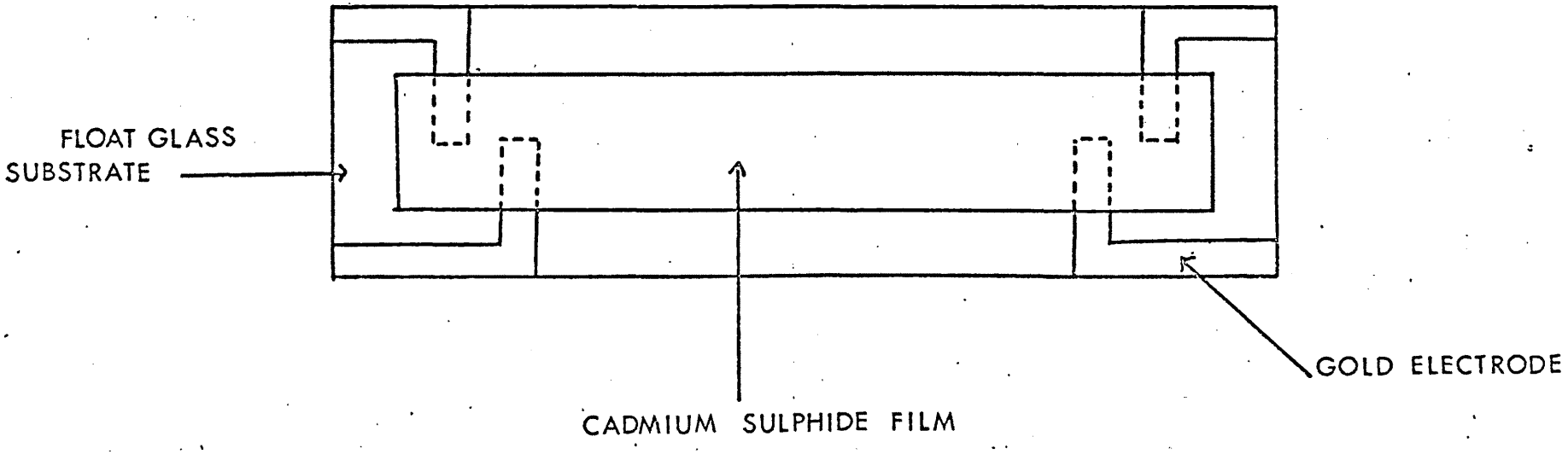

Figure (4.4) Specimen configuration for the 4 point probe resistivity measurements.

500 Å film of cadmium sulphide grown on an unheated float glass substrate are shown in Plates (4.3) and (4.4). The diffraction pattern indicates a randomly oriented film having a hexagonal close packed structure. From the pattern, interplanar spacings were calculated using equation (4.2), which relates the camera constant $2\lambda L$ of the microscope to the diameter D of the diffracted rings

$$dD = 2\lambda L \qquad (4.2)$$

where d is the interplanar spacing

λ is the wavelength of the electrons

L is the distance from the specimen to the viewing screen in the electron microscope.

The experimentally calculated d spacings were then compared with theoretical ones calculated from the equation

$$\frac{1}{d^2} = \frac{4}{3}\,\frac{(h^2 + hk + k^2)}{a^2} + \frac{\ell^2}{c^2} \qquad (4.3)$$

where $h\ k\ \ell$ are the Miller indices

a and c are the lattice constants of the material.

The two sets of d spacings are listed in Table (4.1) and we see that the diffraction pattern is indicative of a remarkably good stoichiometric film. The electron micrograph indicated that the cadmium sulphide had a crystallite size of 200 Å. To produce an evenly condensed film on the glass substrate a very slow rate of deposition $\sim$ 100 Å min^{-1} was used and the source temperature (determined by optical pyrometry) was $\sim 850^{\circ}C$. The film had a yellow appearance, unlike thicker films which were dark brown. The good stoichiometry of this film was attributed to the low source temperature since Shalimova et al. (1963) have indicated that at temperatures of $800^{\circ}C$ cadmium sulphide is only 20% dissociated. In the present work thicker films (>2000 Å) grown at higher deposition rates (500 Å min^{-1}) and high source temperatures ($1000^{\circ}C$) resulted in non stoichiometric films. The dark brown colour and the

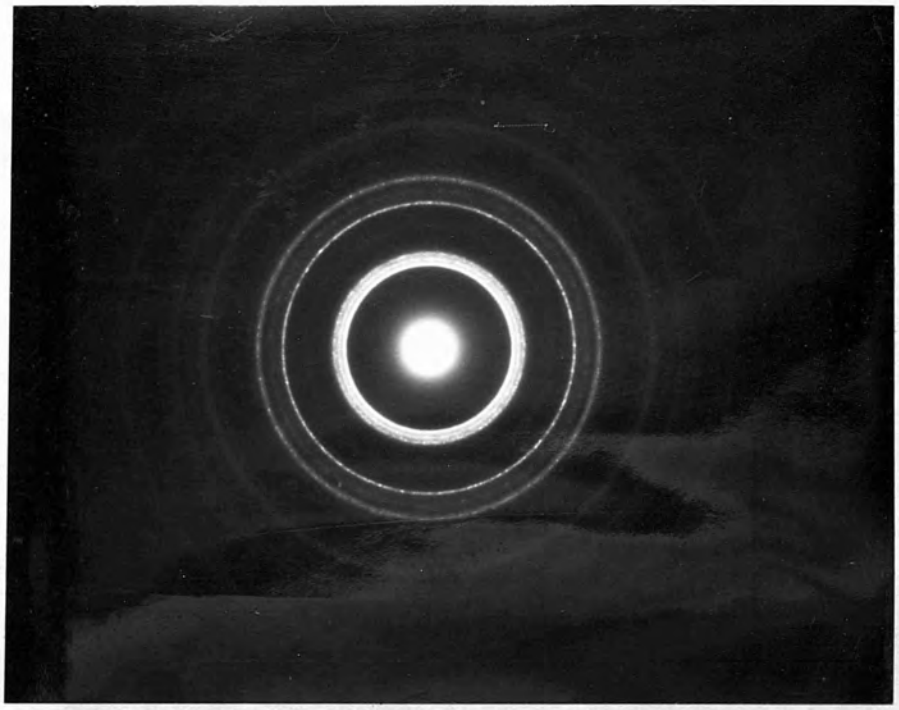

PLATE (4.3) Transmission electron diffraction pattern of a 500Å film of cadmium sulphide grown on a float glass substrate at room temperature (Accelerating voltage 100KV).

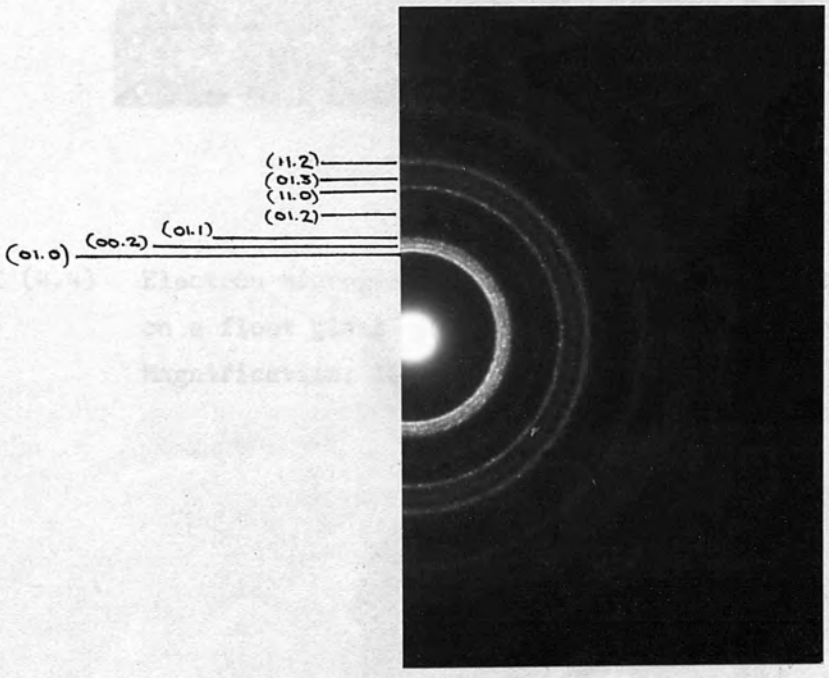

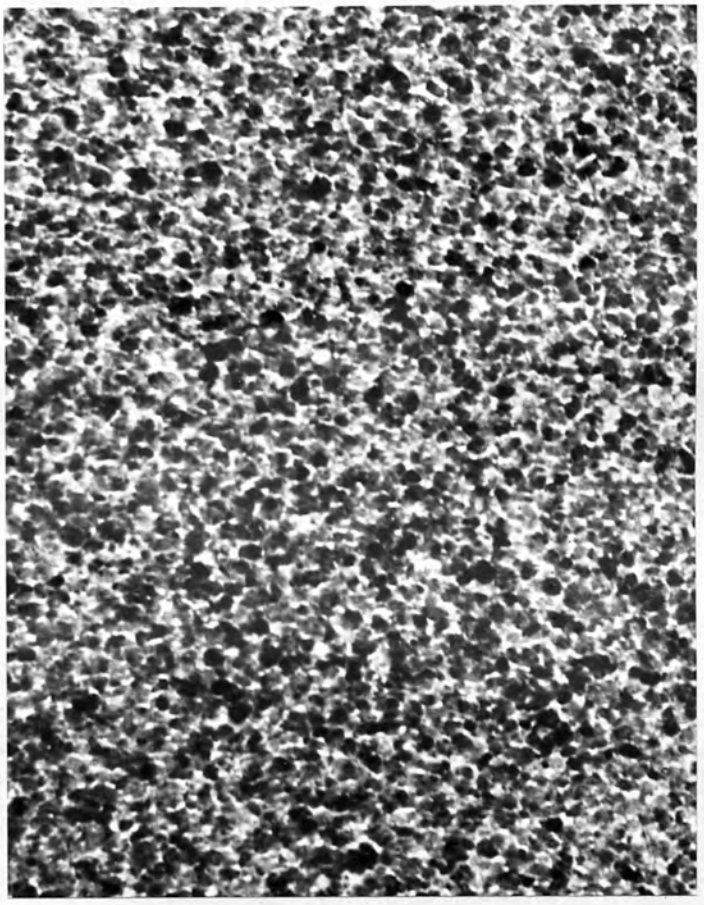

PLATE (4.4) Electron micrograph of a 500Å cadmium sulphide film grown on a float glass substrate at room temperature. Magnification: 100KX

TABLE 4.1

h k ℓ	Calculated d spacings (Å)	Measured d spacings (Å) from Plate (4.4)
00.1	6.691	-
01.0	3.577	3.63
00.2	3.346	3.44
01.1	3.154	3.11
01.2	2.443	2.46
00.3	2.230	-
11.0	2.065	2.07
11.1	1.973	-
01.3	1.893	1.90
02.0	1.788	-
11.2	1.757	1.77

Lattice parameters of cadmium sulphide (Wyckoff 1965)

$$a = 4.130 \text{ Å}$$

$$c = 6.691 \text{ Å}$$

high conductivity of cadmium sulphide films deposited on cold substates has been attributed to the occurrence of excess cadmium (Foster 1965). Reflection electron diffraction analysis of the films grown in the present work gave no evidence of a discrete cadmium phase. Shallcross (1966), in an x-ray diffraction study of films of cadmium sulphide, also found no evidence of the cadmium phase.

Films deposited onto substrates held at temperatures between 180 and 200°C were found to give stoichiometric and highly resistive ($\sim 10^4$ Ω cm) films. The sticking coefficient of the cadmium sulphide was found to decrease drastically as the substrate temperature increased and it was found to be extremely difficult to deposit a film on substrates held above 200°C. High energy reflection electron diffraction analysis indicated that for a film 1200 Å thick, grown on a substrate held at 185°C, a randomly oriented hexagonal close packed structure was formed. An example of such a film is shown in Plate (4.5). Films ranging in thickness from 2000 to 8000 Å deposited on substrates held at 180°C grew in a well ordered orientation see Plate (4.6). Plate (4.7) shows the same film, described above, seen in transmission on a Vickers Projection microscope, the crystallite size being $\sim$ 1 μm. Shallcross (1966) has also found that as the substrate temperature and film thickness increase, oriented growth is observed and the crystallite size increases. All the cadmium sulphide films forming part of the optical modulator were deposited on substrates held at 185°C.

4.8 Choice and preparation of the dielectric layer

In the present work several materials have been evaporated for use as dielectrics. For use in the optical modulator the dielectric needed to have a breakdown strength between 10^7 and 10^8 Volts metre^{-1}. The electrical characteristics of the dielectric films were investigated by fabricating thin film capacitors. Aluminium was chosen as the electrode material; large-grained films such as are formed by lead and tin are unsuitable since

PLATE (4.5) High energy reflection electron diffraction pattern of a 1200Å cadmium sulphide film. Substrate temperature 185°C.

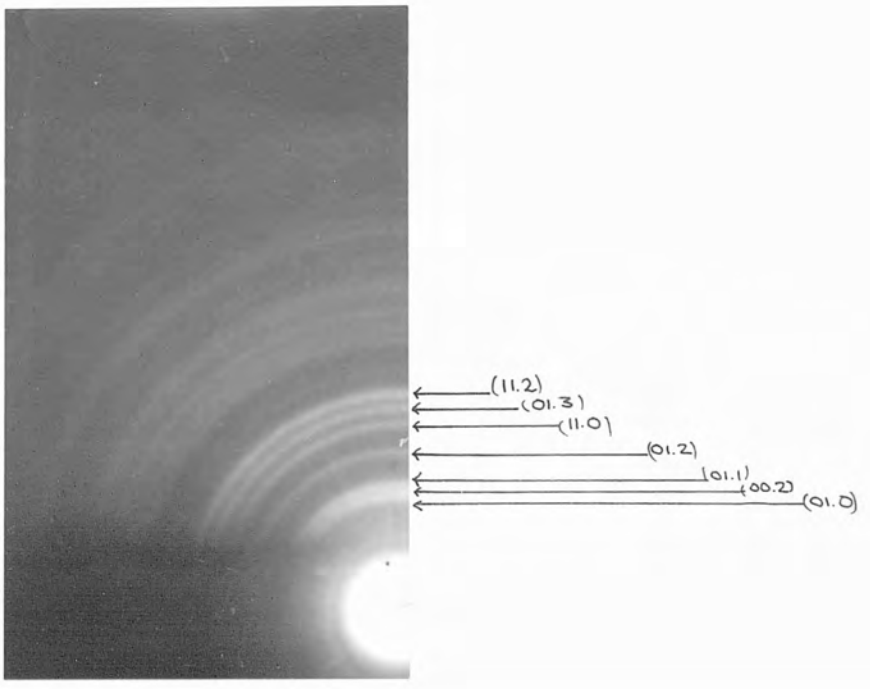

PLATE (4.6) High energy reflection electron diffraction pattern of a 5000Å cadmium sulphide film grown on a float glass substrate at 180°C.

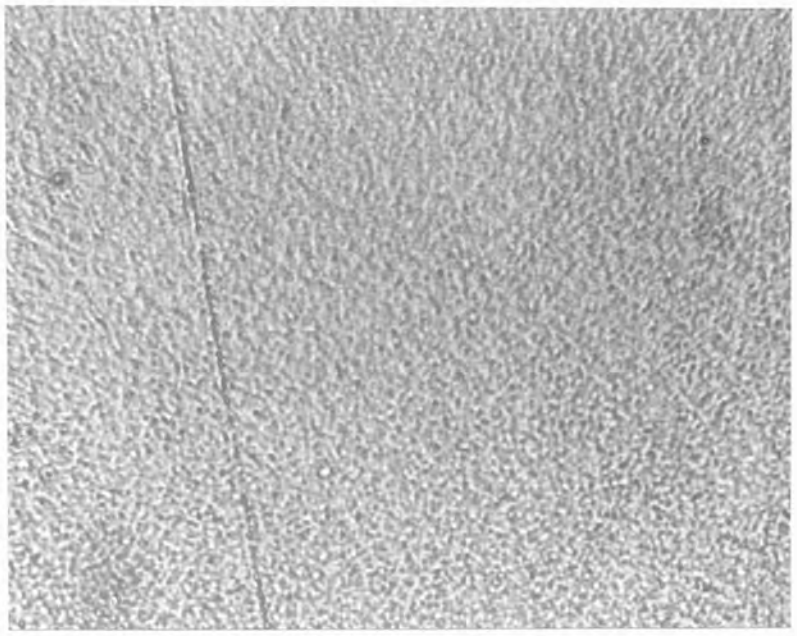

PLATE (4.7) Optical micrograph of the cadmium sulphide film shown in Plate (4.6), seen in transmission on a vickers projection microscope.
Magnification: 800X

they have a high surface roughness. Capacitors with electrodes of high boiling point metals break down more readily than otherwise, probably because the dielectric is penetrated during electrode deposition by the high energy condensate (Hass and Thun 1968) So as to reduce the possibility of metallic or other contamination of the dielectric films, a vacuum system was kept exclusively for the deposition of the latter, and the aluminium electrodes were grown in a separate system.

Aluminium oxide, niobium oxide, soda glass, borosilicate, quartz, magnesium fluoride and silicon monoxide were investigated as dielectric materials. Because of their relatively high melting points, 2045°C and 1520°C respectively, aluminium oxide and niobium oxide were evaporated by electron bombardment from carbon or cermet crucibles. The films produced from the alumina evaporation did not give systematically good dielectric behaviour. Many of the films were light brown in colour, this colouration being attributed to a reaction of the charge material with the crucible. Those alumina films that were non-conducting had a very low breakdown strength. Breakdown paths always appeared at a weak point in the dielectric at the sharp step of the bottom aluminium electrode (Figure (4.5a)). To eliminate this weak point, aluminium films having a diffuse edge rather than a sharp step were produced by moving the stainless steel electrode mask 2 or 3 mm away from the glass substrate. The resulting capacitor configuration is shown in Figure (4.5b). Although this improved the breakdown strength of some of the alumina films, many of the films grown were light brown and highly conducting, even though a cermet crucible was used.

Niobium oxide was evaporated from either the ring gun or from a molybdenum boat. Films produced from both sources were highly conducting and it was thought that the material dissociated upon heating causing free niobium to be present in the film. After evaporation, the charge material, being initially in the form of white granules, had turned to a blue-black deposit. Reliable capacitors could not be produced with any of the glasses. Films which were more than 200 Å thick grown on cold soda glass substrates always showed signs of strain after removal from the vacuum chamber. Neither heating the

Figure (4.5a) Capacitor configuration

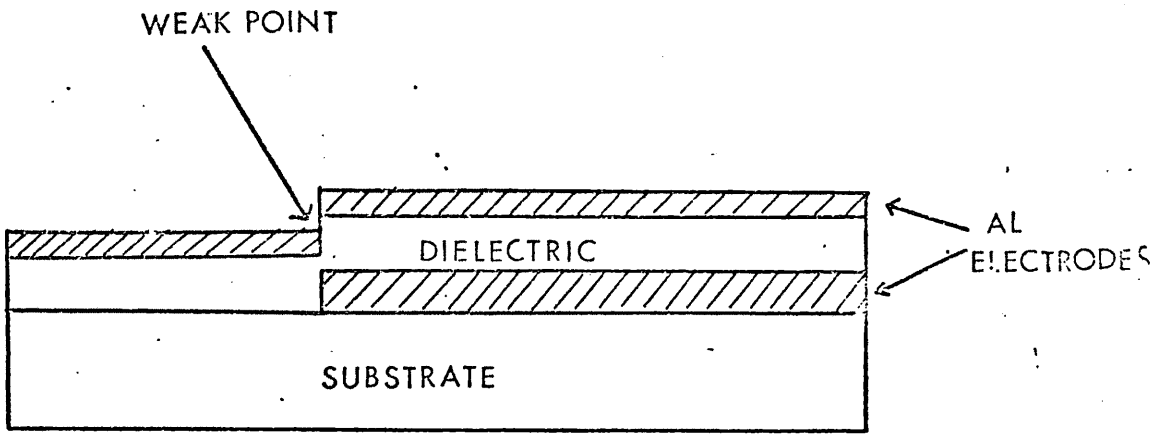

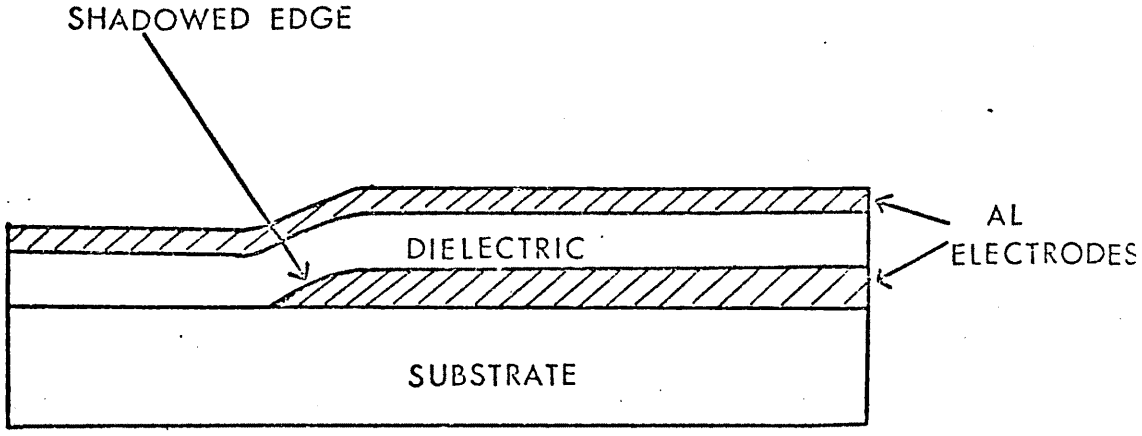

Figure (4.5b) Capacitor configuration with diffuse bottom electrode

substrate nor deposition onto borosilicate substrates improved the film quality.

Films of silicon monoxide and magnesium fluoride were found to give the best dielectric characteristics. Silicon monoxide has been extensively studied by Hass (1950) and Siddall (1959) who found that the optical constants and the physical structure of a film varied considerably with the rate of evaporation and the residual gas pressure. Films deposited at pressures $> 10^{-5}$ torr were found to have a porous structure. In the present work silicon monoxide (B.D.H. Vactran grade 8-120 mesh) was evaporated from a tantalum baffled source (Nordiko S.10) to prevent the charge material from spattering the substrate. The source is shown in Plate (4.8). The rate of deposition was 11 Å sec^{-1} and the base pressure during evaporation was 8×10^{-7} torr. A marked gettering action was observed as the material began to evaporate, showing rapid absorption of the residual gases in the chamber. All the films evaporated under these conditions were slightly yellow in colour. Absorption edges (monitored by a Perkin Elmer spectrophotometer Model 137 UV) of films evaporated at different rates are shown in Figure (4.6). The absorption at 4000 Å of the film deposited at the fastest rate (20 Å sec^{-1}) is much greater than the film deposited at 11 Å sec^{-1}. Capacitors made from films grown at the higher rate (20 Å sec^{-1}) had a high conductivity. Hass (1950) has indicated that for fast evaporation rates the resultant film contains free silicon. All the films used in the optical modulator were deposited at rates of 11 Å sec^{-1}. Plate (4.9) shows a transmission electron diffraction pattern of a film grown at a rate of 11 Å sec^{-1} onto a freshly cleaved (100) surface of rocksalt. The pattern indicates an amorphous structure, and the average interplanar spacing calculated from the halo was $\sim$ 3.50 Å. The interplanar spacing of stoichiometric films is $\sim$ 3.60 Å (Hass 1950). The diffraction pattern showed no ring of silicon or of silica (SiO_2). Although these films were not strictly stoichiometric the capacitors constructed from them had a very high breakdown strength $\sim 10^7$ to 10^8 Volts $metre^{-1}$. Typical capacitances measured using a Marconi Universal

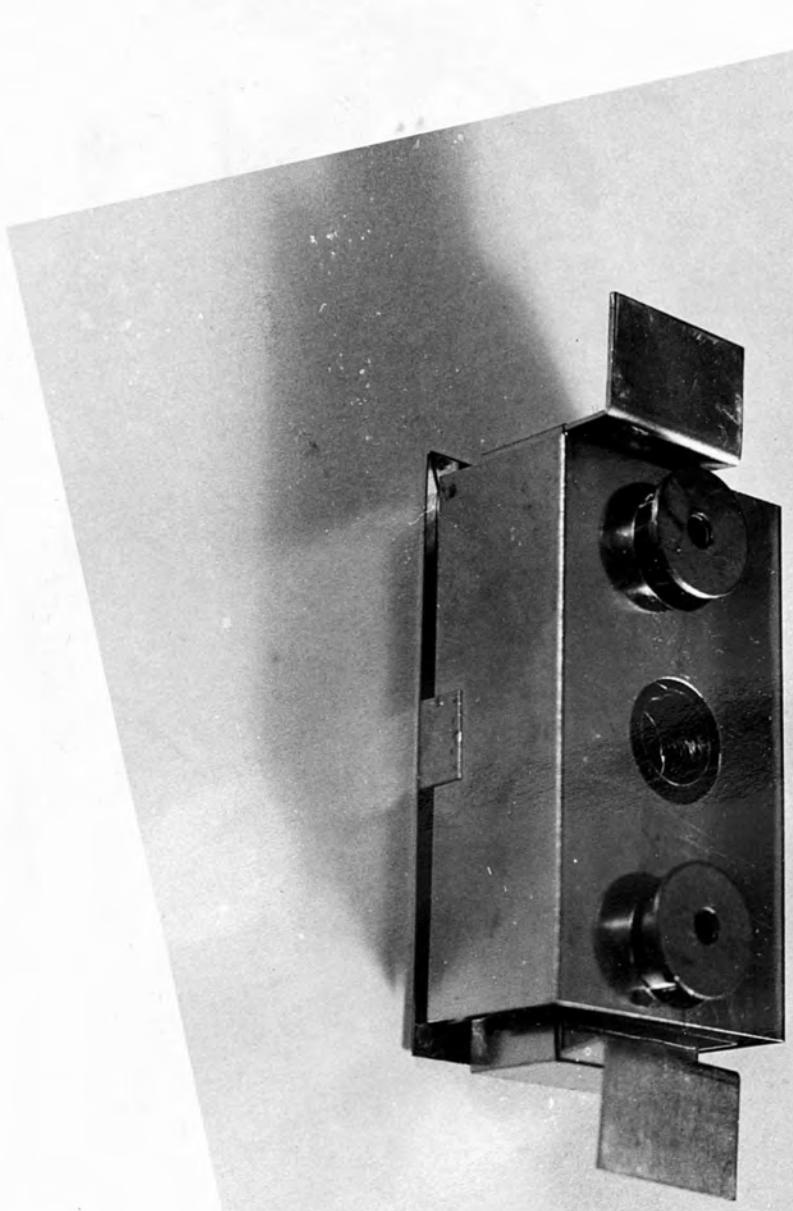

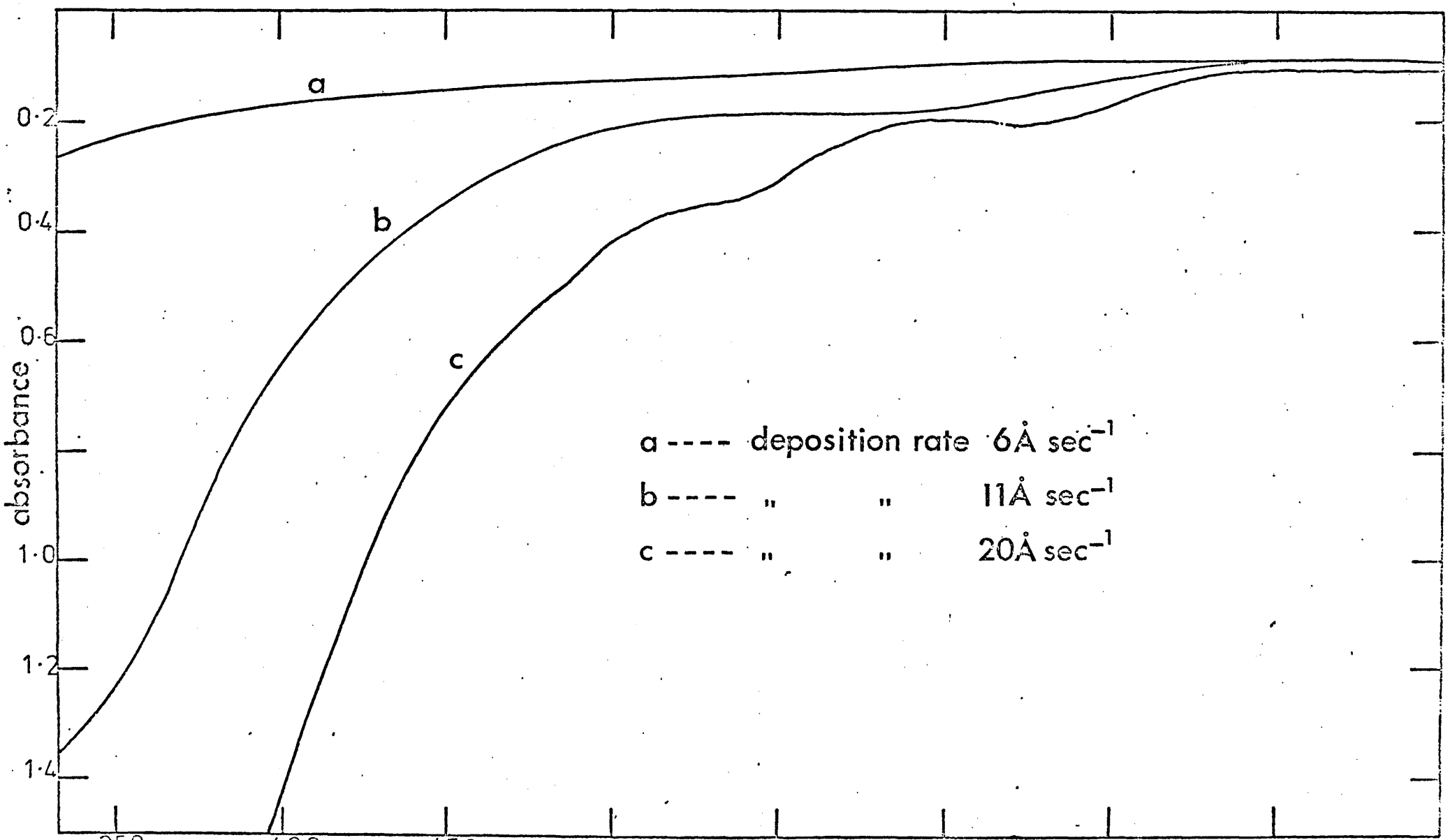

FIGURE (4·6) Absorption edges of Si_xO_y films

PLATE (4.9) Transmission electron diffraction pattern of a silicon monoxide film grown on the (100) face of a rocksalt crystal. Deposition rate: $\sim 11\text{Å}\ \text{sec}^{-1}$.

Bridge were of the order 10^{-10} Farads. Direct current measurements showed that the capacitors would withstand voltages of 30 volts (or more) with associated currents of the order of 10^{-9} to 10^{-11} amps, leakage current characteristics were measured with a Pitman 437 electrometer. All the capacitors investigated had dielectric thicknesses in the range 2000 to 3000 Å. Films deposited at low rates (< 6 Å sec^{-1}), although transparent in the wavelength range 3500 to 7500 Å, always showed signs of strain whether removed from the vacuum chamber immediately or a few hours later.

Magnesium fluoride was evaporated from a molybdenum boat onto heated substrates (films > 1000 Å thick showed signs of strain on cold substrates). Capacitors with magnesium fluoride as the dielectric had typical capacitances of $\sim 10^{-9}$ Farads. With 30 volts applied to the capacitor, leakage currents were typically 10^{-7} to 10^{-8} amps. Since the leakage currents of the capacitors using silicon monoxide as the dielectric were smaller than those using magnesium fluoride, the former was used as the dielectric material for the integrated thin film optical modulator.

CHAPTER V

The thermally modulated optical properties of opaque films of gold and copper

(5.1) Introduction

In this chapter the thermally modulated optical properties of opaque films (≃ 2000Å thick) of gold and copper are examined. The modulated reflectance response has been expressed in terms of the more significant quantities $\Delta\varepsilon_1$ and $\Delta\varepsilon_2$, the changes in the real and imaginary parts of the dielectric constant respectively, by the methods described in (2.5), $\Delta\varepsilon_2$, in particular, is then correlated with the existing band structure calculations which are available for gold and copper.

Gold was the first metallic element to be studied by the thermoreflectance method (Scouler 1967). Scouler thermally evaporated gold films ∿ 2000 Å thick onto glass, mylar and silicon substrates. The thermoreflectance measurements were performed at 120K at a pressure of 10^{-6} torr and films deposited on the different substrates gave the same results. The measurements were made over an extensive spectral range 2 to 10 eV, and was the first time modulation measurements had extended to the vacuum ultraviolet. The experiment was later repeated by Rosei and Lynch (1972) at two temperatures: 120K and 340K, but the photon energy range was less extensive than in Scouler's work. Both workers found that the thermoreflectance response of gold had dominant structure near 2.5 eV and also smaller subsidiary structure located at 2.9 eV and 3.2 eV. Essentially the purpose of the present work was to use gold as a reference material, to determine the spectral position of the dominant structure and to ascertain whether the detection system had sufficient sensitivity to locate the two subsidiary peaks.

The thermally modulated optical properties of polycrystalline opaque films of copper were also examined. Mueller and Phillips (1967) and Janak et al. (1975) have calculated the imaginary part of the dielectric constant,

ε_2. The results represent the only calculations made of this type and thus provide an opportunity for comparisons to be made between experiment and a comprehensive theoretical calculation.

(5.2) The preparation of the gold films

The gold films were prepared in an ordinary high vacuum environment (Birvac T4150), and the growth conditions for a typical film are given below:-

(i) The film was grown from a 99.9% pure sample of gold wire supplied by Johnson and Matthey.

(ii) The film was deposited in the configuration described in (4.5), onto glass substrates at room temperature, from a molybdenum boat.

(iii) The ordinary high vacuum system was evacuated to 10^{-6} torr and the boat and evaporant outgassed by passing a current of 60 amps for 3 minutes.

(iv) After the outgassing procedure the system was allowed to attain its base pressure of $\sim 4 \times 10^{-7}$ torr. The boat was heated until the evaporant melted. The current was then raised to 90 amps and the shutter shielding the substrate was opened, allowing the film to condense onto the float glass slide.

(v) The source-substrate distance was 8cm and the rate of deposition was ~ 20 Å sec^{-1}. The film was deposited in one evaporation and during the course of the evaporation the pressure in the system rose to 2×10^{-6} torr.

(vi) Three float glass substrates were incorporated in the system in any one evaporation. One sample was used to measure the film thickness, a glass cover slip being attached to the substrate to give the required step. Of the other two samples, one was mounted for analysis by high energy reflection electron diffraction and the remaining sample was transferred to the experimental chamber.

Directly after removal from the vacuum chamber the sample slide was mounted on the cryostat; this entailed exposing the film to the atmosphere. The sample was mounted in the experimental chamber within 10 minutes of removal from the growth system and was generally under a pressure of $\sim 10^{-6}$ torr within 30 minutes of starting the pump down. Copper electrical leads were indium - soldered to the ends of the film. A chrome-alumel thermocouple was also indium-soldered to the surface of the film, so that it did not interfere with the incident light beam. Of the two remaining samples, one was mounted on a stud for analysis by high energy reflection electron diffraction in a JEM 6A electron microscope. The sample was mounted on the stud with Acheson Dag 1950, a 3 to 4 hour period being necessary for drying, during which time the specimen was stored at 10^{-6} torr. The other sample was silvered and its thickness measured using multiple beam Fizeau fringes (Tolansky 1963).

Plate (5.1) is a high energy reflection electron diffraction pattern of a typical gold film. We note that the ring grouping is typical of a face centred cubic structure. The diffraction pattern indicates that the film was randomly polycrystalline with a crystallite size in the order of 1000 Å.

(5.3) The thermally modulated reflectance measurements

The specimen was subjected to thermal modulation after the vacuum system reached 8×10^{-7} torr. For convenience of experimental layout initial measurements were made at oblique incidence at 45° with the light plane polarized parallel to the plane of incidence. Measurements were made at 107K and 323K. In the former case the specimen was cooled by the introduction of liquid nitrogen into the cryostat and for the high temperature measurements the cryostat was water-cooled. Measurements were always taken in a low-high-low or high-low-high temperature cycle in order to ascertain whether any changes observed in the modulated reflectance response were repeatable and whether any hysteresis effects were present.

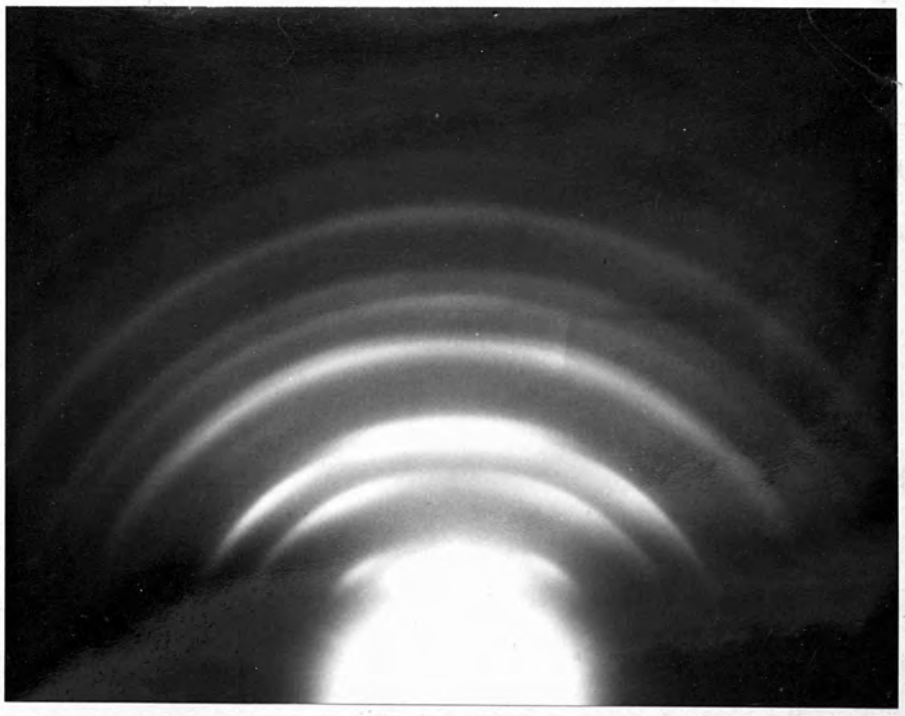

PLATE (5.1) High energy reflection electron diffraction pattern of a gold film (accelerating voltage 100KV).

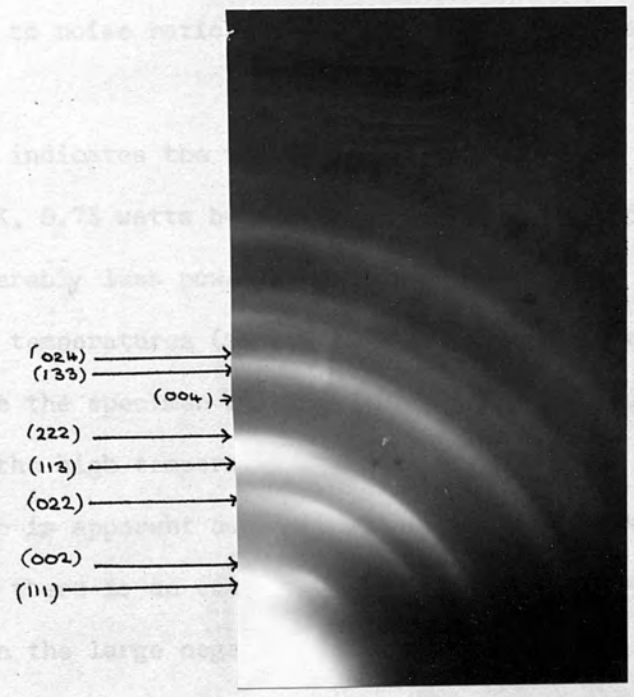

Figure (5.1) indicates the thermally modulated reflectance response of a typical gold film at 320K for two different values of power dissipation in the sample. We see that a larger ($\Delta Rp/Rp$) response is observed on increasing the power dissipation. The thermocouple registered a 40K mean rise in the temperature of the sample on application of the modulating current. We note that the modulated reflectance response consists of two main peaks situated at 2.425 eV and 2.625 eV. Additional structure can also be seen at 3.0 eV and Figure (5.2) indicates this response. The diagram represents a trace of the actual signal ($\Delta Rp/Rp$) displayed on the pen recorder and we see that as lower wavelengths are approached the noise in the detection system increases. The experiment was performed scanning from 1.8 eV to 3.2 eV. The spectralpositions of structure in the thermally modulated reflectance responsewere found at the same photon energy regardless of whether the spectral range was scanned from 1.8 to 3.2 eV or from 3.2 to 1.8 eV. This indicated that the wavelength scan speed matched the time constant of the lock-in amplifier. Measurements could only be taken down to 3.2 eV since in order to maintain a constant 1 volt d.c. signal on the photomultiplier it was necessary to run the photomultiplier high voltage supply at 700 volts at this photon energy. This resulted in a drastically decreasing signal to noise ratio and repeatable readings could no longer be obtained.

Figure (5.3) indicates the thermoreflectance response when the specimen was cooled to 107K, 0.75 watts being dissipated in the sample. It was found that considerably less power had to be dissipated in the samples maintained at low temperatures ($\sim$ 107K) than those at higher temperatures ($\sim$ 320K) otherwise the specimen cracked. The low temperature trace is superimposed on the high temperature response and we note that at 107K the same structure is apparent as at 323K but it is considerably sharpened. Also we note that there is an energy shift of 0.063 ± 0.004 eV towards higher energies in the large negative peak near 2.4 eV. However there is

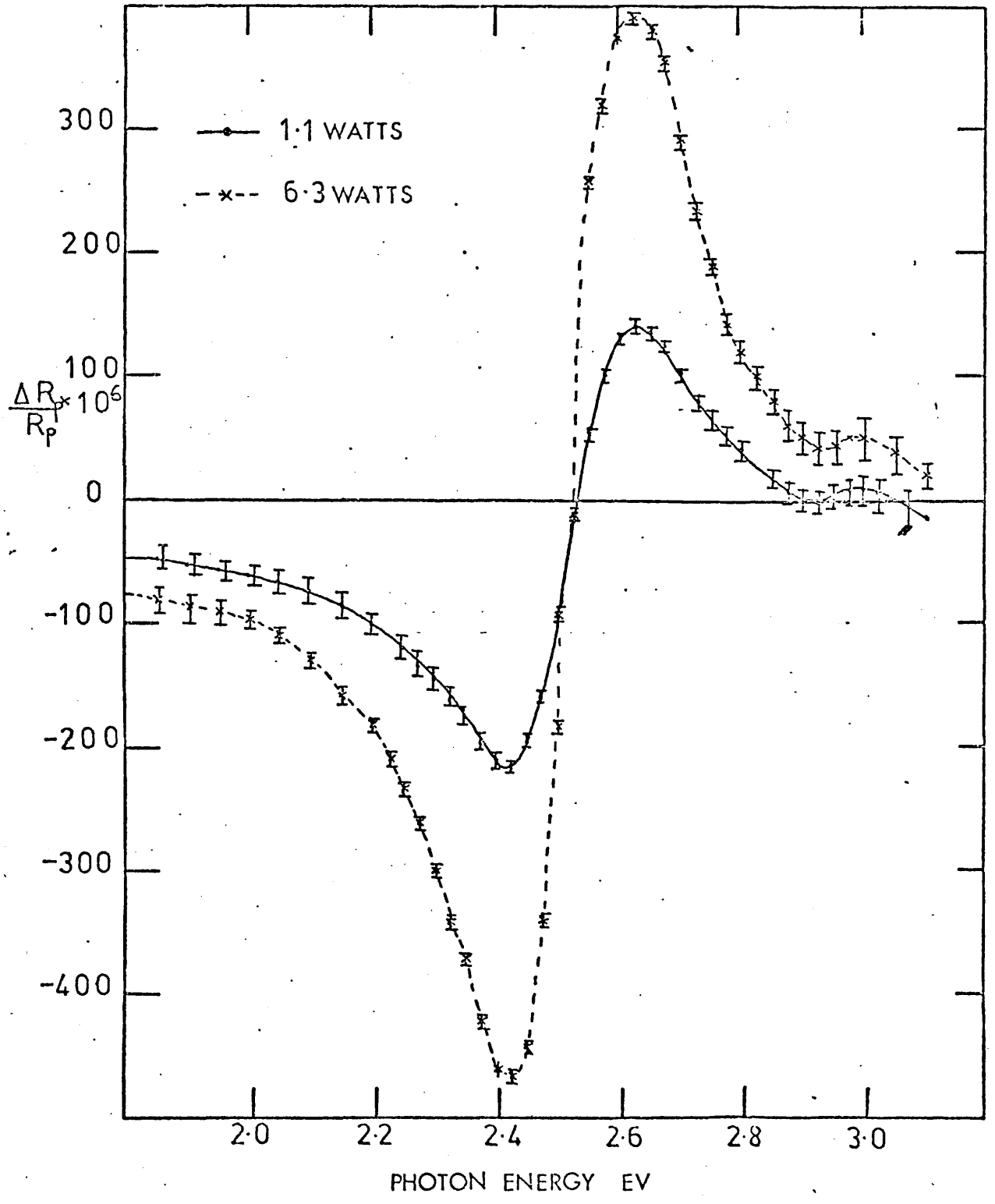

Figure (5.1) The thermally modulated reflectance spectra of a polycrystalline gold film.

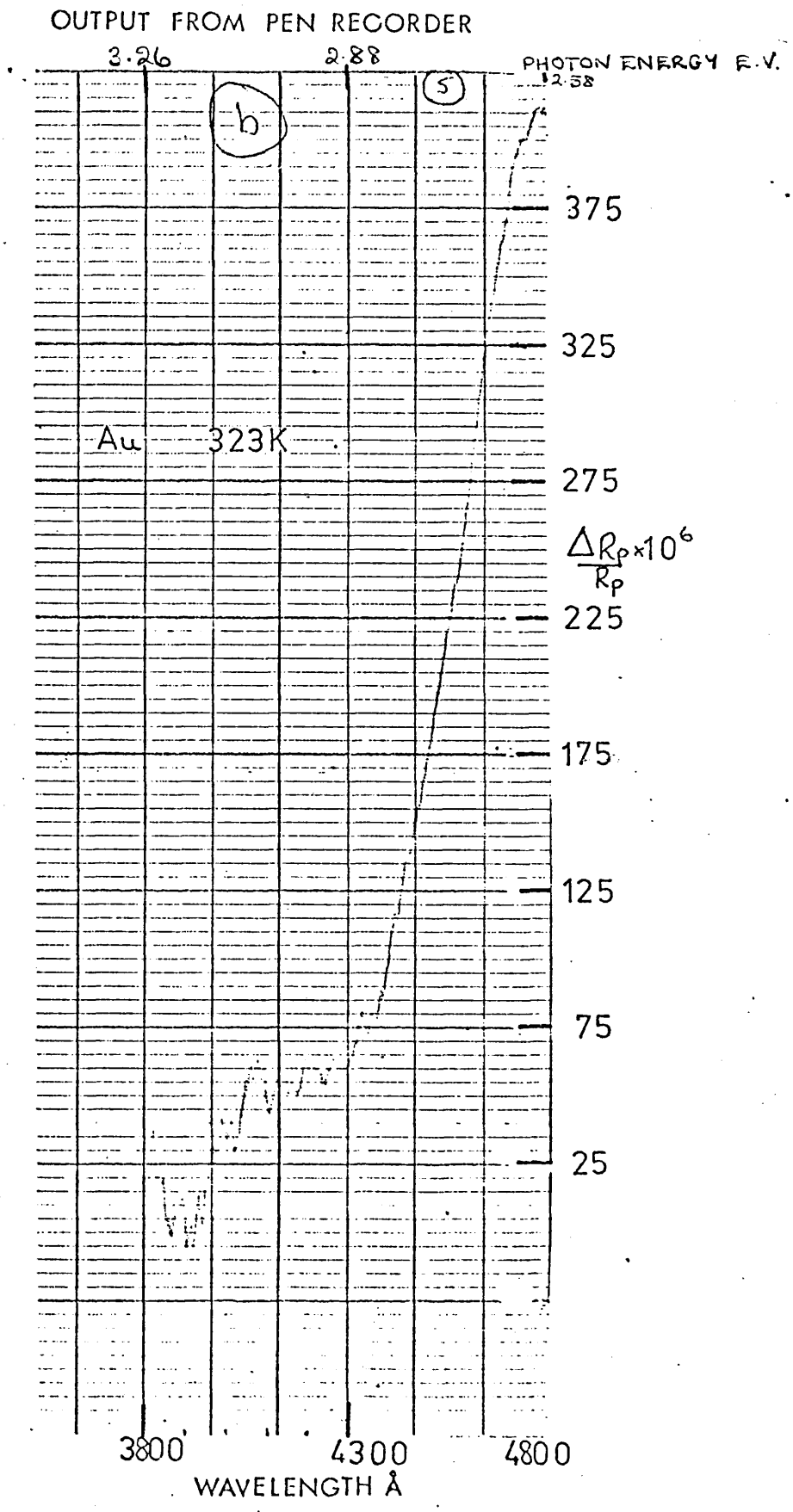

Figure (5.2) Pen recorder output showing the (ΔR/R) response of a gold film.

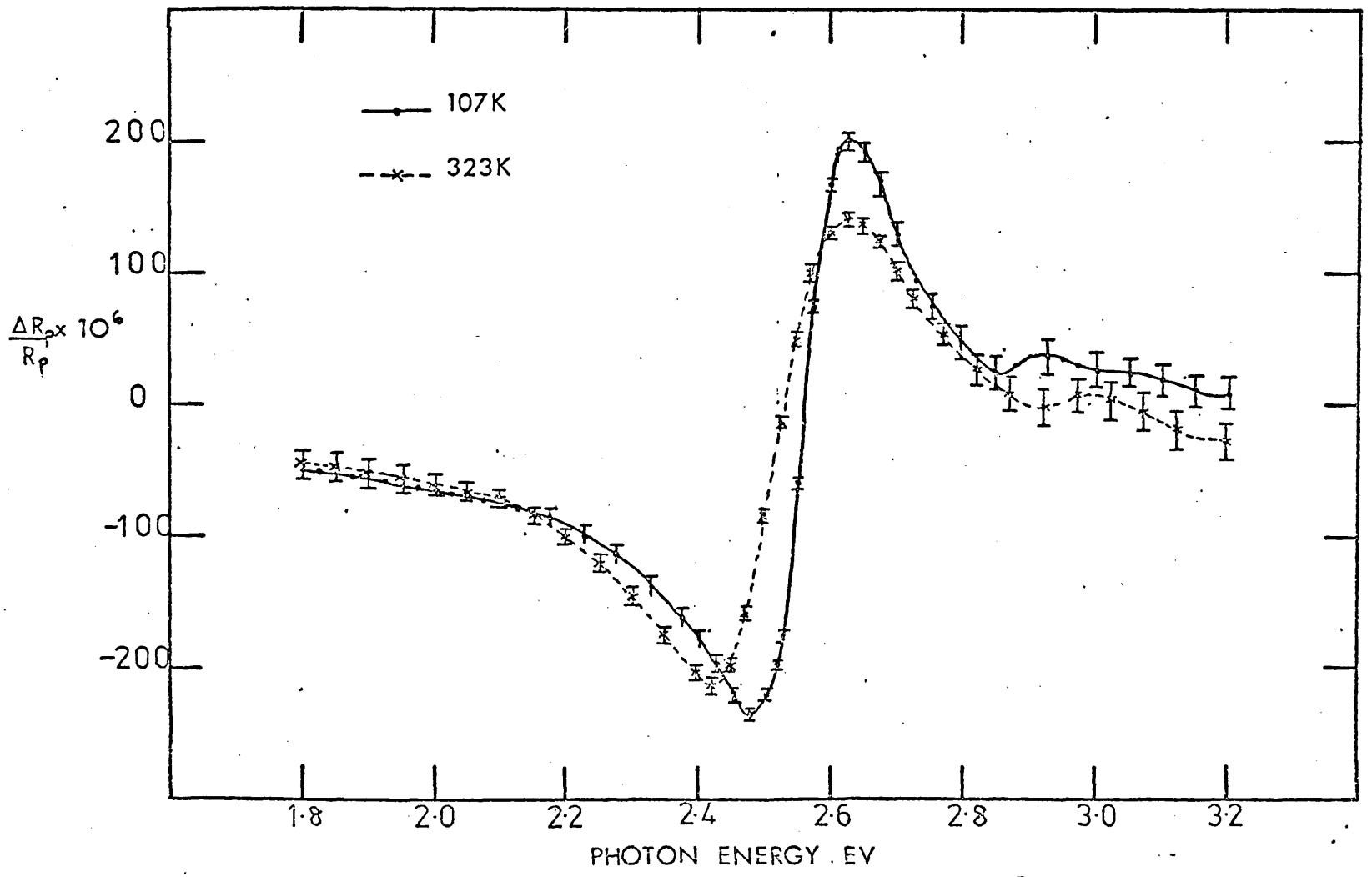

Figure (5.3) The (ΔRp/Rp) spectra of a polycrystalline gold film at 107K and 323K.

no change in the position of the positive peak. An energy shift is also noted in the subsidiary structure around 3.0 eV: the shift of 0.010 ± 0.004 eV is towards lower energies on lowering the temperature.

As a check on these results and to confirm that the spectral positions of structure changed on lowering the temperature of the sample the experiment was repeated at near normal incidence using the mirror configuration shown in Figure (3.4). Near-normal incidence geometry was chosen primarily for two reasons, namely:-

(i) Rosei and Lynch (1972) and Scouler (1967) obtained their data at near normal incidence.

(ii) Work by Fischer and Seraphin (1967) and Schmidt and Knausenberger (1969) on the electroreflectance response of germanium indicates that the position of structure in modulated reflectance can depend on the angle of incidence.

The thermal modulation experiment at near normal incidence was performed on the same sample used in the oblique incidence measurements. However the experimental chamber had to be let up to atmospheric pressure in order to align the mirrors, thus exposing the sample to the atmosphere. The film was exposed for approximately 20 minutes before pump down recommenced. Figure (5.4) indicates the thermally modulated reflectance responses for measurements taken at near normal incidence at 323K and 107K. The spectral positions of structures do not change with angle of incidence and on lowering the temperature there is again an energy shift of 0.063 eV in the negative peak.

In order to ascertain whether the observed peak position shift with temperature was associated with strain in the films caused by differential thermal expansion of the substrate and film, the substrate was changed to Spectrosil B. The thermal expansion coefficients of Spectrosil B, soda glass and gold are (Kaye and Laby 1955).

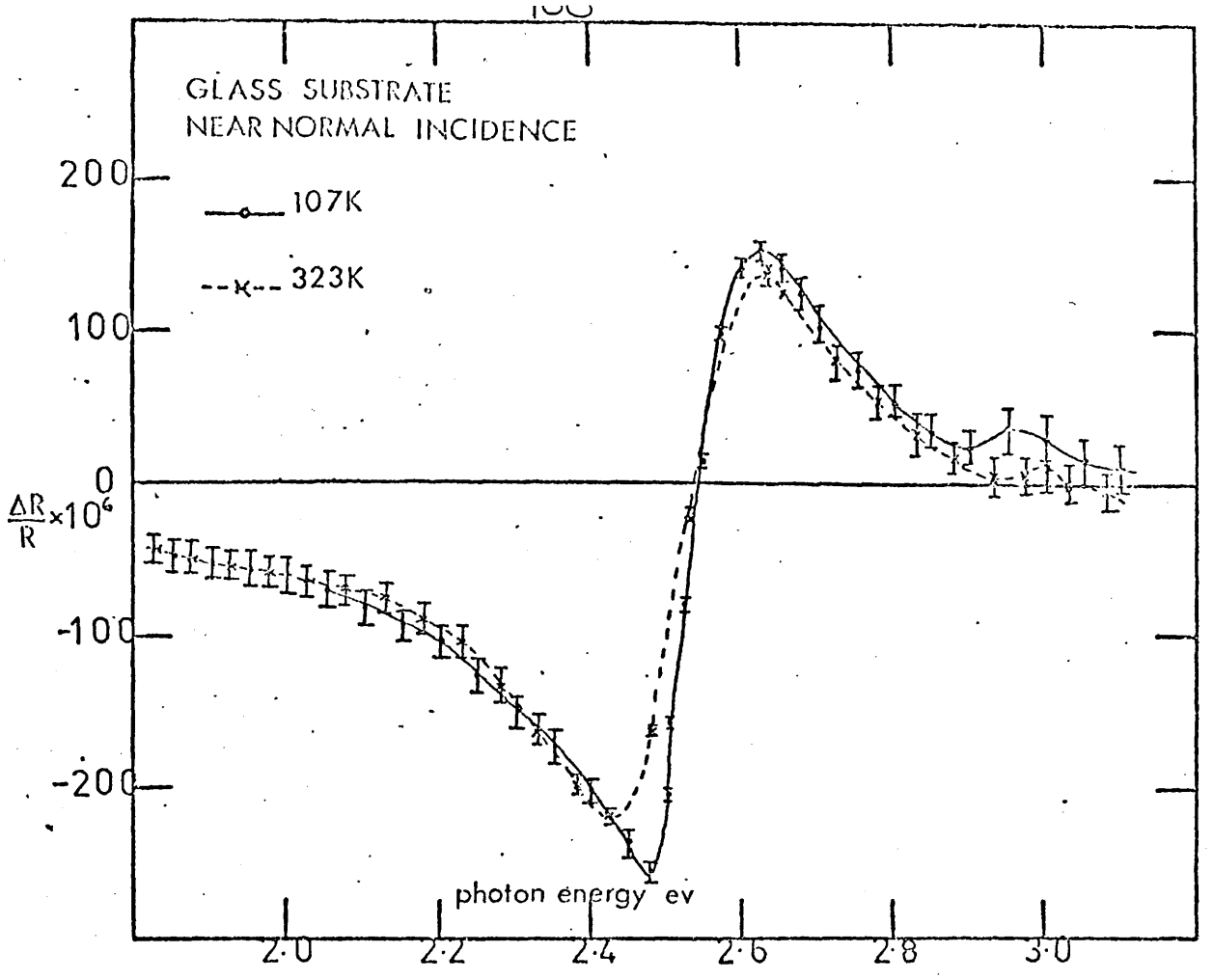

Figure (5.4) The (ΔR/R) responses of a gold film at 107K and 323K at near normal incidence

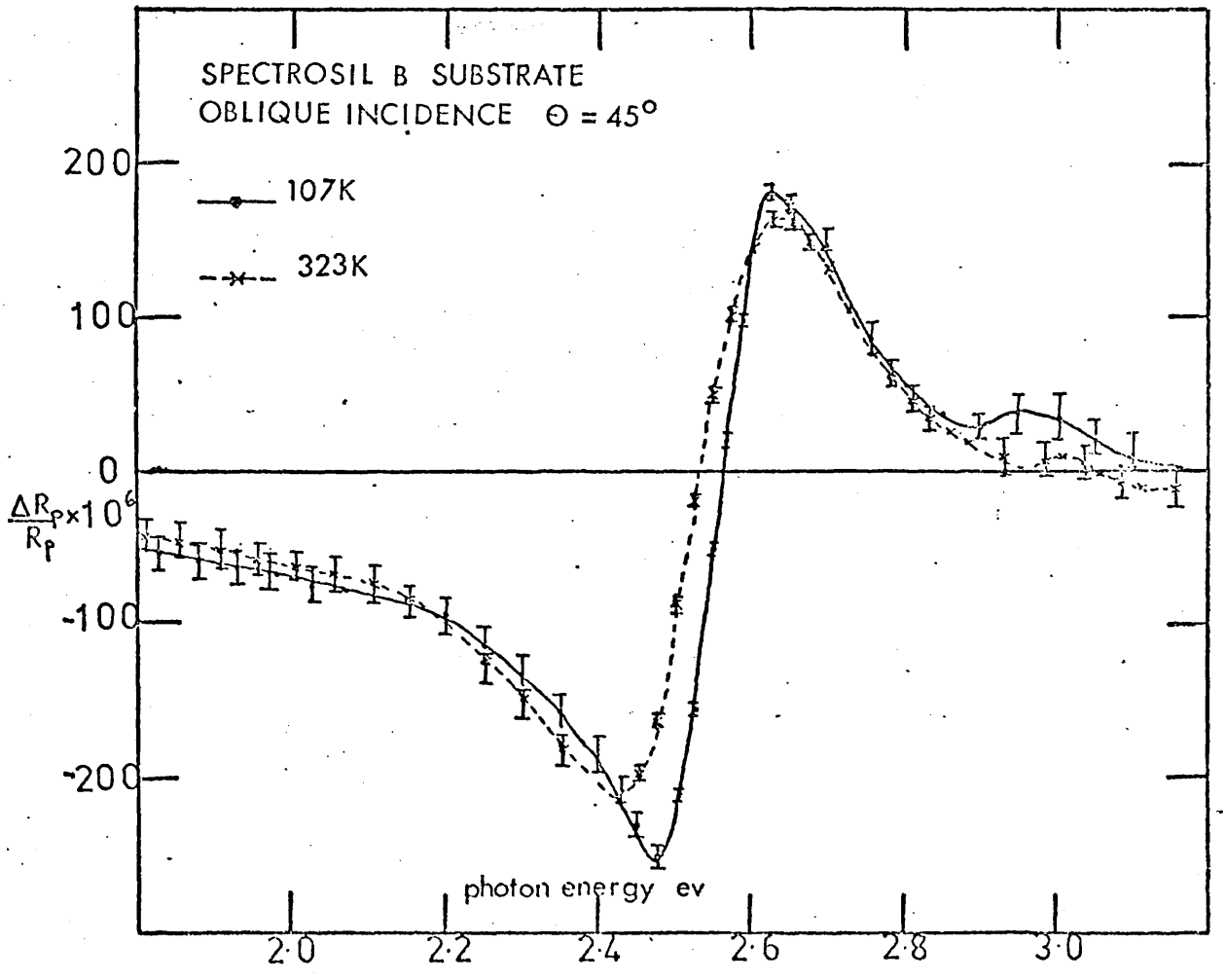

Figure (5.5) The (ΔRp/Rp) responses of a gold film deposited on a spectrosil substrate at 107K and 323K

	SPECTROSIL B	GLASS	GOLD
Expansion Coefficient per ^{o}C	0.45×10^{-6}	9.80×10^{-6}	15×10^{-6}

We see that Spectrosil B has a thermal expansion coefficient an order of magnitude less than that of glass. The gold film was grown on the quartz substrate under the same conditions as for the float glass substrate - however a slight difference in film thickness was noted. The film grown on the float glass substrate was 1430 Å thick and that on the quartz substrate 1350 Å thick. On repeating the optical measurements no difference in the peak positions or magnitude of the main peak shift with temperature was observed. This behaviour is shown in Figure (5.5).

At this point it is worth considering the foregoing results on this structure at 2.4 eV in the light of those obtained by Cheyssac (1973), who measured the thermally modulated reflectance, piezoreflectance and electroreflectance response on the same polycrystalline gold film. Cheyssac's results are shown in Figure (5.6) and we see that the peak in the thermoreflectance response near 2.4 eV is considerably sharper than the peak due to the piezoreflectance and electroreflectance response. Cardona (1969) has indicated that this behaviour suggests transitions to the Fermi surface as a possible cause of this structure. If this is so then the thermally modulated reflectance response at this energy would be due in large part to the "smearing" of the Fermi distribution as the temperature is raised. However, part of the structure will be due to strain, because the sample is constrained to the substrate and thermal expansion will cause shear stress. We see from Figure (5.6) that the electroreflectance response is not so sharp as the thermally modulated reflectance response. Prostak and Hansen (1967) attribute the occurrence of electromodulation in metals to a modulation of the free carrier concentration. The electron

Figure (5.6) Comparative modulation spectra of a polycrystalline gold film (Cheyssac 1973).

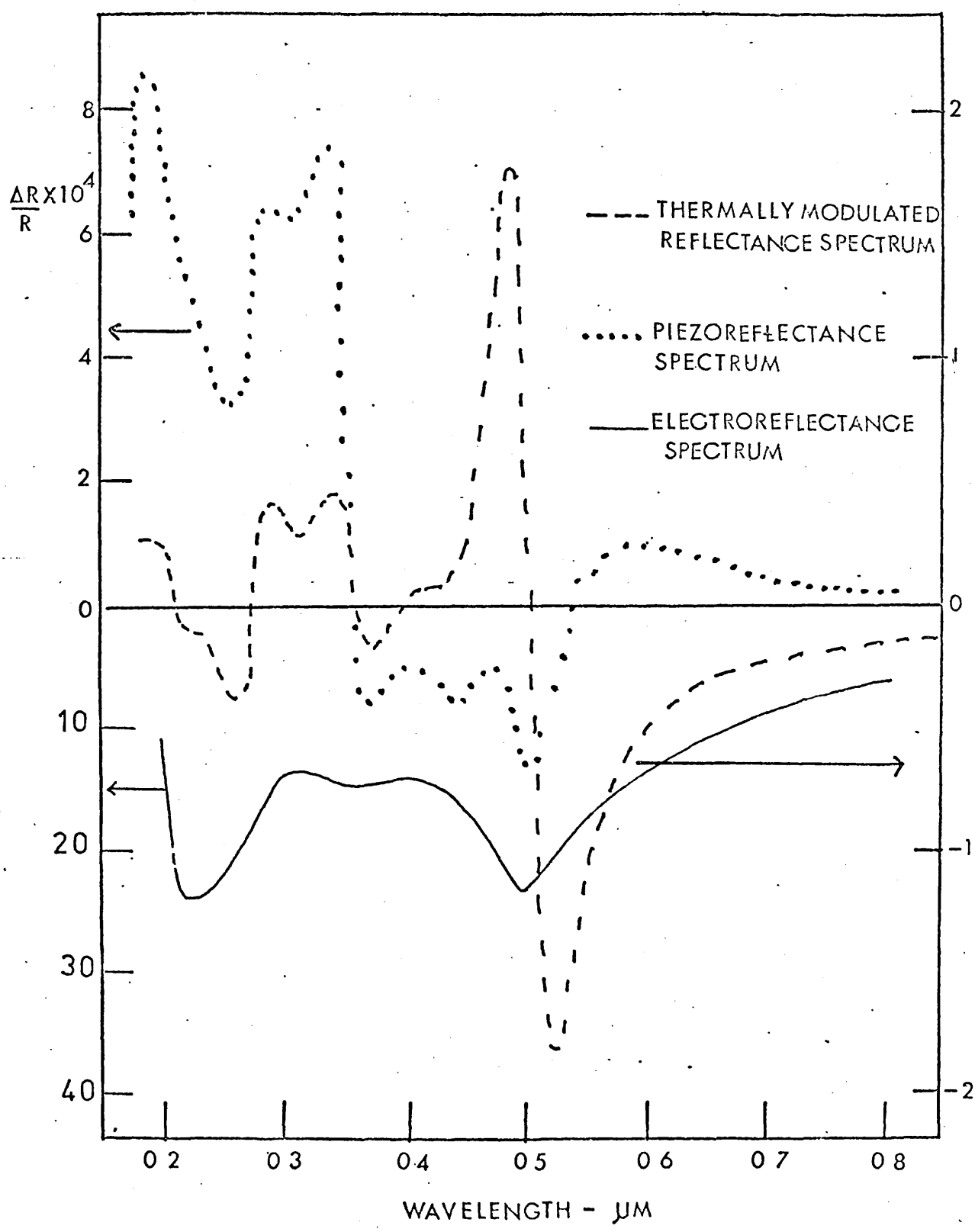

concentration, n, is related to the Fermi energy by

$$E_f = \hbar^2/2m\ (3\pi^2 n_e)^{2/3} \qquad (5.1)$$

where

E_f is the Fermi energy.

$\hbar$ is the reduced Planck's constant

m is the electron mass

n_e is the electron density

Clearly, a change in n will produce a change in the Fermi level.

(5.4) The thermally modulated $\Delta\varepsilon_1$ and $\Delta\varepsilon_2$ results

The changes in the real and imaginary parts of the dielectric constant $\Delta\varepsilon_1$ and $\Delta\varepsilon_2$ were computed by the method described in (2.5). The thermal modulation data was taken from the pen recorder readout in 0.025 eV steps and inserted in the computer program. In order to compute $\Delta\varepsilon_1$ and $\Delta\varepsilon_2$ it is still necessary to have some knowledge of the optical constants of the material. In the transformation of the thermally modulated reflectance data we have used the optical constants taken from Johnson and Christy (1972) and Pells and Shiga (1969). Although other workers have determined optical constants of gold films (Schultz and Tangherlini 1954, Theye 1970 and Irani et al. 1971), they do not cover such an extensive photon energy range. Although both Johnson and Christy, and Pells and Shiga measured n and k as a function of temperature for both gold and copper, measurements were not performed near 80K for gold. In computing $\Delta\varepsilon_1$ and $\Delta\varepsilon_2$ from thermal modulation measurements taken at 107K we have therefore had to use values of n and k derived from measurements made at 295K.

Figure (5.7) indicates the temperature modulated phase change $\Delta\psi_p(w)$ computed from equation (2.47) for the low and high temperature

Figure (5.7) The variation of $\Delta\psi p$, the temperature modulated phase change with photon energy.

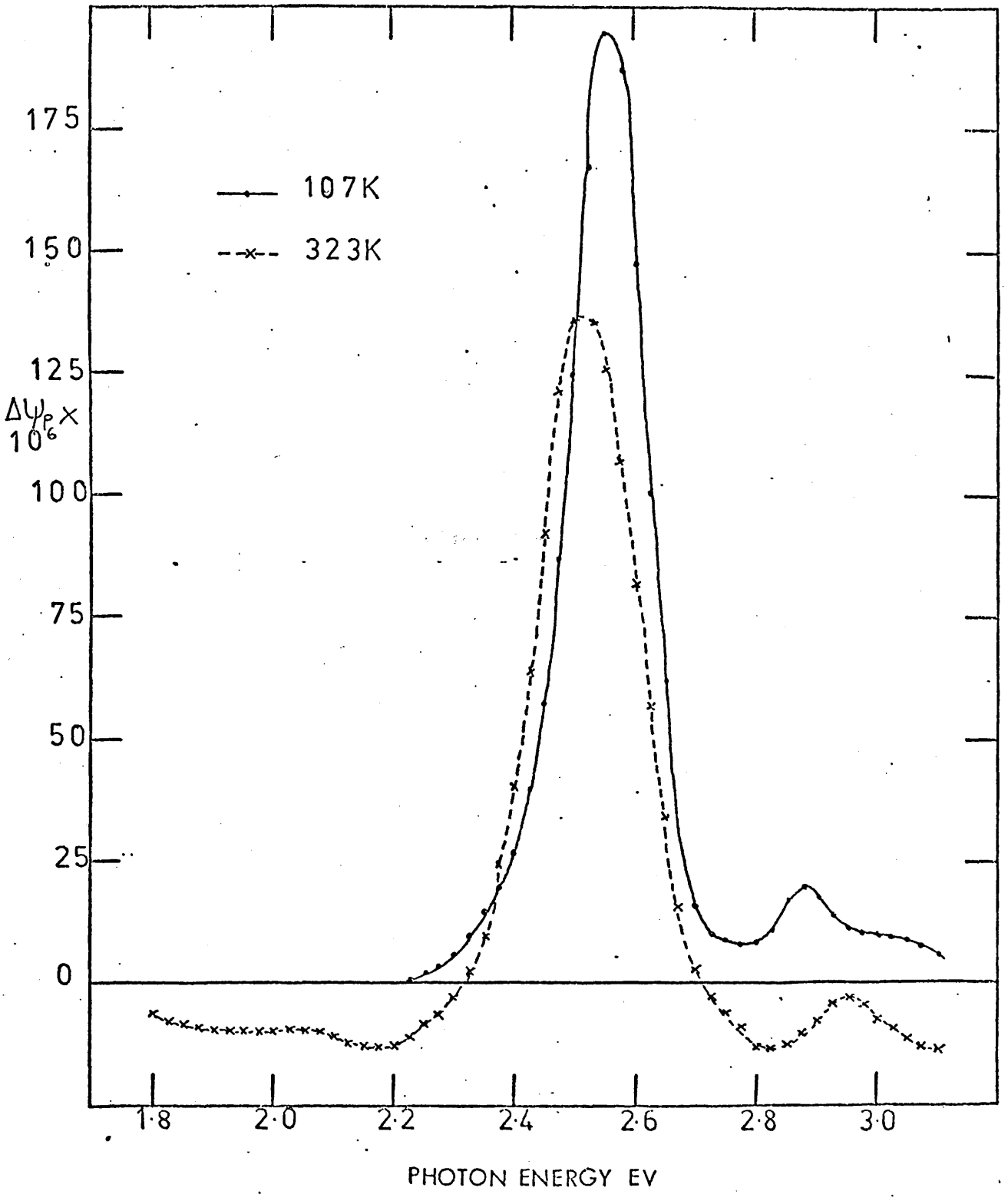

measurements. We note that the response has a principal peak at 2.50 eV for 323K, and at 2.55 eV for 107K, and the low temperature curve is again much sharper than the high temperature response. We also note that the subsidiary structure near to 3.0 eV seen in the modulated reflectance spectra appears again in the $\Delta\psi_p(w)$ curves and there is a shift to lower photon energies on lowering the temperature.

Figures (5.8) and (5.9) show the thermally modulated $\Delta\varepsilon_1$ and $\Delta\varepsilon_2$ spectra, the former is given for completeness, but the discussion will mainly be concerned with the $\Delta\varepsilon_2$ spectra since this parameter may be correlated with band structure calculations. The data shown here were computed using n and k values taken from Johnson and Christy (1972). The effect of using n and k from Pells and Shiga's(1969) measurements has already been discussed in (2.5) where it was shown that the spectral positions of the structures in the $\Delta\varepsilon_2$ curve were unchanged. The sharpening of the modulated reflectance response at low temperatures is repeated in the transformed results and a shift of 0.05 eV in the energy of the main peak is observed. A shift in the subsidiary peak to lower energy is also seen on lowering the temperature: at 323K it occurs at 2.950 eV, and at 107K it is at 2.875 eV.

We note that the observed peak positions in the thermal modulation $\Delta\varepsilon_2$ spectra are in good general agreement with previous thermal modulation results (Scouler 1967, Cardona 1969 and Rosei and Lynch 1972). We have not been able to detect the subsidiary peak at 3.2 eV observed by Scouler, probably because of the increasing noise in the detection system due to the reduced output of the quartz-iodine lamp in this region.

(5.5) The correlation of $\Delta\varepsilon_2$ with band structure calculations

The thermally modulated $\Delta\varepsilon_2$ spectra have been correlated with a relativistic augmented plane wave (R.A.P.W) band calculation for gold performed by Christensen and Seraphin (1971). The authors show that for

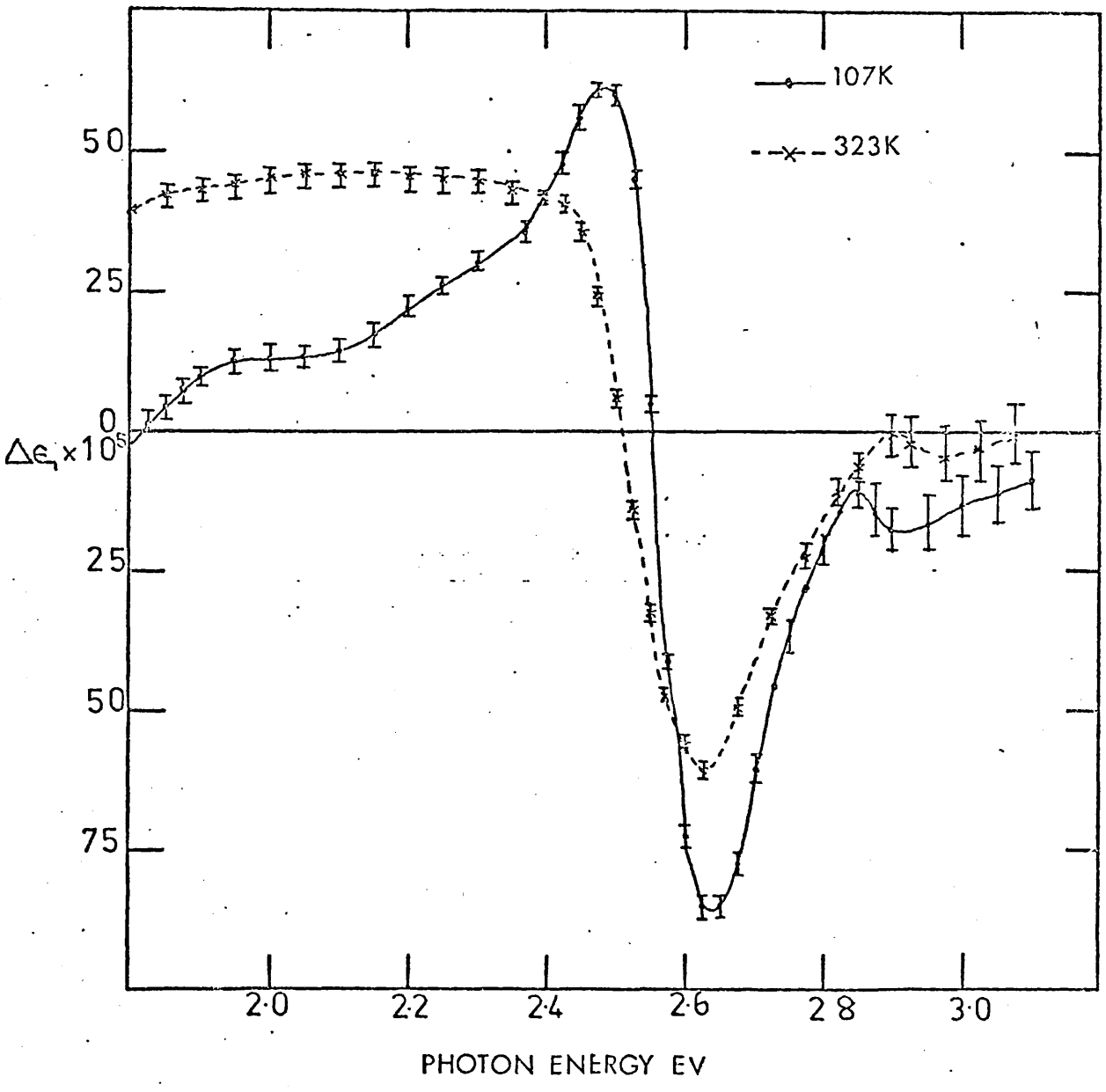

Figure (5.8) The thermally modulated $\Delta\epsilon_1$ spectra of gold at 107K and 323K.

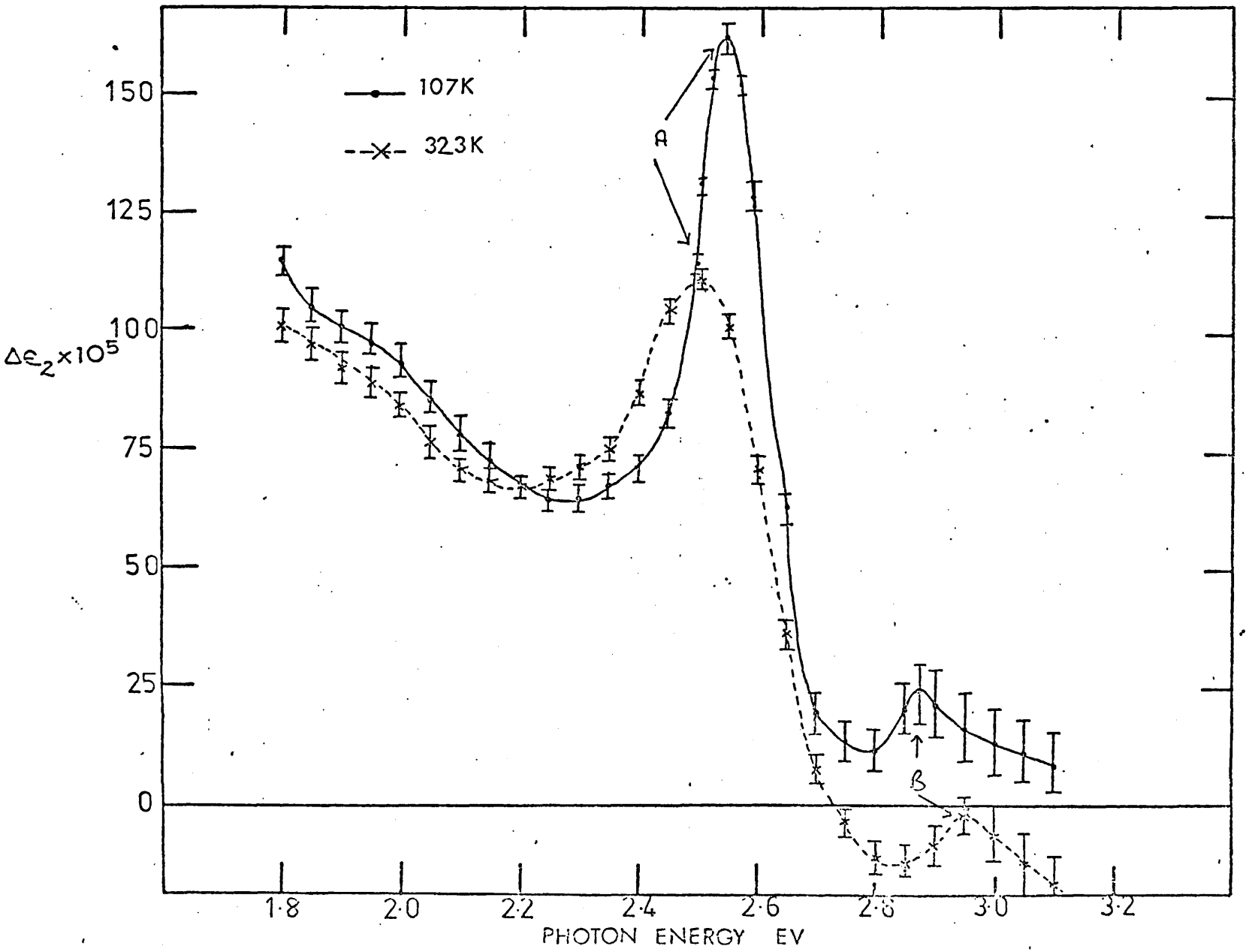

Figure (5.9)
The thermally modulated $\Delta\varepsilon_2$ spectra of gold at 107K and 323K.

gold which has atomic number Z = 79, relativistic effects are important and cause significant differences when compared with non-relativistic A.P.W. calculations (Jacobs 1968). Spin-orbit splitting of energy levels sometimes reaches values of the order of magnitude of the energy gaps. Although other R.A.P.W. calculations for gold have been performed (Sommers and Amar 1969, Kupratakuln 1970 and Ramchandani 1970) Christensen's calculation is the only one which gives eigen values of energy bands for both expanded (T = 920K) and normal volume lattices (T = 0K). This is particularly important, since temperature coefficients of some transitions may be interpolated from the results, which may then been compared with the experimentally determined coefficients from the thermal modulation measurements.

The results of Christensen and Seraphins' R.A.P.W. calculation are shown in Figure (5.10) and Figure (5.11) indicates the appropriately labelled first Brillouin zone of the face-centred cubic crystal lattice. The two peaks denoted by A and B in Figure (5.9) have been tentatively assigned by Christensen and Seraphin (1971) as

$$(Q_3 + Q_4)^5 \rightarrow E_f(Q_3 + Q_4)^6 \quad \text{Peak A}$$

and

$$\Delta_{6 \text{ or } 7}^2 \rightarrow E_f(\Delta_6^3) \quad \text{Peak B}$$

At this point we note that the shift of the structures A and B with temperature has not previously been observed in thermal modulation experiments on gold. However, although Scouler (1967) only made measurements at 120K he does comment that the position of the large negative peak in the thermally modulated reflectance response is shifted to higher energies relative to that observed in a room temperature piezoreflectance experiment on polycrystalline gold films (Garfinkel 1966). Scouler does not however, give the magnitude of the energy shift. Although Rosei and Lynch (1972) performed thermal modulation experiments at 120K and 340K on polycrystalline gold films they do not report any observed shift of peak position. This lack of observable shift with temperature in their

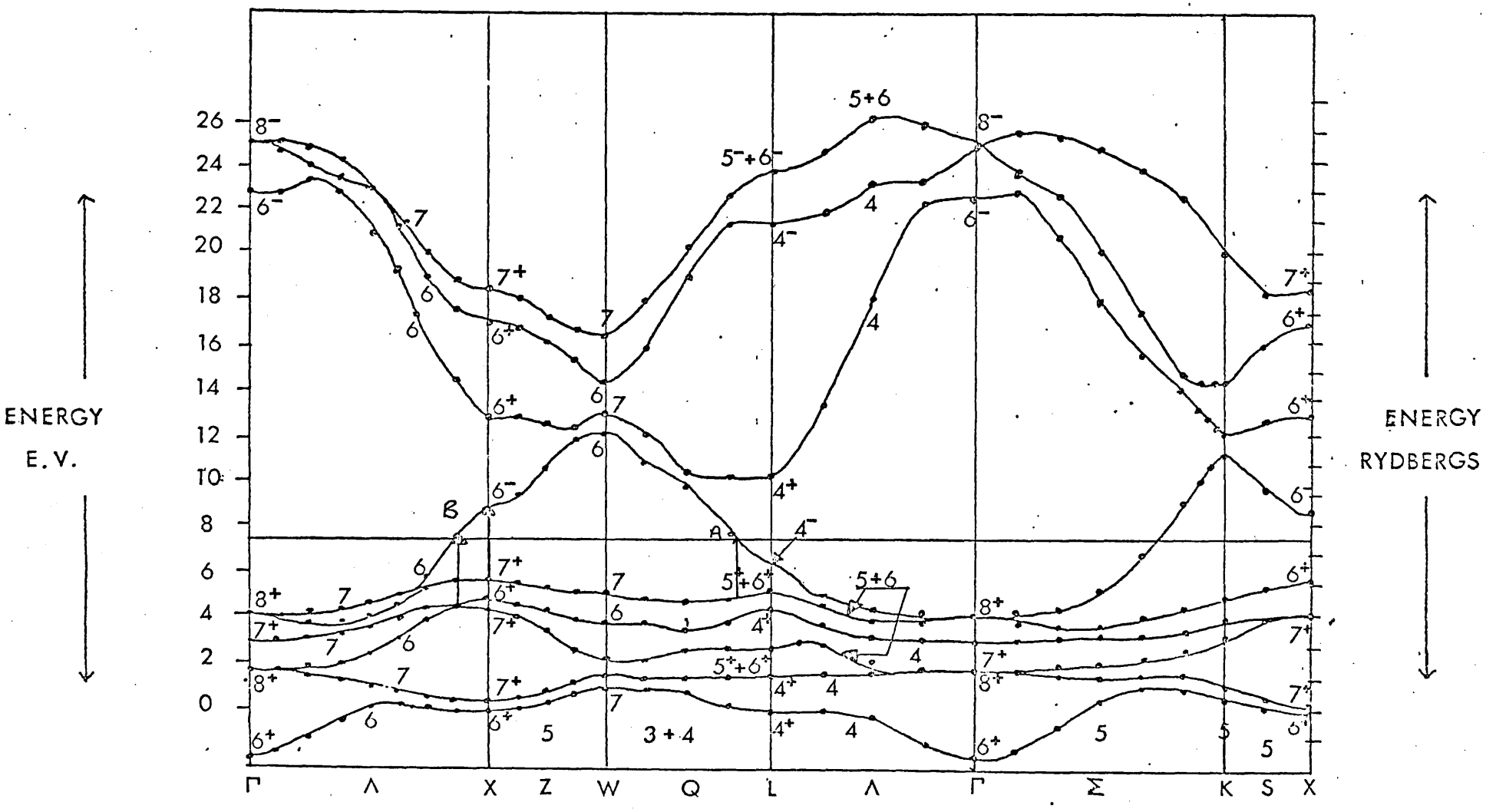

Figure (5.10) Energy bands of gold (Christensen and Seraphin 1971).

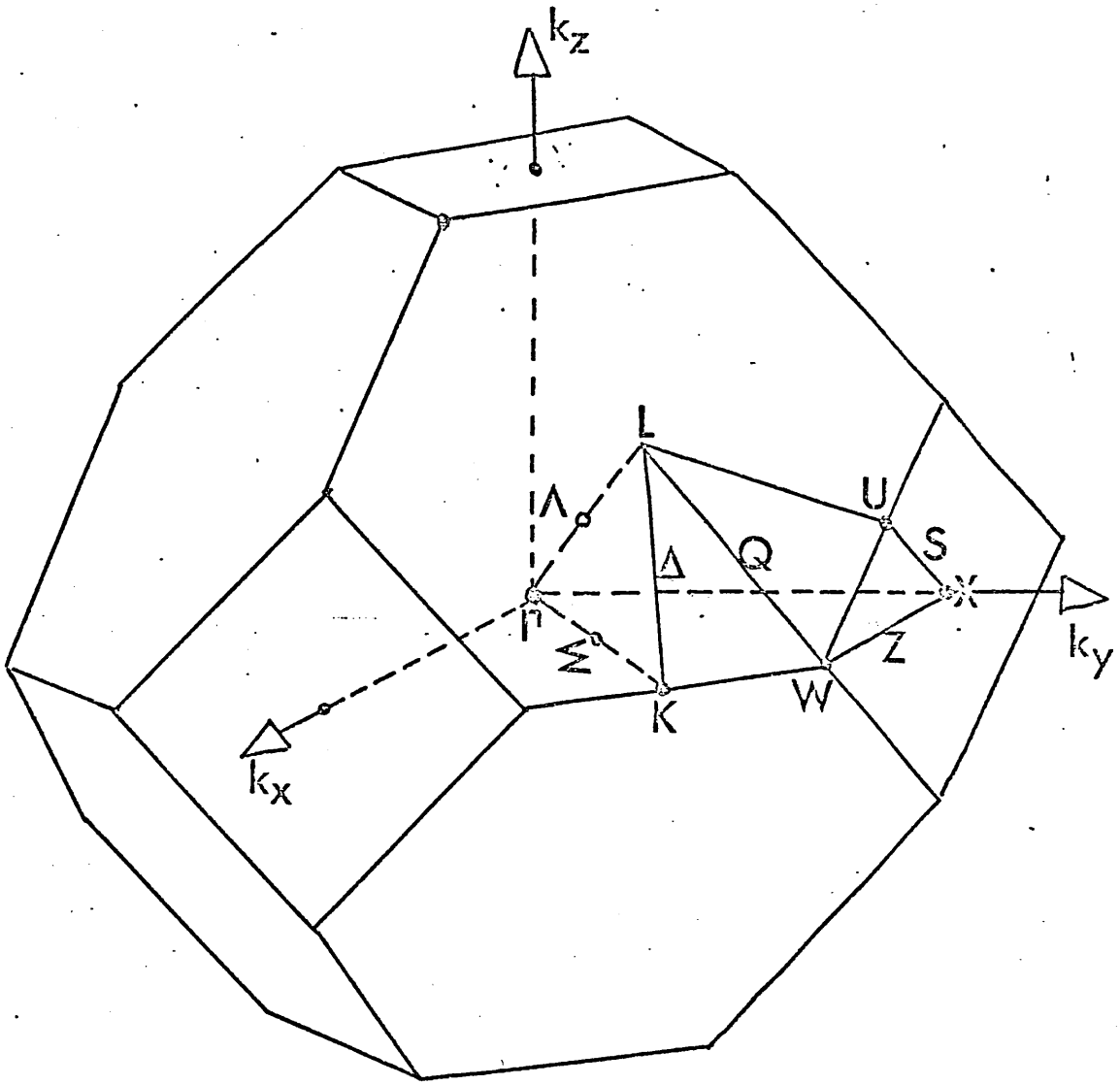

Figure (5.11) Labelled first Brillouin zone for the f.c.c. lattice.

experiments is difficult to explain but might be due to a rather lower energy resolution (estimated from their data as being $\sim$ 0.03 eV) in their optical measurements, than in the present work. We note also that measurements were performed on much thinner films - in the order 300 to 400 Å thick, the properties of which may differ from those of thick films.

Shifts in the principal absorption edge of gold have been observed by other workers using other modulation techniques. Welkowsky and Braunstein (1971) and Stokes et al. (1972) have observed a shift of -2.3×10^{-4} eV/K and -1.7×10^{-4} eV/K respectively in wavelength modulation experiments. It should be noted that these results indicate shifts in the $1/R(dR/dE)$ response with temperature. Although Welkowsky and Braunstein compute ε_2, values at 80K only are given and thus it is not possible to estimate the magnitude of the temperature shift of the main absorption edge. Grobman and Eastman (1972) performed a temperature modulated photoemission experiment and report a shift of the edge of the d band upward at a rate of 2 to 6×10^{-4} eV/K with respect to the Fermi energy E_f. However, these conclusions contradict those of Pells and Shiga (1969) who polarimetrically determined the optical constants of gold, and found that the principal absorption edge at 2.5 eV broadened while the central position remained constant, from 295K to 770K. On further numerical analysis of their data Winsemius (1973) does find a shift of the edge with temperature. By plotting:-

$$(\varepsilon_2(470K) - \varepsilon_2(295K))/(470-295)$$

and

$$(\varepsilon_2(570K) - \varepsilon_2(470K))/(570-470)$$

against photon energy, which he calls the thermovariation spectrum, a response qualitatively similar to the thermally modulated $\Delta\varepsilon_2$ response is seen. From this analysis Winsemius found a shift of the principal absorption edge of -0.02×10^{-4} eV/K. However it should be noted that such a shift is only seen after the experimental data had been reduced and is not a direct result of the experiment, unlike the measurements obtained

from the modulation experiments. From the expanded lattice R.A.P.W. band calculation for gold, Christensen (1971) calculated a shift of -0.5×10^{-4} eV/K assuming a completely linear temperature dependence of the lattice expansion. In the present experiment the observed peak shift is -2.3×10^{-4} eV/K. It can be seen that all the experimental results for the temperature shift, with the exception of the thermovariation results of Winsemius, are roughly an order of magnitude larger than the theoretically estimated shift, (Winsemius results are an order of magnitude less than the theoretical value). This discrepancy may be due to the method by which Christensen and Seraphin estimated the order of magnitude of the shifts in the conduction states due to thermal vibrations. The authors themselves admit the model is rather crude and in the calculation of some of the parameters involved, the elastic constants of gold are needed. The authors use elastic constants derived from the experiments of Neighbors and Alers (1958) at very low temperature and always apply the same elastic constants, although in reality they vary with temperature.

Scouler (1967), Rosei and Lynch (1972) and Cheyssac (1973) have observed subsidiary structure in $\Delta\varepsilon_2$ between 2.7 and 3.0 eV in thermal modulation experiments. In the present thermal modulation experiment, subsidiary structure has been observed at 2.95 eV at 323K, and 2.875 eV at 107K. Structure at this photon energy is also seen in the low temperature thermovariation spectra calculated by Winsemius. As already discussed, Christensen assigns this structure as being due to transitions to the Fermi level. Grobman (1972) in a photoemission experiment has confirmed that the structure originates from initial states in the d bands. The thermovariation spectra calculated by Winsemius indicates that the structure moves to higher photon energies as the temperature of the sample increases. This positive shift with temperature is also noted in the present thermal modulation work, the magnitude of the shift being $+3.4 \times 10^{-4}$ eV/K. According to Christensen's expanded lattice band calculations, such a relatively large positive temperature induced shift

is expected by transitions near the X symmetry point. From Figure (5.10) we see that the transition $X_{7_3}^{+} \rightarrow X_{6}^{-}$ (where 3 indicates the third 7^{+} band from the abscissa) is located at 3.01 eV at 0K. This transition is located at 3.11 eV at 920K i.e a shift of $+ 1.1 \times 10^{-4}$ eV/K. From Christensen's results it is not possible to calculate the temperature coefficient of the transition Δ_6^2 or $7 \rightarrow E_f(\Delta_6^3)$. However we note from Christensen's work that on increasing the temperature the Fermi energy moves to lower energies and the d band is considerably broadened. This implies that the energies of transitions from d bands to the Fermi surface will decrease as the temperature is increased. This assignment to transitions that do not involve the Fermi surface is further supported by the comparative modulation studies made by Cheyssac (1973), the responses being shown in Figure (5.6). The structure centred at 3.0 eV in the thermoreflectance response is at least the same order of magnitude as that in the piezoreflectance response. This behaviour indicates that lattice expansion is the dominant influence. In their expanded lattice band calculation for gold Christensen and Seraphin (1971) find that the states at the regions near the X and L symmetry points are the most sensitive to strain. These are just the regions where the Fermi surface exhibits the larges deviations from spherical shape (Schoenberg and Roaf 1962), indicating that electrons on the Fermi surface sense the crystal potential particularly strongly. In the present thermal modulation work we see from Figure (5.9) that the structure in $\Delta\varepsilon_2$ around 2.90 eV is not sharpened to the same degree as the principal peak is on lowering the temperature. Our results seem to indicate that the transition is of the X type since we have observed a positive shift in energy with increasing temperature of the structure near 2.90 eV, also a scan of the band diagram in Figure (5.10) does not reveal another transition having this energy. To come to more definite conclusions would require further work on the origin of the structure.

(5.6) The preparation of the copper films

Like the gold films, all the copper films were prepared in an ordinary high vacuum environment and the growth parameters of a typical film are summarized below:-

(i) The films were grown from a 99.9% pure sample of copper wire obtained from Johnson and Matthey, the film being deposited on float glass substrates at room temperature from a molybdenum boat at a source-substrate distance of 8 cm.

(ii) Outgassing procedures were the same as those employed in the growth of the gold films, the vacuum chamber being allowed to attain its base pressure after the outgassing procedure had been completed.

(iii) The film was deposited in one evaporation at the rate of deposition of 20 Å sec^{-1} for a boat current of 70 amps.

Plate (5.2) is a high energy reflection electron diffraction pattern of a typical copper film. The film has a face-centred cubic structure. The pattern has been indexed and we note the existence of additional rings designated by A and B in Plate (5.2) between the bright central spot and the (111) reflection, and between the (200) and (220) reflections. Pashley and Stowell (1963) have observed such extra rings in electron diffraction patterns obtained from polycrystalline thin films of gold and have attributed these rings to the occurrence of double diffraction at microtwin bounderies or to the existence of a hexagonal close packed phase. In the present work it has not been possible to determine whether the extra rings are due to double diffraction or the occurrence of the hexagonal close packed phase since the visibility of the patterns obtained was poor and prevented accurate measurements being made.

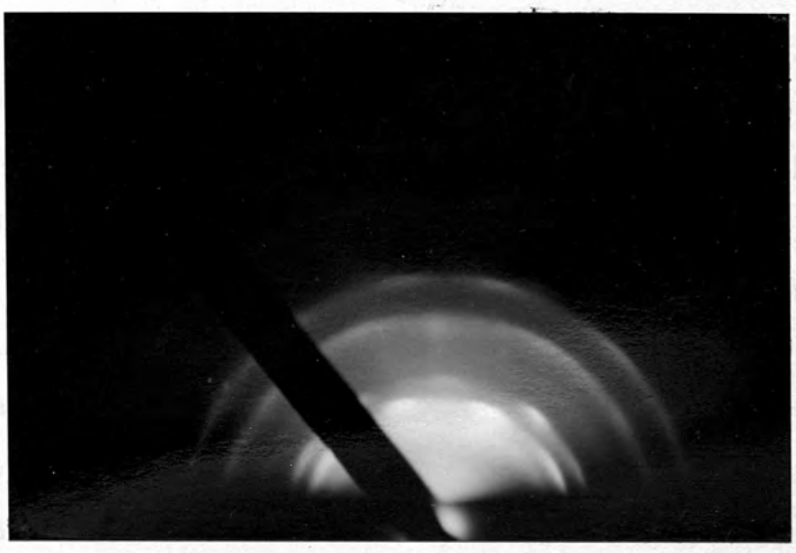

PLATE (5.2) High energy reflection electron diffraction pattern of a copper film (accelerating voltage 100KV).

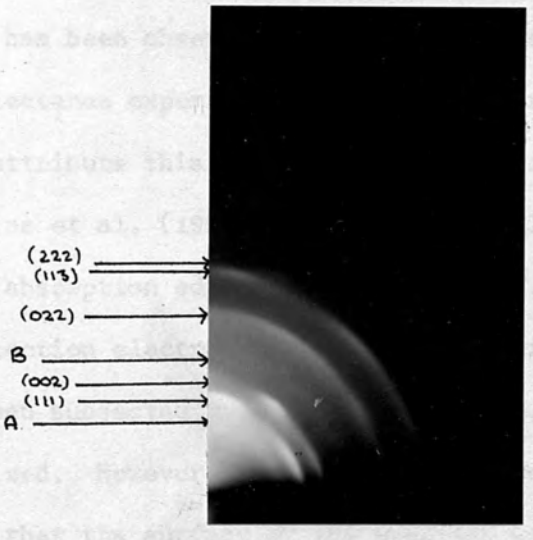

(5.7) The thermally modulated reflectance response of copper films

The measurements were made in the same manner as for the gold films. It was found that in some cases electrical leads could not be indium soldered to the film and the arrangement of copper pads described in (3.7) was used to make electrical contact to the film. The sample was again exposed to the atmosphere on removal from the growth system. Some preliminary thermal modulation experiments were performed in air at near normal incidence using the optical cell arrangement described in (3.5). All measurements were performed at room temperature. All the films showed signs of overheating (a discolouration was observed) after being subjected to thermal modulation. However, a thermal modulation response was measured and is shown in Figure (5.12a). We note that the response consists of two main peaks at 2.125 eV and 2.275 eV together with subsidiary structure at 2.025 eV. Of the five films whose thermally modulated reflectance response were measured in this manner all spectra displayed structure near to 2.0 eV, but in some cases it was more marked than in others. Figure (5.12b) indicates the thermally modulated $\Delta\varepsilon_2$ response computed using optical constants reported by Johnson and Christy (1972). The response consists of a main peak centred at 2.175 eV and a subsidiary peak at 2.025 eV. Subsidiary structure has been observed by Garfinkel et al. (1966) at 2.0 eV in a piezoreflectance experiment performed in air on polycrystalline copper films. They attribute this structure to the existence of cuprous oxide (Cu_2O). Nikitine et al. (1968) have experimentally observed that cuprous oxide has an absorption edge starting at 2.0 eV. In the present work high energy reflection electron diffraction analysis was attempted after the film had been subjected to thermal modulation, to ascertain if the copper had been oxidized. However, no clear diffraction patterns were observed, indicating that the surface of the specimen was amorphous or had a very small crystallite size.

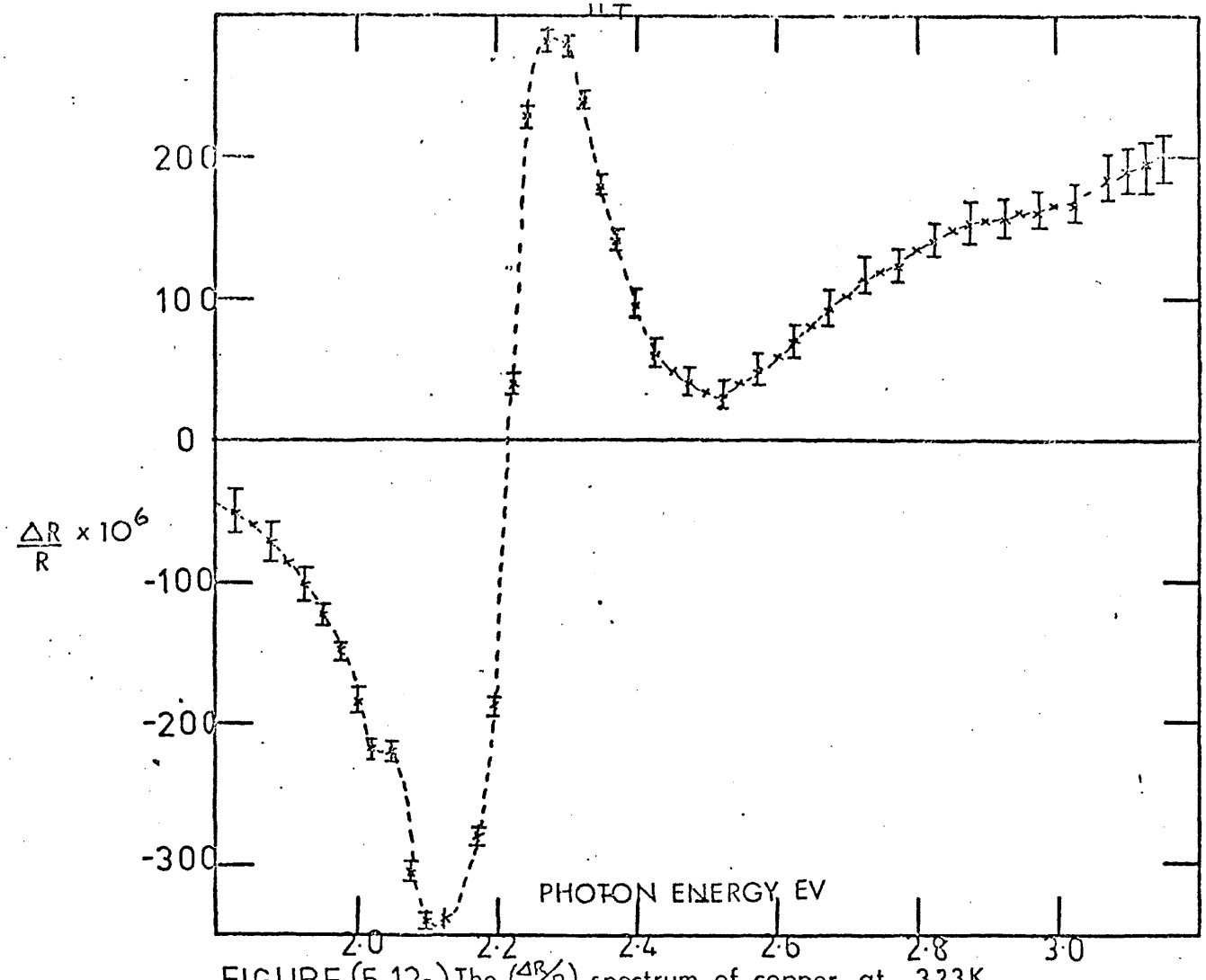

FIGURE (5·12a) The $(\Delta R/R)$ spectrum of copper at 323K

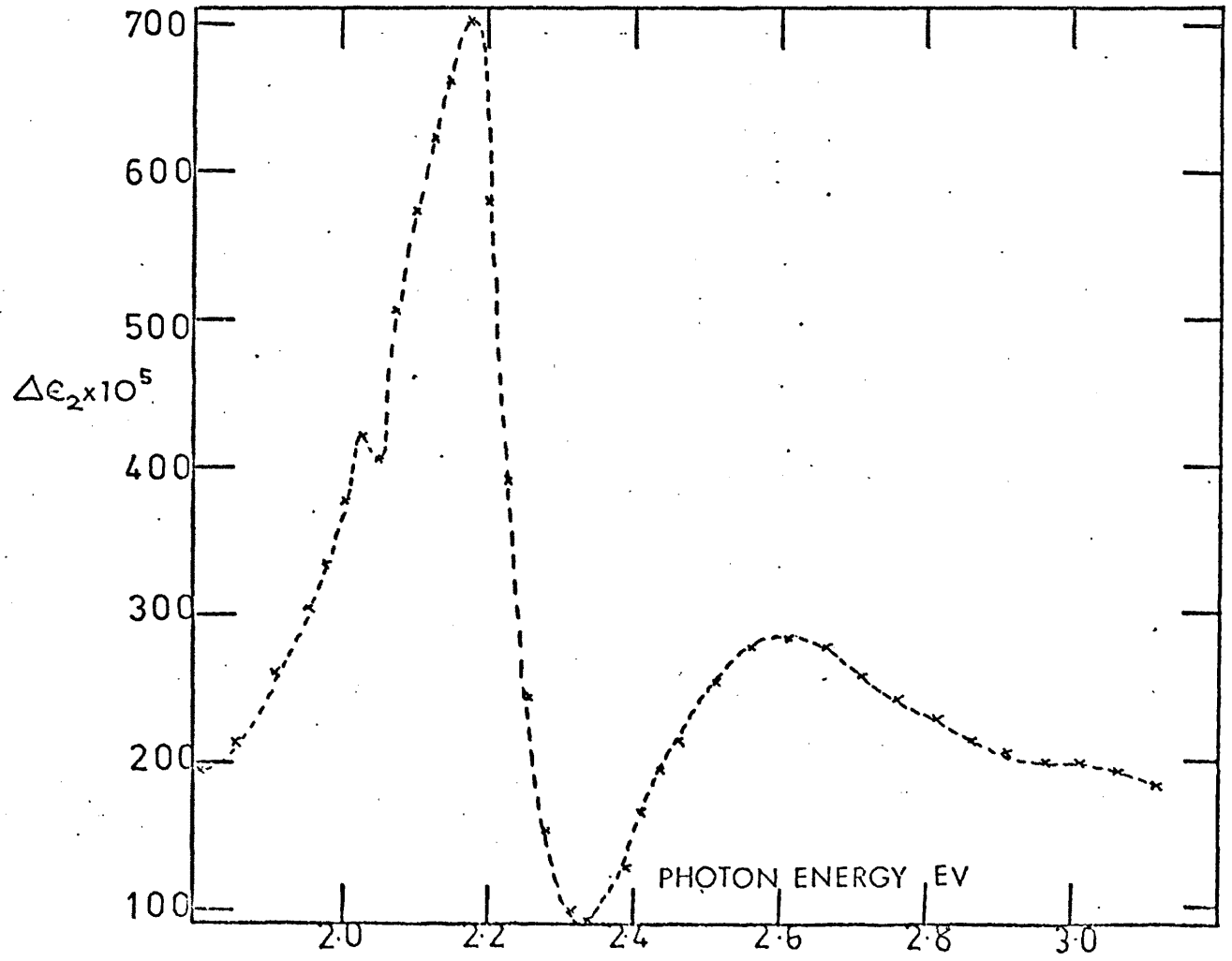

FIGURE (5·12b) The thermally modulated $\Delta\epsilon_2$ spectrum of copper

All further measurements on the copper films were made in the O.H.V. environment at a 45° angle of incidence. Figure (5.13) shows typical thermally modulated reflectance responses of polycrystalline copper films at 323K and 107K, powers of 6.3 watts and 1.3 watts being respectively dissipated in the sample. The response consists of two peaks located at 2.125 eV and 2.275 eV at 323K, and 2.175 eV and 2.275 eV at 107K. Subsidiary structure is seen at 2.55 eV and 2.575 eV at 323K and 107K respectively. As in the case of gold, the dominant structures in the curves are considerably sharpened on lowering the temperature of the sample. The position of the large negative peak is shifted by - 0.05 eV, the position of the positive peak remaining at the same energy. It is interesting to compare the modulated reflectance at 323K in Figure (5.13a) with that obtained in air in Figure (5.12a). We see that apart from the disappearance of the structure near 2.0 eV the main peak positions are located at the same photon energy. However at higher photon energies the size of the $(\Delta R/R)$ response measured in air is considerably greater than that of the $(\Delta Rp/Rp)$ response measured in vacuum. The structure near 2.55 eV is absent in the air measurements. It would appear that the effect of a possible oxide layer on the film surface still allows the main absorption peak of the pure metal to dominate the spectrum although there is considerable difference in the results in the ultra-violet end of the spectrum.

(5.8) The thermally modulated $\Delta\varepsilon_1$ and $\Delta\varepsilon_2$ spectra

The changes in the real and imaginary parts of the dielectric constant $\Delta\varepsilon_1$ and $\Delta\varepsilon_2$ were computed as before. Optical constant data was taken from Pells and Shiga (1969) and Johnson and Christy (1975). Figure (5.14) indicates the temperature modulated phase change $\Delta\psi_p(w)$ computed using Johnson and Christy's n and k values. We note that the response has a principal peak centred at 2.20 eV at 323K, and at 2.25 eV at 107K. Subsidiary structure is seen at 2.525 eV and 2.5000 eV at 323K and 107K

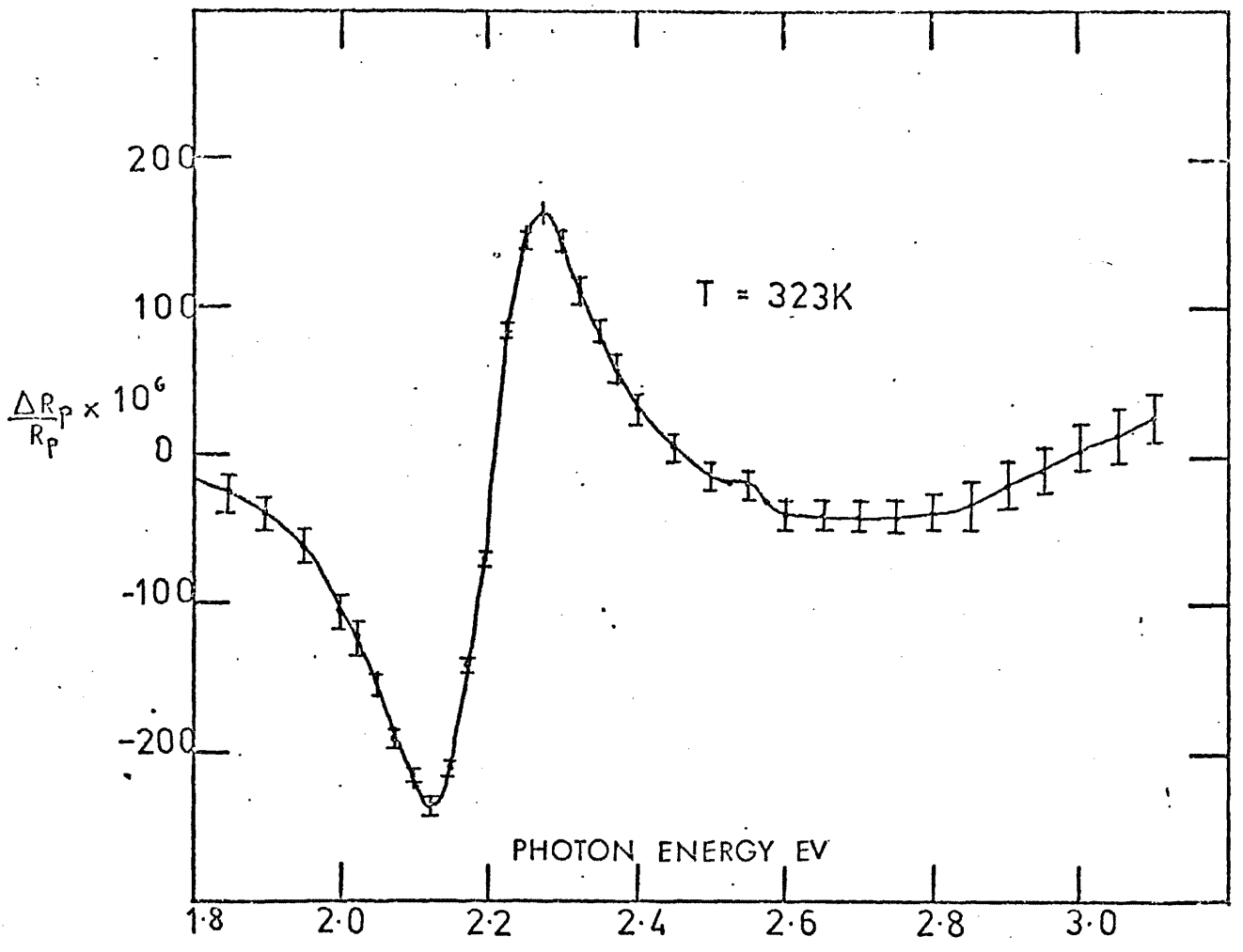

Figure (5.13a) The (ΔRp/Rp) spectrum of copper at 323K

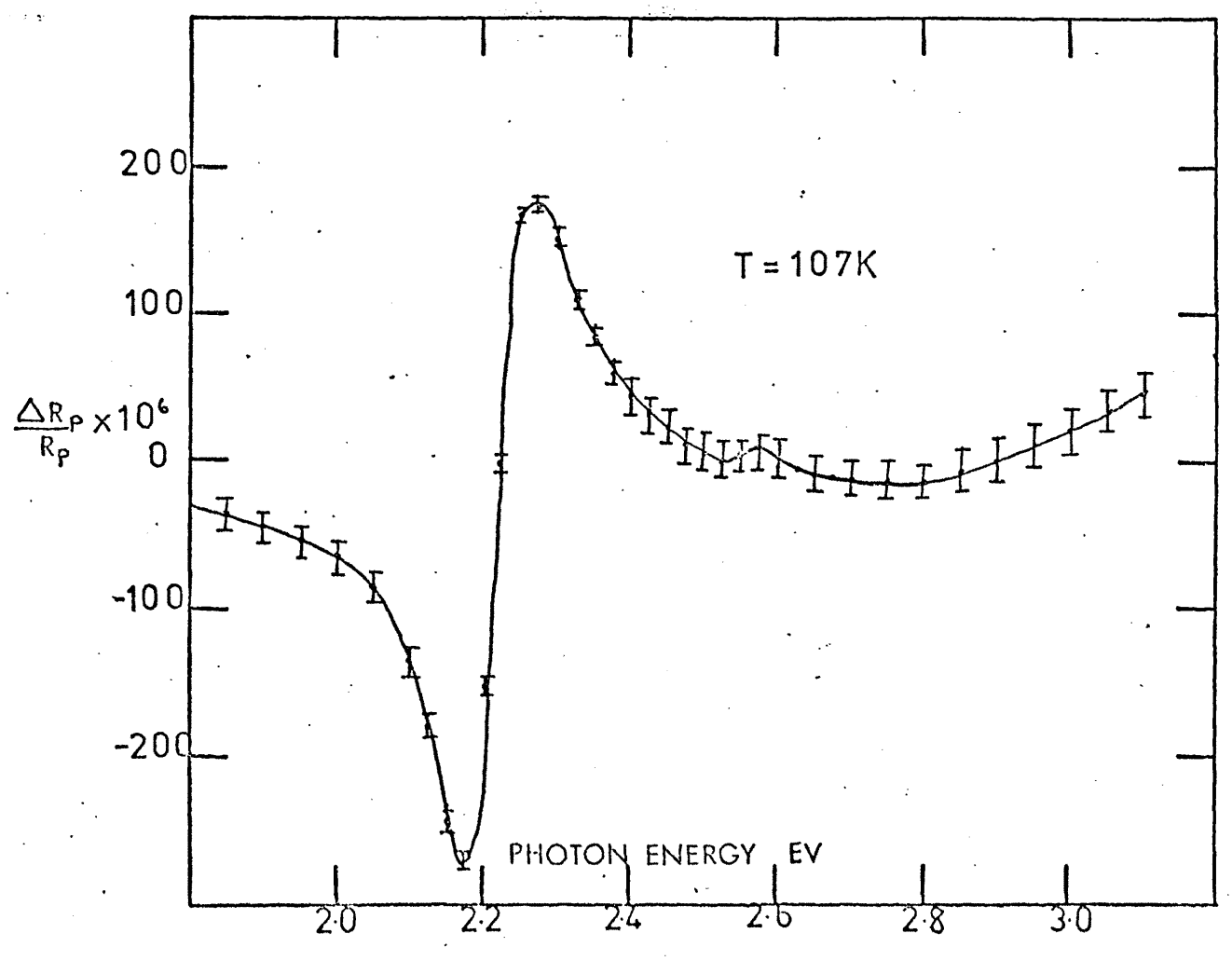

Figure (5.13b) The (ΔRp/Rp) spectrum of copper at 107K.

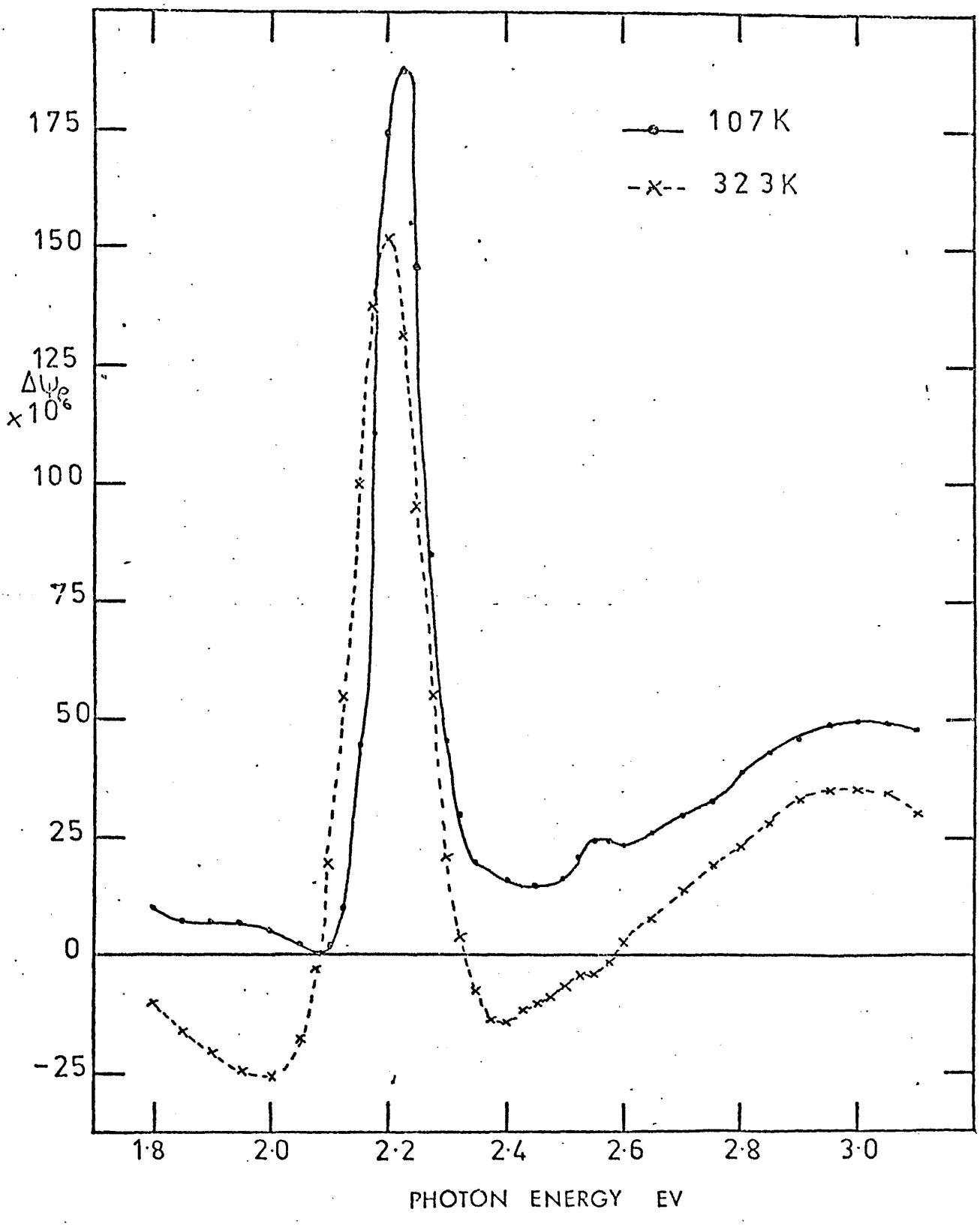

Figure (5.14) The variation of $\Delta\psi p$ with photon energy for copper.

respectively. Figures (5.15a) and (5.15b) show the effect of the differing sets of optical constants on the $\Delta\varepsilon_2$ spectra. We see that the principal peak at 323K is located at 2.125 eV using n and k from Pells and Shiga and at 2.175 eV using data from Johnson and Christy. At 107K the peaks are located at 2.175 eV and 2.200 eV. The spectral positions of the subsidiary structure seen near 2.55 eV is unaffected by the different sets of optical constants. The discrepancy in location of peak positions is not surprising since Pells and Shiga's values of ε_2 are as much as 50% larger than those of Johnson and Christy's. It is however perhaps surprising that the spectral position of the subsidiary structure near to 2.55 eV is unaffected by the different sets of optical constants. Close inspection of Pells and Shiga's optical constants and Johnson and Christy's optical constants reveals that there is a 4% difference in k values and only a 3% difference in n values at 2.55 eV. At 2.2 eV, the photon energy of the principal peak, the spectral position of which is affected by the different sets of optical constants, there is a 22% difference in n values and a 12% difference in k values. It is suggested that the large difference in ε_2 values derived by Pells and Shiga and Johnson and Christy may be due to the methods of surface preparation of the sample. Johnson and Christy made reflection and transmission measurements on thin copper films $\sim$ 300 to 500 Å thick, in an ordinary high vacuum system $\sim 10^{-6}$ torr. Pells and Shiga made polarimetric measurements on samples which were mechanically polished and then annealed under ultra-high vacuum 10^{-8} to 10^{-9} torr. Their polarimetric method of determining n and k has been shown to be highly dependent on good surface preparation (Roberts 1960). For these reasons more credance is placed on the $\Delta\varepsilon_1$ and $\Delta\varepsilon_2$ results obtained using Johnson and Christy's n and k data. For completeness, the $\Delta\varepsilon_1$ spectra are shown in Figure (5.16). We note that the sharpening of the modulated reflectance response at low temperature is repeated in the transformed $\Delta\varepsilon_2$ results and a shift of $-0.025 + 0.004$ eV in the energy of the main peak is observed

Figure (5.15a) The thermally modulated $\Delta\varepsilon_2$ spectra of copper at 323K.

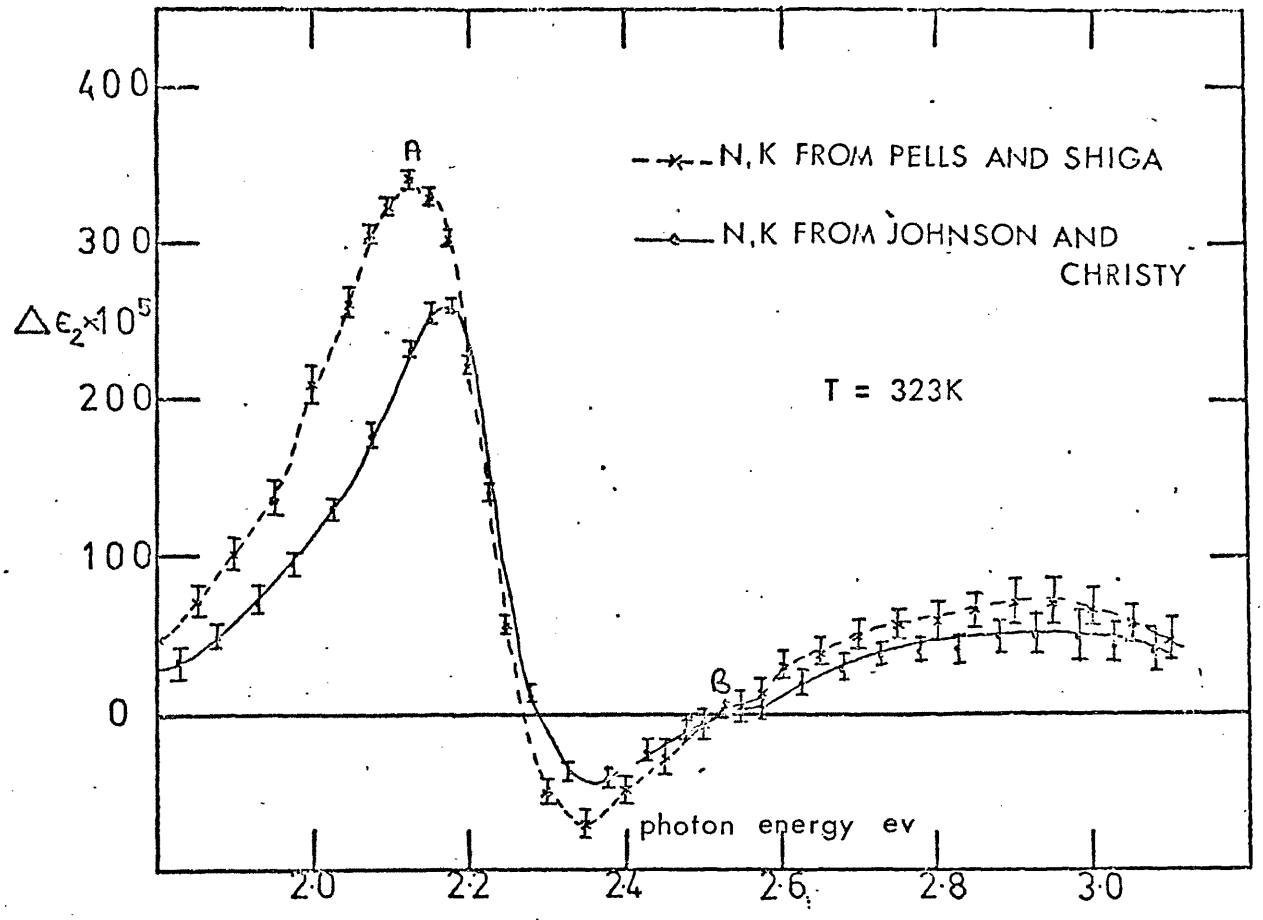

Figure (5.15b) The thermally modulated $\Delta\varepsilon_2$ spectra of copper at 107K.

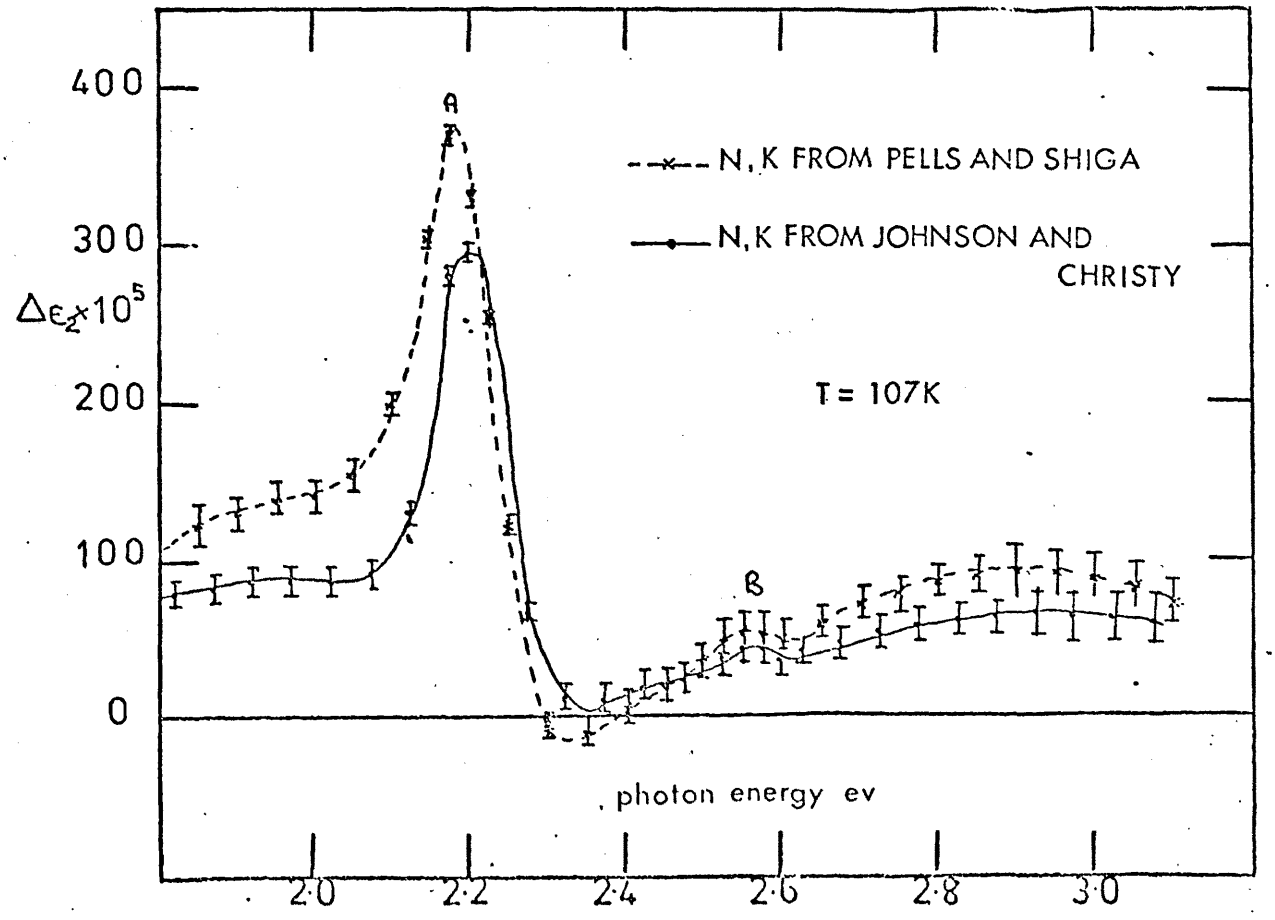

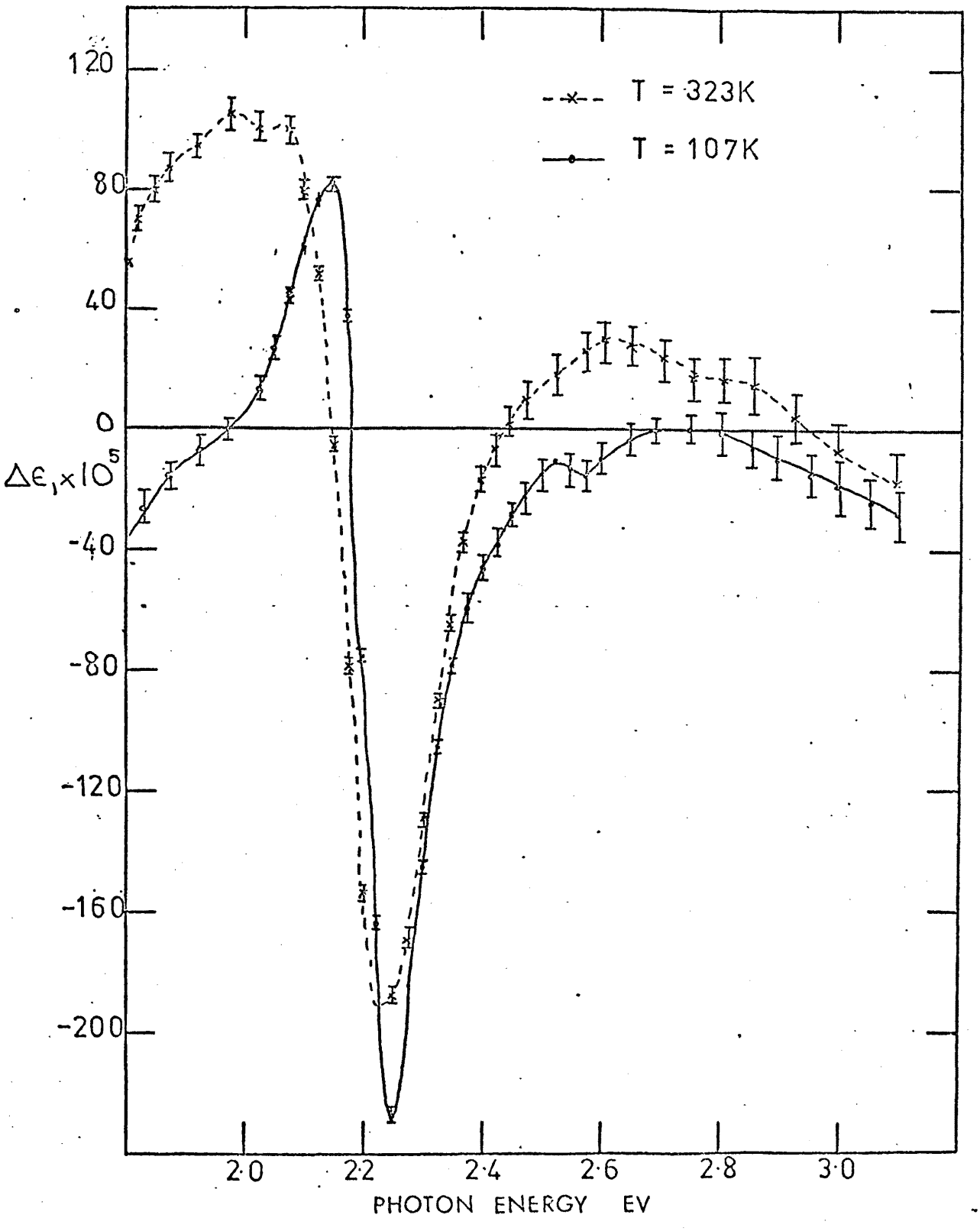

Figure (5.16) The thermally modulated $\Delta\epsilon_1$ spectra of copper at 107K and 323K.

(- 0.050 ± 0.004 eV. for Pells and Shiga's n and k). A shift, and considerable sharpening, of the subsidiary peak is also seen on lowering the temperature. At 323K it is centred at 2.538 eV and at 107K at 2.563 eV. We note that the observed main peak positions in the thermal modulation $\Delta\varepsilon_2$ spectra are in good agreement with previous thermal modulation results (Rosei and Lynch 1972). However, Rosei and Lynch make no specific reference to structure near 2.55 eV, although in their $\Delta\varepsilon_2$ curves at 120K and 350K a shoulder appears near this photon energy.

(5.9) The correlation of $\Delta\varepsilon_2$ with band structure calculations

The thermally modulated $\Delta\varepsilon_2$ spectra of copper have been correlated with a non-relativistic augmented plane wave (A.P.W.) band calculation performed by Burdick (1963) (Relativistic effects are considered to be unimportant in the case of copper since Z, the atomic number = 29). This band structure calculation is in excellent qualitative agreement with de Haas-van Alphen effect Fermi surface measurements (Shoenberg 1962). The results of Burdick's calculation are shown in Figure (5.17). The two peaks denoted by A and B in Figures (5.15a) and (5.15b) have been tentatively assigned as

$$L_3(Q_+) \rightarrow E_f(L_2') \qquad \text{Peak A}$$

$$L_3(Q_-) \rightarrow E_f(L_2') \qquad \text{Peak B}$$

At this point we note that the shift or the structures A and B with temperature has not previously been observed in any modulation experiment. Rosei and Lynch's thermal modulation experiment detected no shift in the principal absorption peak on lowering the temperature of the sample, this result has already been discussed in (5.5). Similarly Welkowsky and Braunstein (1971), in their wavelength modulation experiment, found no shift of the principal absorption edge of copper with temperature. The absence of a shift is difficult to explain since they quote the energy

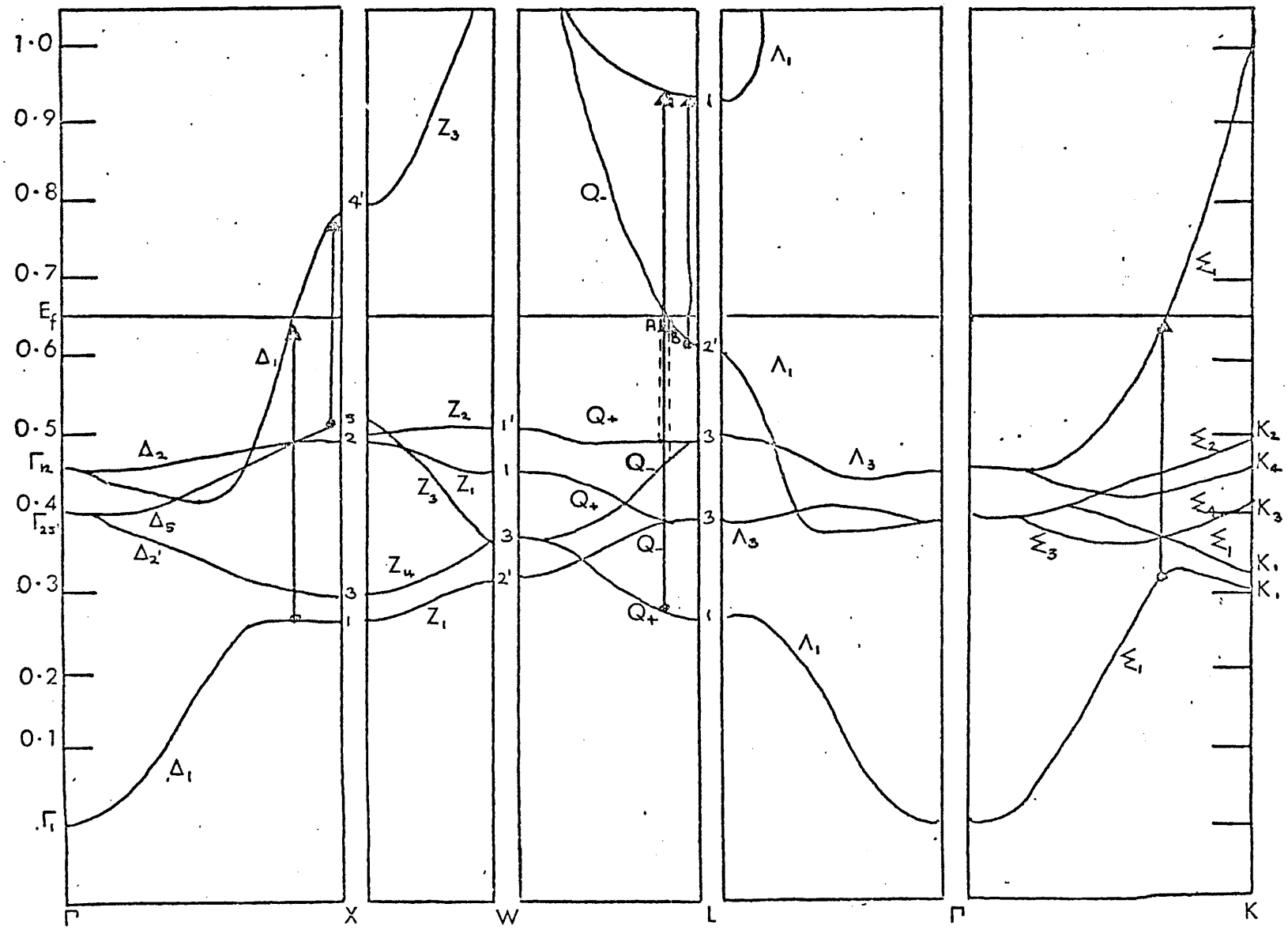

FIGURE (5·17) Energy bands of copper (Burdick 1963)

resolution of their system as 0.003 eV, which is only marginally less than the resolution in the present thermal modulation experiment. Pells and Shiga (1969), using a polarimetric method, found no shift in the absorption edge with temperature, although Johnson and Christy (1975) found that the onset of interband transitions occurs at lower photon energies as the temperature of the sample is decreased.

Expanded lattice band structure calculations for copper have been performed by several workers. Snow (1973), using a self-consistent augmented plane wave method, finds that as the temperature increases the Fermi energy moves to lower energy and the transition $E_f \rightarrow L_3$ (that signifying the principal absorption edge) moves to lower energies. Davis (1968) using a Korringa-Kohn-Rostoker (KKR) method concludes that the transition moves to lower energies as the temperature increases. Since both workers merely give results for various percentage volume expansions it is difficult to estimate the temperature coefficients of the shifts. Neither worker gives any indication of the temperature dependence of the $L_3(Q_-) \rightarrow E_f(L_2')$ transition.

(5.10) Summary of the gold and copper data

The thermally modulated optical properties of polycrystalline thin films of gold and copper have been studied. The observed structures in the thermally modulated $\Delta\varepsilon_2$ spectra of both metals are in good general agreement with previously published results. However, a shift in the principal absorption edge with temperature for both elements has been observed. This shift, although predicted theoretically in expanded lattice band structure calculations has not previously been observed in thermal modulation experiments.

CHAPTER VI

The thermally modulated optical properties of opaque films of gadolinium, terbium, dysprosium and erbium

6.1 Introduction

In this chapter the thermally modulated optical properties of opaque ($\sim$ 2000Å) films of gadolinium, terbium, dysprosium and erbium are discussed. The electronic and optical properties of the rare earth metals have been principally studied by the following experimental techniques: reflection spectroscopy (Krizek 1975, Meyers 1976, Miller 1974), magneto-optical measurements (Erskine and Stern 1973) and photo-emission experiments (Blodgett et al. 1966). The main objectives of these measurements have been to investigate the predictions of electronic band model calculations and to obtain data which may be used to further improve these models. However, modulation spectroscopy has not previously been used to experimentally investigate the rare earth metals. We preface the results of the thermal modulation experiments by a synopsis of some of the properties of the rare earth metals:

The elements having atomic numbers Z = 57 to 71 inclusive, appearing in group IIIa of the periodic table, are known collectively as the rare earths or the lanthanides. The series is further subdivided into the "light" rare earths and the "heavy" rare earth metals. The latter include the elements gadolinium (Gd), terbium (Tb), dysprosium (Dy), holmium (Ho), erbium (Er) and thulium (Tm). The lanthanides have similar chemical properties because the outer electron configuration remains essentially unchanged throughout the series. A general representation of the electron structure may be written as:-

$$Xe(1s - 4d)4f^{n}\ 5s^{2}\ 5p^{6}\ 5d^{(1)}\ 6s^{2}$$

where n increases from 0 to 14 from La (Z = 57), to Lu (Z = 71) and Xe denotes the Xenon core. The parentheses for the 5d state are used to

indicate that in many of the elements, once the 4f shell contains electrons, the 5d electron is transferred to the 4f shell. The outer electrons $5d^{(1)}$ and 6s are readily removed to become conduction electrons, leaving a trivalent ion core (with the exception of europium and ytterbium which are divalent).

All the heavy rare earth metals have a h.c.p. crystal structure, transitions to a b.c.c. phase occurring at temperatures $\sim$ 1550K for Gd, Tb, Dy and Ho (Taylor and Darby 1972). Some workers have indicated that when grown in thin film form the heavy rare earths transform to a f.c.c. phase (Curzon and Chlebek 1973, Bist et al. 1972). However, this latter phase has now been shown (Gasgnier et al. 1974) to be the metal dihydride, which has a lattice parameter very close to that estimated for a f.c.c. phase of the metal.

Most of the lanthanides exhibit some form of ordered spin structure in the temperature range 4K to 300K. On cooling below room temperature, the elements Gd, Tb, Dy, Ho, Er and Tm become ferromagnetic at temperatures characteristic of the individual metals. All except gadolinium transform into this magnetic state from a higher temperature antiferromagnetic phase which forms directly from the paramagnetic phase. The observed magnetic structures of the heavy rare earths in zero applied magnetic field are shown in Figure (6.1) (Taylor 1970). It is the 4f electron which gives rise to their magnetic properties but the 4f levels are buried deep in the atom and the coupling mechanism between atoms, which is necessary for magnetic order to exist, cannot occur by direct overlap of the electrons in the incomplete shell (as it does for Ni, Co and Fe) and some other exchange mechanism is essential. The origin of the exchange interaction observed in the lanthanides is ascribed to a second mechanism formulated by Ruderman and Kittel (1954), Kasuya (1956) and Yosida (1957). They indicate that the exchange interaction responsible for this coupling between 4f orbitals is an indirect one which involves the polarization of the conduction electrons. The conduction electrons moving through the lattice serve as a medium whereby

Figure (6.1) The magnetic structures of the heavy rare earth metals.

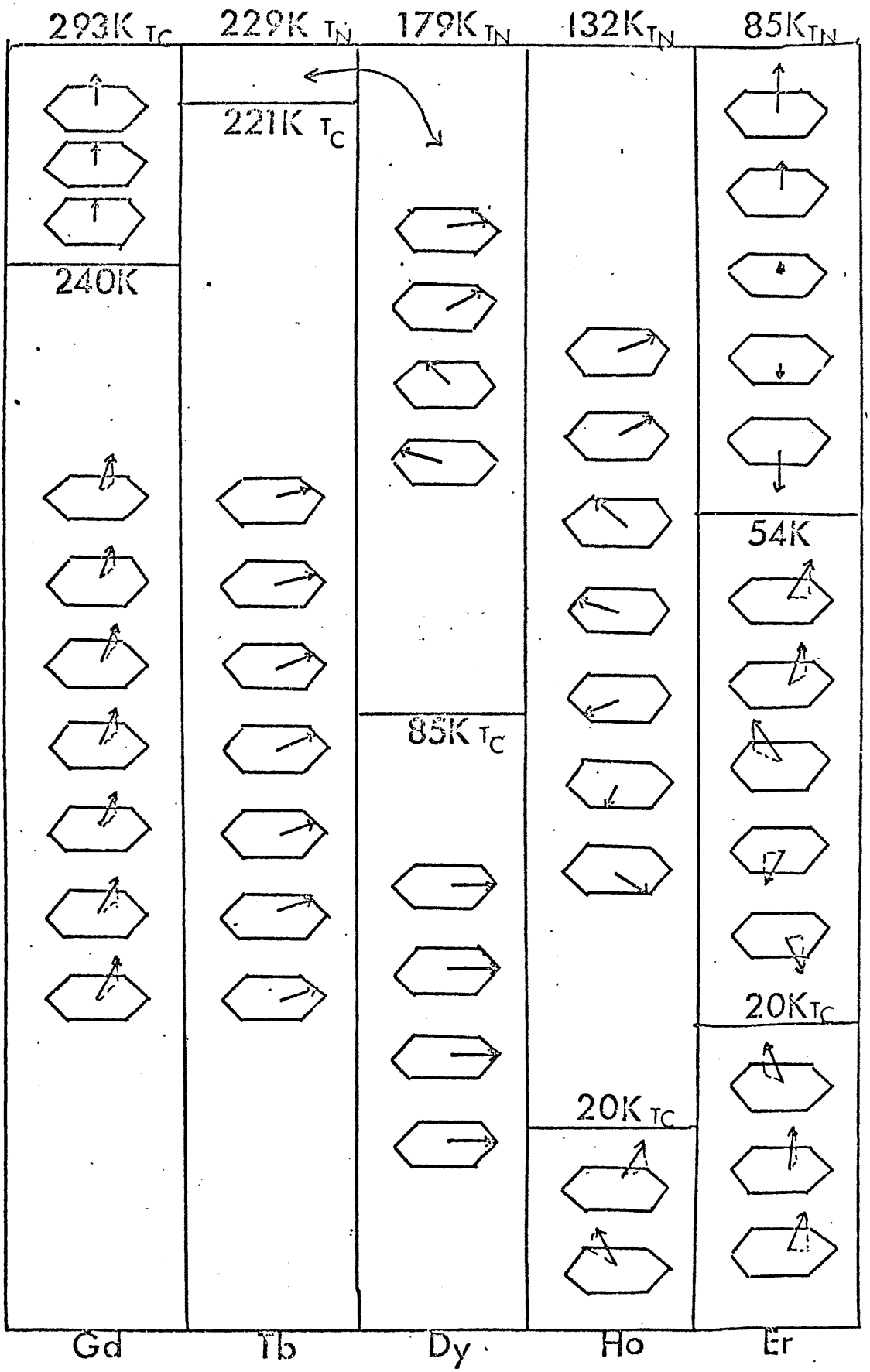

the orientation of the moment on one ion can influence the neighbouring ions. The metals may thus be regarded as consisting of ions with well localized moments due to 4f shells in a sea of conduction electrons which contribute little to the magnetic properties directly but provide the medium for exchange interaction. The interaction is oscillatory in nature and has a long range and is thus capable of giving rise to a variety of periodic spin structures such as those observed.

The band structures of many of the heavy rare earths have been calculated by Loucks (1967) who has developed a systematic procedure based on Hartree-Fock-Slater calculations for free-atoms. All these calculations have used the relativistic augmented plane wave (R.A.P.W.) approach and at present R.A.P.W. calculations of Gd, Dy and Er have been performed (Keeton and Loucks 1966, 1968) and on Tb by Jackson (1969). A relativistic calculation has not been performed for holmium although a nonrelativistic A.P.W. calculation has been reported by Williams et al. (1966). As in all band structure calculations there is some uncertainty as to which atomic configurations are most appropriate and also it should be noted that all the calculations have been made for the metals in the paramagnetic state.

The optical properties of a few rare earth metals have been previously studied (Hodgson and Cleyet 1969, Pétrakian 1972, Miller et al. 1974, Meyers 1976). The agreement between the existing optical data is poor and in many cases the results do not agree even qualitatively. The present thermal modulation expeirments were performed with a view to resolving some of these discrepancies. Miller et al. (1974) using an optimized reflection ratio technique (measurement of (Rp/Rs) at two selected angles of incidence) found that the optical conductivity, $\sigma(w)$, dispersion curves of gadolinium and terbium had fine structure superimposed on them. Hasan (Ph.D. thesis 1975) found similar structure in the $\sigma(w)$ dispersion curves, measurements being made in air on thin films of gadolinium, terbium, dysprosium and holmium grown in both ordinary and ultra high vacua. Both workers explain the presence

of the fine structure as being due to allowed optical transitions between certain symmetry points in the first Brilloiun zone of the hexagonal close packed lattice. To date these are the only experiments in which fine structure has been observed in the $\sigma(w)$ curves.

In the thermal modulation measurements made on thick absorbing films of gold and copper (see (5.4) and (5.8)) we have seen that the technique is capable of locating very fine structure e.g. the transition located at 3.0 eV for gold (Figure 5.9) and that at 2.55 eV for copper (Figure 5.15a). It was thought that the technique would be a good diagnostic tool to investigate the existence of the fine structure in the $\sigma(w)$ curves of the heavy rare earth metals reported by Miller (1974) and Hasan (1975). In the present work the modulated reflectance measurements were made in an ordinary high vacuum environment on films grown under both O.H.V. and U.H.V. conditions. Experimental details are given below.

6.2 The growth of the gadolinium films

Gadolinium was chosen as the first metal to be studied since it has been most extensively studied by other experimental techniques and its band structure has been calculated. Also, from Figure (6.1) we see that it has the highest ferromagnetic Curie temperature $T_c = 293$ K and exhibits only a ferromagnetic ordered phase, unlike the other heavy rare earths, most of which exhibit a variety of magnetic orderings.

Gadolinium films were grown in both U.H.V. and O.H.V. environments. The conditions necessary for the production of an opaque continuous film in the U.H.V. chamber were determined by performing several trial runs in an O.H.V. system. The tantalum boat, prepared as described in (4.4) was placed in the U.H.V. chamber and the system evacuated to its base pressure. Further outgassing of the boat was then found to be necessary. A current of 50 amps was passed through the boat with the shutter shielding the substrate from the evaporant. During this time the pressure in the system rose to 10^{-6} torr and the boat was allowed to outgas for 5 minutes.

During the outgassing the mass spectrometer indicated that H_2O, N_2 and H_2 were evolved. After the outgassing procedure had been completed the substrate holder was rotated (using the rotary drive) so as to be perpendicular to the evaporation source. Adjustment of the height of the substrate holder was also necessary in order to ensure complete coverage or both microscope slides during the evaporation. Of the two specimens produced, one was used as the sample for the thermal modulation experiments and the other was cut in half, one half being used for a thickness measurement and the other for structure analysis by high energy reflection electron diffraction. The growth conditions of a typical gadolinium film grown in the U.H.V. environment are given below:-

(i) The residual gases in the system were H_2O, N_2 and CO_2. The total integrated pressure measured on the Bayard-Alpert ionization gauge was $3. \times 10^{-10}$ torr.

(ii) The film was grown from a 99.9% pure sample of gadolinium in wire form (1mm diameter) obtained from Goodfellows Metals.

(iii) Wherever possible the film was grown in one evaporation. As the evaporation proceeded a pressure rise in the system was usually observed, probably caused by the effects of further outgassing of the boat and charge material or by the outgassing of the chamber walls due to the heating from the boat. If the pressure approached 10^{-8} torr the current was switched off and the system allowed to return to its base pressure. This process was repeated until an opaque film had been grown; usually the maximum number of evaporations necessary to produce such a film was two.

(iv) For the film described here a current of 60 amps was passed for 4 minutes, this time representing the total time taken for two evaporations.

(v) The measured film thickness was 2000Å (a deposition rate of 500Å/min).

(vi) The film was grown on a float glass substrate at room temperature.

The growth conditions of a typical gadolinium film grown in the O.H.V. system ($\sim 10^{-7}$ torr) are summarized below. To give a fast evaporation rate the film was grown from a tungsten helical filament.

(i) The loading of the tungsten filament with the charge material has been previously described in (4.4). The filament and evaporant were outgassed to a pressure of 10^{-6} torr for 5 minutes by passing a current of 50 amps through the filament.

(ii) After the outgassing procedure was completed the system was allowed to achieve a pressure of 8×10^{-7} torr.

(iii) The material was evaporated by passing 60 amps through the filament for 30 seconds which resulted in the formation of an opaque film. We note that as the evaporation began there as a marked gettering action, the pressure in the system falling to 4×10^{-7} torr. Towards the end of the evaporation period the pressure had risen to 2×10^{-6} torr.

(iv) The film was deposited in one evaporation onto a glass substrate at room temperature and the source-substrate distance was 8cm.

(v) The measured film thickness was 2200Å (a deposition rate of 73Å/sec).

On removal from the U.H.V. and O.H.V. growth chambers the films were exposed to the atmosphere. High energy reflection electron diffraction patterns of the films are shown in Plates (6.1) and (6.2). We see that the film grown in the U.H.V. environment exhibits a high degree of preferred orientation, and the pattern is indicative of a hexagonal close packed structure. Considerable difficulty was found in obtaining a diffraction pattern from the gadolinium films grown in the O.H.V. chamber. Immediately the specimen was placed in the electron microscope a ring pattern was clearly defined but before the image could be recorded the pattern disappeared. This result probably indicates that the high energy electron beam (75 $\sim$ 100KV) caused changes in the specimen surface. Owing to the poor visibility of the

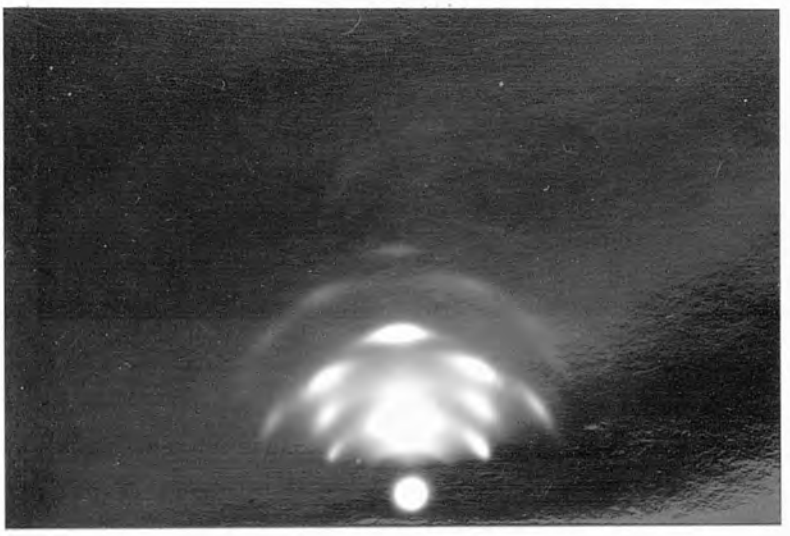

PLATE (6.1) High energy reflection electron diffraction pattern of a U.H.V. grown gadolinium film.

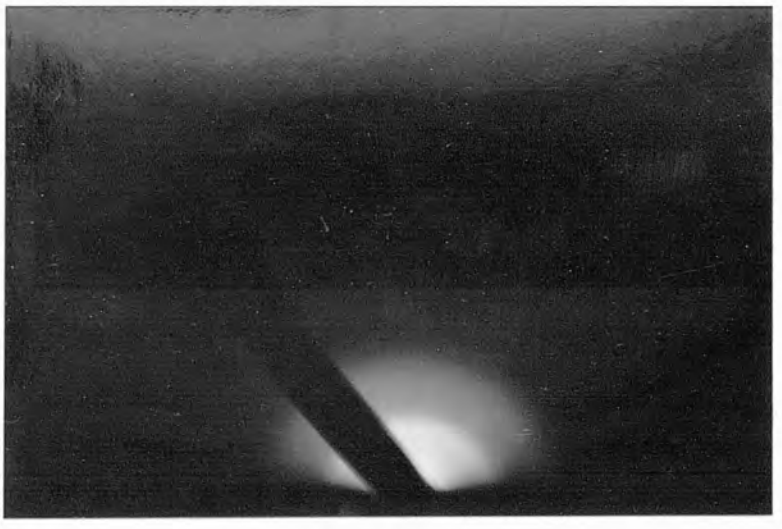

PLATE (6.2) High energy reflection electron diffraction pattern of an O.H.V. grown gadolinium film.

diffraction pattern in Plate (6.2) the interplanar spacings could not be calculated. It would appear from the diffraction pattern that the film had a very small crystallite size or was amorphous. The gadolinium films grown in the different vacuum enviroments also appeared visibly different. The O.H.V. grown film appeared very dark and absorbing compared with the highly reflecting nature of the U.H.V. grown film. A resistance measurement revealed that O.H.V. grown films of similar thickness to U.H.V. films had a higher resistance. These differences are not surprising when we consider the nature of the growth environment. A necessary condition for an evaporated film to be free fromcontamination by the residual gas in the chamber is that the atoms of the evapcrant have a long mean free path compared with the source-substrate distance. An estimate shows that this condition is satisfied even at 10^{-4} torr so that the contamination produced by collisions with the residual gas molecules during evaporation may be ignored. However, if we consider the rate at which gas molecules strike the surface then the pressure limitations become much stricter. From kinetic theory the number of molecules, N, striking unit area in unit time is given by

$$N = pN_A/(2\pi MRT)^{\frac{1}{2}} \qquad (6.1)$$

where T is the absolute temperature of the gas

p is the pressure of the gas

R is the gas constant

N_A is Avogadro's number

M is the mass of the molecule.

From equation (6.1) we see that low mass numbers are the most important. Typically the partial pressure of water vapour in the U.H.V. system was 5×10^{-11} torr. Using this in equation (6.1) we get

$$N = 2.4 \times 10^{10} \text{ molecules/sec.}$$

If we take the area covered by a water vapour molecule to be $1.5(\text{Å})^2$, the time taken for the formation of a monolayer of water vapour is 77 hours

assuming unit sticking probability. The partial pressures of the residual gases in the O.H.V. chamber were not measured, so an estimate of the partial pressure of water vapour must be made. The partial pressure of water vapour was taken to be $\sim 5 \times 10^{-6}$ torr. Using this figure in equation (6.1) we get

$$N = 2.4 \times 10^{15} \text{ molecules/sec}$$

Again assuming ever molecule sticks to the surface we see that a monolayer is formed $\sim$ 3 seconds. Contamination of the film by residual gases is thus occurring during the course of the evaporation in the O.H.V. system. The absorbing nature and higher resistivity of the O.H.V.-grown gadolinium film arethus explicable in terms of contamination by residual gases as the film is being grown.

6.3 The thermally modulated reflectance spectra of gadolinium films

The measurements were taken in the same manner as those for gold and copper except that a different current pulser with a higher output impedance was necessary in this case. Electrical leads could not be indium-soldered directly to the surface of the film and the copper pad arrangement described in (3.7) was again used. The chrome alumel thermocouple was indium-soldered to the glass substrate at a point near to the gadolinium film. After their removal from the growth chamber the films were usually under a vacuum of 10^{-6} torr. within 30 minutes of transfer ence to the experimental chamber.

The thermally modulated reflectance spectra measured at an angle of incidence $\theta_o = 45^o$ with light polarized parallel to the plane of incidence, of U.H.V. grown gadolinium films are shown in Figure (6.2). The measurements were taken at 97K and 315K with powers of 5.0 watts and 7.8 watts respectively dissipated in the sample. The high temperature trace thus corresponds to the paramagnetic phase and the low temperature trace to the ferromagnetic phase of gadolinium. During the course of the measurements the pressure in the experimental chamber was 3×10^{-7} torr. From Figure (6.2) we see that the high temperature ($\Delta Rp/Rp$) response is rather featureless but the low

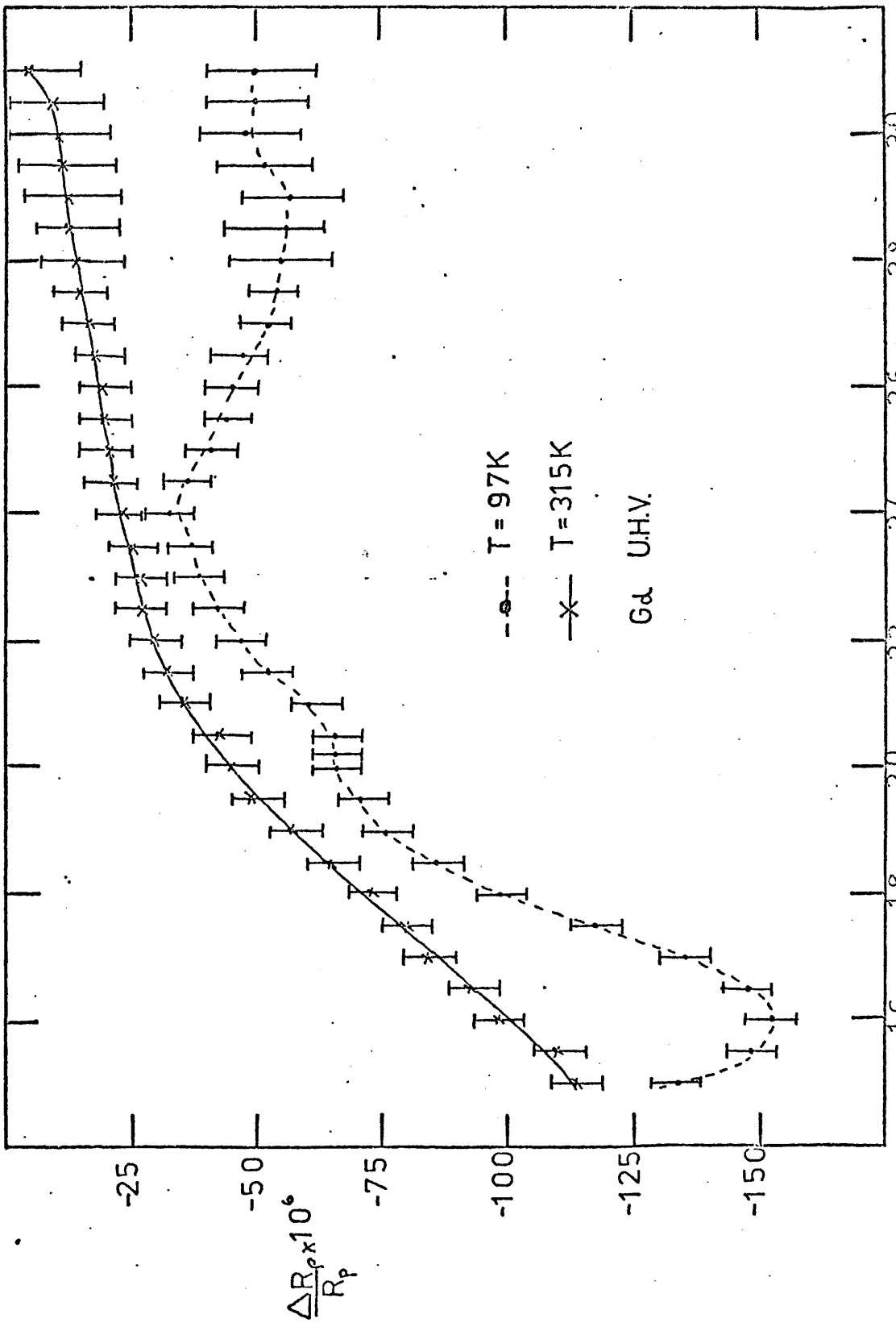

Figure (6.2) The ($\Delta R_p/R_p$) spectra of a U.H.V. grown gadolinium film at 97K and 315K.

temperature trace has structure located at 1.6 eV, 2.0 eV and 2.4 eV. The structure near to 2.0 eV although weak appeared in all five films measured and Figure (6.3) gives some indication of the reproducibility of the low temperature $\Delta Rp/Rp$ spectra for 4 gadolinium films. We see that the 3 pieces of structure are located at the same photon energies for all the films. Figure (6.3a) shows a pen recorder trace of the thermoreflectance response of a gadolinium film at 97K. Measurements were always taken in a high-low-high-low temperature cycle, the results indicating that structure in the low temperature spectra was due to the effect of lowering the temperature of the sample rather than oxidation or annealing of the film as a current was pulsed through the sample.

The thermally modulated reflectance spectrum of an O.H.V. - grown gadolinium film at 315K with a power of 5.2 watts dissipated in the sample is shown in Figure (6.4). We see that at low photon energies the trace is very similar to the high temperature results obtained from the U.H.V. grown film. However, at higher photon energies around 2.4 eV there is a rapid increase in the $(\Delta Rp/Rp)$ response. Similar behaviour of the thermally modulated reflectance spectra at high photon energies has been observed for copper films measured in air, see (5.7). Julien (1973 Ph.D. thesis) has indicated that U.H.V. grown gadolinium films showing evidence of comtamination yielded optical conductivity curves which rose sharply at the ultra-violet end of the spectrum. Systematic results could not be obtained from the O.H.V. - grown films and on removal from the growth chamber many of the specimens appeared brown at the edges. As discussed in (6.2) the high energy reflection electron diffraction patterns obtained from the O.H.V. grown films were very poor and unfortunately they could not be analysed satisfactory. However, to give an indication of the high reactivity of the O.H.V. - grown gadolinium films, during the course of one evaporation the tungsten filament with the charge snapped leaving a partially grown film which appeared semitransparent and was $\sim$ 500Å thick. The specimen was left exposed to the atmosphere for 24 hours and after this period the metallic

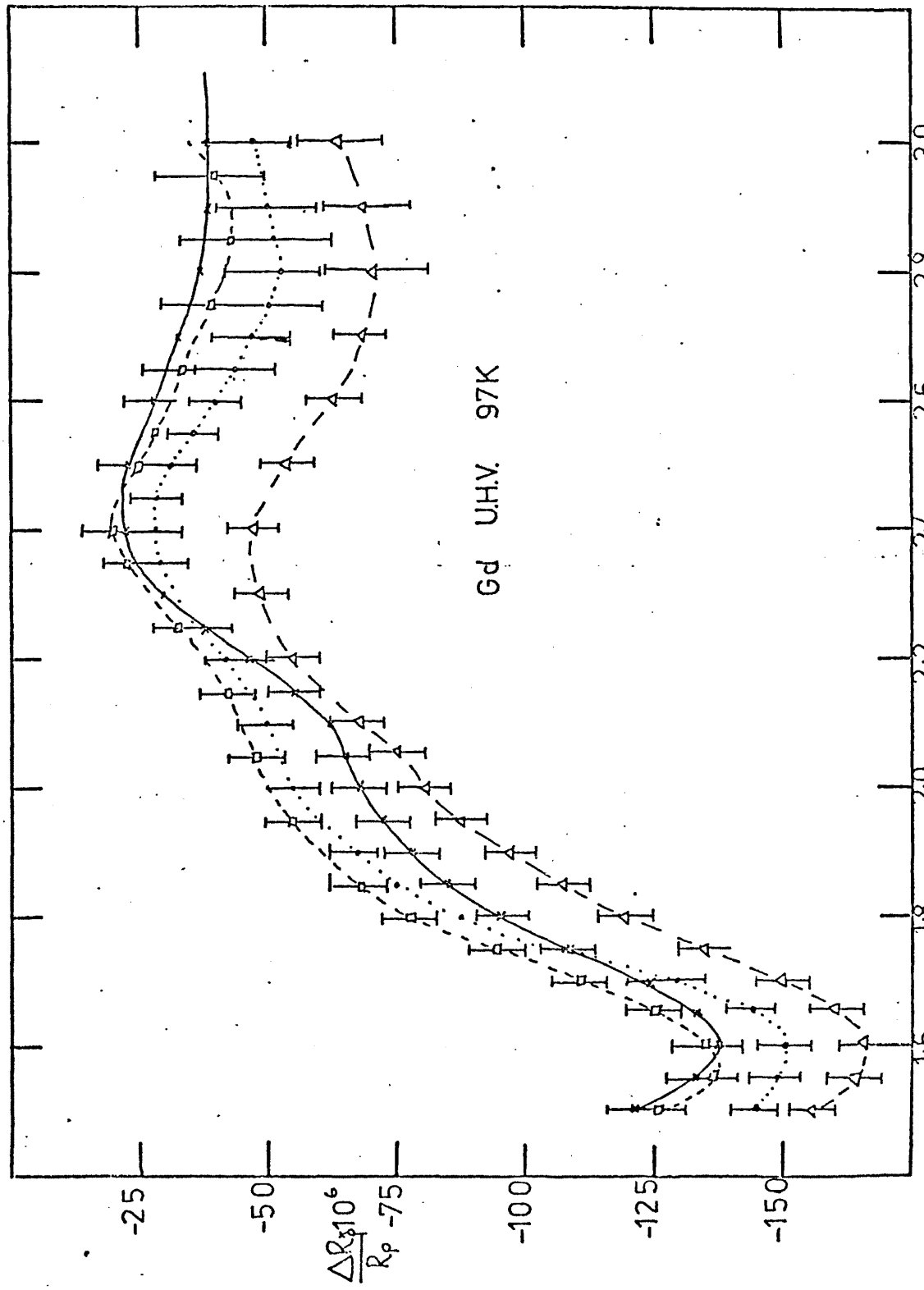

Figure (6.3) Additional data on gadolinium.

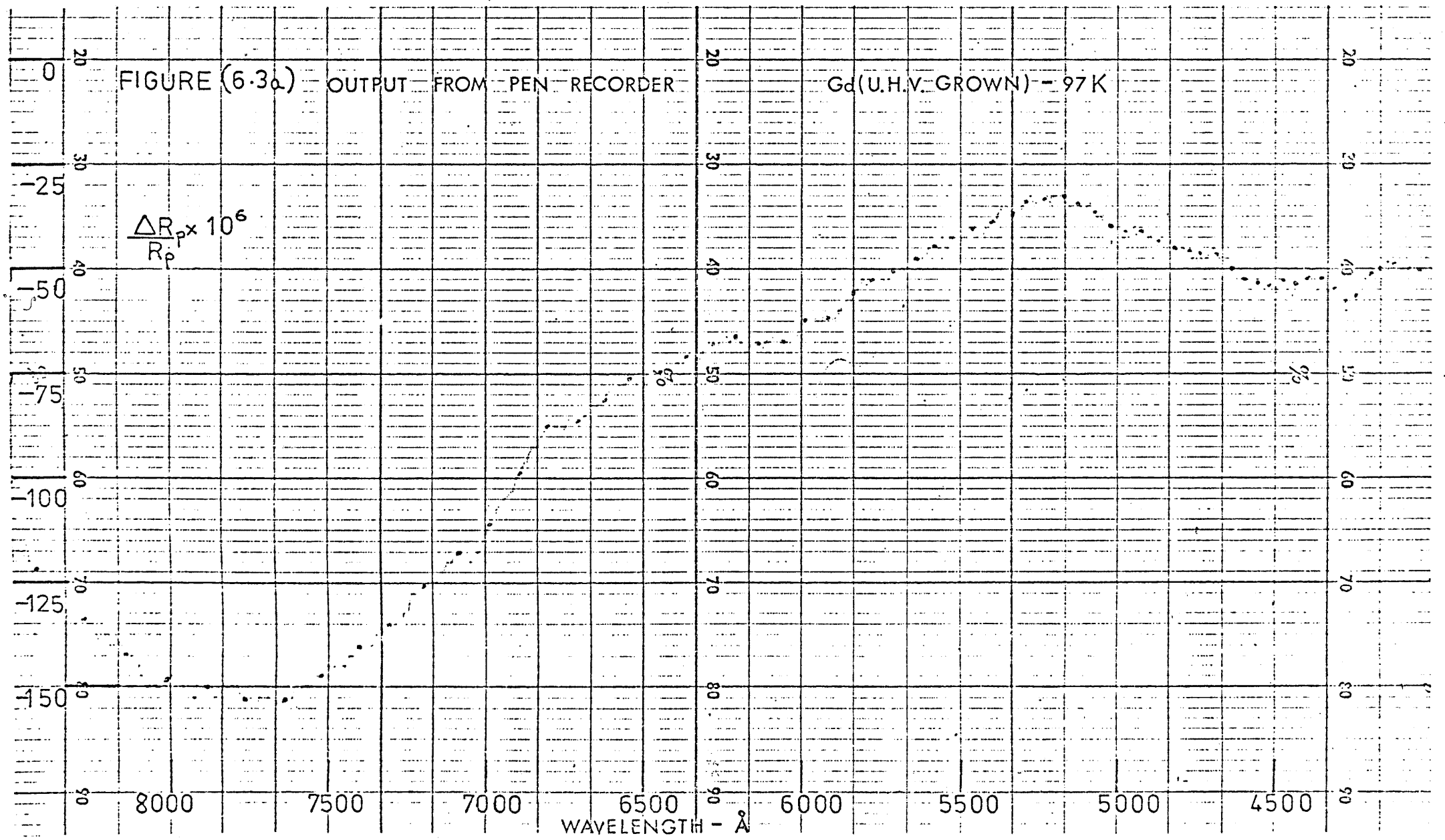
FIGURE (6·3a) — OUTPUT FROM PEN RECORDER — Gd (U.H.V. GROWN) – 97 K
$\frac{\Delta R_p}{R_p} \times 10^6$
0
−25
−50
−75
−100
−125
−150
8000
7500
7000
6500
6000
5500
5000
4500
WAVELENGTH – Å

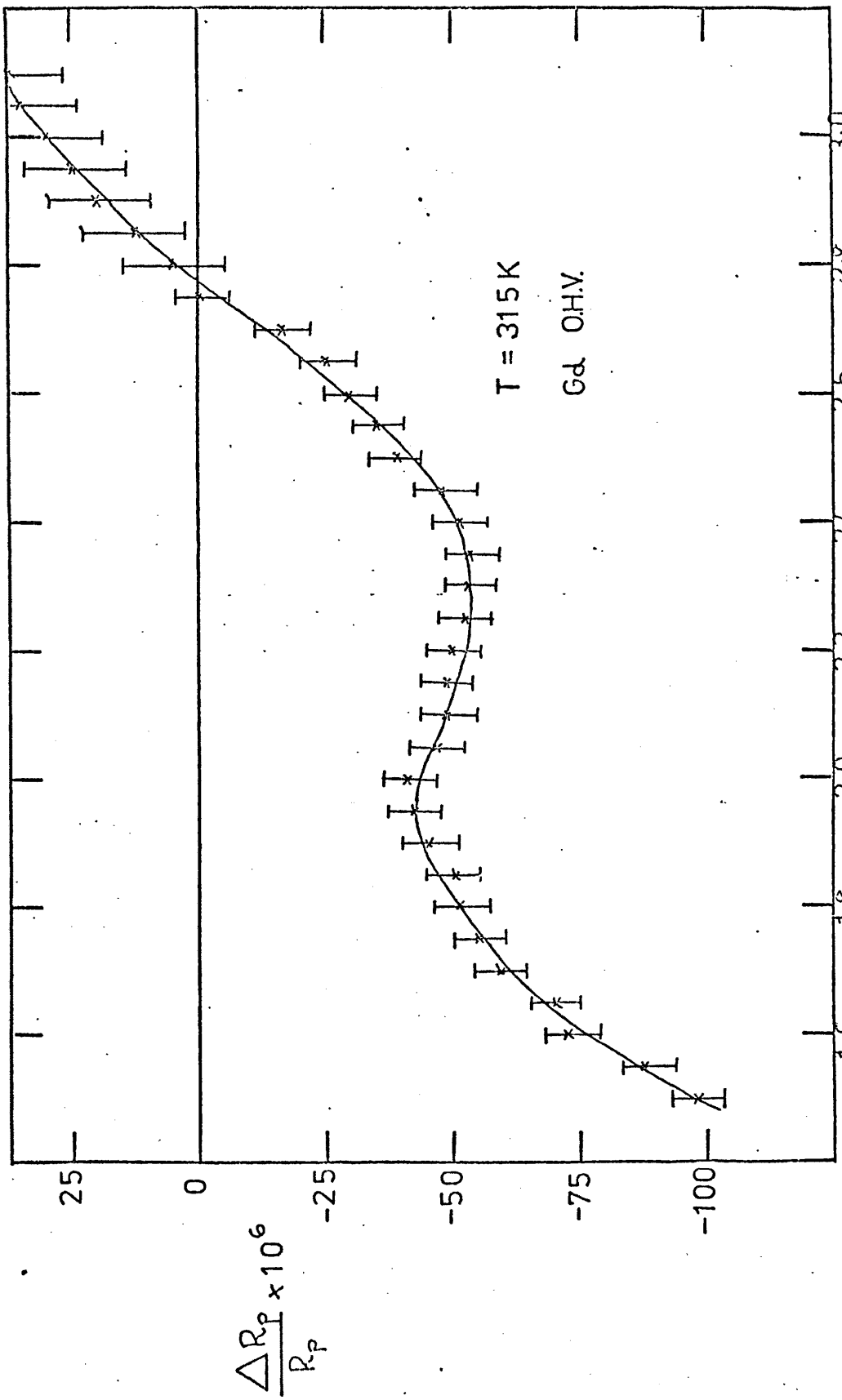

Figure (6.4) The ($\Delta Rp/Rp$) spectrum of an O.H.V. grown gadolinium film at 315K.

nature of the film had completely disappeared leaving a transparent film on the glass substrate. All of the thermal modulation measurements on the O.H.V. - grown gadolinium films were disregarded and it was inferred that the high ($\Delta Rp/Rp$) values in the near ultra-violet part of the spectrum were due to specimen contamination.

6.4 The growth of the terbium films

Following the thermally modulated reflectance studies on gadolinium it was decided to investigate terbium, this being the next element in the rare earth series. The terbium films were grown under conditions similar to those described in (6.2). The growth conditions for typical terbium films grown in the U.H.V. and O.H.V. systems are summarized below.

(a) U.H.V. characteristics

(i) The film was prepared from a 99.9% pure sample of terbium wire supplied by Goodfellows metals.

(ii) The film was grown by condensation of a horizontal vapour stream from a tantalum boat and the measured base pressure of the system was 3×10^{-10} torr.

(iii) The films were grown in two evaporations, by passing a current of 65 amps. The total time of evaporation was 4 minutes.

(iv) The measured film thickness was 2055Å (a deposition rate of 514Å/min).

(b) O.H.V. characteristics

(i) The terbium was evaporated from a tungsten helical filament.

(ii) The usual outgassing procedures were followed, a current of 60 amps being passed through the filament for 5 minutes.

(iii) The source-substrate distance was 8 cm.

(iv) The base pressure of the system prior to evaporation was 7×10^{-7} torr. A current of 70 amps was passed through the filament for 45 secs. A slight gettering action was observed as the evaporation proceeded, the pressure falling to 5×10^{-7} torr. We note that the gettering

action was not so marked as during the growth of the gadolinium films. At the end of the evaporation the pressure in the system had risen to 2×10^{-6} torr.

(v) The film was deposited in one evaporation and the measured thickness was 1800Å, a deposition rate of 2400Å/min.

Plates (6.3) and (6.5) show the high energy reflection electron diffraction patterns obtained from the terbium films grown in the U.H.V. and O.H.V. environments respectively. Once again we see that the U.H.V. grown film exhibits an oriented growth and the pattern is indicative of a hexagonal close packed crystal structure. The O.H.V. grown film appears to have either a very small crystallite size or to be amorphous. As the pattern was not clearly defined interplanar spacings could not be calculated. The reflection electron diffraction analysis was also performed on samples that had been subjected to thermal modulation. We see from Plates (6.4) and (6.6) that the patterns remain essentially unchanged, although the patterns are perhaps not so clearly defined as those obtained prior to the thermal modulation measurements.

6.5 The thermally modulated reflectance spectra of terbium films

A total of 8 terbium films were grown, 4 under ultra-high vacuum conditions and the remainder in O.H.V. The thermal modulation measurements were made in the usual manner. The pressure in the experimental chamber was always $< 4 \times 10^{-7}$ torr when measurements were made. Figure (6.5) shows the thermally modulated reflectance response of a typical U.H.V. grown terbium film at 97K and 315K, powers of 8.1 watts and 5.5 watts being dissipated respectively in the sample. As in the case of gadolinium the high temperature ($\Delta Rp/Rp$) response is rather featureless. On lowering the temperature of the sample to 97K a minimum in ($\Delta Rp/Rp$) appears at 1.675 eV and fine structure is seen in the vicinity of 2.65 eV. These features were apparent on all four of the U.H.V. grown films measured. Further ($\Delta Rp/Rp$)

PLATE (6.3) High energy reflection electron diffraction pattern of a U.H.V. grown terbium film before thermal modulation.

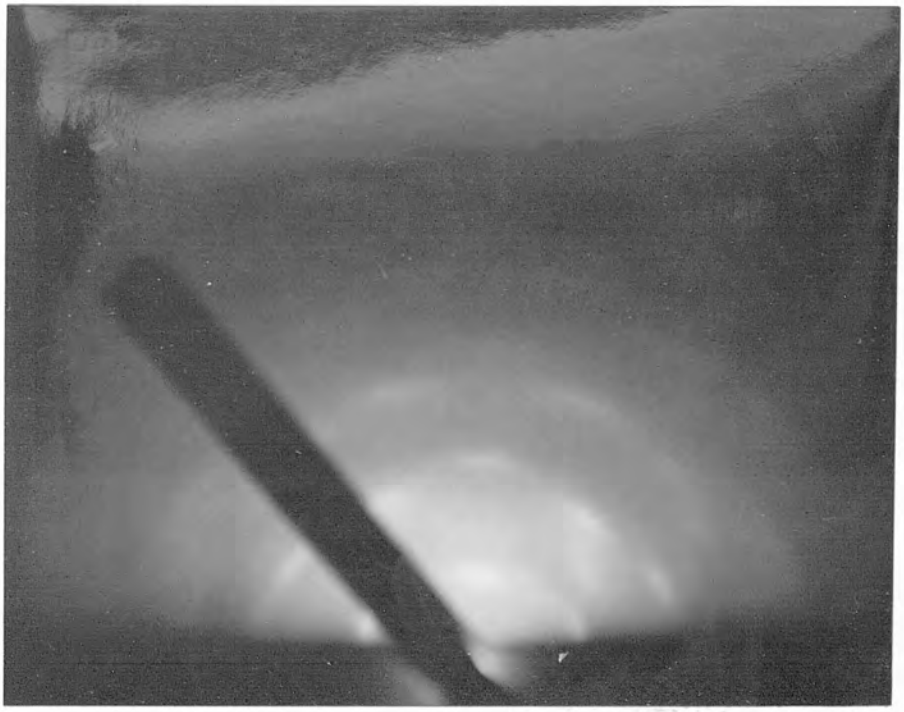

PLATE (6.4) High energy reflection electron diffraction pattern of a U.H.V. grown terbium film after thermal modulation.

PLATE (6.5) High energy reflection electron diffraction pattern of an O.H.V. grown terbium film before thermal modulation.

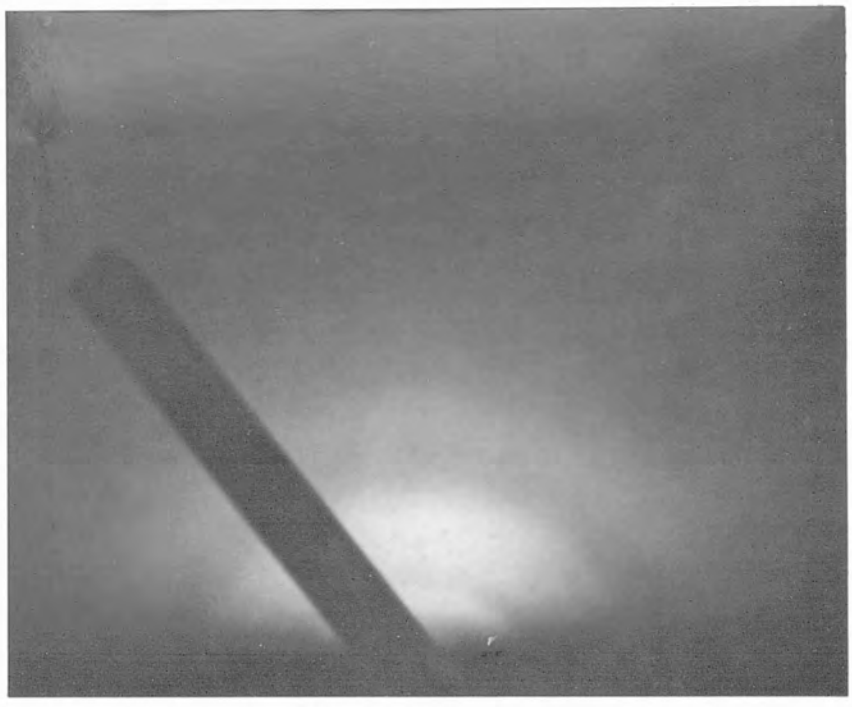

PLATE (6.6) High energy reflection electron diffraction pattern of an O.H.V. grown terbium film after thermal modulation.

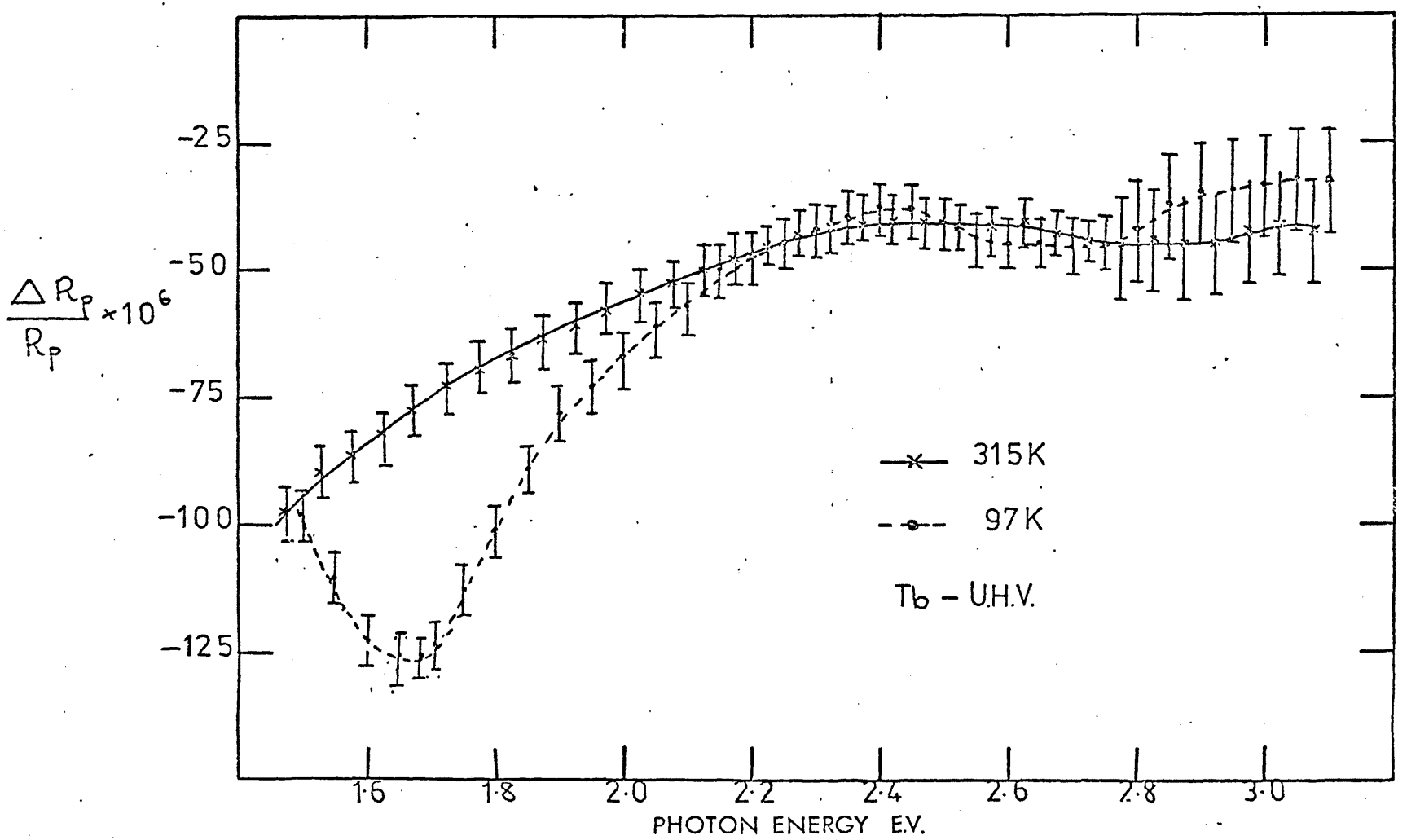

Figure (6.5) The (ΔRp/Rp) spectra of a U.H.V. grown terbium film at 97K and 315K.

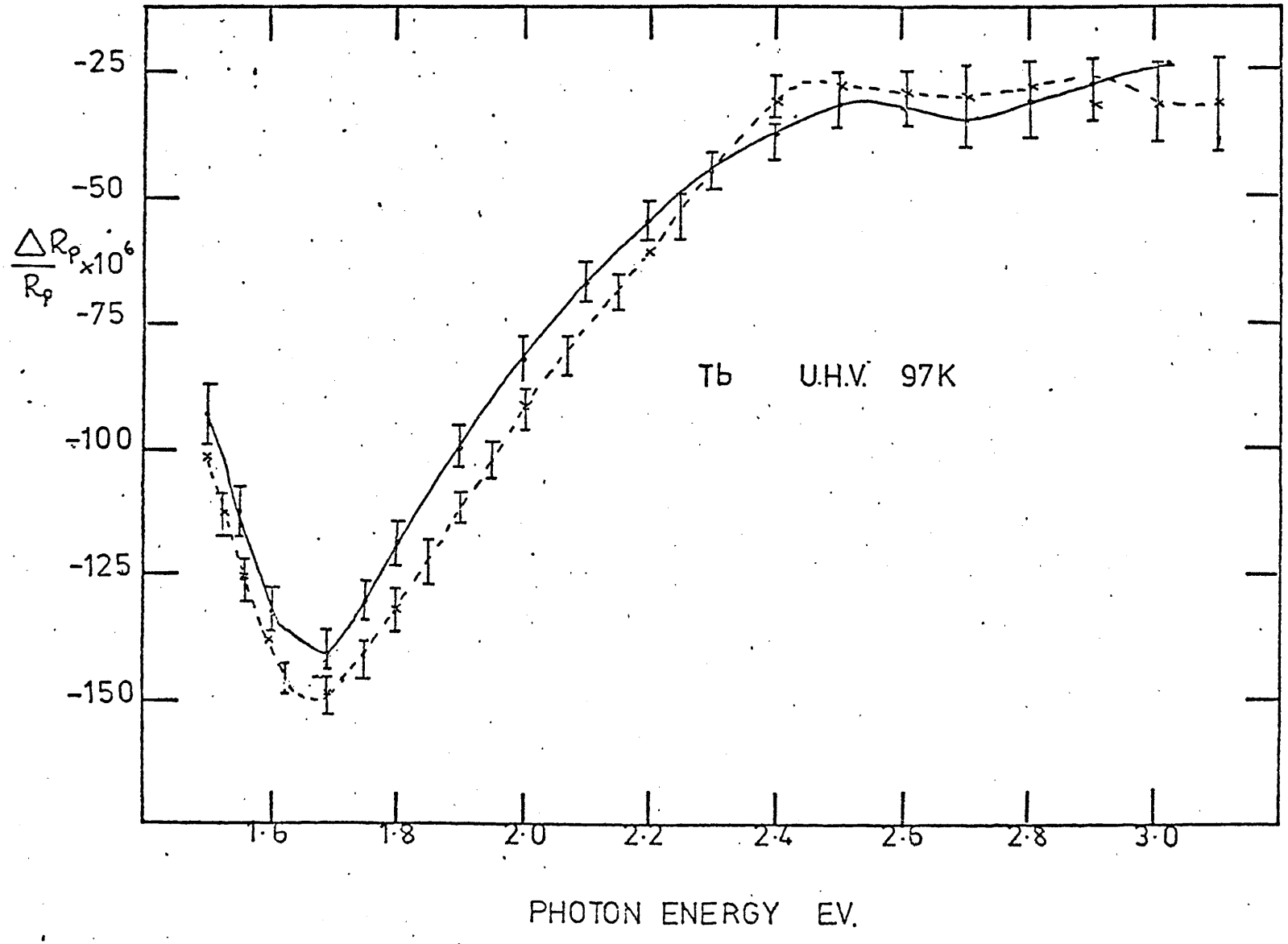

Figure (6.5a) Additional data on U.H.V. grown terbium films.

data for terbium at 97K is presented in Figure (6.5a). As in the case of the gadolinium measurements (see Figure 6.3a) we see that there is some variation in the magnitude of the $(\Delta Rp/Rp)$ values obtained from each film. It is thought that this variation is probably due to slightly different levels of power dissipation in the sample and to "phasing errors" on the lock-in amplifier when initially setting the system up for each $(\Delta Rp/Rp)$ dispersion response to be measured. We note that the high temperature $(\Delta Rp/Rp)$ response corresponds to measurements made on terbium in the paramagnetic state and the low temperature response to the ferromagnetic phase. The high and low temperature $(\Delta Rp/Rp)$ responses of a typical O.H.V. - grown terbium film with powers of 9.5 watts and 6.5 watts being dissipated respectively in the sample are shown in Figure (6.6). Comparing Figures (6.5) and (6.6) we see that there are slight differences in the $(\Delta Rp/Rp)$ response for the U.H.V. and O.H.V. terbium films at 315K at low photon energies. The $(\Delta Rp/Rp)$ response for the O.H.V. film appears to have a plateau region near to 1.5 eV which is not apparent in the response of the U.H.V. specimen. Also the minimum in the $(\Delta Rp/Rp)$ response at 97K is located at 1.65 eV for O.H.V. films compared with 1.675 eV for U.H.V. films. Some differences in optical behaviour are to be expected since the terbium films grown at higher pressures $\sim 10^{-7}$ torr appeared to be very dark and absorbing compared with films grown at pressures of 10^{-10} torr.

6.6 The growth of the dysprosium and erbium films

Following the thermally modulated reflectance measurements on gadolinium and terbium further studies were made on thick absorbing films of dysprosium and erbium. However, these metals were not studied so extensively as gadolinium and terbium. Only 4 dysprosium films were grown: 2 in O.H.V. conditions and 2 in U.H.V. conditions. The 2 erbium films studied were grown in an O.H.V. environment.

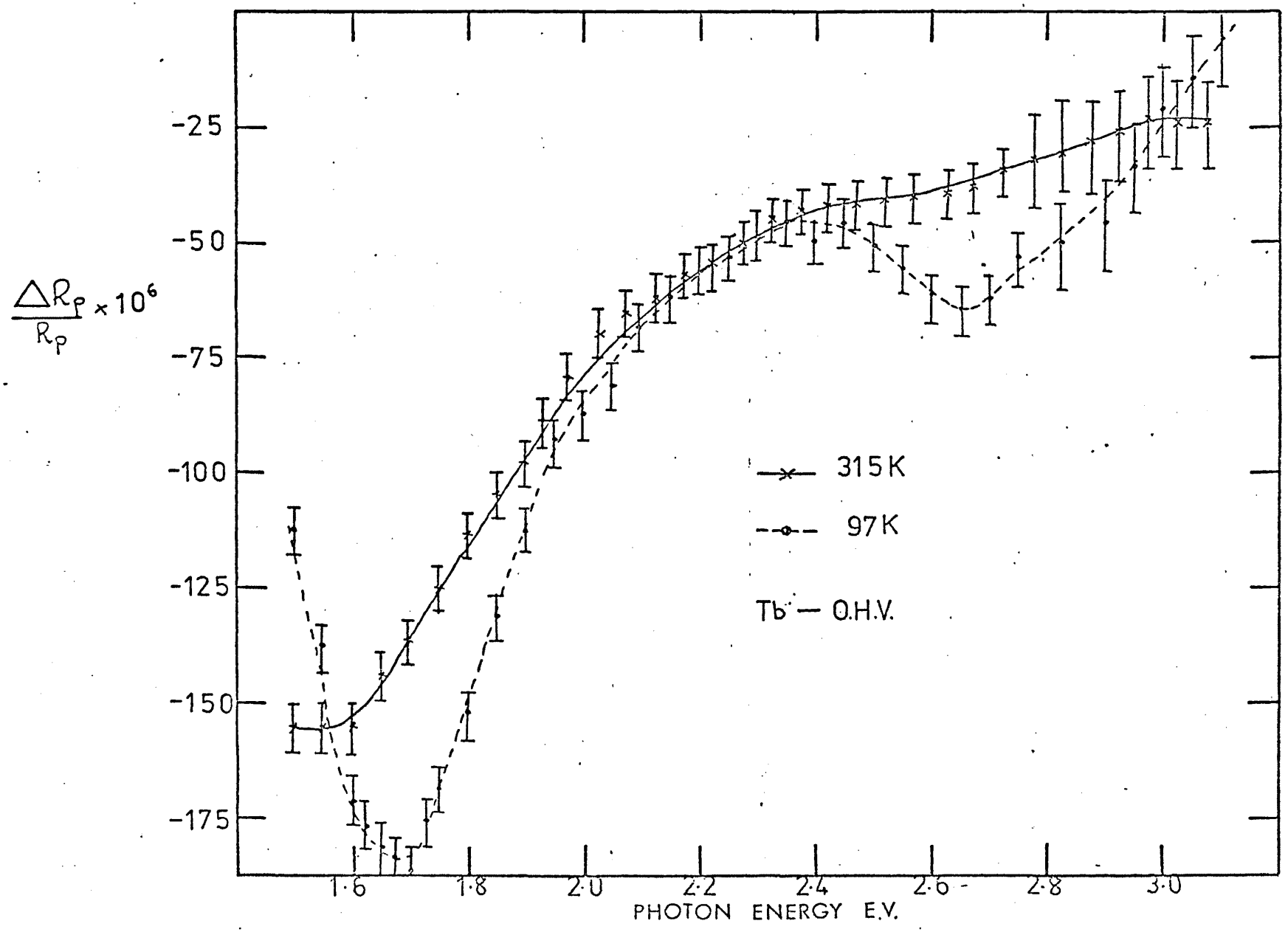

Figure (6.6) The (ΔRp/Rp) spectra of an O.H.V. grown terbium film at 97K and 315K

The growth parameters of these metals were slightly different from those for gadolinium and terbium, since dysprosium sublimes at 750°C at 10^{-6} torr and 625°C at 10^{-8} torr, and erbium sublimes at 775°C at 10^{-6} and 650°C at 10^{-8} torr (Balzers chart for the vacuum evaporation of metals). It was thus extremely important to have a well loaded filament or boat in order to produce an opaque film since much of the evaporant was lost by sublimation during the outgassing procedure. The growth conditions of both elements are given below:-

(a) The growth characteristics of dysprosium and erbium films in O.H.V.

(i) A tungsten helical filament was used as the source, dysprosium and erbium in wire form, 99.9% pure were supplied from Goodfellow Metals.

(ii) The source-substrate distance was 7 cm.

(iii) The filament and charge material were outgassed by passing a current of 30 amps for 5 minutes. A microscope slide positioned above the filament revealed that some of the charge material was lost by sublimation during the outgassing.

(iv) After the outgassing procedures had been completed the system was allowed to reach its base pressure of $< 4 \times 10^{-7}$ torr.

(v) An evaporation current of 40 amps was passed through the filament. At the start of the evaporation a pressure burst was observed, the pressure rising to 3×10^{-6} torr. To ensure that the pressure did not exceed this value during the remainder of the evaporation period the current was pulsed through the filament for 45 seconds.

(vi) The measured film thickness of the dysprosium and erbium films were 2140Å and 1680Å respectively, giving deposition rates of < 50Å/sec for both metals.

(b) The growth characteristics of a typical dysprosium film grown in U.H.V.

(i) The film was grown from a tantalum boat and the base pressure of the U.H.V. chamber prior to evaporation was $< 5 \times 10^{-10}$ torr.

(ii) The film was grown in one evaporation by passing a current of 70 amps for 1.5 minutes, the pressure in the system rising to 8×10^{-9} torr during the course of the evaporation.

(iii) The measured film thickness was 1980Å, a deposition rate of 22Å/sec.

Plates (6.7) to (6.9) inclusive show the reflection electron diffraction patterns obtained from the dysprosium and erbium films.

6.7 The thermally modulated reflectance spectra of dysprosium and erbium films

The thermally modulated reflectance spectra of a typical dysprosium film grown in an O.H.V. enviroment is shown in Figure (6.7). As in the case of both the gadolinium and terbium films the ($\Delta Rp/Rp$) spectrum obtained at 315K is rather featureless. On lowering the temperature of the sample to 97K a sharp minimum is observed near to 2.1 eV and fine structure is seen at 2.70 eV. The thermally modulated reflectance responses at 97K and 315K of the 2 U.H.V. grown dysprosium films are shown in Figures (6.8) and (6.8a). We see that the ($\Delta Rp/Rp$) responses obtained from the U.H.V. grown sample are in good overall agreement with the ($\Delta Rp/Rp$) spectra obtained from the O.H.V. grown films. Both O.H.V. and U.H.V. grown samples exhibit ($\Delta Rp/Rp$) responses with sharp minima near to 2.15 eV and fine structure located near to 2.7 eV at 97K. However, although the high temperature ($\Delta Rp/Rp$) responses are rather featureless for both O.H.V. and U.H.V. grown films the ($\Delta Rp/Rp$) response of the U.H.V. grown film has a much steeper slope than that of the O.H.V. grown film.

The thermally modulated reflectance responses of the two O.H.V. grown erbium films at 315K and 97K with powers of 4.0 watts and 5.0 watts dissipated respectively in the samples are shown in Figures (6.9) and (6.9a). As appears to be the general trend in the series, the response at 315K is rather featureless but on lowering the temperature of the sample an overall sharpening of the spectra is observed, with structure appearing at 2.0 eV

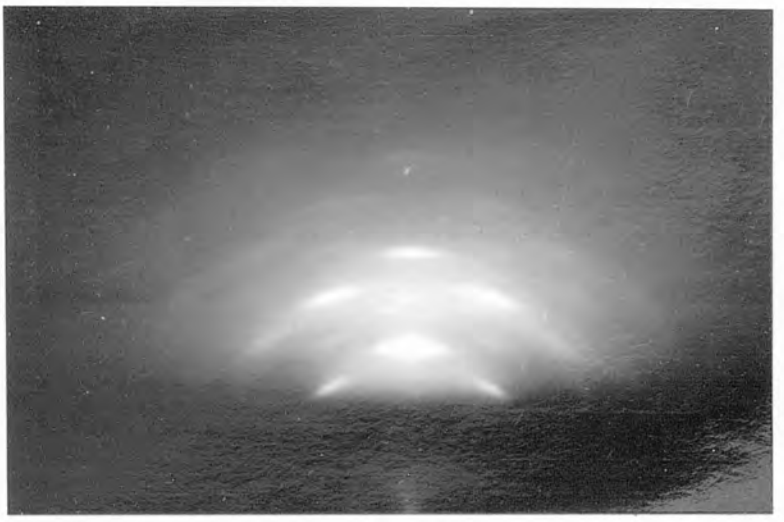

PLATE (6.7) High energy reflection electron diffraction pattern of an U.H.V. grown dysprosium film.

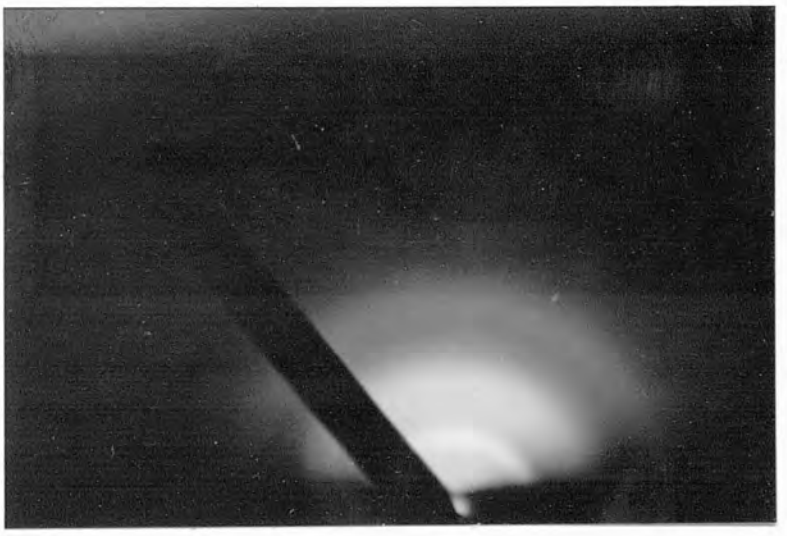

PLATE (6.8) High energy reflection electron diffraction pattern of an O.H.V. grown dysprosium film.

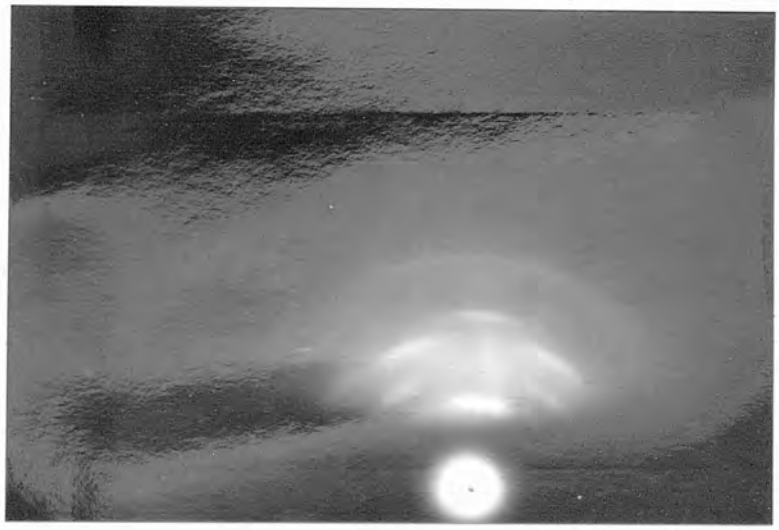

PLATE (6.9) High energy reflection electron dirfraction pattern of an O.H.V. grown erbium film.

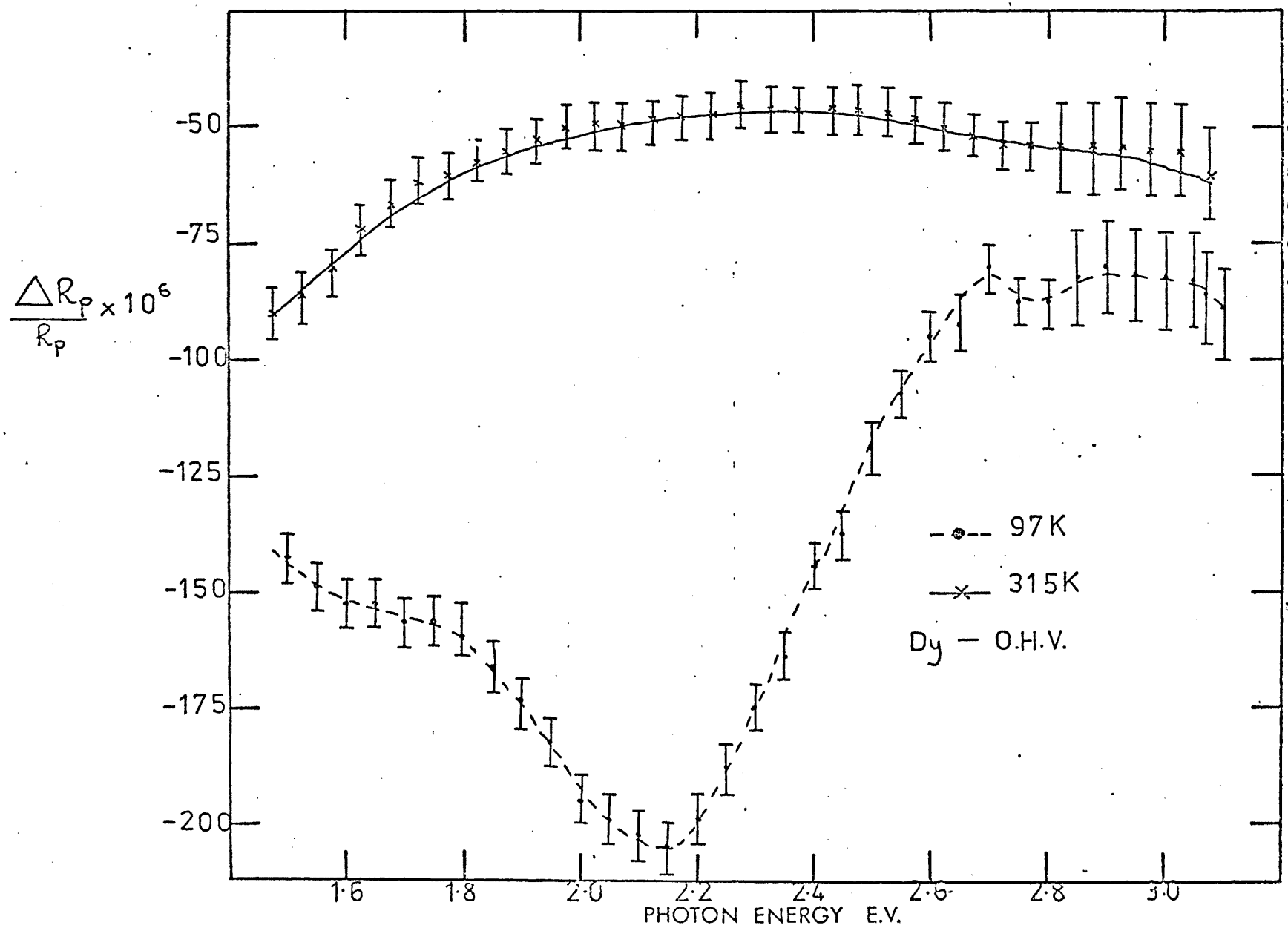

Figure (6.7) The ($\Delta Rp/Rp$) spectra of an O.H.V. grown dysprosium film at 97K and 315K.

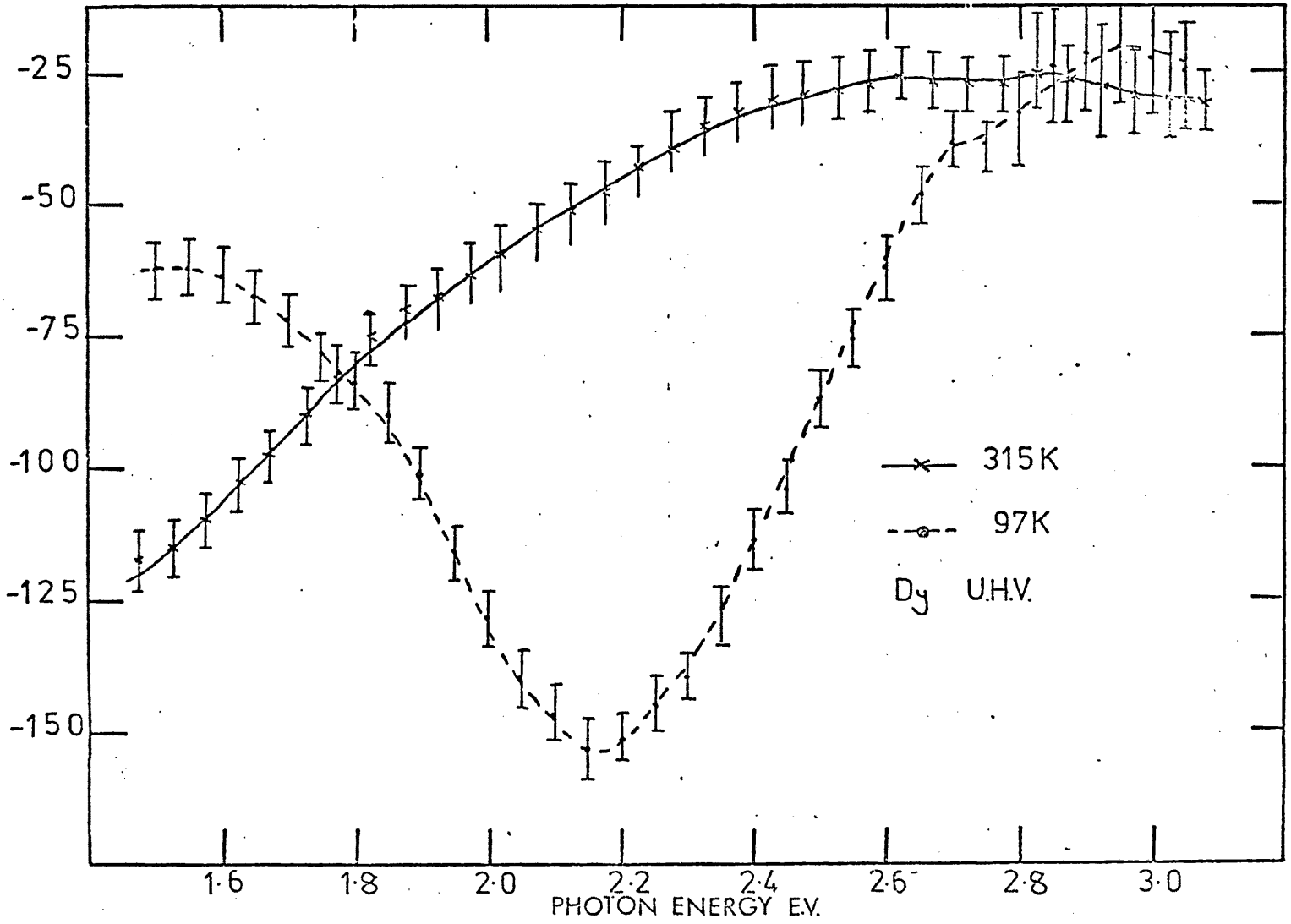

Figure (6.8)
The (ΔRp/Rp) spectra of a U.H.V. grown dysprosium film at 97K and 315K

Figure (6.8a)
Further data on dysprosium

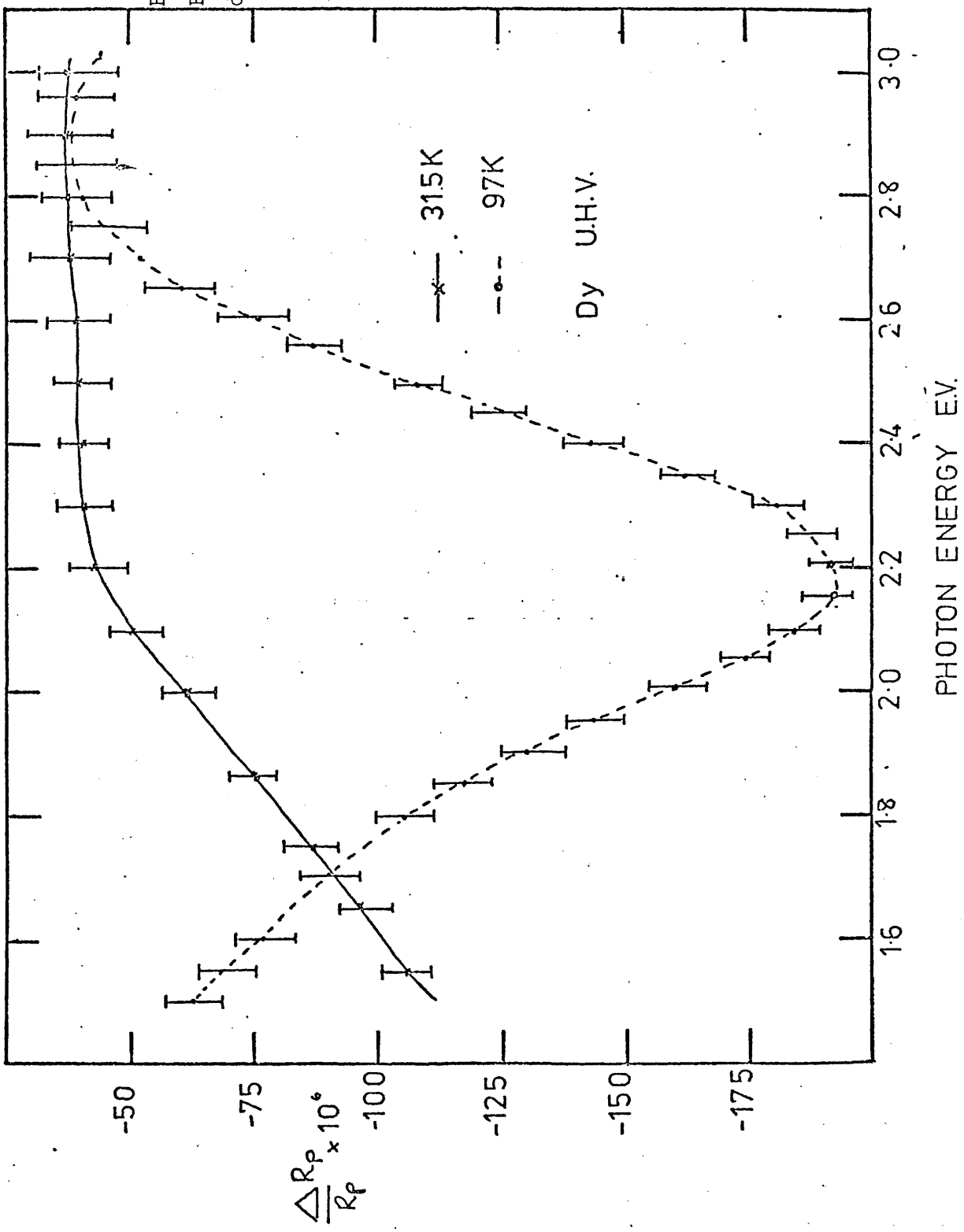

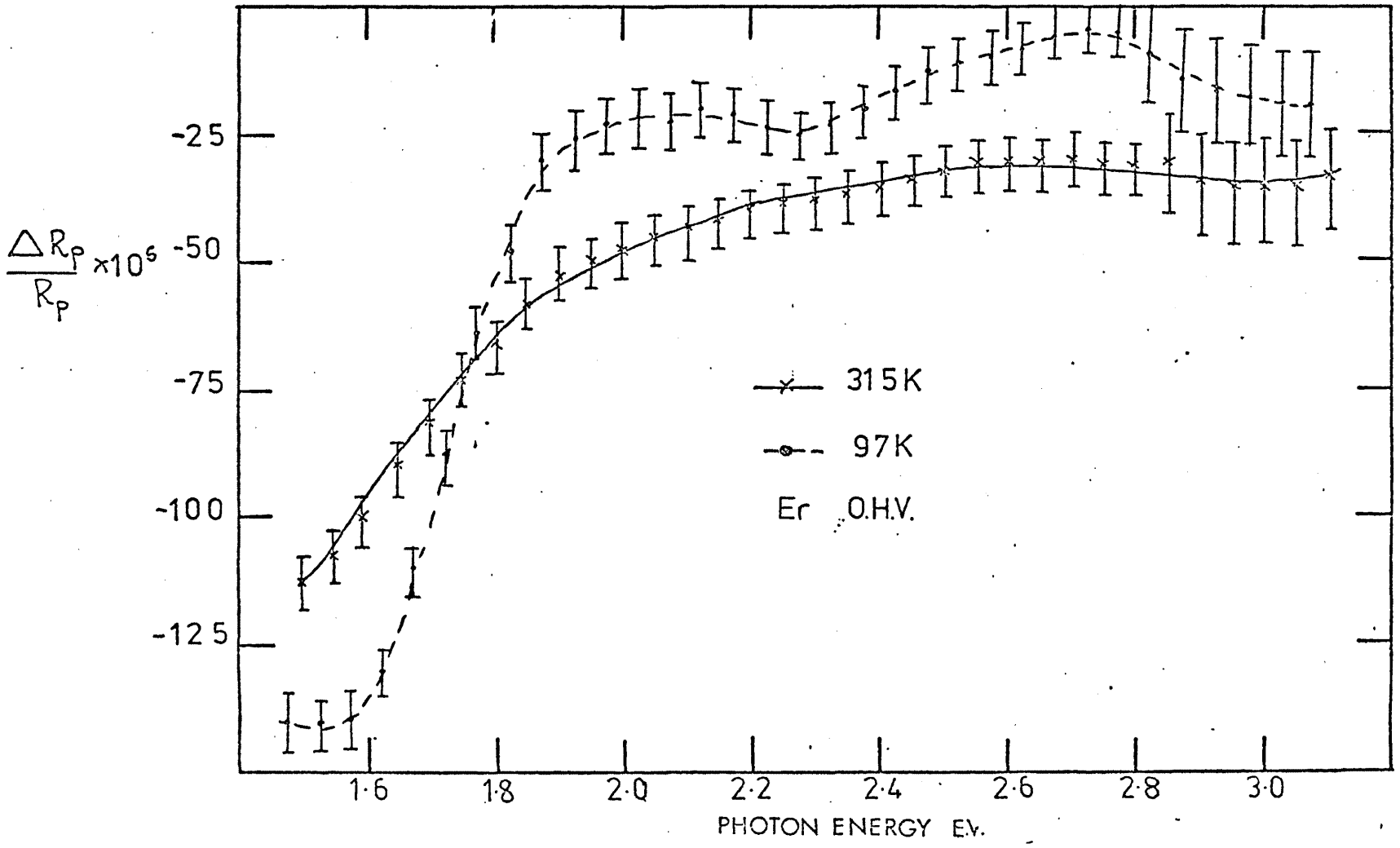

Figure (6.9) The (ΔRp/Rp) spectra of an O.H.V. grown erbium film at 97K and 315K

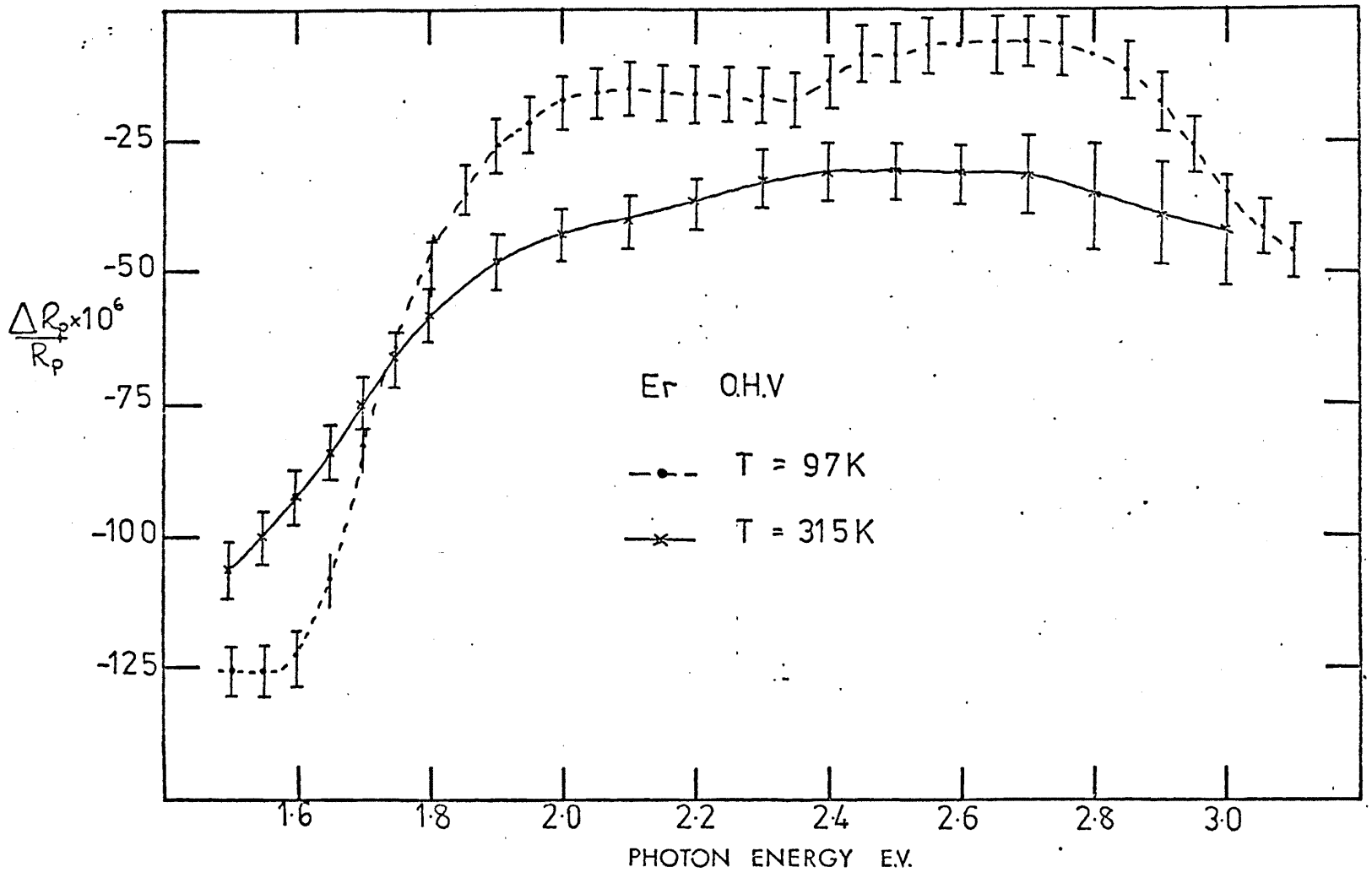

Figure (6.9a) Further data on erbium

and 2.7 eV. From Figure (6.1) we see that both the high and low temperature traces correspond to measurements taken when erbium was in the paramagnetic state.

6.8 The thermally modulated reflectance spectra of gadolinium terbium and dysprosium as a function of temperature.

In the preceding sections we have seen that on lowering the temperature of films of the heavy rare earth metals to 97K the thermally modulated reflectance dispersion curves are considerably sharpened and new structure appears. With the exception of erbium, all the elements studied are known to exhibit magnetic ordering in the temperature range 90K to 295K. The first theoretical prediction of changes in the optical properties of the rare earth metals caused by magnetic ordering were reported by Miwa (1963) who used the free electron model to evaluate energy gaps at superzone boundaries resulting from the antiferromagnetic helical spin configuration. It was later concluded (Cooper and Reddington 1965) that observed optical changes were connected with the onset of magnetic ordering, rather than changes in the periodicity of the ordering. In view of these facts it was decided to study more closely the behaviour of the ($\Delta Rp/Rp$) response as a function of temperature so as to ascertain what effect, if any, magnetic ordering had on the observed spectra.

The experiments were performed in the following manner: after the ($\Delta Rp/Rp$) dispersion curves at high and low temperature had been recorded, the current pulser was switched off, the cryostat was filled with liquid nitrogen and the system allowed to stablize at low temperature. The monochromator was set at a fixed wavelength and current was pulsed through the sample. The output of the lock-in amplifier (recording ($\Delta Rp/Rp$)) and the output of the thermocouple were fed to two pen recorders (Panax Servoscribe SREC 2p). Both the thermally modulated reflectance response and the temperature of the sample could thus be monitored as a function of time

during the course of the experiment. As the current was pulsed through the film, the temperature of the cryostat and sample slowly increased. The experiment was terminated when the sample temperature was some 20K above room temperature. This temperature was chosen because gadolinium has the highest magnetic ordering temperature (T_c = 293K) of all the elements studied.

Figures (6.10) and (6.11) show the ($\Delta Rp/Rp$) response as a function of sample temperature of U.H.V. - grown gadolinium and terbium films respectively. The measurements were made at 1.6 eV for gadolinium and at 1.675 eV for terbium. These energies were chosen since we see from Figures (6.2) and (6.5) that the ($\Delta Rp/Rp$) dispersion curves at low temperature show a maximum divergence from the curves obtained at higher temperatures at these photon energies. Figures (6.12) and (6.13) show typical thermally modulated reflectance responses, as a function of temperature, for a range of photon energies for an O.H.V. - grown dysprosium film. Of particular interest in Figures (6.10) to (6.13) inclusive is the occurrence of a marked change in slope at the points denoted by A. Table (6.1) gives the temperature at which this change occurs together with the magnetic transition temperatures of the 3 elements, gadolinium, terbium and dysprosium. We see that the anomalous behaviour of the thermally modulated reflectance response occurs very near to the magnetic ordering temperatures. However, before we infer that these changes in slope indicate changes in the optical properties of the rare earth metals at the magnetic transition temperatures, the behaviour of other factors affecting the thermal modulation response must be considered. From (3.2) the modulation efficiency γ is given by:

$$\gamma = 0.405Q\tau/C \qquad (6.1)$$

where Q the heat leak per unit time and unit temperature difference between sample and sink.

τ the periodicity of the current.

C the heat capacity of the sample

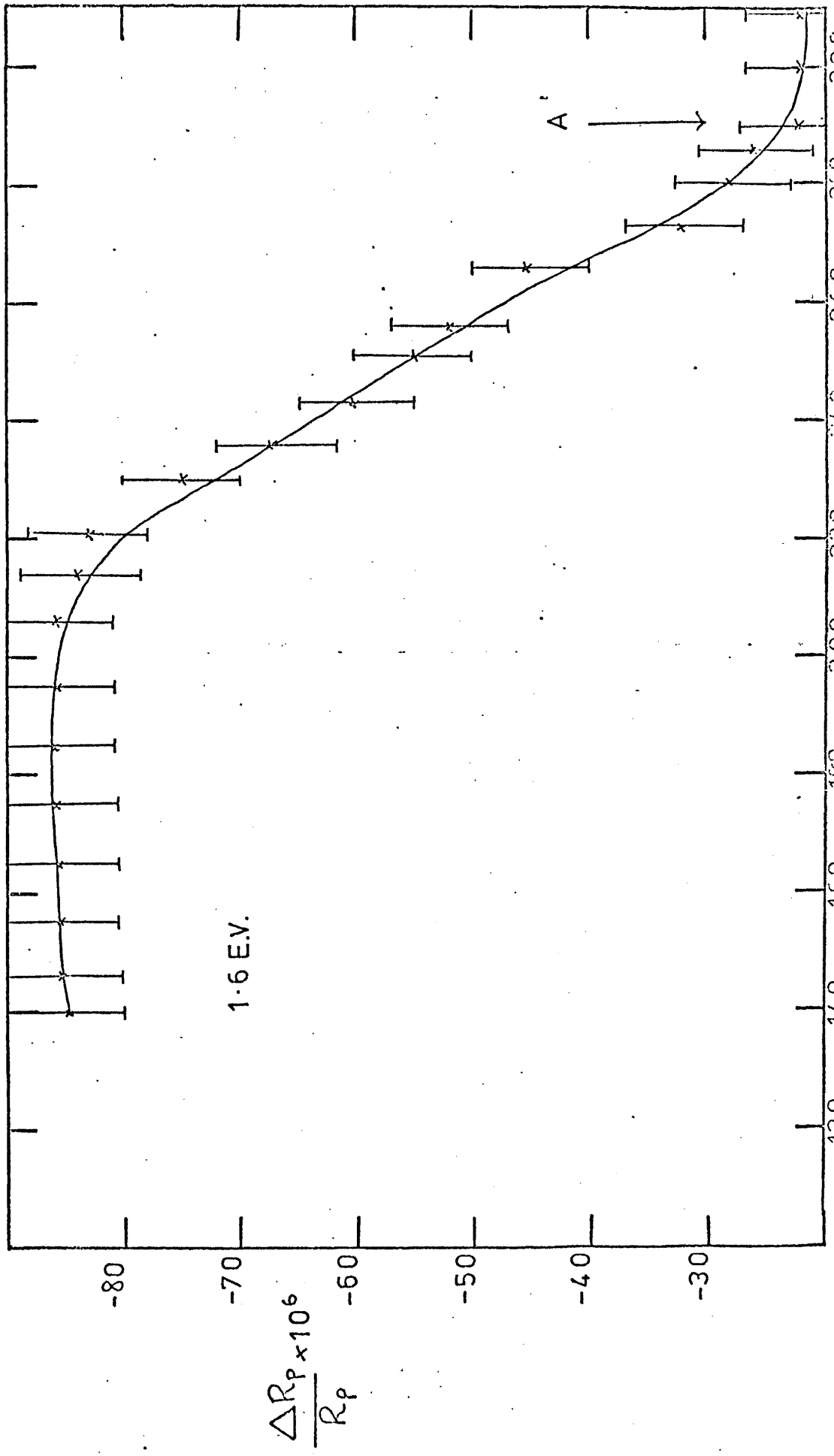

Figure (6.10) The ($\Delta Rp/Rp$) response as a function of temperature for a U.H.V. grown gadolinium film.

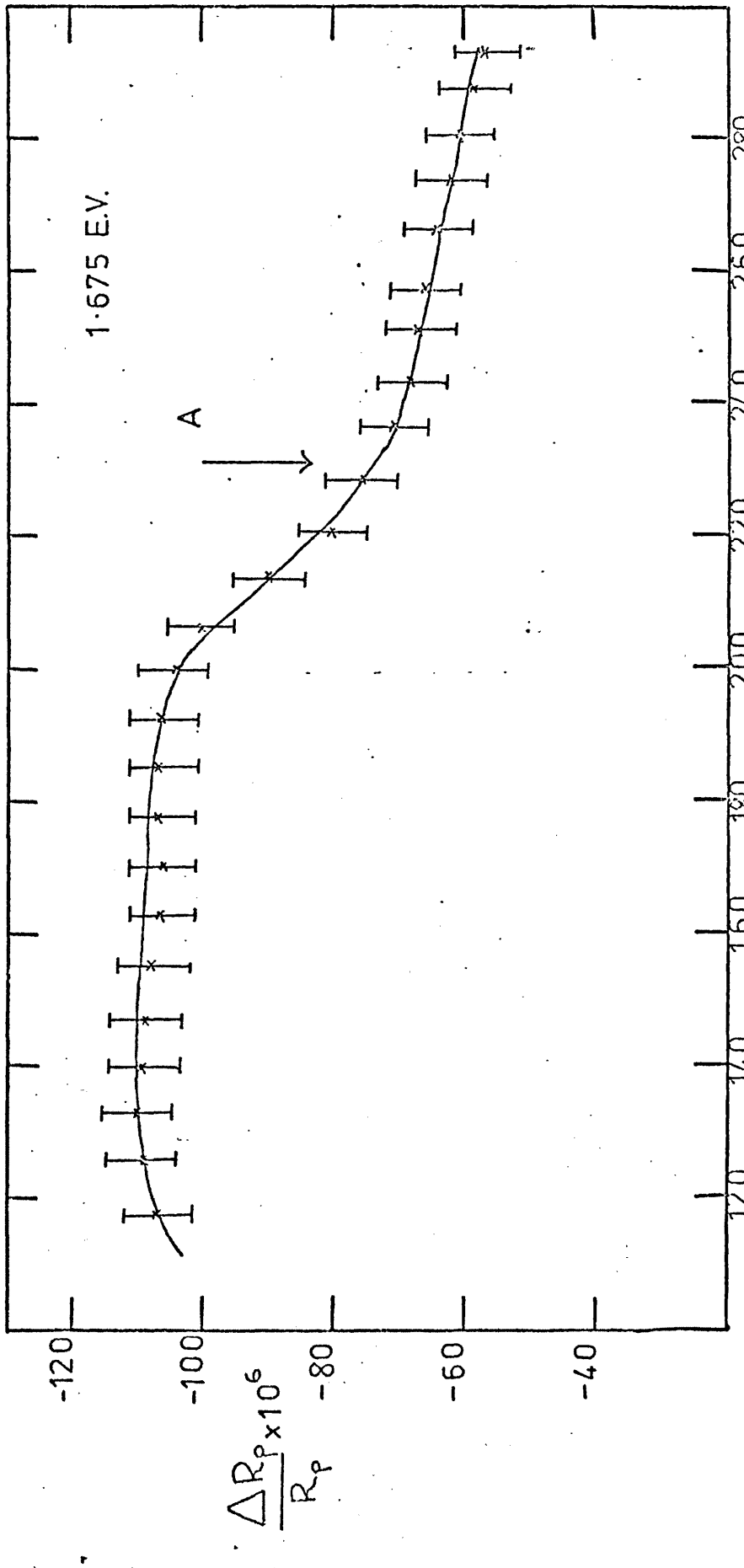

Figure (6.11) The (ΔRp/Rp) response as a function of temperature for a U.H.V. grown terbium film.

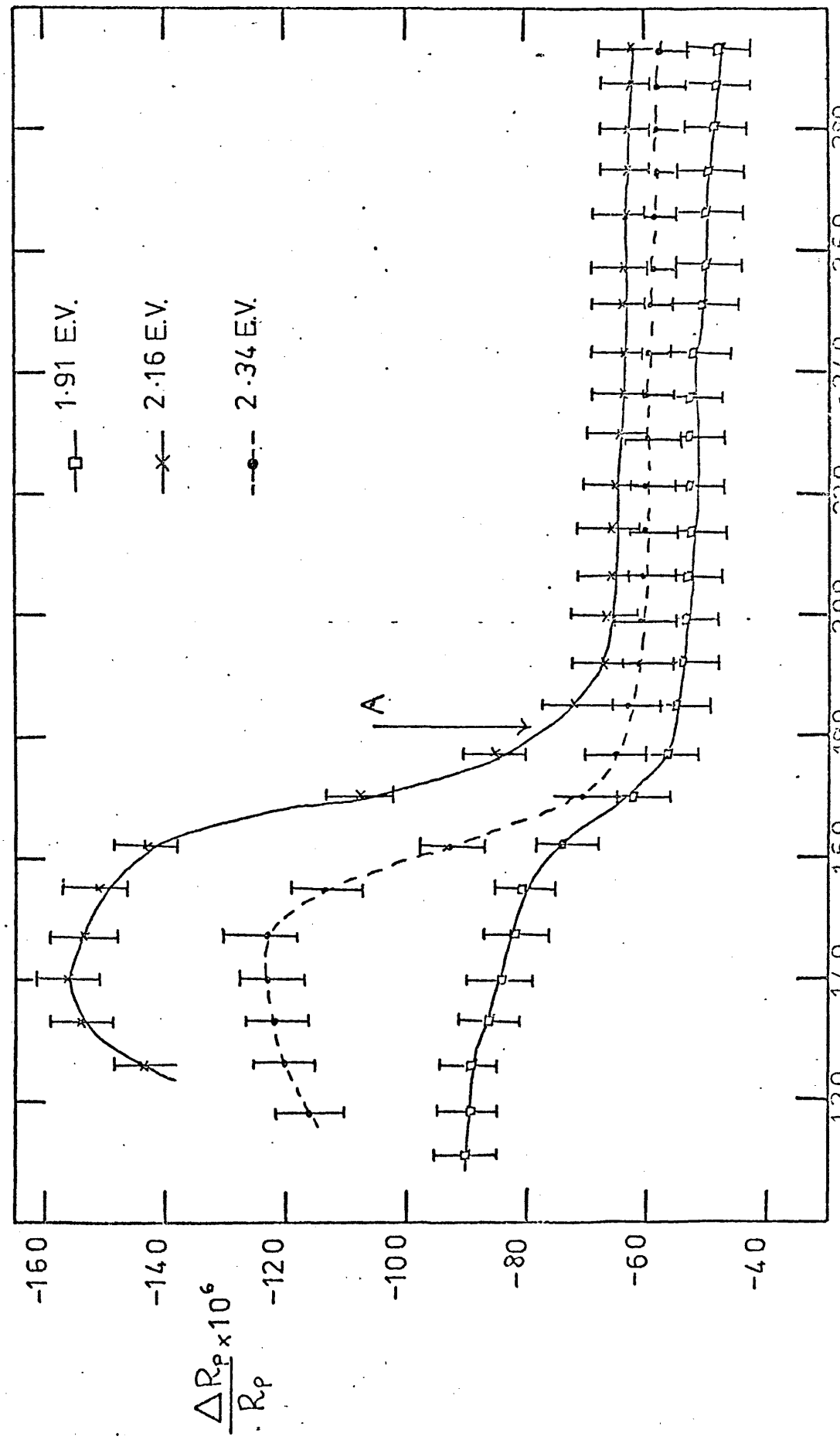

Figure (6.12) The ($\Delta R_p/R_p$) response as a function of temperature for an O.H.V. grown dysprosium film.

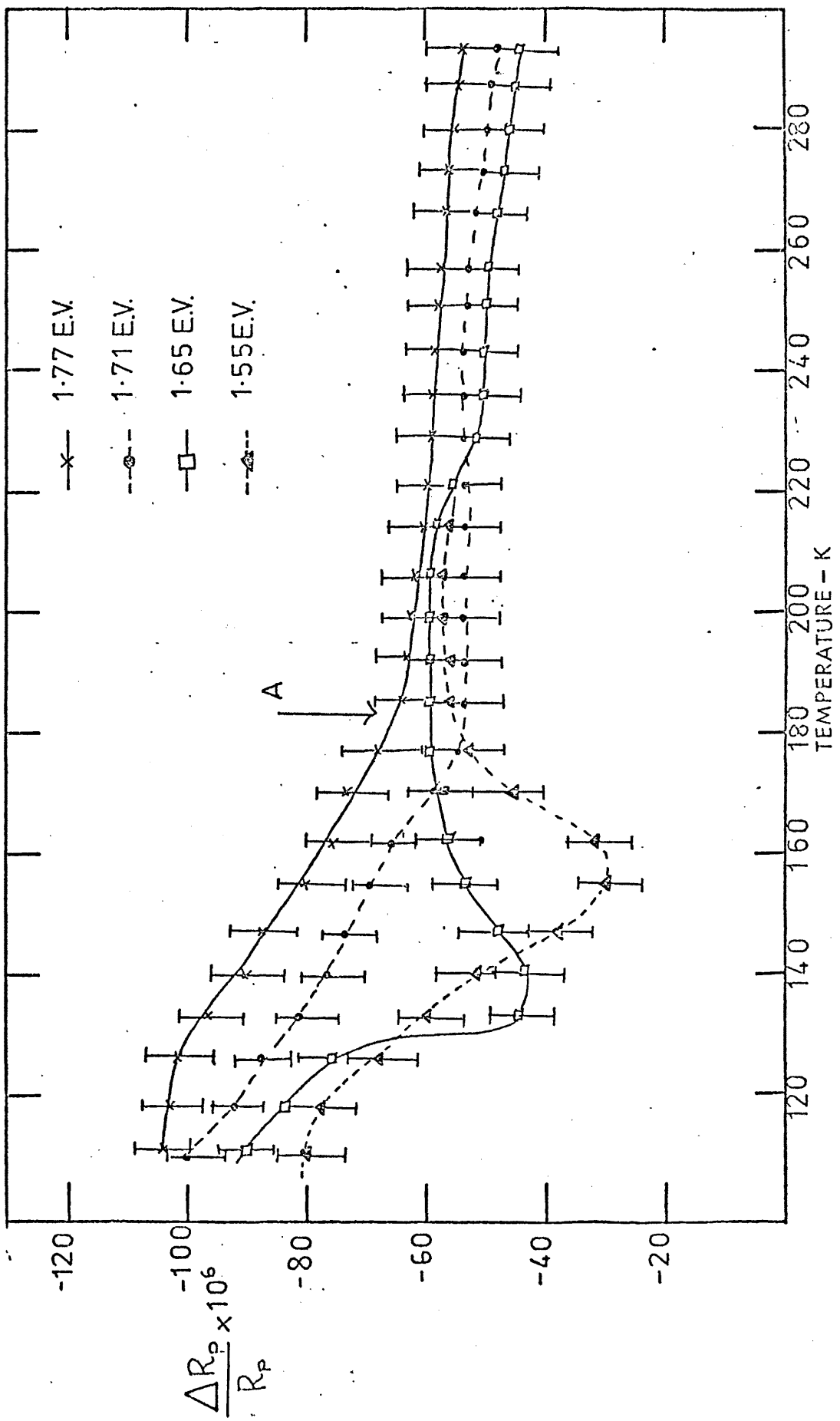

Figure (6.13) The (ΔRp/Rp) response as a function of temperature of an O.H.V. grown dysprosium film.

TABLE 6.1

ELEMENT	TEMPERATURE AT WHICH CHANGE IN SLOPE OF (ΔRp/Rp) OCCURS	CURIE POINT	NÉEL POINT
GADOLINIUM	290K (± 5k) (1.60 eV)	293K	-
TERBIUM	230K (± 5k) (1.675 eV)	221K	229K
DYSPROSIUM	185K (± 5k) (2.16 eV)	85K	179K
	177K (± 5k) (2.34 eV)		
	180K (± 5k) (1.91 eV)		
	182K (± 5k) (1.77 eV)		
	177K (± 5k) (1.71 eV)		

Table 6.1 indicates the temperatures at which the change in slope of the (ΔRp/Rp) against temperature curve occurs for the elements Gd, Tb and Dy, together with the magnetic transition temperatures of these elements.

and $Q_{max} = K/d$, where K is the thermal conductivity of the sample and d the thickness.

The magnitude of the thermally modulated reflectance response also depends on the electrical power dissipated in the sample, which in turn is directly related to the resistivity of the specimen. The electrical resistivity, ρ, and the thermal conductivity, K, of polycrystalline bulk samples of the heavy rare earth metals have been measured as a function of temperature between 90K and 300K by Chuah and Ratnalingham (1973). Figure (6.14) indicates their results for dysprosium, and we see that anomalous behaviour of both ρ and K was observed at the magnetic ordering temperatures. Similar results were obtained for gadolinium, terbium and holmium. Griffel et al. (1957) have measured the specific heat of dysprosium as a function of temperature. From their results, shown in Figure (6.15), we again see anomalous behaviour at the magnetic ordering temperatures; similar results were obtained from the other rare earth metals. The effects of the anomalous behaviour of ρ, K and C with temperature on the thermally modulated reflectance response of a dysprosium film are summarized below. It should be noted that the analysis may be applied to gadolinium and terbium.

On raising the temperature of dysprosium through the Néel point:-

(i) K increases more rapidly with increasing temperature T causing γ and hence $(\Delta Rp/Rp)$ to increase more rapidly with increasing T.

(ii) ρ increases less rapidly with increasing tempeature and hence the power dissipated in the sample will decrease less rapidly causing $(\Delta Rp/Rp)$ to decrease less rapidly with increasing T.

(iii) The specific heat drastically decreases with increasing T causing γ and hence $(\Delta Rp/Rp)$ to increase.

In Figures (6.11) to (6.13) we see that for gadolinium, terbium and dysprosium the modulus of the $(\Delta Rp/Rp)$ response decreases with increasing temperature and clearly (i) and (iii) above seem to have negligible effect

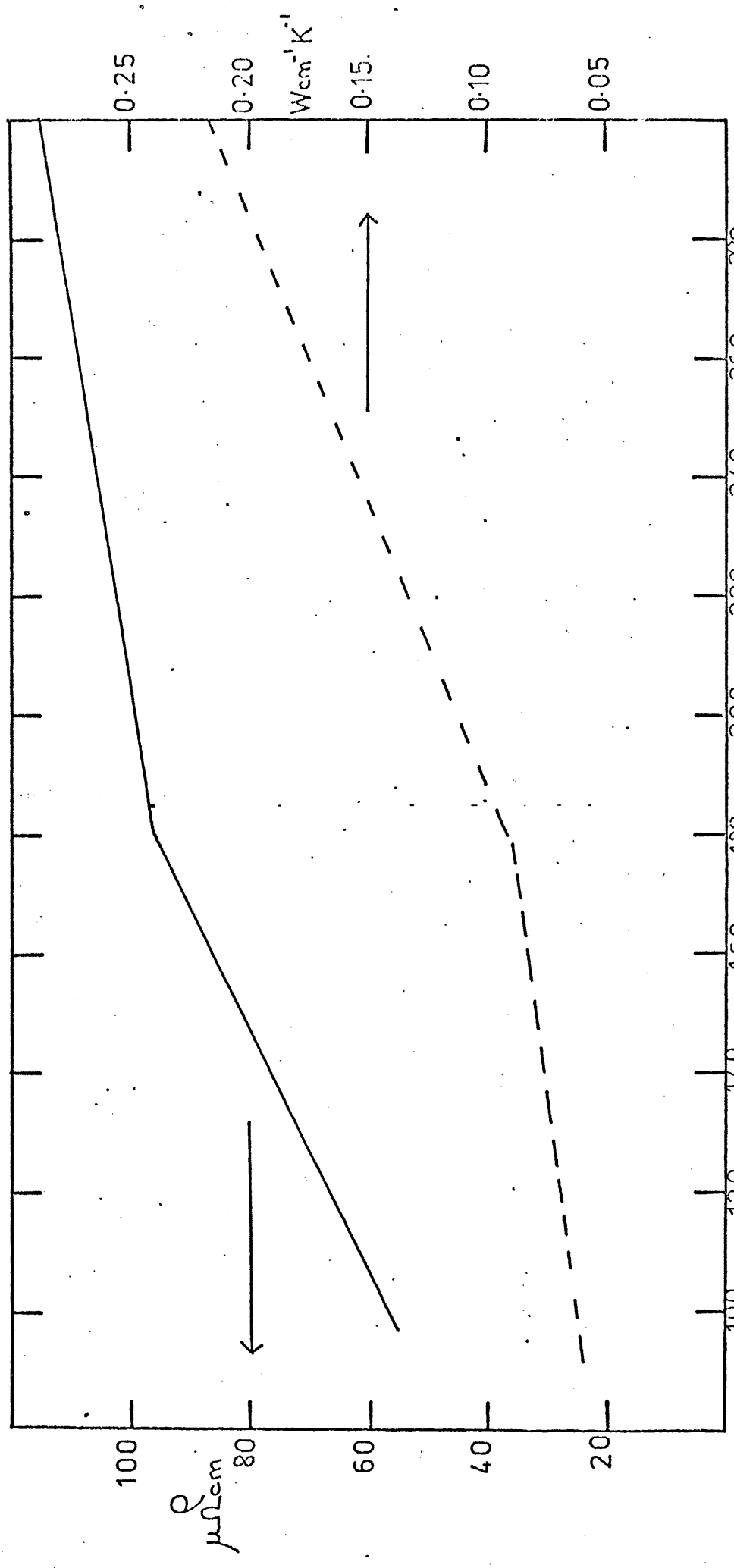

Figure (6.14) The temperature dependence of the electrical resistivity and thermal conductivity of polycrystalline dysprosium (Chuah and Ratnatingham 1974).

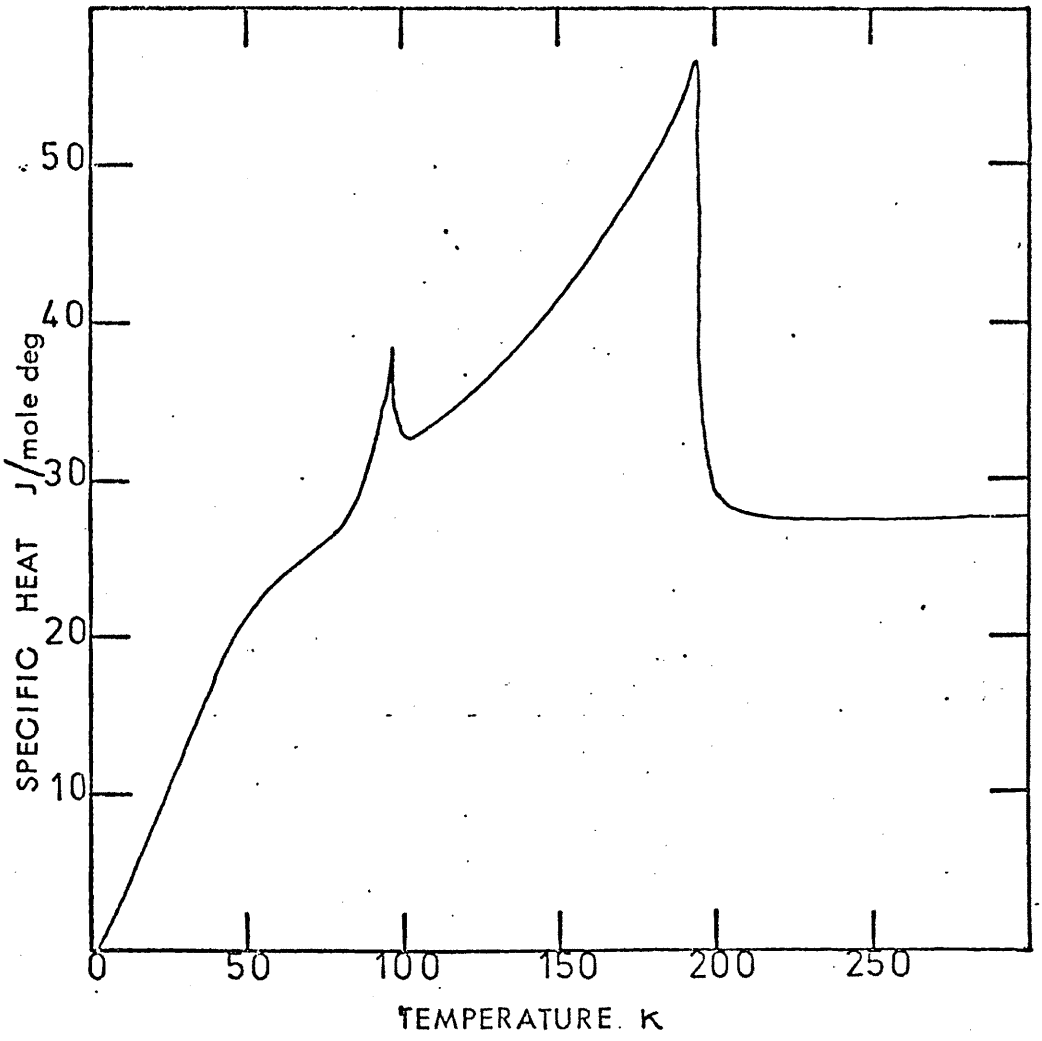

Figure (6.15) The temperature dependence of the specific heat of dysprosium (Griffel et al. 1957).

on the response since these two factors would cause an increase in the $(\Delta Rp/Rp)$ response on increasing the temperature. However, the anomalous behaviour of the resistivity of the sample causes the $(\Delta Rp/Rp)$ response to decrease less rapidly with increasing temperature, which is the effect observed in the present experiments. Although the anomalous behaviour of the thermally modulated reflectance response at the magnetic ordering temperatures or gadolinium and terbium films could be purely electrical in origin, this is not the case with dysprosium. In Figures (6.12) and (6.13) we see that the $(\Delta Rp/Rp)$ against temperature response is not independent of photon energy, anomalous behaviour occurring in the near infra-red part of the spectrum. It may thus be concluded that the anomalies in the thermally modulated reflectance response of dysprosium films observed at the magnetic ordering temperatures are genuinely optical in origin and not caused by variations in other factors which might affect the modulated reflectance response. However, we cannot come to such conclusions for the gadolinium and terbium samples since owing to experimental constraints the $(\Delta Rp/Rp)$ response as a function of temperature for an extensive range of photon energies could not be measured. The maximum $(\Delta Rp/Rp)$ response observed for gadolinium and terbium at 97K was 1.6 eV and 1.675 eV respectively and the limit of the spectral range in the present experiment (determined by the response of the photomultiplier) was 1.5 eV.

Changes in the optical properties of the rare earth metals above and below the magnetic transition temperatures have been previously observed using static optical techniques (Schuler 1966, Hodgson and Cleyet 1969, Erskine et al. 1974 and Krizek 1975) Schuler, Hodgson and Cleyet and Krizek observe changes at very much lower photon energies ($\sim$ 0.5 eV) than those reported in the present work. Only Erskine et al. and Hodgson and Cleyet report changes in the visible and near infra red parts of the spectrum. Hodgson and Cleyet find that the optical conductivity, $\sigma(w)$, dispersion curve of gadolinium is sharpened on lowering the temperature of the sample, the main peak moving from 1.6 eV at 293K to 1.8 eV at 105K.

Although Erskin et al. report a similar shift in the peak of $\sigma(w)$ for gadolinium they find that the main peak is broadened on cooling the specimen. Erskine et al. extended their studies to terbium and dysprosium where similar behaviour is observed, the main peak in $\sigma(w)$ terbium moving from 1.8 eV at 293K to 1.6 eV at 80K, No changes in the $\sigma(w)$ values of dysprosium are observed until photon energies of 2.5 eV are reached, the $\sigma(w)$ values being lower at 80K than 300K.

In the present work it is difficult to firmly identify a single mechanism to explain the occurrence of the thermally modulated reflectance anomalies at the Néel Point of dysprosium, without further experimental and theoretical studies being undertaken. There are 3 mechanisms which may cause changes in the optical properties of the rare earth metals and these are summarized below:-

(i) Exchange splitting of the conduction electron bands due to ferromagnetic ordering.

(ii) The effect or magnetic superzone boundaries in the antiferromagnetic phase. Miwa (1963) has suggested that optical transitions can occur across energy gaps at superzone boundaries induced by a periodic spin structure. The theory predicts changes in the optical conductivity dispersion curve at the transition between the antiferromagnetic and ferromagnetic phases.

(iii) Magnetostriction: Magnetostriction is characterised by sudden changes in the lattice constants of a material at the magnetic transition temperatures. These changes produce changes in the band structure which in turn influence the optical constants of the material. Large magnetostrictive strains have been found in the heavy rare earth metals and sudden changes in the lattice constants of dysprosium in zero applied magnetic field have been observed at the magnetic transition temperatures (Clark 1965). The large changes at the Curie point have been shown to arise because of an orthorhombic distortion of the hexagonal close-packed crystal lattice (Darnell and Moore 1963).

In order to find which mechanism is responsible for the occurrence of the anomalies in the thermally modulated reflectance response at the magnetic transition temperatures it is felt that further measurements need to be made over a more extensive spectral range down to at least 0.5 eV. (This is the photon energy at which Schuler (1966), Hodgson and Cleyet (1969) and Krizek (1975) observe large changes in the optical properties of the rare earth metals). In the present work the lowest temperature which could be attained was 90K, which meant that out of all the heavy rare earths studied, terbium and gadolinium were the only metals with Curie temperatures in this range. Cooling with liquid helium would allow measurements to be taken down to at least 20K, which would allow the thermally modulated reflectance response at the Curie point of dysprosium and the Curie and Néel points of erbium to be studied. At present no band structure calculations have been performed for variations in the lattice constants of the heavy rare earth metals. Such calculations would show whether new optical transitions occurred at particular photon energies when the lattice constants of the material are perturbed, as they are in the case of magnetostriction.

As a final comment on the studies of the thermally modulated reflectance responses of the heavy rare earth metals as a function of temperature it should be noted that we have been able to locate anomalies, either optical or electrical in nature, at the magnetic transition temperatures of the elements themselves. This is a good indication that the composition of our thin film samples was predominantly that of the pure element rather than of the dihydride or an oxide since both dihydrides and oxides of the rare earth metals have magnetic transition temperatures at much lower temperatures than the elements themselves (Wallace 1972, Henry 1955).

6.9 A summary of the results of the thermally modulated reflectance dispersion curves of the heavy rare earth metals

In (6.3) to (6.7) inclusive we have seen that the thermally modulated reflectance spectra at 315K of gadolinium, terbium, dysprosium and erbium in the spectral range 1.5 eV to 3.0 eV is rather featureless. The fine structure observed in the optical conductivity dispersion curves of gadolinium and terbium by Miller et al. (1974) has not been observed in the present thermal modulation experiments. In (2.3) we have seen that it is unwise to correlate the thermally modulated reflectance response directly with band structure calculations since the coefficients $\alpha_{p,s}$ and $\beta_{p,s}$ in equation (2.16) are themselves dispersive. Structure seen in the $(\Delta Rp/Rp)$ response may thus be due to structure in the coefficients themselves. Figure (6.10 shows the coefficients $\alpha_{p,s}$ and $\beta_{p,s}$ for gadolinium as a function of photon energy. The coefficients have been computed for an angle of incidence of 45° since all the thermal modulation measurements were undertaken at this angle. The optical constants used in the calculation or the coefficients were taken from Krizek (1975) since his data covered the spectral range of the present experiments. A calculation of $\alpha_{p,s}$ and $\beta_{p,s}$ using optical constants taken from Miller et al. (1974) gave similar results in the range 1.8 eV to 3.0 eV (their data only extends to 1.8 eV). We see from Figure (6.16) that in the spectral range of the present thermal modulation studies $|\alpha_p|$ is always greater than $|\beta_p|$, and similar results were obtained for the other rare earth metals. Although we have no knowledge of the theoretical shapes of the $\Delta\varepsilon_1$ and $\Delta\varepsilon_2$ dispersion curves, (the changes in the real and imaginary parts of the dielectric constant respectively), the behaviour of the coefficients α_p and β_p would imply that the $(\Delta Rp/Rp)$ response is dominated by $\Delta\varepsilon_1$. Figure (6.17) shows a comparison between the $(\Delta Rp/Rp)$ response of a gadolinium film obtained in the present work with the change in the real part of the dielectric constant

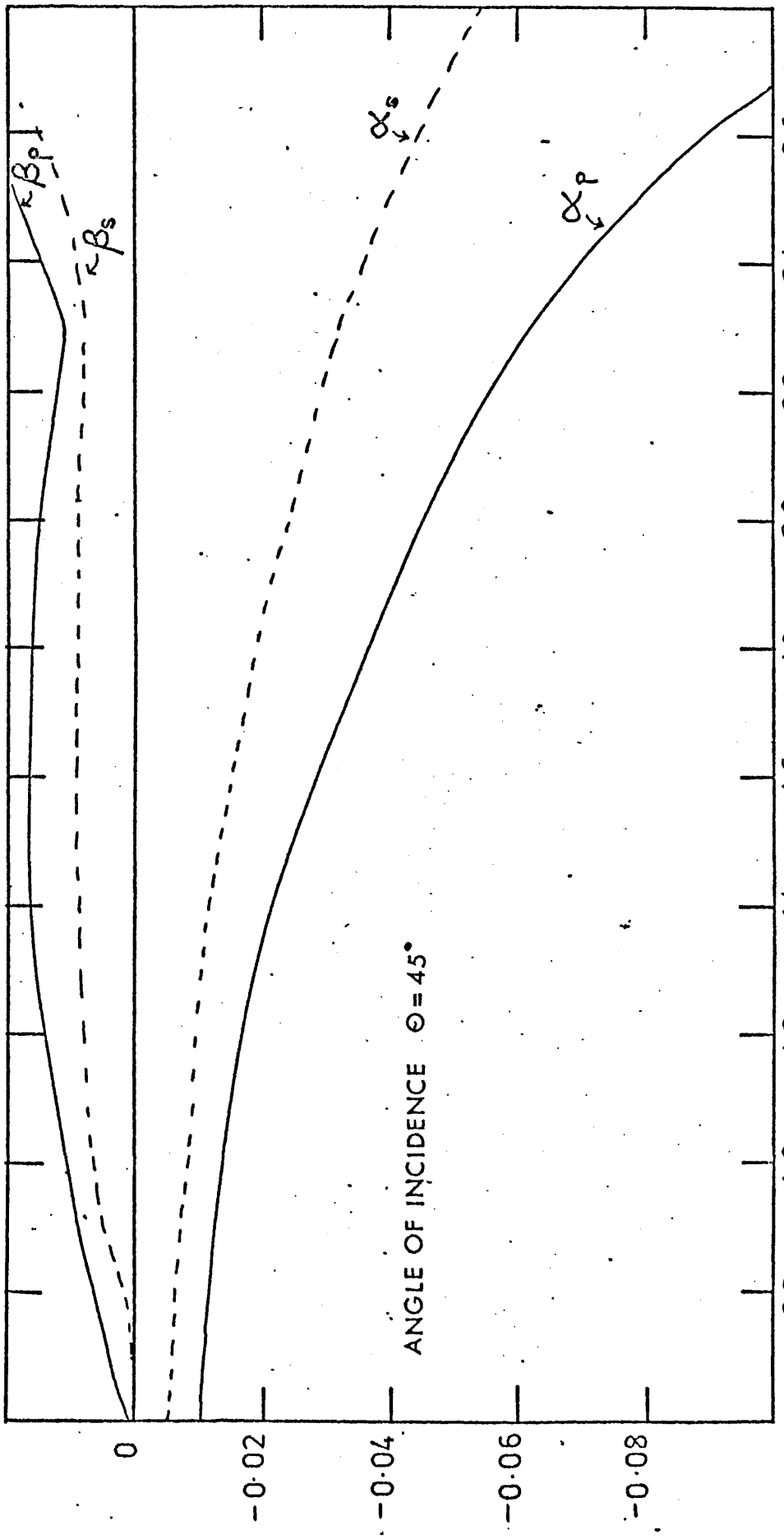

Figure (6.16) The spectral dependence of α and β for gadolinium at θ = 45°

Figure (6.17) The change in ϵ_1 with temperature interpolated from Hodgson and Cleyet (1969) compared with the $(\Delta Rp/Rp)$ response at 97K obtained from a gadolinium film in the present work.

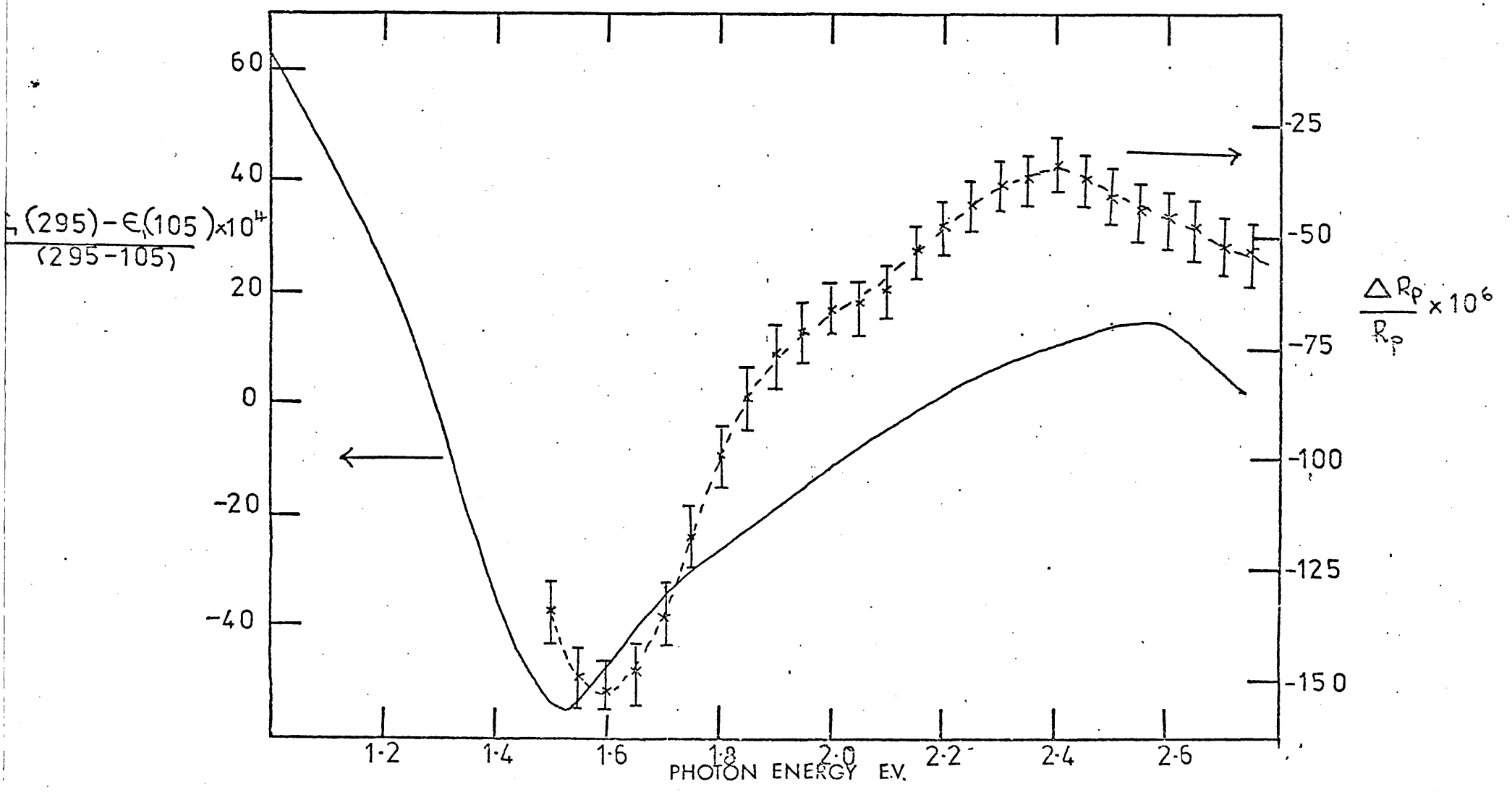

$$(\varepsilon_1(295K) - \varepsilon_1(105K))/(295-105)$$

interpolated from the results of Hodgson and Cleyet (1969) on gadolinium. We see that there is quite good agreement between the two curves, a minimum occurring near to 1.50 eV in Hodgson and Cleyet's results, compared with a minimum of 1.60 eV from the present work. Structure is also seen near 2.55 eV in Hodgson's work compared with structure at 2.4 eV in the thermal modulation measurements. It would seem from Figure (6.17) that the $(\Delta Rp/Rp)$ response is dominated by changes in the real part of the dielectric constant. At this point we note that fine structure in the ε_1 dispersion curves obtained by Miller et al. (1974) was not so predominant as that in the $\sigma(w)$ dispersion curves.

Attempts were made to analyse the $(\Delta Rp/Rp)$ data obtained from the rare earths by the Kramers-Kronig method of analysis. Unfortunately, the form of the response for these elements is such that this method of analysis is inappropriate without an extended range of data. Unlike the analysis of the gold and copper results a constant extrapolation is not appropriate at the low energy limit of the data. Clearly, further measurements need to be made over a much wider spectral range in order that the thermally modulated reflectance data may be analysed and correlated with electronic band structure calculations.

CHAPTER VII

THE ELECTRO-OPTICAL CHARACTERISTICS OF A TOTALLY INTEGRATED THIN FILM OPTICAL MODULATOR

7.1 Introduction

In this chapter we briefly discuss the theory underlying the effect of a uniform electric-field on the optical properties of insulators and semiconductors. The preparation and electro-optical characteristics of a totally integrated thin film optical modulator based on the Franz-Keldysh effect with a cadmium sulphide film as the active medium, are then described (the configuration and optimum growth conditions of the films comprising the modulator have been described in Chapter IV). Although the modulator designed in the present work overcomes some of the disadvantages of conventional electro-optic modulators (see (4.6)) this results in a reduced performance in terms of the modulation efficiency, η, where η is defined as:

$$\eta = (T - Te)/I_o = \Delta T/T_o \qquad (7.1)$$

where T is the transmitted light intensity in zero applied electric field

Te is the transmitted light intensity with an applied electric field.

and I_o is the incident light intensity.

However, we see in (7.5) that by suitable filter design this limitation may be partially overcome. In order to accomplish the filter design a computer program has been developed to calculate the optical properties of a multilayer stack of thin films having an arbitrary number of layers with generally complex refractive indices. The program uses the matrix method proposed by Abeles (1948) and both the program and method are fully described in (7.5).

We have seen in Chapter 1 that one of the most surprising results from the use of an electrolytic electro-modulation technique was observed by Feinleib (1966), who reported electric field modulation of the reflectance from metal-electrolyte interfaces. In view of this work, a "dry package"

technique was used in the present work to study the electromodulation of metals. In (4.8) we have seen that the electrical characteristics of the dielectric films to be used in the optical modulator were investigated by fabricating thin film capacitors and investigating the electro-optical properties of the thin film metallic electrodes. The results of this investigation are described in (7.8) together with a computer simulation of a model for the electromodulation mechanism at a metal-electrolyte interface. The computer studies showed that the electroreflectance effect could be reproduced if one assumed the formation of a thin absorbing layer in the electrolyte during the application of the electric field. From this work, and the results of the "dry package" experiments, we tentatively conclude that electromodulation effects in metals are not primarily due to changes in the optical properties of the metal, but to changes in the optical properties of the electrolyte.

7.2 The theory of electroabsorption in insulators and semiconductors

The tunnelling of carriers in semiconductors under the influence of strong electric fields was initially predicted by Zener and Wills (1934) and later more accurately by Houston (1940). However, it was not until 1958 that Franz and Keldysh independently studied the effect of high electric fields ($\sim 10^5$ to 10^6 Volts/cm) on the optical properties of insulators and semiconductors, by using the wavefunctions calculated by Houston. The Franz-Keldysh effect as it later became known is described in terms of the tunnelling of electrons in valence and conduction bands into the states of the forbidden band, the effect of the electric field causing a shift of the absorption edge of the material to longer wavelengths. Basically, the application of an electric field to a crystal breaks the symmetry of the Hamiltonian of the system in the direction of the field by adding a potential energy term $-eF.\underline{r}$ (for a uniform electric field). The term $-eF.\underline{r}$ shifts the origin of the energy with $\underline{r}$ as indicated in Figure (7.1).

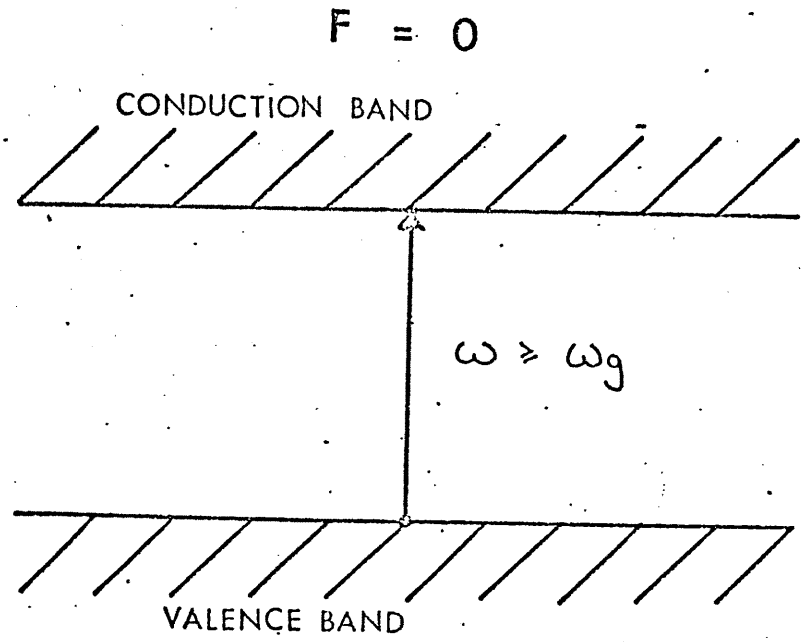

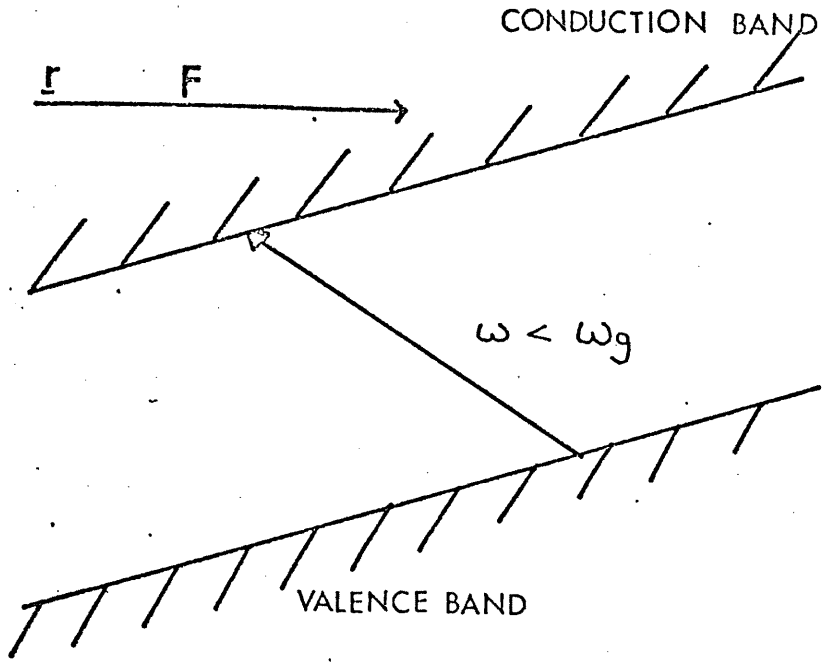

Figure (7.1) The effect of an applied electric field on energy bands.

The one electron Hamiltonian of the system is now no longer invariant to lattice translations in the direction of the electric field and transitions between the valence and the conduction bands are now possible for energy smaller than the band gap, Eg. Franz (1958) and Keldysh (1958) showed that for an "Urbach type" absorption edge, where the absorption coefficient has an exponential form as given below:

$$\alpha = \alpha_o \exp\ (bh\nu/kT) \qquad (7.2)$$

where α is the absorption coefficient

h is Planck's constant

ν is the frequency

b is the logarithmic slope of the absorption edge

T is the absolute temperature

k is Boltzmann's constant

the change in the absorption coefficient, $\Delta\alpha$, due to the effect of an applied electric field is given by

$$(\Delta\alpha/\alpha) = \hbar^2 e^2 b^3 F^2 / 24(kT)^2 m^* \qquad (7.3)$$

where m^* is the reduced effective mass

e is the electronic charge

$\hbar$ is the reduced Planck's constant

F is the electric field strength

and b, k, and T have the same meaning as in equation (7.2). However, we note that the theory developed by Franz and Keldysh was restricted to perfect crystals, direct optical transitions and to photon energies below the absorption edge. Callaway (1963, 1964) and Tharmalingham (1963) obtained more general results for direct transitions which were valid at photon energies both above and below the absorption edge. Tharmalingham has shown that for an M_o type absorption edge an explicit expression for the absorption coefficient α, as a function of electric field strength, F is given by:

$$\alpha(\omega,F) = R\theta_F^{\frac{1}{2}}/\omega \left|dAi(\beta)/d\beta\right|^2 - \beta|Ai(\beta)|^2 \qquad (7.4)$$

where

$$\theta_F = (e^2F^2/2\mu h)^{1/3} \qquad (7.5)$$

$$\beta = (\omega_1 - \omega)/\theta_F \qquad (7.6)$$

$$R = 2e^2C_o^2/\hbar\omega cnm^2(2\mu/\hbar)^{3/2} \qquad (7.7)$$

where C_o is a matrix element between periodic parts of the Bloch states at band energies

n is the refractive index of the material

m is the electron mass

μ is the reduced mass

e is the electronic charge

$\hbar\omega_1$ is the energy of the band gap

and the Airy Function $Ai(\beta)$ is given by:-

$$Ai(\beta) = \frac{1}{\pi^{\frac{1}{2}}} \int_0^\infty \cos(u^3/3 + u\beta)du \qquad (7.8)$$

where $Ai(\beta)$ is the solution of the differential equation

$$\omega'' - \beta\omega = 0 \qquad (7.9)$$

(see Abramowitz and Stegun 1964).

Tharmalingham was in fact the first to predict that there would be electric field induced oscillations in the electroabsorption spectra at photon energies above the fundamental absorption edge. Aspnes (1966, 1967) extended Tharmalingham's results to include all four types of critical point (M_o, M_1, M_2, M_3). Aspnes et al. (1968) unified the theory of electroabsorption by showing that both Callaway's and Tharmalingham's approaches led to the same result. Yacoby (1965) discussed the change in absorption for both direct and indirect transitions and obtained expressions for $\Delta\alpha$ which were valid below and above the fundamental absorption edge. Yacoby found

that agreement between theory and experiment was satisfactory for silicon in the vicinity of the fundamental absorption edge but at photon energies higher than this, the experimental results could not be explained by the exisiting theories. These discrepancies were explained as a result of an oversimplified approximation of the energies of electrons and holes in the conduction band.

The first experimental confirmation of Franz and Keldysh's theoretical predictions was observed by Williams (1960) who studied the electroabsorption response of single crystal bulk cadmium sulphide using an electrolytic technique described in Chapter I. However, the first electrooptical observations were probably made by Harrick (1956, 1960) who used an electric field to modulate the number of carriers in the space charge region of semiconductor surfaces. At photon energies close to the band edge large modulation effects were observed which could not be explained by free carrier absorption.

7.3 The preparation of the thin film optical modulator

The specimen geometry of the integrated thin film optical modulator designed in the present work has been discussed in (4.6). Devices were initially fabricated with thermally evaporated semi transparent ($\sim$ 200Å thick) films of aluminium as both top and bottom electrodes. Aluminium was chosen as the electrode material since it has a relatively flat transmission response over the visible part of the spectrum. However, it was found that when using aluminium films as the electrodes the transmitted light intensity of the entire device was so low that accurate electroabsorption measurements could not be made. Although the use of thinner aluminium films < 200Å increased the light transmission such films oxidised very quickly and did not retain their electrical conductivity. In view of this, attempts were made to grow films of stannous oxide (SnO_2) by thermal evaporation in ordinary high vacuum. Stannous oxide was chosen as the

electrode material since it combines the properties of good electrical conductivity together with optical transparency over the visible part of the spectrum. The material (B.D.H. powder form) was evaporated from a molybdenum boat onto float glass substrates at room temperature. Slow heating of the boat was required to prevent decrepitation of the charge material and eventually a "crust" was formed over the tin oxide. The deposited film was slightly yellow in colour and was highly insulating, and although heating in air at 250°C for 4 hours gave a transparent film, it was still insulating. Tin films $\sim$ 500Å thick were deposited onto float glass substrates by evaporation using an electron gun. These films were also heated in air at 250°C for 6 hours in an attempt to oxidise the tin. Although a transparent film was produced, it was insulating. In view of the difficulties encountered in depositing a transparent and electrically conducting thin film of stannous oxide a commerical grade of "conducting glass" (Baltracon grade) was used as the bottom electrode of the device and a 200Å thin film of aluminium as the top electrode. The "conducting glass" consisted of a 3000Å film of stannous oxide deposited by chemical vapour deposition and doped with antimony, deposited on float glass substrates. In the present work "conducting glass" with a sheet resistance of 150 Ω per square was used. The conducting glass sheet was cut into 2.5cm squares and the bottom electrode of the light modulator defined by painting a 2.5 cm x 0.3cm strip of molten paraffin wax onto the glass substrate. The wax was allowed to solidify and the tin oxide was etched in a 10% solution of orthophosphoric acid dispersed with zinc powder, at room temperature. (This is a standard etchant for metallic oxides). Typical etch times for the removal of the stannous oxide was $\sim$ 5 minutes, the etchant being agitated throughout this period. The sample was then taken out of the etch solution and rinsed in distilled water and then placed in acetone which dissolved the paraffin wax. The substrates were then placed in a degreasing agent (Decon 90) and the cleaning procedures described in (4.5) adopted.

The glass substrates were then placed in the Edwards 12EA O.H.V. system

and a thin film of cadmium sulphide deposited. The growth conditions of a typical film are given below:-

(i) The film was grown from cadmium sulphide granules (B.D.H. Vactran grade 4-40 mesh).

(ii) The film was deposited in the configuration described in (4.6) onto a "conducting glass" substrate held at 185°C.

(iii) A molybdenum boat was used as the source, the source-substrate distance being 8cm.

(iv) The O.H.V. system was evacuated to 5×10^{-6} torr and the boat and evaporant outgassed by passing a current of 40 amps for 5 minutes.

(v) After the outgassing procedure the system was allowed to attain its base pressure and a current of 60 amps was then passed through the boat and charge material for 10 minutes. The film was deposited in one evaporation. During all the cadmium sulphide evaporations a second float glass substrate was incorporated into the system so that the absorption edge of the film could be monitored and also the film thickness measured. After the deposition of the cadmium sulphide film, the substrate was transferred to a second O.H.V. chamber used exclusively for the evaporation of dielectrics. A film of silicon monoxide was then deposited onto the cadmium sulphide film, the growth parameters being:-

(i) Silicon monoxide (B.D.H. Vactran grade 4-40 mesh) was evaporated from a tantalum baffled source (see Plate 4.8) onto the substrate held at room temperature.

(ii) The rate of deposition was 11 Å sec^{-1} and the base pressure during the evaporation was $\sim 8 \times 10^{-7}$ torr.

A marked gettering action was observed as the material began to evaporate, showing rapid absorption of the residual gases in the chamber. All the films produced in this manner were slightly yellow in colour.

After deposition of the dielectric film, the substrate was transferred to another O.H.V. system and the top aluminium electrode deposited.

The aluminium was thermally evaporated from a tungsten "V" shaped filament onto the substrate at room temperature. The final film deposition consisted of an opaque aluminium film $\sim$ 2000Å thick deposited onto the extremities of the electrodes (see Figure 4.3b) in order that good electrical contact could be made to the modulator without damaging the thin top aluminium electrode.

7.4 The electroabsorption characteristics of the integrated thin film modulator

After the modulator had been fabricated it was placed with the electrode side resting on the brass studs of the sample holder shown in Plate (3.3). The detection system of Figure (3.1) was used with the modifications described in (3.8) to investigate the electroabsorption response of the cadmium sulphide film. A sinusoidal voltage was applied to the device, and the electroabsorption response $(\Delta T/T)$ was detected by lock-in amplifier and displayed on the pen recorder. At this point we define the modulation degree δ by

$$\delta = (T-T_e)/T = \Delta T/T \qquad (7.10)$$

where T and T_e have the same meaning as in equation (7.1).

Figure (7.2) shows the absorption edges, monitored by a Perkin Elmer Model 137 spectrophotometer of two cadmium sulphide films having different thicknesses, 2000Å and 1200Å respectively and we note that the thicker film exhibits a much steeper absorption edge. The importance, from the device viewpoint, of having a steep absorption edge is indicated in Figures (7.3) and (7.4) which show the electroabsorption spectra of two cadmium sulphide films, obtained with a sinusoidal signal applied to the device at a frequency of 38Hz (This frequency was chosen initially as it is not a multiple of "mains" frequency). We see that a much larger electroabsorption response is obtained from the device with the 2000Å cadmium sulphide film and δ_{max} (at the fundamental frequency) is $\sim$ 8% compared with δ_{max} $\sim$ 1.5% for the device having a 1200Å cadmium sulphide film. We also note that for both devices the electroabsorption response was observed at the fundamental

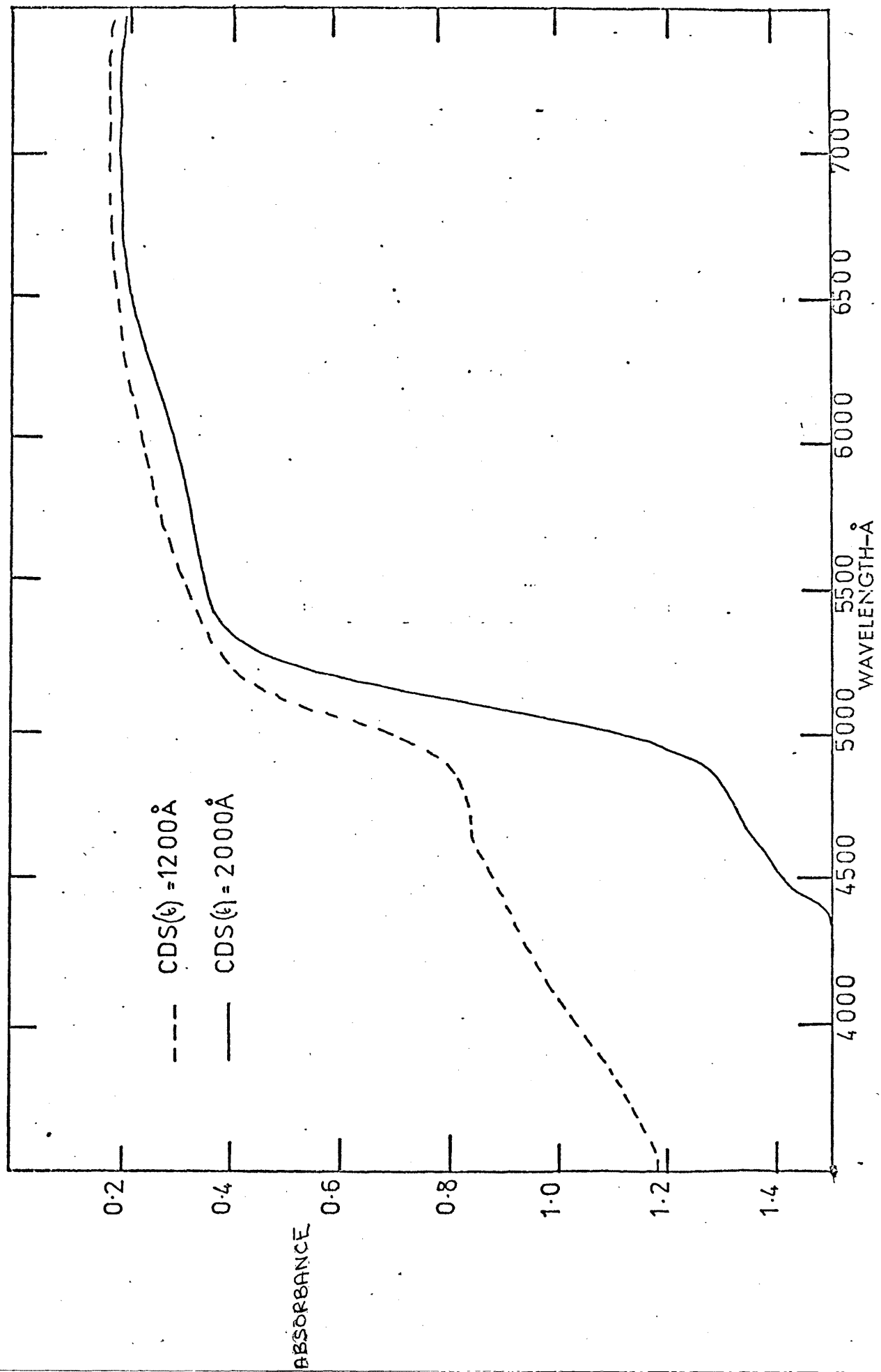

FIGURE (7·2) Absorption edges of cadmium sulphide films

Figure (7.3) The electroabsorption spectra of a 2000Å cadmium sulphide film.

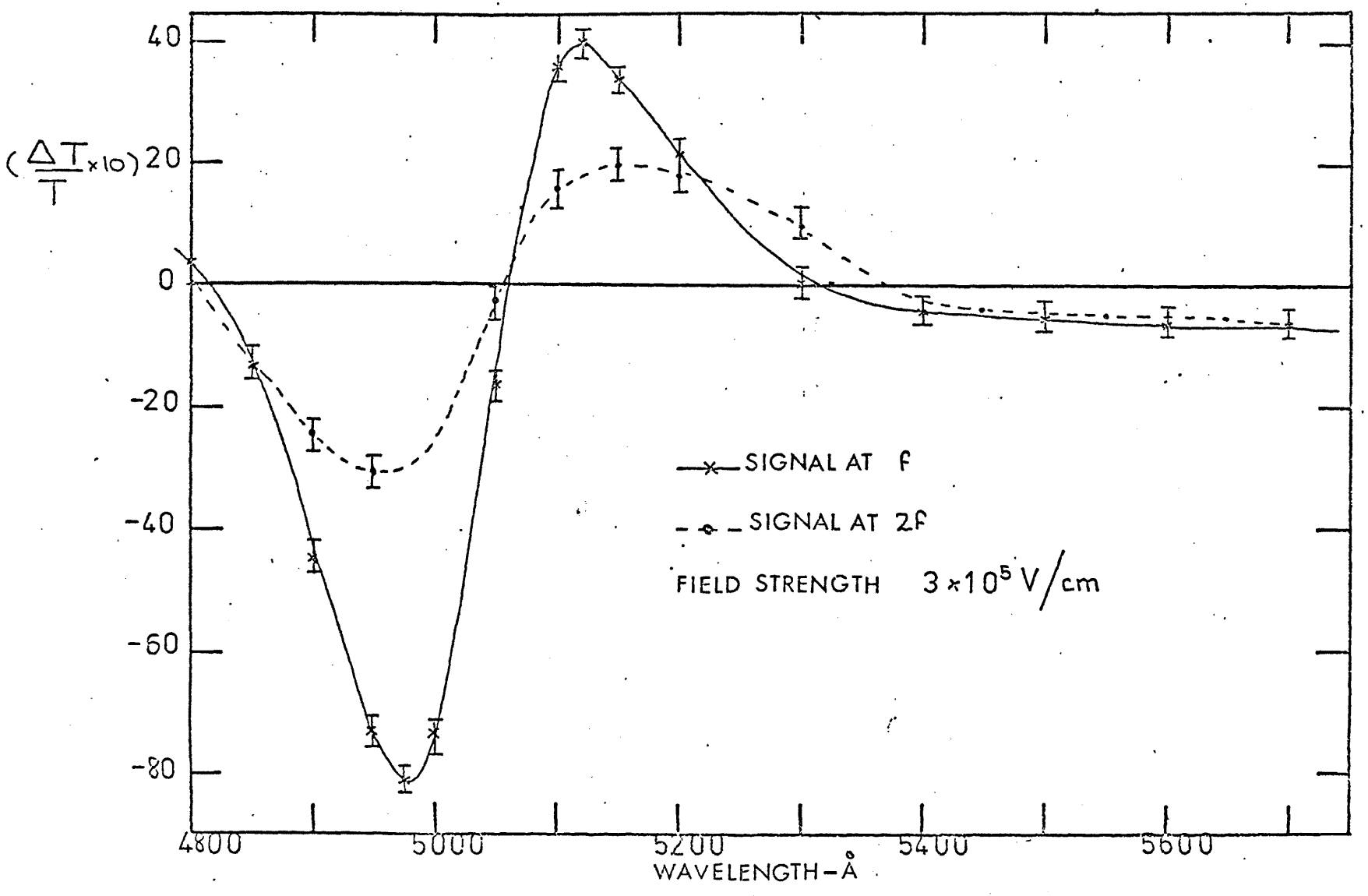

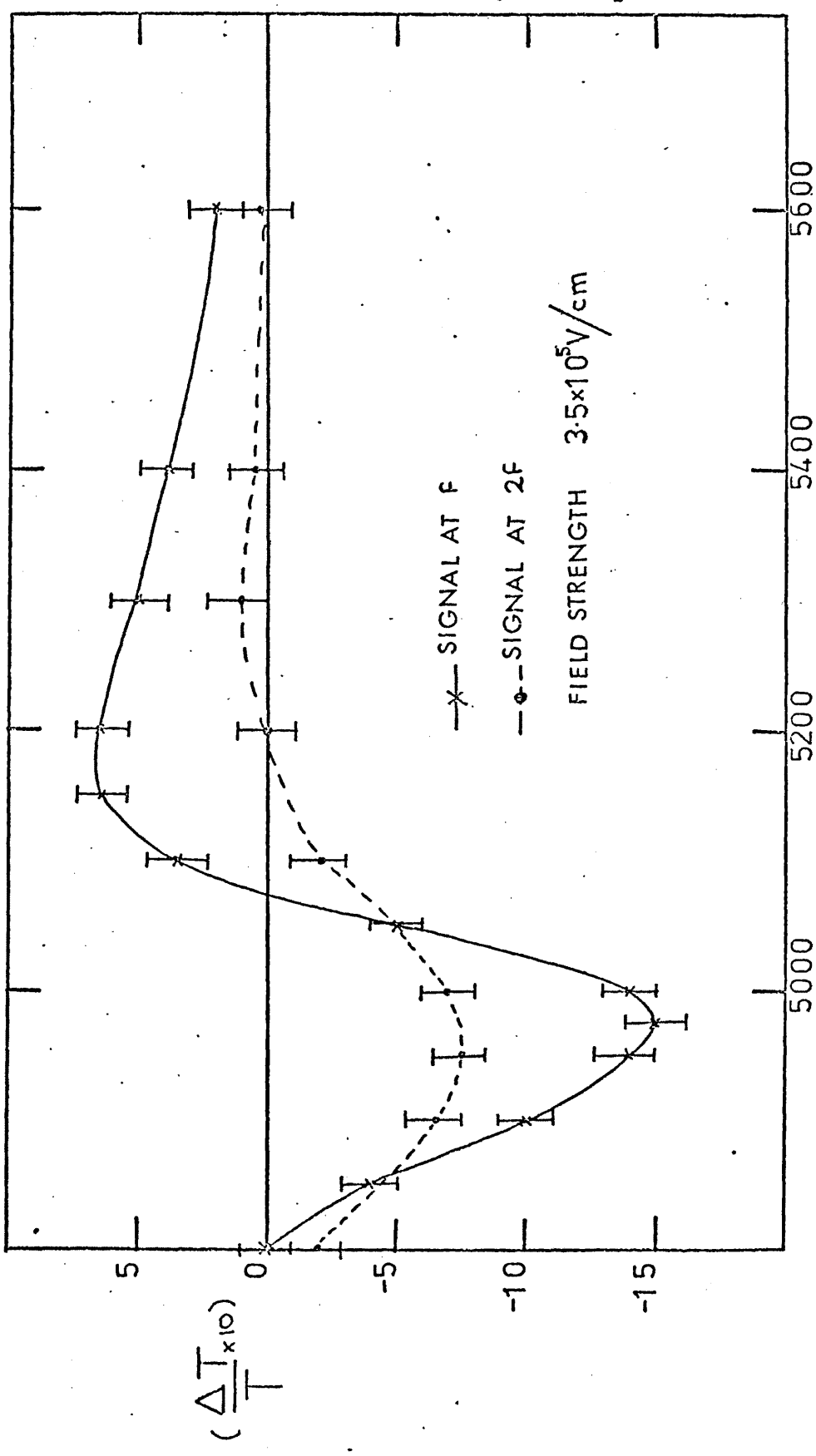

Figure (7.4) The electroabsorption spectra of a 1200 Å cadmium sulphide film.

frequency and the second harmonic, the former being greater than the latter. However, from equation (7.3) we see that for a sinusoidally applied electric field the electroabsorption response is proportional to the square of the electric field strength and thus we would expect only a response at the second harmonic. Plates (7.1a) to (7.1j) show the electroabsorption responses for a range of wavelengths, monitored directly across the anode load resistor or the photomultiplier and displayed on a Tetronix 454 oscilloscope. We see that the electroabsorption response has a rectified nature and Figure (7.5) shows the d.c. electrical characterists of a typical device (measured using a Pitman 437 electrometer). Clearly, as the alternating voltage is applied across the modulator, current will chiefly flow in one direction and during one half cycle the electric field strength across the device will be higher than in the other half of the cycle resulting in the electroabsorption waveform shown schematically in Figure (7.6). The electroabsorption responses observed at f and $2f$ have thus been explained in terms of the rectifying nature of the modulator.

Electromodulation studies of bulk single crystal and thin film polycrystalline samples of cadmium sulphide have been undertaken by many workers. Electroabsorption in the long wavelength tail of cadmium sulphide absorption has been observed by Williams (1960), Britsyn (1965), Kireev (1965) and Gutsche and Lange (1966). These authors interpreted their results in terms of the photon assisted tunnelling model of electroabsorption proposed by Franz (1958) and Keldysh (1958). Snavely (1967) studied the electroabsorption of thin polyscrystalline films of cadmium sulphide at photon energies both above and below the absorption edge in the temperature range 4K to 300K and the electroabsorption response of thin platelets of cadmium sulphide was studied by Hase and Onuki (1969). Perov et al. (1967) extended the measurements to epitaxial thin films of cadmium sulphide grown by thermal evaporation on mica substrates. Two sample configurations were used, which allowed the electric field to be applied either parallel or perpendicular to the film, but no significant differences were found in

PLATES (7.1a → j): Time Scale 10msec/division
Voltage Scale 50mV/division

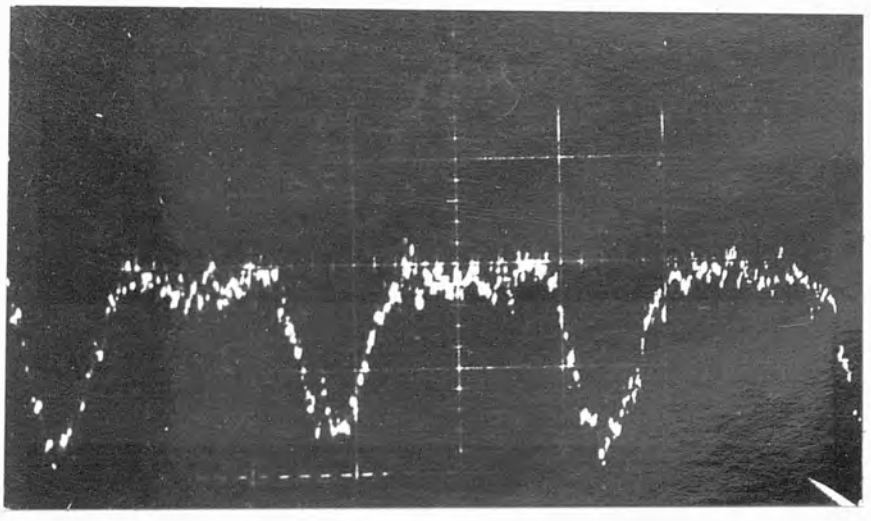

PLATE (7.1a) λ = 4950Å

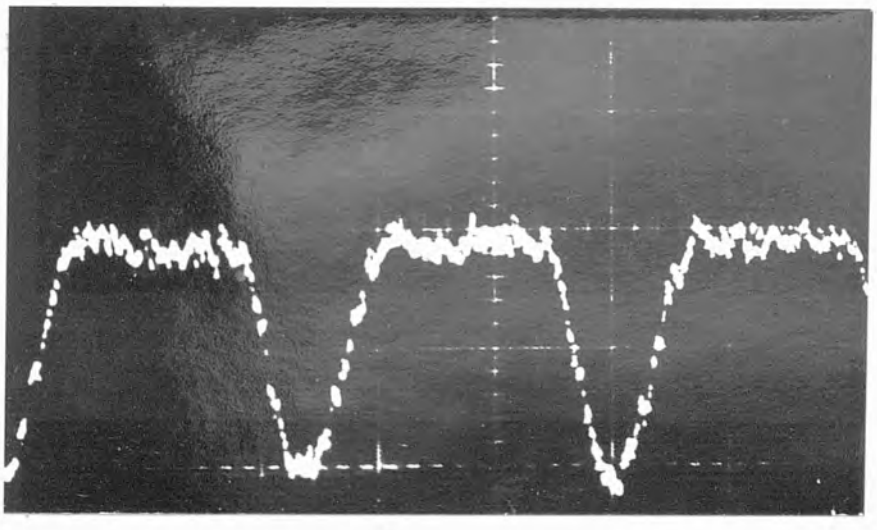

PLATE (7.1b) λ = 5000Å

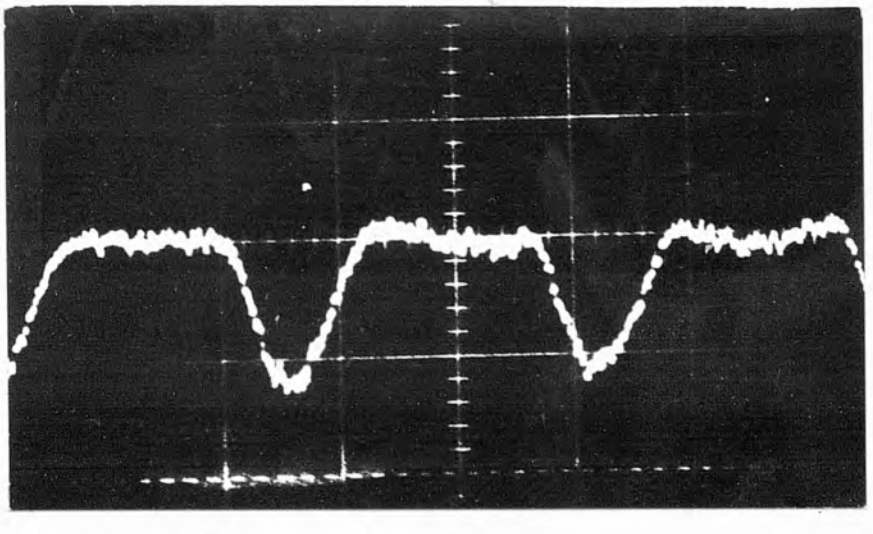

PLATE (7.1c) λ = 5050Å

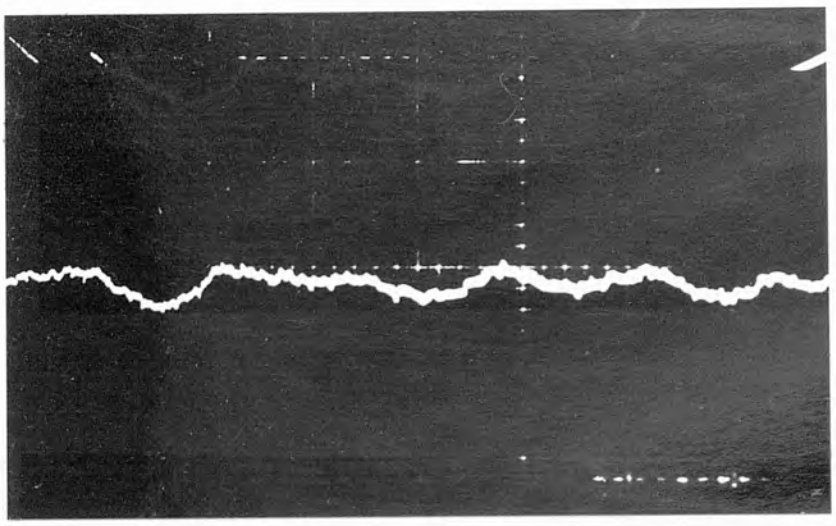

PLATE (7.1d) λ = 5075Å

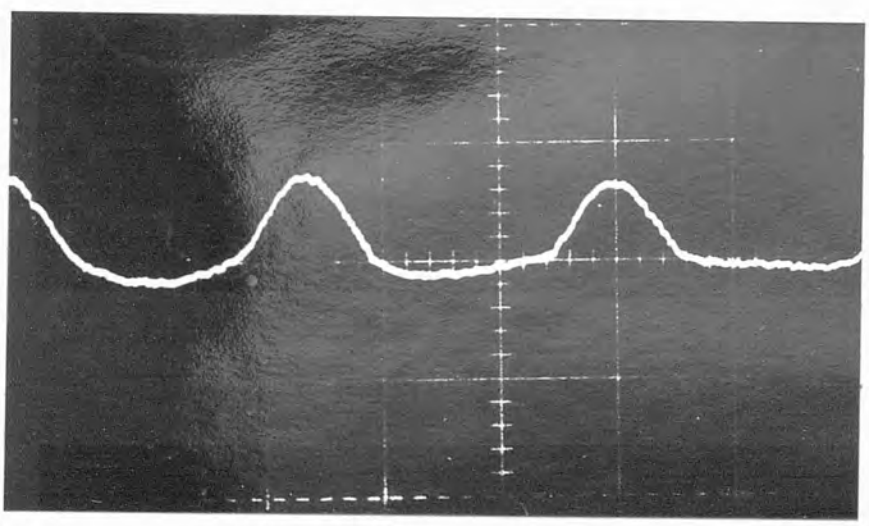

PLATE (7.1e) λ = 5200Å

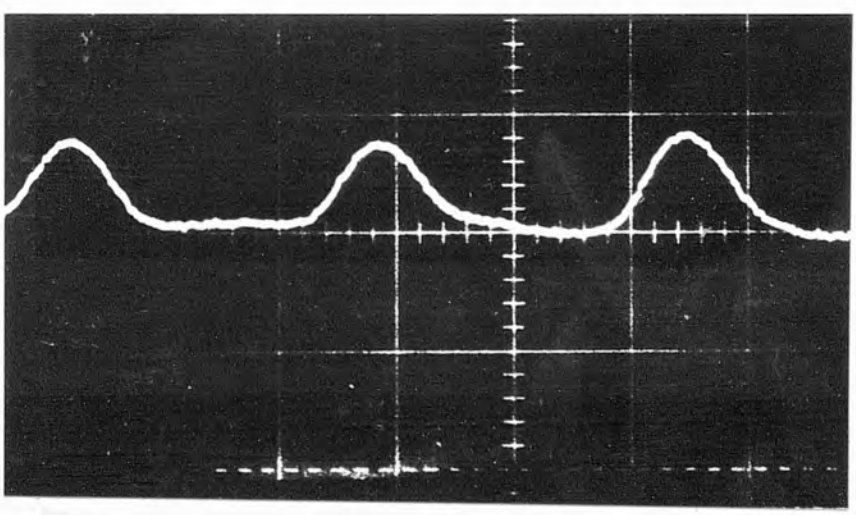

PLATE (7.1f) λ = 5150Å

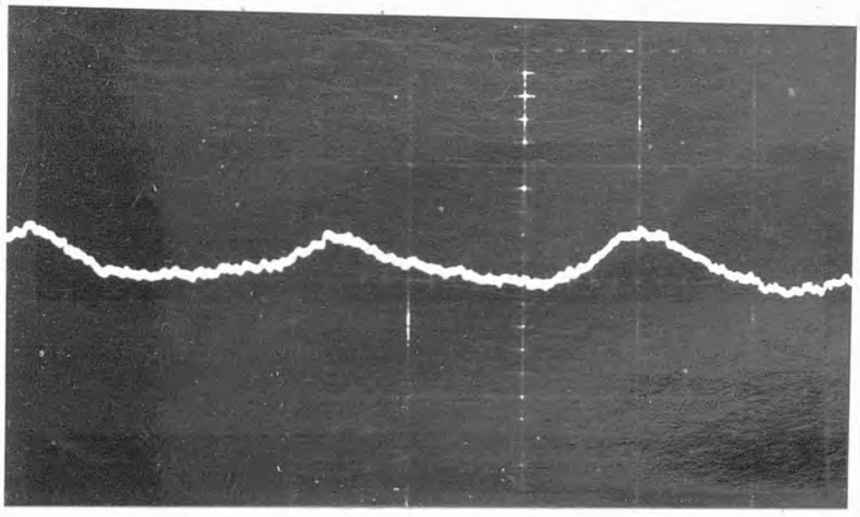

PLATE (7.1g) λ = 5100Å

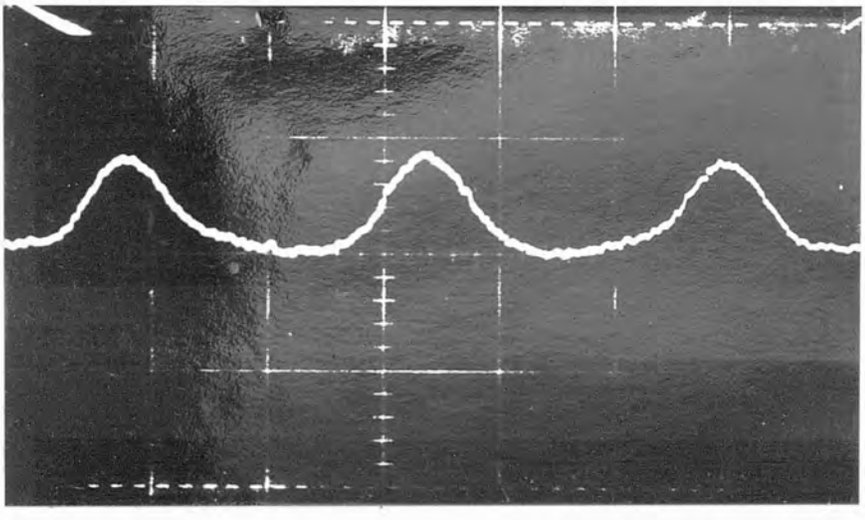

PLATE (7.1h) λ = 5250Å

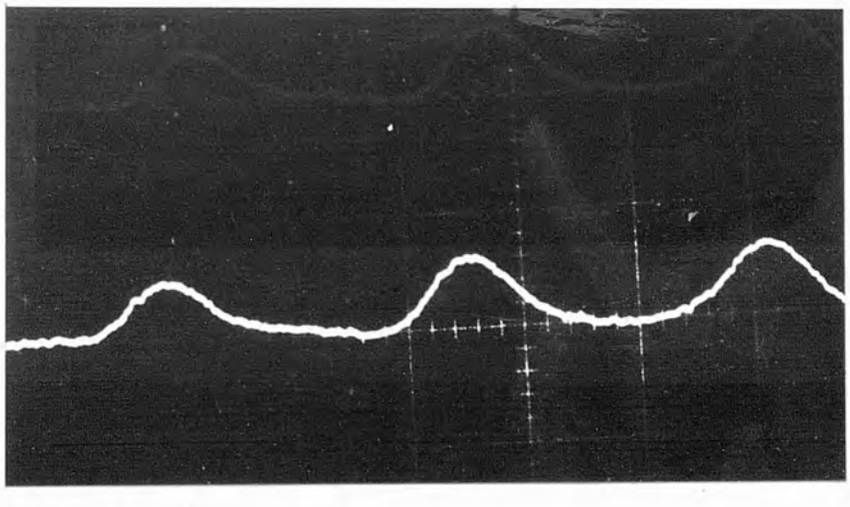

PLATE (7.1i) λ = 5300Å

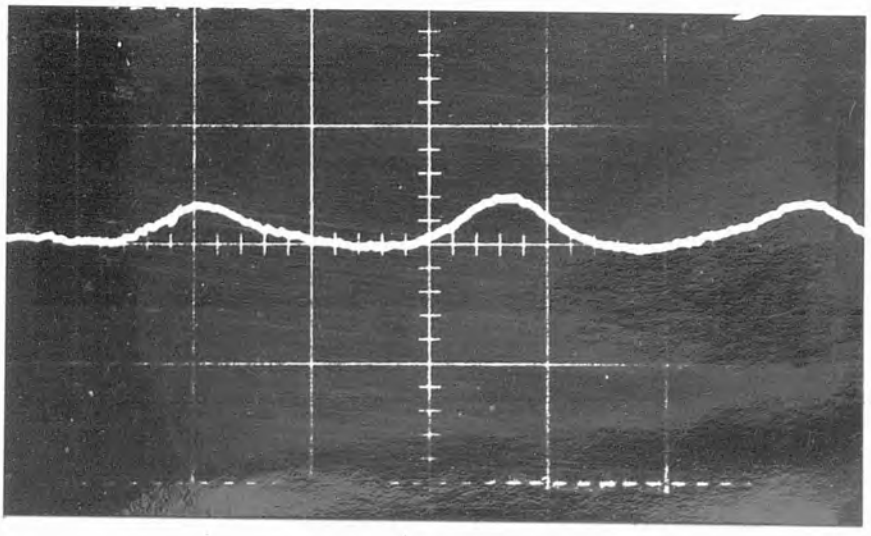

PLATE (7.1j) λ = 5400Å

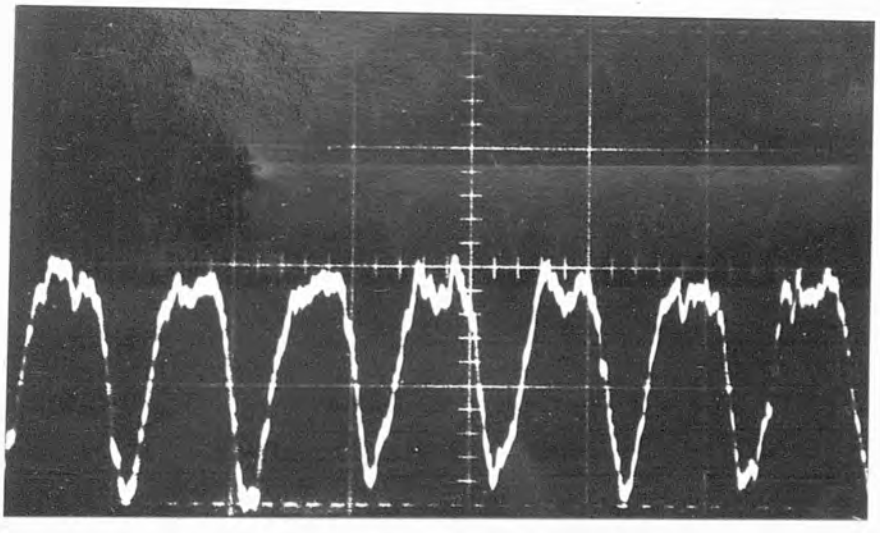

PLATE (7.2) λ = 4950Å 15V applied f = 1kHz.
Voltage scale 50mV/division.

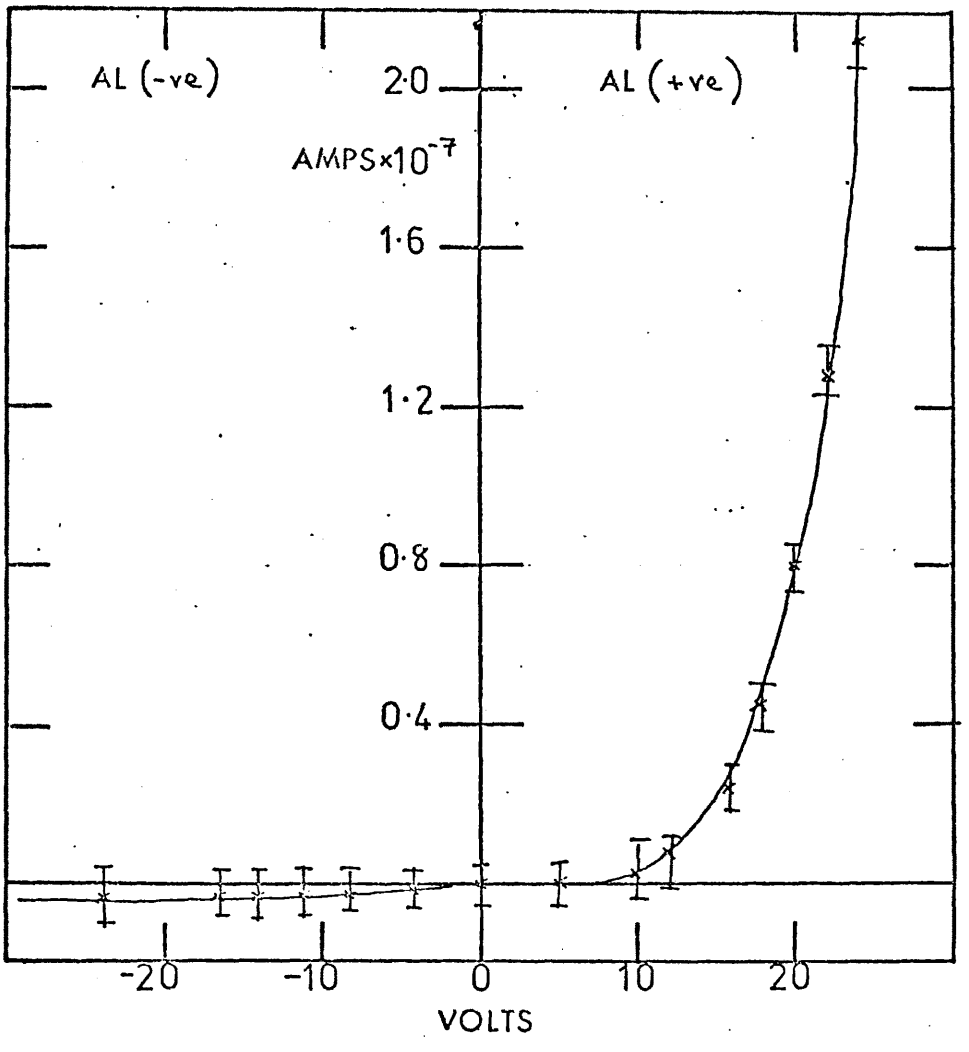

Figure (7.5) The d.c. electrical characteristics of a Al-Si_xOy-CdS-SnO_2 optical modulator.

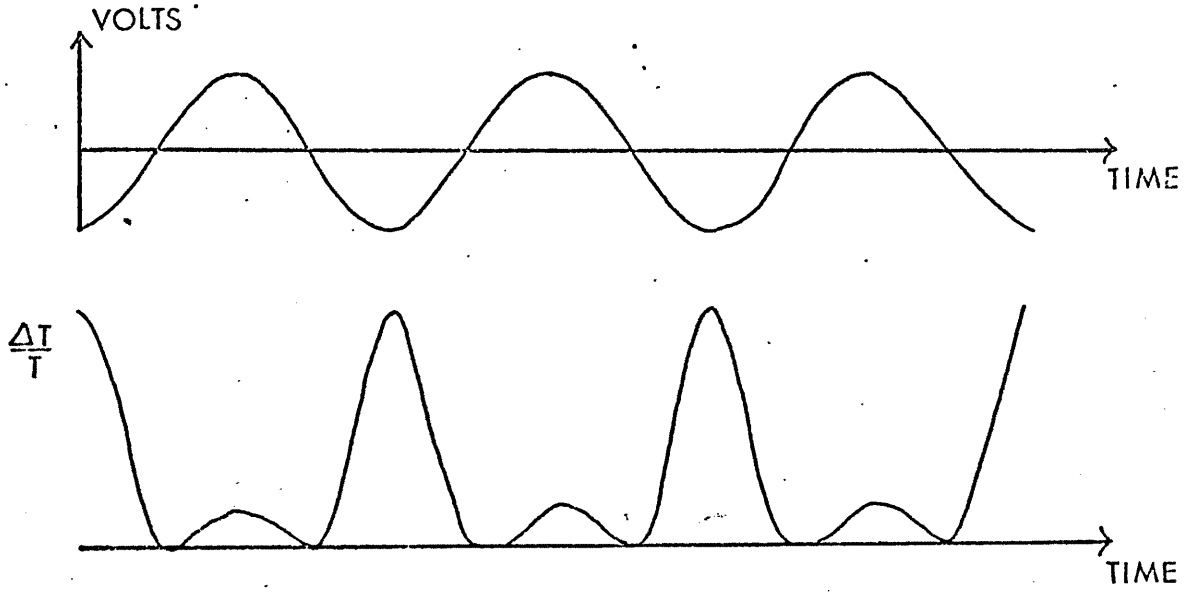

Figure (7.6) Schematic diagram of the electroabsorption response

the electroabsorption response for either configuration. The positions of the negative and positive peaks of the electroabsorption response obtained in the present work are compared with the results of Snavely (1967) Hase and Onuki (1969) and Perov et al. (1967) in Table (7.1) below:-

TABLE (7.1)

Peak Position	Snavely	Hase and Onuki	Perov	Present work
-ve peak	5039Å	4963Å	5000Å	4975Å (f) 4950Å (2f)
+ve peak	5122Å	5028Å	5100Å	5125Å (f) 5150Å (2f)

We see that in the present work the peak to peak separation of the electroabsorption response observed at the fundamental frequency is 150Å compared with separations of 83Å, 65Å and 100Å observed by Snavely, Hase and Onuki and Perov respectively. The variation in peak to peak separation observed by various workers is perhaps related to the different growth conditions of the samples used. Snavely thermally evaporated cadmium sulphide onto glass substrates annealing the films in hydrogen sulphide at 400°C for 1 hour after deposition. The thin crystals of cadmium sulphide used in the measurements of Hase and Onuki were grown by sublimation from the gaseous phase.

In all, 16 devices were fabricated in the configuration described in (4.1) and for a field strength of $\sim 5 \times 10^5$ Volts/cm a modulation degree of 10% was typically observed. In some cases, for slightly increased electric field strengths, a modulation degree of 15% was observed, but, such devices usually could not sustain the applied voltage for more than $\sim$ 5 minutes.
In all the 16 devices fabricated no electroluminescence or photoconductivity effects were exhibited by the cadmium sulphide films. If photoconductivity were present the resistance of the cadmium sulphide film and hence the

electroabsorption response would decrease if the incident light intensity was increased. However, it was found that there was no detectable change in the magnitude of the electroabsorption responses as the incident light intensity (over several orders of magnitude) was increased. It was also found that if the light source was removed no modulated signal was observed indicating that no electroluminescence was present. The applied electric field did not have any influence on the polarization of the incident light. A polarizer, (polariod type) was positioned between the monochromator and the lens in the detection system. The polarizer was then rotated and the electroabsorption response monitored. It was found that for all positions of the polarizer the modulated signal remained constant indicating that there was no polarization modulation by the applied electric field. However, one major limitation of the optical modulator designed in the present work was that the tramsmittance of the device was typically less than 10%. In order to improve on the transmitted light intensity of the device, filter designs based on the Fabry-Perot interference filter with cadmium sulphide as the spacer layer are presented.

7.5 Filter calculation

A computer program has been developed to calculate the optical parameters: reflectance, transmittance and phase change of a multilayer stack of thin films having an arbitrary number of layers with generally complex refractive indices for light incident at any angle of incidence. The program uses the matrix method proposed by Abeles (1948) to calculate the reflectance and transmittance of N films. The design thickness of the spacer layer in the Fabry Perot interference filter was computed using the concept of the "split filter" approach described by Macdonald (1971) and shown schematically in Figure (7.7) where the filter is considered to be split at a non absorbing film. Macdonald (1971) shows that for a particular design wavelength the transmitted light intensity of a Fabry-Perot

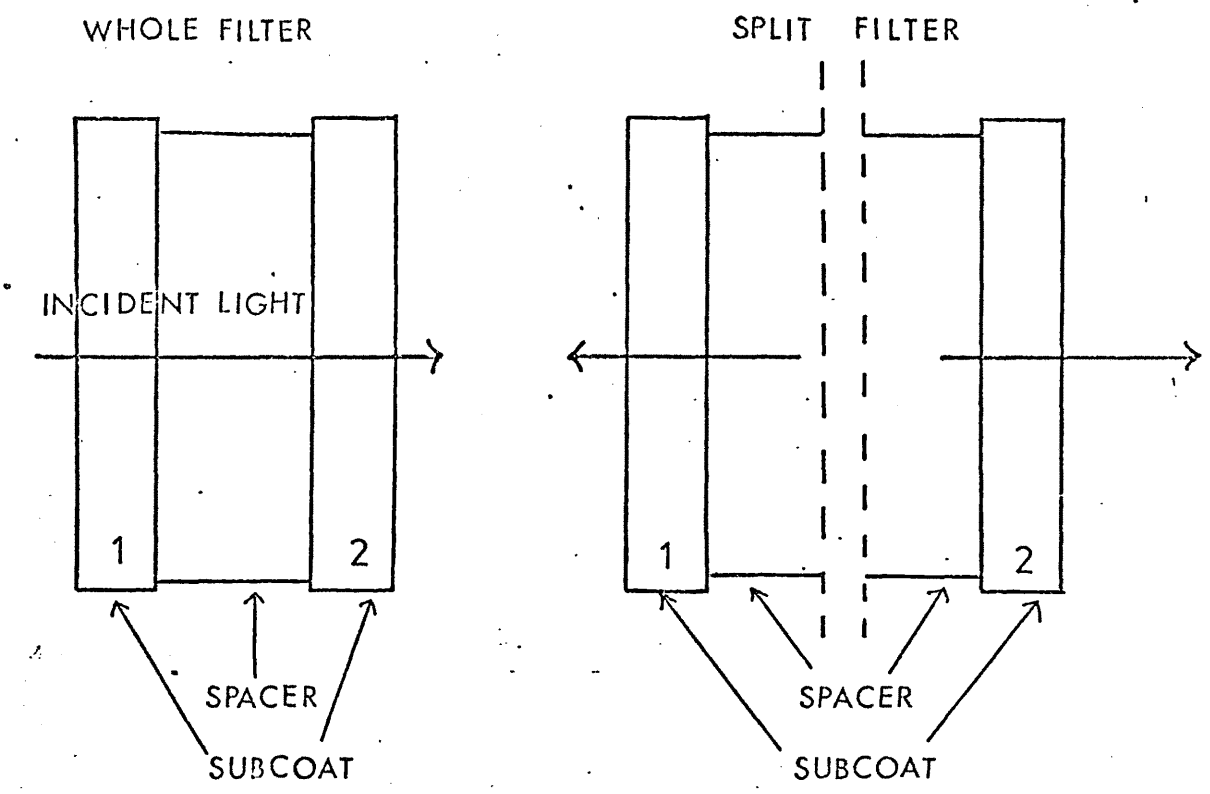

Figure (7.7) The concept of the "split" filter

may be maximized when:

$$2g - (\rho_1 + \rho_2) = 2m\pi \qquad (7.11)$$

for $m = 0,1,2...\ell$, and where g, the phase thickness of the spacer layer is given by

$$g = (2\pi/\lambda)\, ndcos\theta \qquad (7.12)$$

where λ is the design wavelength

n is the refractive index of the spacer layer

d is the metrical thickness of the spacer

θ is the angle of incidence in the spacer,

and $r_1 = |r_1|expi\rho_1$ is the amplitude reflectance of the first subcoat looking from the spacer with the incident medium of the complete filter as the emergent medium, and $r_2 = |r_2|expi\rho_2$ is the amplitude reflectance of the second subcoat looking from the spacer and with the substrate as the emergent medium with

$$\rho_1 = \tan^{-1}\left(\frac{\text{Imaginary part } (r_1)}{\text{Real part } (r_1)}\right) \qquad (7.13)$$

and

$$\rho_2 = \tan^{-1}\left(\frac{\text{Imaginary part } (r_2)}{\text{Real part } (r_2)}\right) \qquad (7.14)$$

In the filter calculations undertaken in the present work the following assumptions have been made:-

(i) The thin films comprising the filter are considered to be homogeneous and optically isotropic.

(ii) The supporting dielectric substrate has negligible absorption and a thickness much greater than the films and has been considered to have a refractive index of 1.52 throughout the calculations.

(iii) No account has been taken of scattering losses that will inevitably arise through the granular strucutre of thermally evaporated thin films.

The filter calculations were carried out on the University of London C.D.C. 6600 computer. The flow diagram of the computer program used in this investigation is shown in Figure (7.8). This program uses several subroutines.

FIGURE (7·8) Flow diagram of program 'Filter'

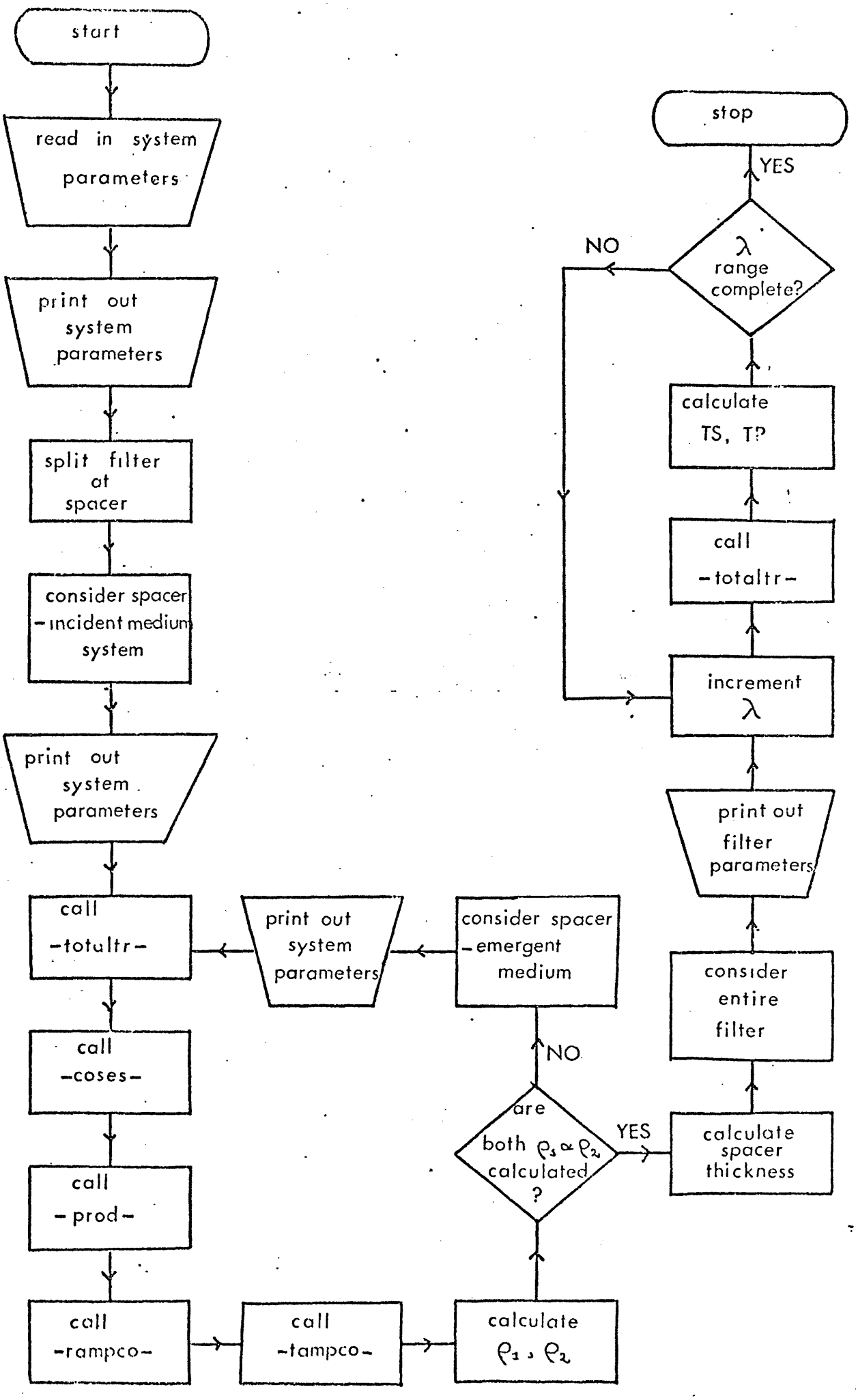

The subroutine called COSES uses Snell's law to calculate the complex angles of refraction in each of the films and subroutines RAMPCO and TAMPCO calculate the amplitude reflectance and transmittance respectively of each interface using the Fresnel equations. Subroutine PROD then calculates the product of the (2 x 2) matrix used in the Abeles method. Subroutine TOTALTR calls these subroutines successively for the number of films comprising the filter and calculates the total reflectance and transmittance. The program allows the phase changes ρ_1 and ρ_2 in equation (7.11) to be computed and hence the metrical thickness of the spacer layer to be calculated. In the present investigation the metrical thickness of the spacer layer was calculated for $m = 0, 1, 2, 3, 4, 5$. In Figures (7.9) and (7.10) we show the results obtained from the filter calculations. Figure (7.9) shows the transmission characteristics of a device designed for maximum transmittance at $\lambda = 5400\text{Å}$. The structure or the filter is:

Ag - Zns - MgF_2 - ZnS - MgF_2 - CdS - MgF_2 - ZnS - MgF_2 - Ag - glass

where the silver electrodes are 300Å thick and the zinc sulphide and magnesium fluoride rilms are one quarter wave layers. The design thickness of the cadmium sulphide spacer layer is 2497Å and we see that the peak transmitted light intensity at $\lambda = 5400\text{Å}$ is 72%. We see, however, that the filter does not have a small half width and a side band is located at 5200Å. This side band may be slightly suppressed by using a higher order of spacer thickness, $t = 4590\text{Å}$. The half width of the filter may be considerably reduced by using thicker silver electrodes but at the expense of the magnitude or the peak transmission. This behaviour is shown in Figure (7.10) where the filter comprised: Ag - ZnS - MgF_2 - CdS - MgF_2 - ZnS - Ag - glass layers and where the silver electrodes were 520Å thick and the spacer thickness = 1974Å and exhibited a peak transmission, at $\lambda = 5400\text{Å}$, of 32%. We note that in both these calculations the transmission of the device is very much greater than the "untuned" optical modulator described in (7.4).

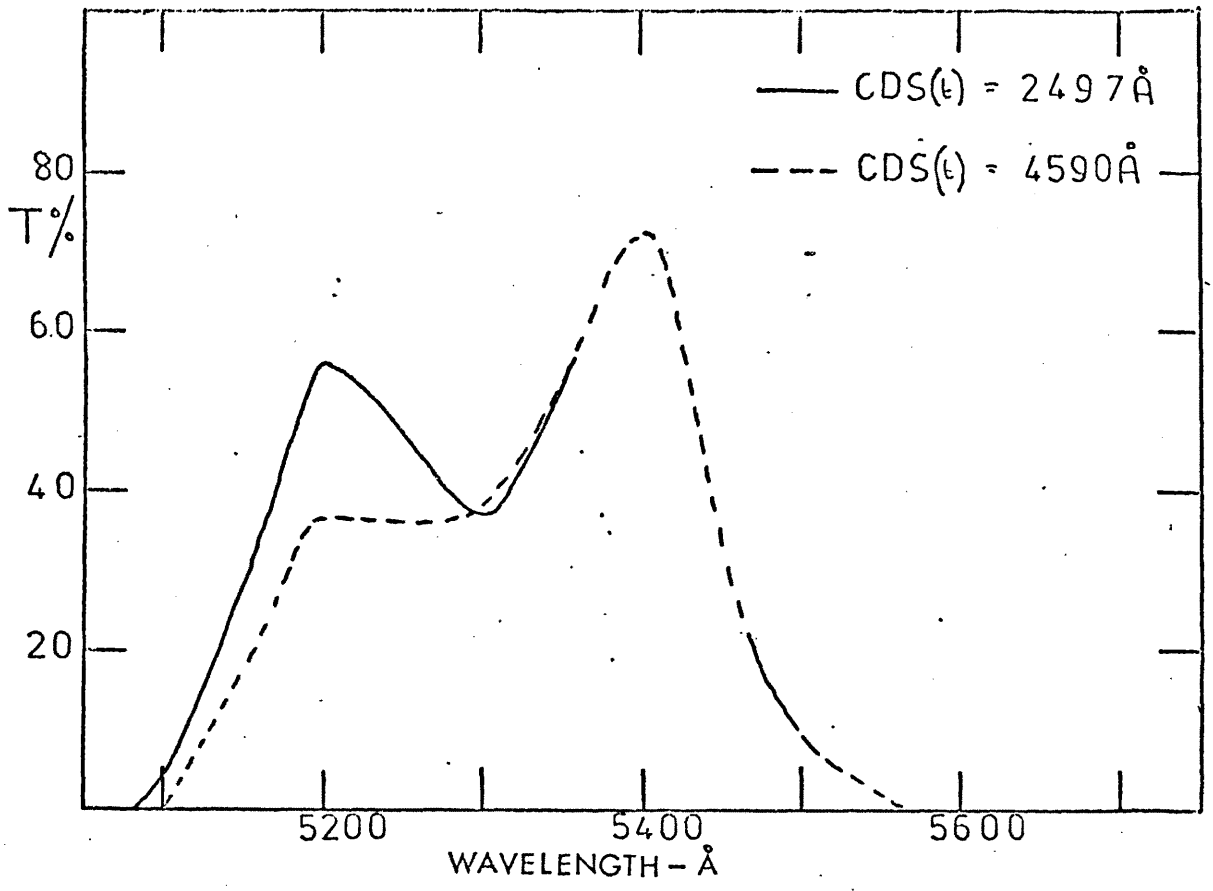

Figure (7.9) Transmission characteristics of a Ag-ZnS-MgF_2-ZnS-MgF_2-CdS-ZnS-MgF_2-ZnS-Ag-glass filter.

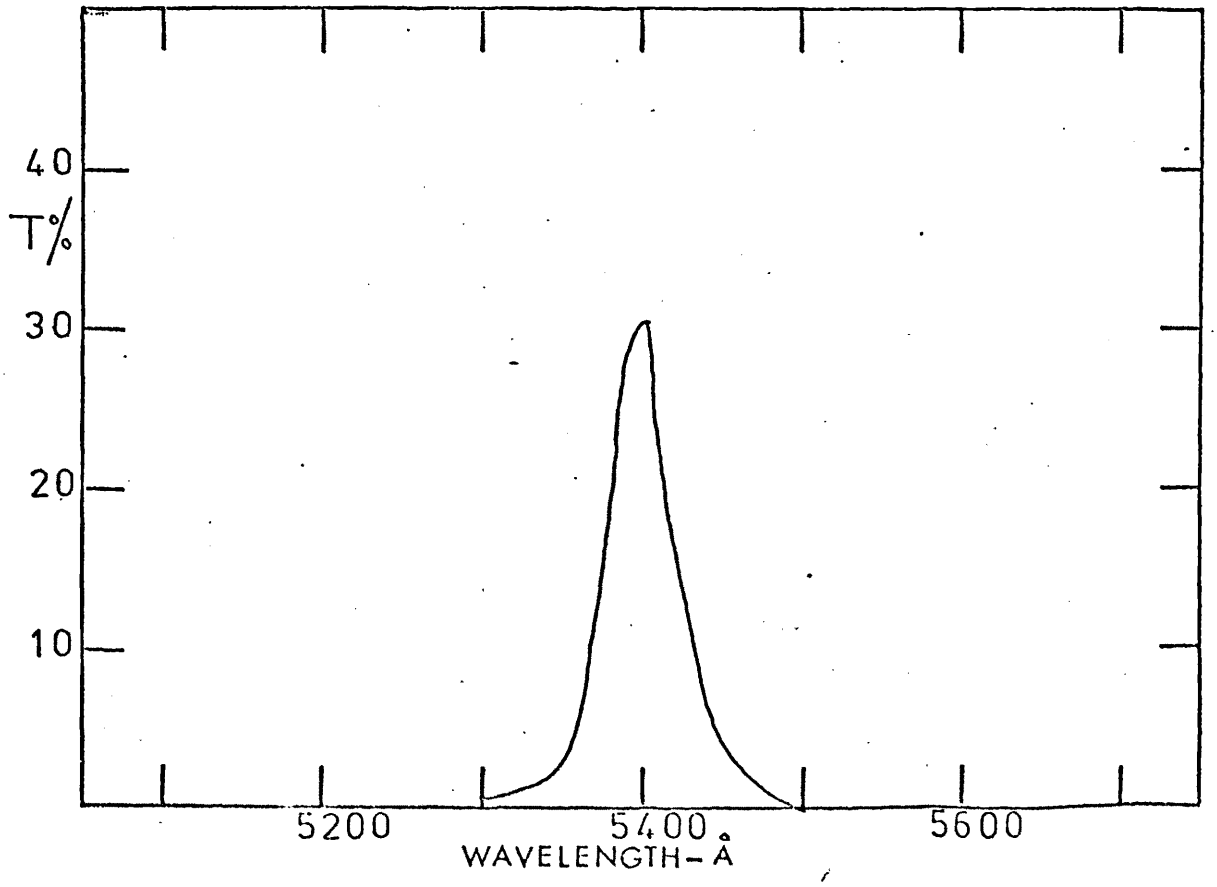

Figure (7.10) Transmission characteristics of an Ag-ZnS-MgF_2-CdS-MgF_2-ZnS-Ag-glass filter.

The effect of introducing absorption into the spacer layer as would occur when an electric field is applied to the device (considering the filter in Figure (7.9)) is shown in Figure (7.11) and we see that for $k = 0.03$ the transmission of the device has fallen to 42%, a modulation degree of $\sim$ 40%. Thus it appears at least possible to produce modulation degrees of $\sim$ 40% and maintain a high transmission coefficient.

The above filter calculations are based on the Franz Keldysh modulation mechanism. However, large electromodulation responses have been observed in ferroelectric materials, in which the large changes in optical properties induced by the applied electric field are not generally thought to be related to shifts in absorption edges. Many of the materials exhibit large electro modulation responses in transparent regions: e.g. $BaTiO_3$ (Frova and Boddy 1966) and rutile, TiO_2 (Frova and Boddy 1967). The authors explained the effect in terms of lattice changes induced by the applied field. Typically, one can expect changes $\sim$ 1% in the real part of the refractive index on application of an electric field of 10^4 Volts/cm. In view of these results attempts were made to grow capacitors with titanium dioxide (rutile phase) as the dielectric in order to study the electroabsorption response of the material. In the present work titanium was evaporated, using an electron gun, onto pyrex substrates. Holland (1966) has indicated that by heating titanium films in air the film is oxidised to rutile, but in the present studies, after heating in air for 6 hours at 400°C, a transparent film was produced which was electrically conducting. However, Weitzel and Kempter (1976) have indicated that high dielectric strength rutile thin films (< 1μm in thickness) may be obtained by chemical vapour deposition. The authors show that the resulting film had a breakdown strength of 5×10^5 Volts/cm. From this work it appears that high dielectric strength rutile films may be grown and in view of this fact a design for an all-dielectric Fabry-Perot optical modulator with rutile as the spacer layer is presented in Figure (7.12). The filter comprises

Figure (7.11) The effect of introducing absorption in the spacer layer.

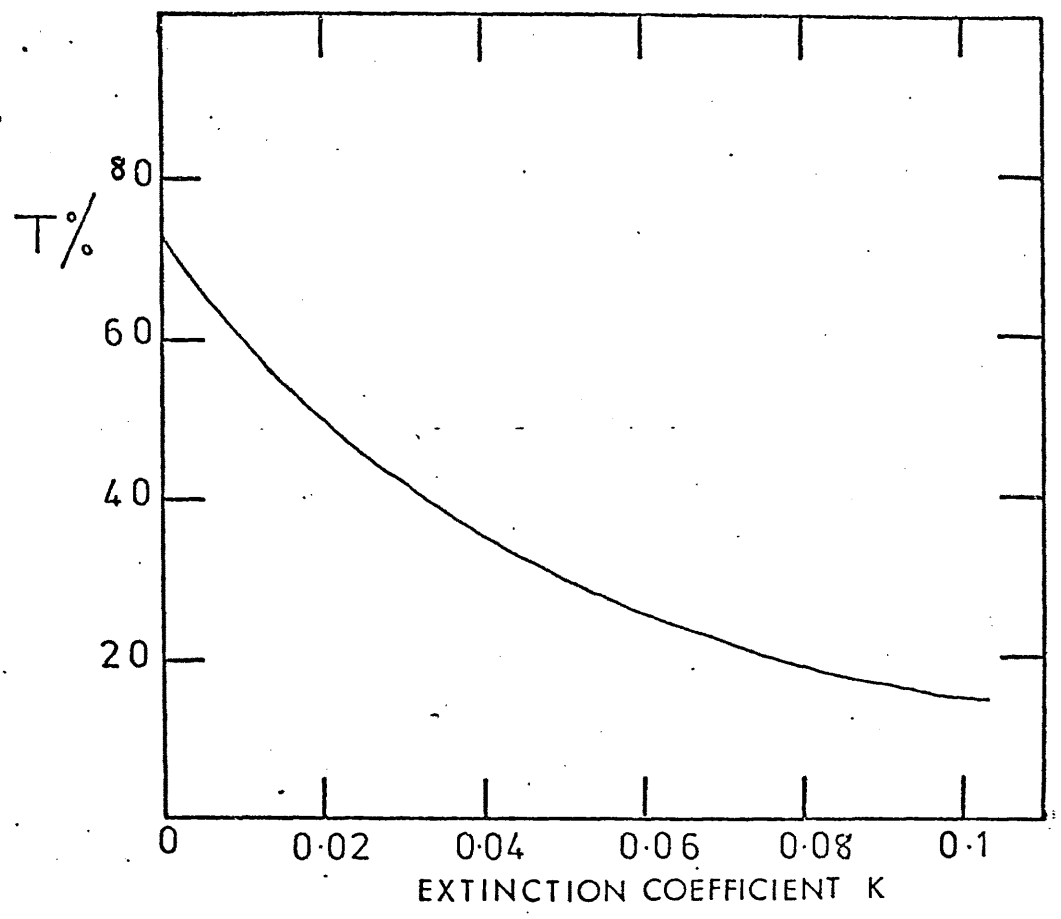

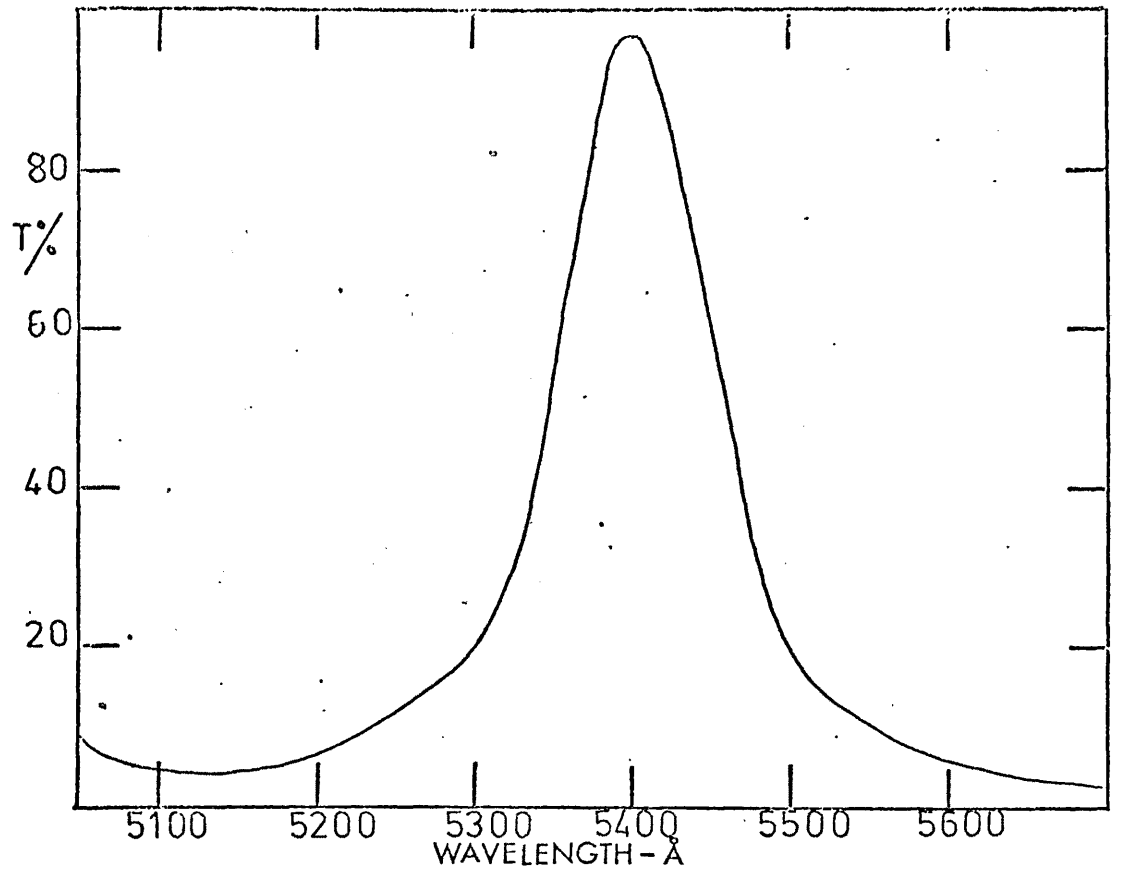

Figure (7.12) Transmission characteristics of an Air-ZnS-MgF_2-SnO_2-MgF_2-TiO_2-MgF_2-SnO_2-MgF_2-ZnS-glass filter.

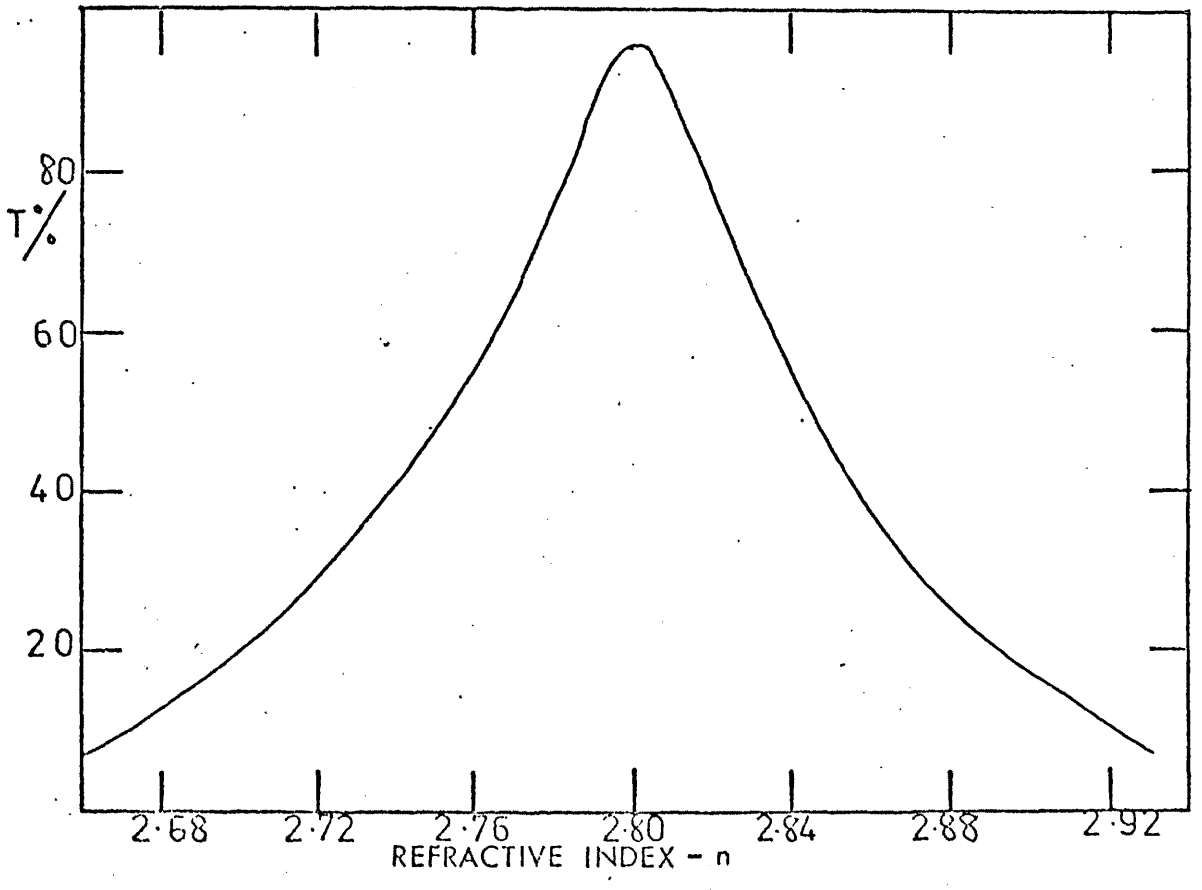

Figure (7.13) The effect of a change in the refractive index of the spacer layer on the transmission characteristics of the filter in Figure (7.12)

$ZnS - MgF_2 - SnO_2 - MgF_2 - TiO_2 - MgF_2 - SnO_2 - MgF_2 - ZnS$ - films

deposited on a glass substrate. The rutile spacer thickness is 2688Å and the zinc sulphide, magnesium fluoride and stannous oxide films are quarter wave layers. The modulating voltage is applied across the conducting stannous oxide electrodes and for a design wavelength of 5400Å a peak transmitted light intensity or 96% is calculated. Figure (7.13) shows the peak transmittance of the device for varying refractive index and we see that for refractive index variation of $\sim$ 2% we may expect modulation degrees of $\sim$ 30%.

7.6 Summary of data

A totally integrated thin film optical modulator has been designed which overcomes some of the disadvantages of conventional electro-optic modulators however, this results in a reduced performance in terms of modulation efficiency. We see in (7.5) that this limitation may be partially overcome by suitable filter design and it has been found possible to design filters that would exhibit peak transmittance of $\sim$ 70% and modulation degrees of $\sim$ 40%. It is felt that the results are sufficiently good to justify attempts to fabricate the devices (particularly a modulator with titanium dioxide as the active medium) in future work.

7.7 A comment on the electromodulation effect in metals

We have seen in Chapter 1 that electromodulation is a powerful tool for investigating the optical transitions in insulators and semiconductor. Its application to metals is however, subject to difficulties of interpretation. Feinleib (1966) reported electroreflectance measurements of gold and silver using an electrolytic technique. These results were rather surprising since it is well known that the penetration of an electric field into a good conductor is limited by the screening of free carriers. The Thomas-Fermi screening length for a static charge in an electron gas is given by

$$\lambda_{TF} = (E_F/6\pi ne^2)^{\frac{1}{2}} \qquad (7.15)$$

where n is the free carrier density

E_F is the Fermi energy.

In lightly doped semiconductors the screening length for the electric field can be of the order or the wavelength of visible light. However, in good conductors the screening occurs within atomic dimensions from the surface, leaving a field free region in the bulk of the metal. In copper, for example, the screening length, λ_{TF}, is $\sim$ 0.5Å. Despite these considerations Feinleib reported the electromodulation of metals, the change in the observed reflectance of gold in some parts of the spectrum being as high as 0.5% which is comparable with the magnitude of the effect seen in semiconductors using the electrolytic method (Cardona 1969). Unlike the Franz-Keldysh effect the electroreflectance effect in metals was observed at the fundamental frequency of the applied field. In view of these aspects Feinleib (1966) interpreted his results as a modulation of the real part of the refractive index of the electrolyte (occuring in the Gouy layer). A model calculation of this effect by Hansen and Prostak (1967) indicated that it was not possible to interpret the electroreflectance spectrum in this manner and a peak of the correct shape was obtained for gold if the optical constants of a very thin layer $\sim$ 1Å of the metal were modulated. This semi-empirical model predicted an electroreflectance dispersion curve which resembled the derivative of the reflectance spectrum. However, the model has been found to be only applicable to gold, and anomalies exist for copper and silver. Discussion still continues as to whether electromodulation of metals occurs at all. It should also be noted at this point that almost all studies of the electromodulation of metals have been carried out using the electrolytic technique (Buckman and Bashara 1968, Garrigos et al. 1974, Hansen et al. 1975). The only dry package study has been reported by Ishibashi and Stadler (1969) who investigated the electroreflectance of evaporated polycrystalline thin films of gold caused by the reversal of the ferroelectric polarization of the barium titanate substrates.

Although a similar response was observed to that seen in "wet package" configuration it was not clear whether the response seen was totally due to electro reflectance effects or partially due to a piezoreflectance component. In view or these studies a "dry package" configuration has been used in the present work to investigate the electromodulation of metals.

7.8 "Dry package" studies of the electromodulation of metals

In the course of the work done in producing the integrated thin film optical modulator it was necessary to determine the electrical characteristics of dielectric films, by fabricating thin film capacitors. These capacitors were then subsequently used to investigate the electroabsorption response of the thin film ($\sim$ 300Å) metallic electrodes. The sample configuration is shown in Figure (7.14) and the electroabsorption studies were performed at normal incidence using the detection system described in (3.8). Figures (7.15) and (7.16) show the electroabsorption response obtained from test capacitors having the following composition: Au - Si_xOy - SnO_2 and Aℓ - Si_xOy - SnO_2. The gold and aluminium electrodes were 200Å and 300Å thick respectively and the silicon monoxide thickness was 3000Å in each device. We see in both cases that electroabsorption responses were observed at the fundamental frequency and at the second harmonic. This behaviour is explained, as with the optical modulator, in terms of the rectifying characteristics of the capacitor. The d.c. current-voltage characteristics of the Aℓ - Si_xOy - SnO_2 capacitor are shown in Figure (7.17a, 7.17b) From Figure (7.15) we see that the maximum electroabsorption response is observed near to 4100Å for both the signal at the fundamental frequency and the second harmonic. For the Aℓ - Si_xOy - SnO_2 capacitor a maximum response is again seen near to 4000Å. At this point we refer to Figure (4.6) which shows the absorption edges of silicon monoxide films deposited at various rates. We see that the films deposited at 11Å sec^{-1} and 20Å sec^{-1} exhibit absorption edges starting near to 4000Å. The electroabsorption

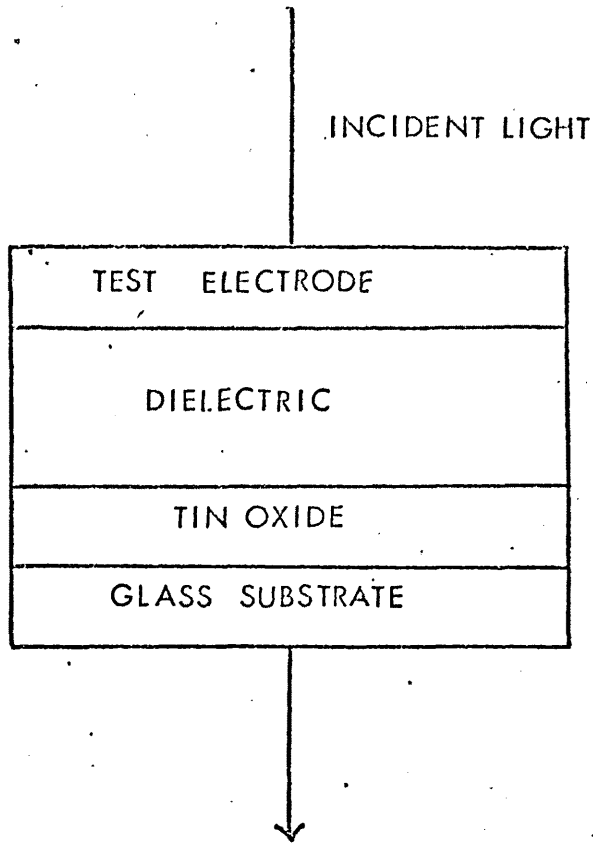

Figure (7.14a) Capacitor configuration for electroabsorption studies.

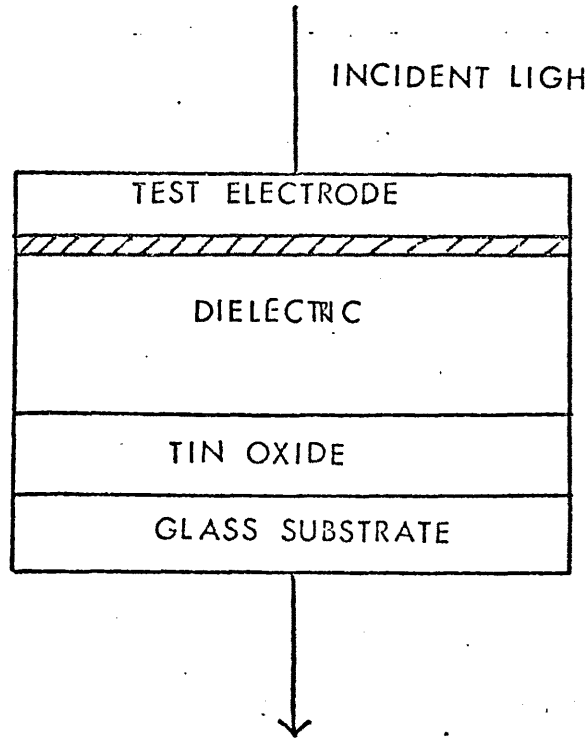

ASSUMED REGION OF MODULATED OPTICAL CONSTANTS

Figure (7.14b) Capacitor configuration with assumed region of modulated optical constants of the metal electrode.

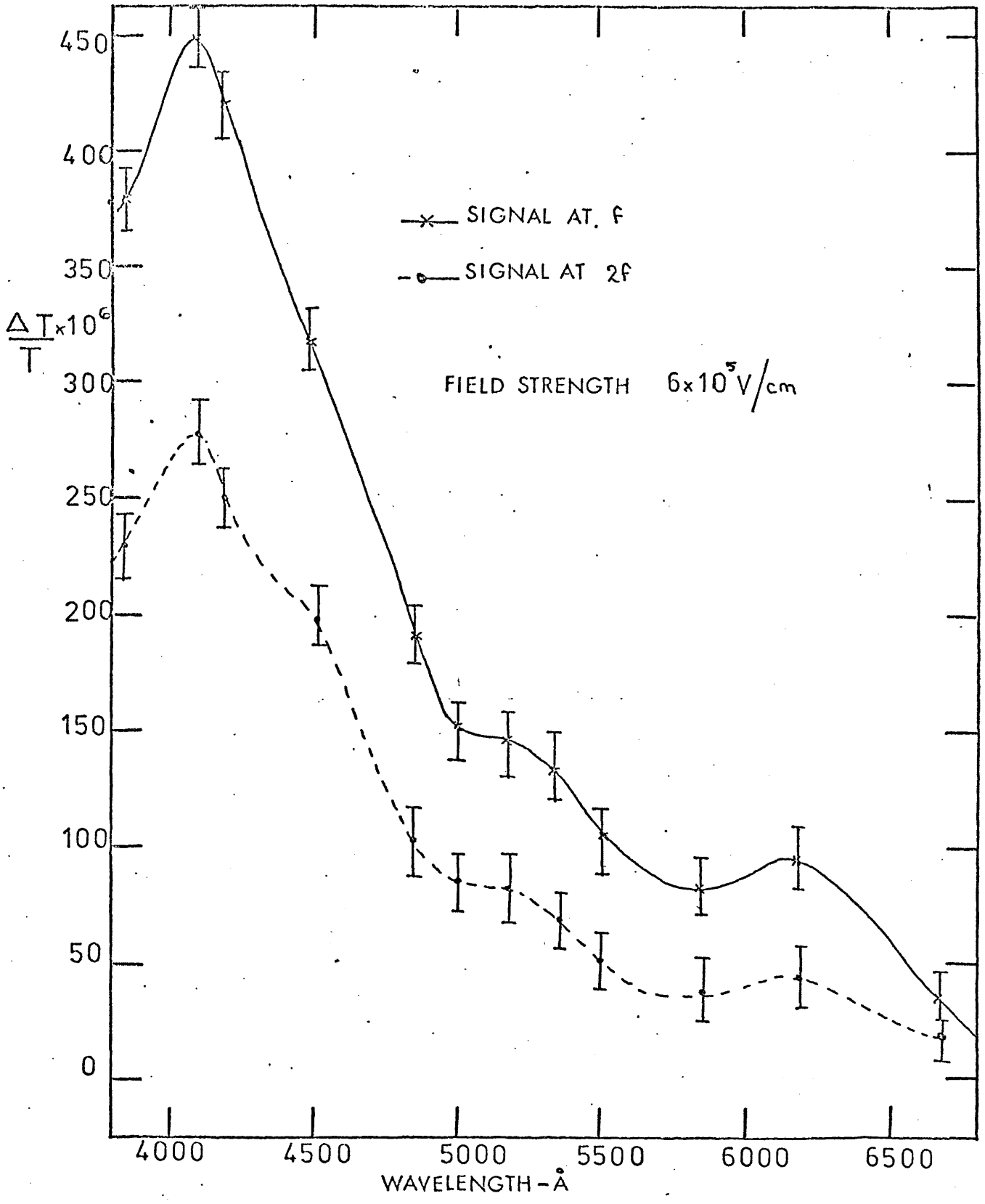

Figure (7.15) The electroabsorption responses of an Au-Si_xOy-SnO_2 capacitor.

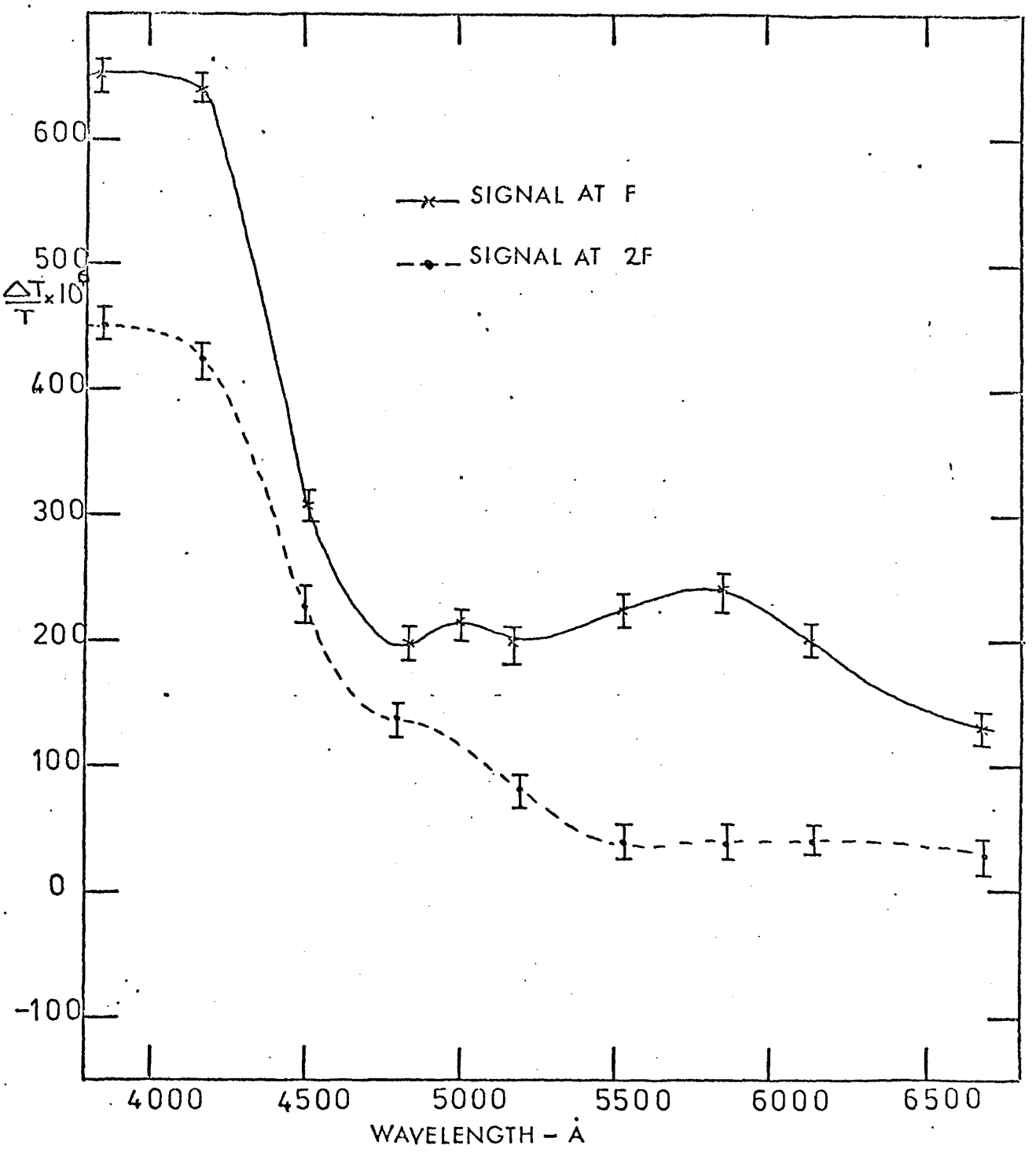

Figure (7.16) The electroabsorption responses of an Al-Si_xOy-SnO_2 capacitor.

Figure (7.17a) The d.c. electrical characteristics of an $Al\text{-}Si_xOy\text{-}SnO_2$ capacitor

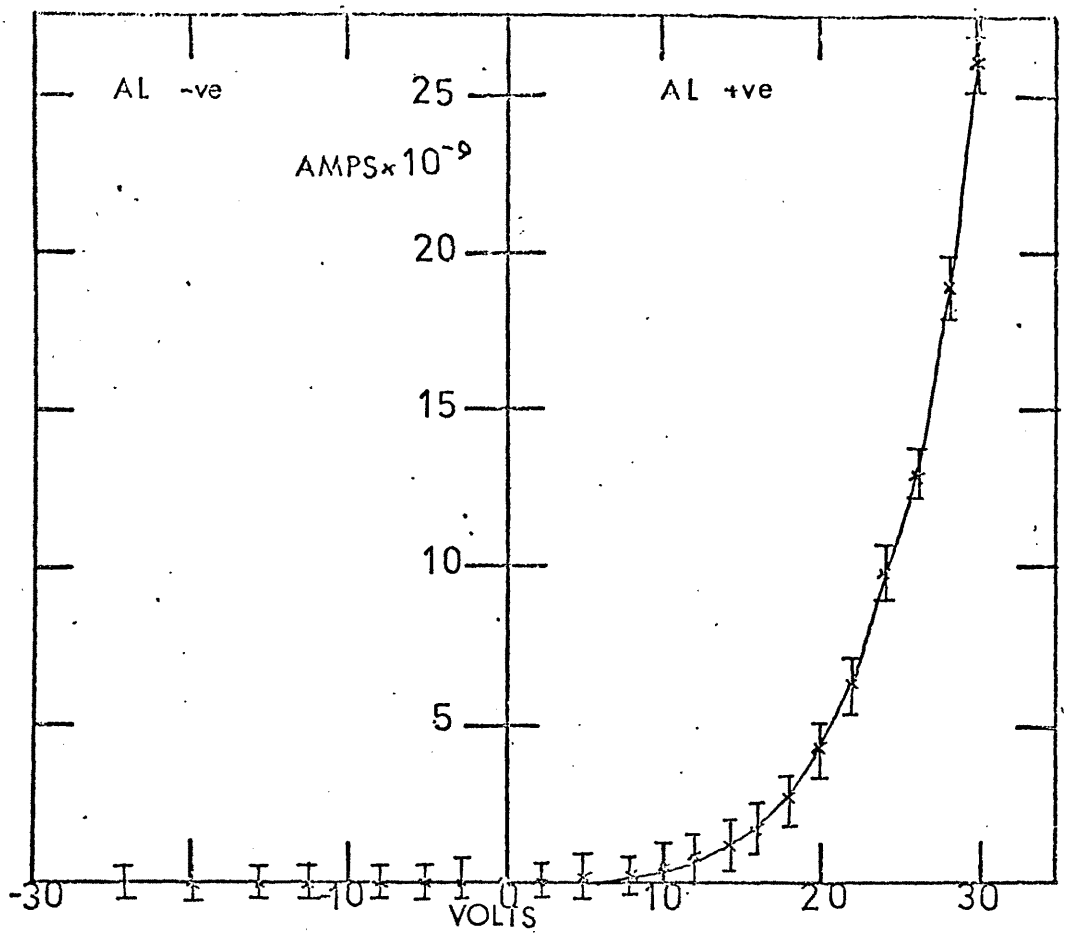

Figure (7.17b) Expanded current scale, with Al,-ve polarity

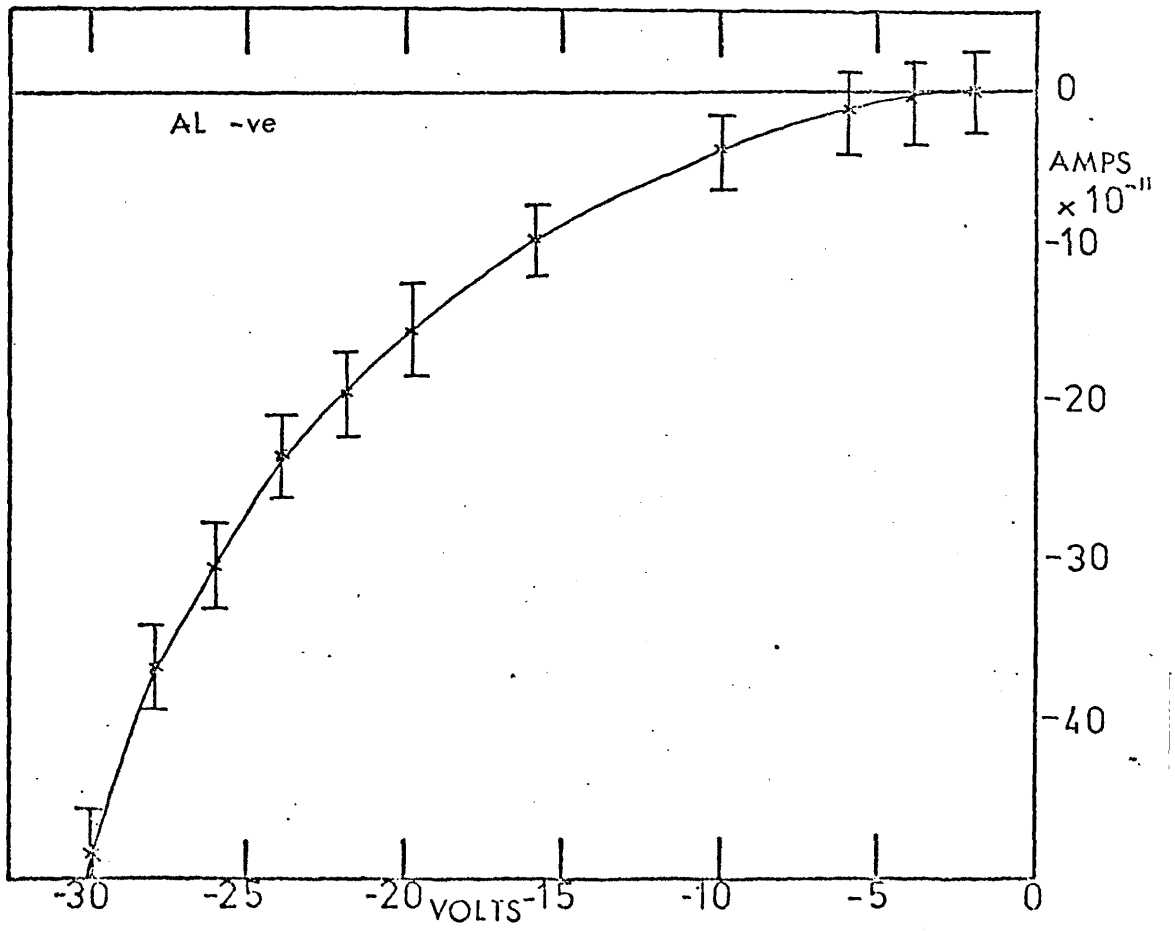

responses seen could thus be the effect of the electric field on the absorption edge of the silicon monoxide film. In view of this, test capacitors were fabricated with magnesium fluoride as the dielectric. This material was chosen since is is known to have no absorption edge in the visible part of the spectrum. In all devices, Aℓ - MgF_2 ≃ SnO_2, Au - MgF_2 - SnO_2 no electroabsorption response was observed at either the fundamental frequency of the applied electric field or the second harmonic even though field strengths of ∿ 5 x 10^5 Volts/cm were applied.

We note that the electromodulation responses of metals observed by other workers using "wet package" techniques were not observed in the present "dry package" investigations. In view of this null result a computer simulation of the electromodulation response observed using an electrolytic technique was undertaken. The computer program was based on the matrix method developed by Abelès (1948) for determining the reflectance and transmittance of a system of N films. Although Hansen and Prostak (1967) found that the modulation of the real part of the refractive index of the electrolyte in the Guoy layer did not produce the correct shaped spectra to explain the electromodulation observed at a copper-electrolyte or gold electrolyte interface, we have found in the present computer investigation that if a thin absorbing layer is assumed to form in the Gouy layer during the application of an applied electric field then a response similar to that observed in the electroreflectance studies of gold, copper and silver is found. The following assumptions have been made in the computational studies

(i) The Gouy layer is considered to be a homogeneous thin film.

(ii) No account is taken or spatially dependent optical constants within the Gouy layer.

(iii) The induced absorption in the electrolyte is assumed to be non dispersive.

Essentially, the computer program calculates the reflectance or a metal-electrolyte interface at an angle of incidence of 10° (all the electroreflectance studies reported in the literature have been undertaken at near normal incidence) and then recalculates the reflectance of the system assuming the formation or a thin absorbing layer in the electrolyte. The computational analysis has been undertaken for gold, copper and silver-electrolyte interfaces and the optical constant data taken from Johnson and Christy (1972). Figures (7.18), (7.19), (7.20) and (7.21) show the simulated electroreflectance responses of copper, gold and silver electrolyte interfaces respectively. We see that there is quite good agreement between the computed response and the experimentally observed electroreflectance responses interpolated from Garrigos et al. (1971) for copper and Buckman and Bashara (1968) and Feinleib (1966) for silver. However, we see that the agreement between theory and experiment (Feinleib 1966) is not so encouraging for the gold-electrolyte interface. It is felt that this is probably due to the simple model used in the present simulation. The computational analysis could be refined by

(i) introducing a dispersion into the induced absorption

(ii) considering the effect of spatially dependent optical constants within the Gouy region.

FIGURE (7·18) The computed and interpolated electroreflectance response of copper

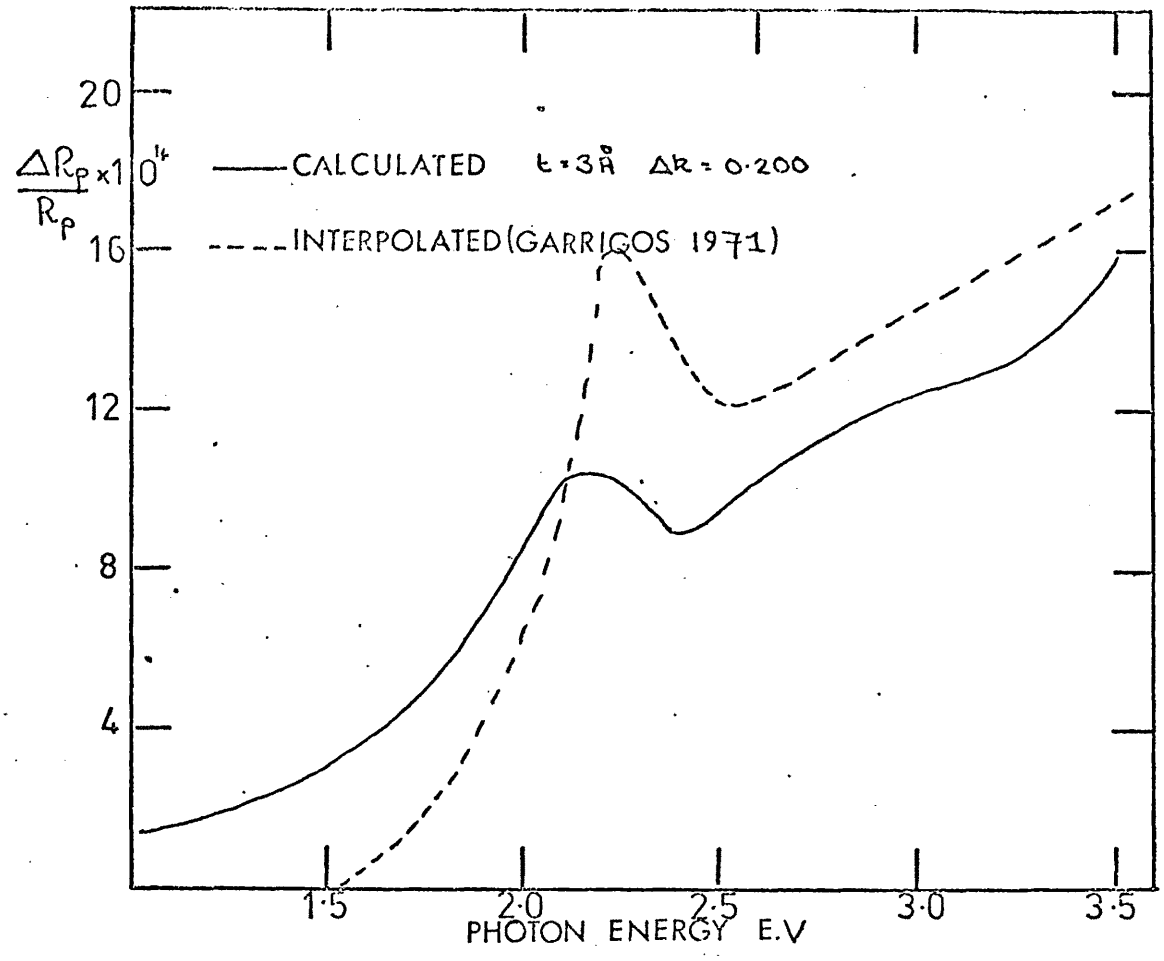

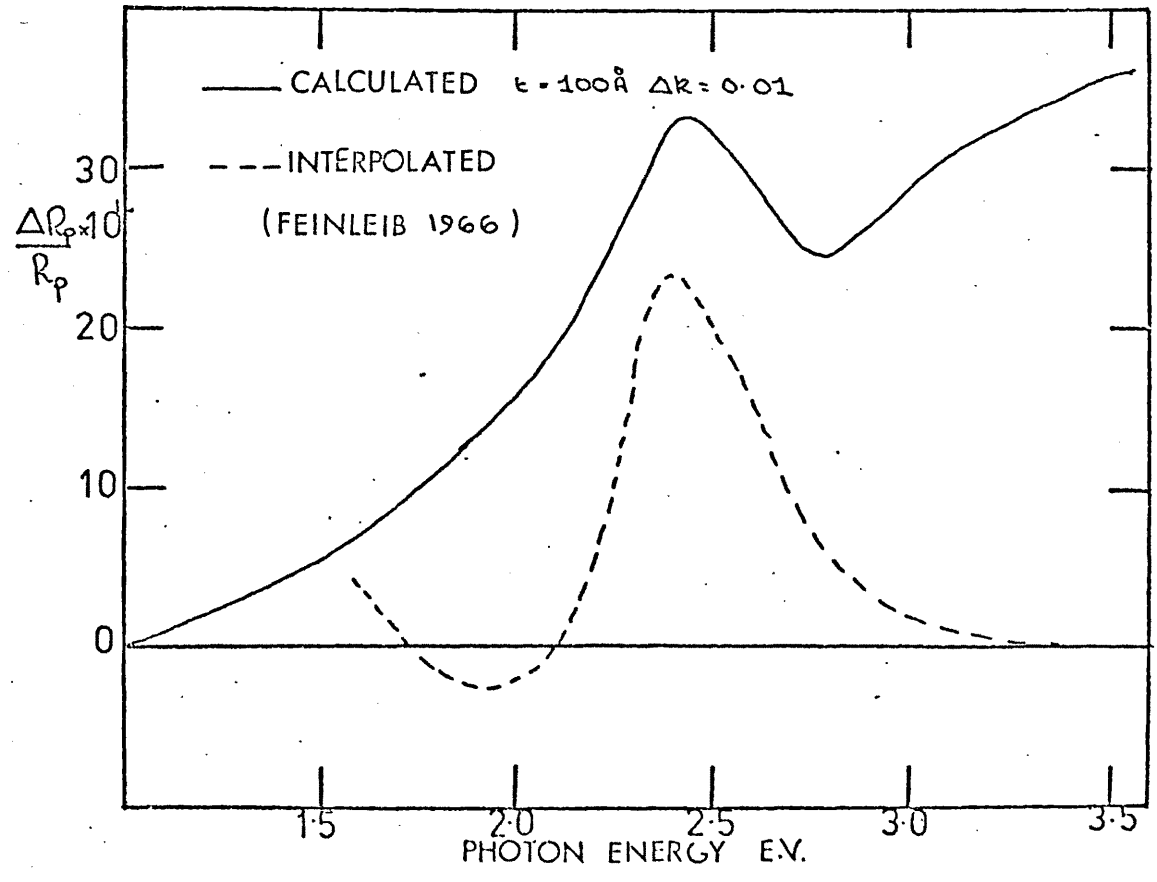

FIGURE (7·19) The computed and interpolated eletroreflectance response of gold

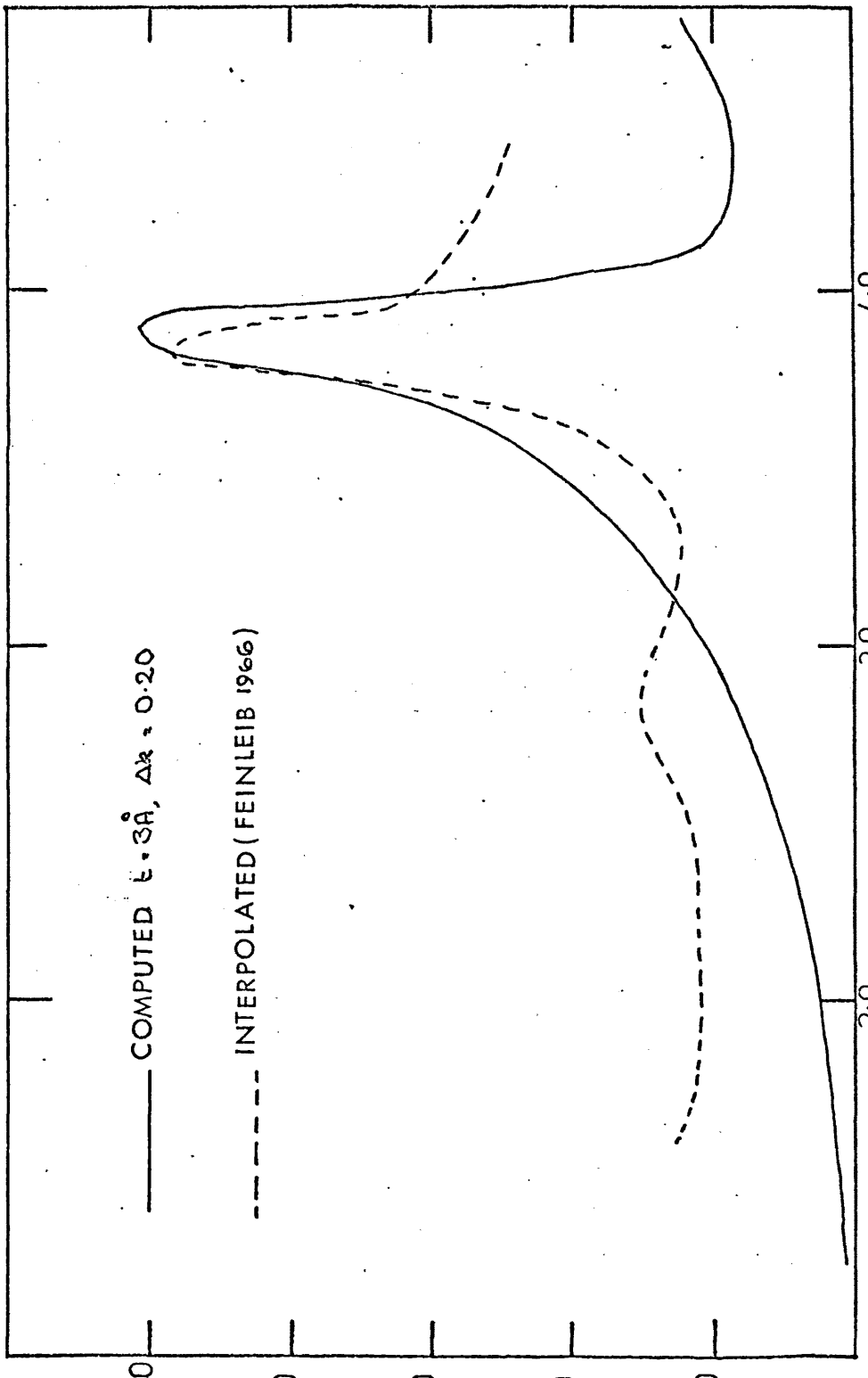

Figure (7.20) The computed and interpolated electroreflectance spectra of silver

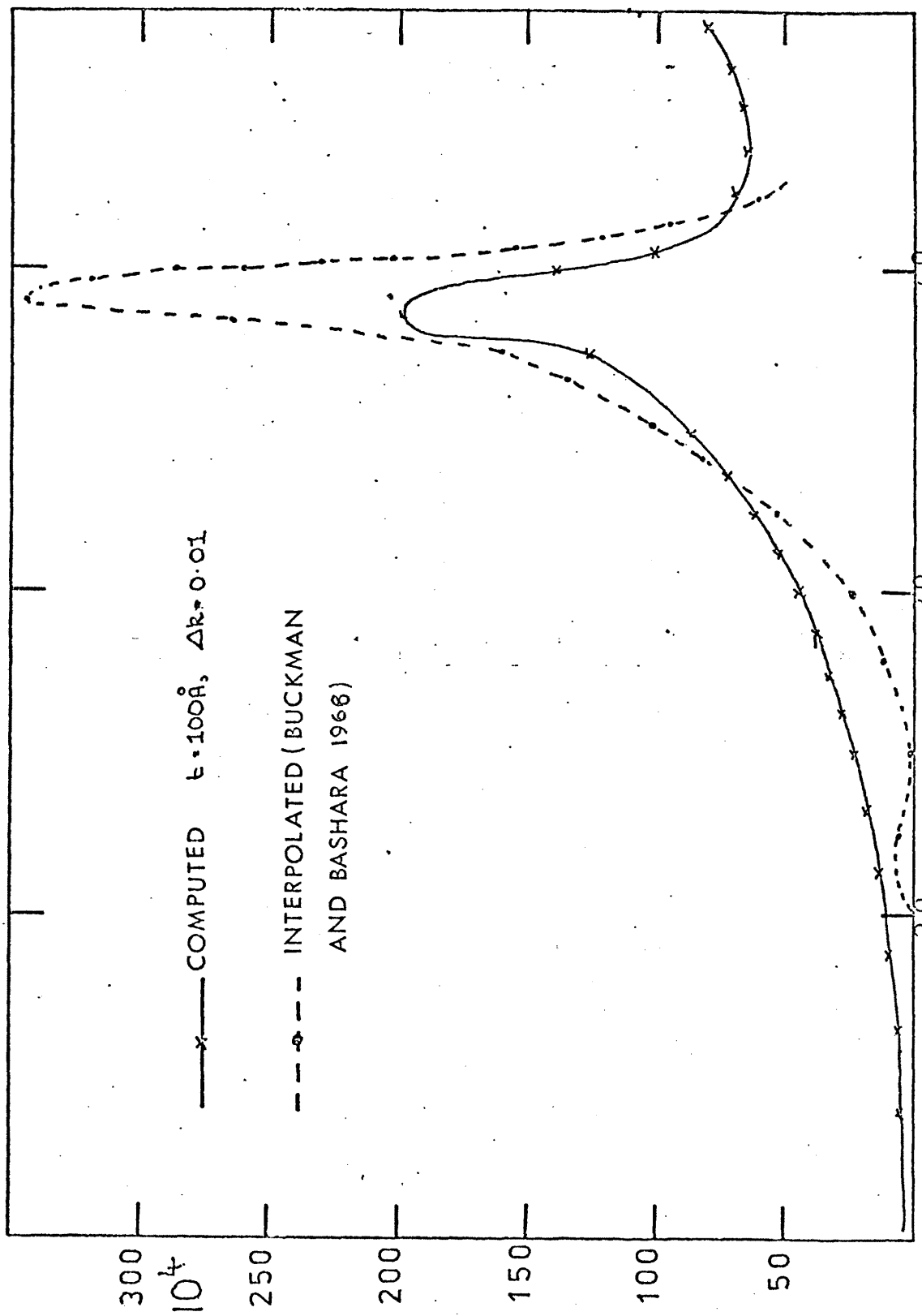

Figure (7.21) The computed and interpolated electroreflectance spectra of silver.

CHAPTER VIII

Conclusions and suggestions for further work.

The work described in this thesis has been primarily concerned with the use of an optical modulation technique as a solid state diagnostic. An experimental system has been set up to study the thermoreflectance response of opaque thin films ($\sim$ 2000Å thick) at oblique incidence, over a spectral range 1.5 to 3.2 eV and in the temperature range 90K to 240K, (and at a pressure of $\sim 10^{-6}$ torr). The initial thermoreflectance measurements were performed on opaque, polycrystalline thin films of gold and copper. The purpose of this work was to use gold as a reference material, to determine the spectral position of the dominant structure and to ascertain whether the detection system had sufficient sensitivity to locate subsidiary structure previously observed by Scouler (1967). Although the thermoreflectance response of gold and copper films has been previously reported (Scouler 1967, Rosei and Lynch 1972, Cheyssac 1973) the present study has yielded new information. The observed structures in the thermally modulated $\Delta\varepsilon_2$ spectra of both metals were found to be in good general agreement with previously published results. However, a shift in the principal absorption edge with temperature for both elements has been observed. This shift, although predicted theoretically in expanded lattice electronic band structure calculations by Christensen and Seraphin (1971) for gold and Snow (1973) for copper, has not previously been observed in thermal modulation experiments. The lack of observable shift of the principal absorption edge with temperature in previous thermal modulation studies is explicable by the rather lower energy resolution compared with that in the present work.

It would thus seem that a thermal modulation study is an excellent technique for experimentally determining the temperature coefficients of optical transitions. However, in (2.3) we have seen that in order to

compute the thermally modulated $\Delta\varepsilon_2$ spectra, we must have a knowledge of the optical constants n and k of the material. We have seen in (5.8) that in using different sets of n and k data for copper, taken from Johnson and Christy (1975) and Pells and Shiga (1969), structure in the resulting $\Delta\varepsilon_2$ dispersion curve appears at different spectral positions and the temperature coefficients of the transitions also differ. Thus the determination or temperature coefficients of optical transitions depends not only on the experimental observables but also on data derived by other workers. It is proposed that this limitation of the thermal modulation technique could be overcome by effectively determining the optical constants of the film under study during the course of the thermal modulation experiment. This may be achieved by considering the relationship between the thermally modulated reflectance response, $\Delta R/R$, and the thermally modulated changes in the dielectric constant, $\Delta\varepsilon_1$ and $\Delta\varepsilon_2$, viz:

$$(\Delta R/R) = \alpha\Delta\varepsilon_1 + \beta\Delta\varepsilon_2 \qquad (8.1)$$

Clearly, if four such measurements were made for two different polarizations at two angles of incidence θ_1 and θ_2 i.e.

$$\left(\frac{\Delta Rp}{Rp}\right)_{\theta_1} = \alpha_{p_1}\Delta\varepsilon_1 + \beta_{p_1}\Delta\varepsilon_2 \qquad (8.2)$$

$$\left(\frac{\Delta Rs}{Rs}\right)_{\theta_1} = \alpha_{s_1}\Delta\varepsilon_1 + \beta_{s_1}\Delta\varepsilon_2 \qquad (8.3)$$

$$\left(\frac{\Delta Rp}{Rp}\right)_{\theta_2} = \alpha_{p_2}\Delta\varepsilon_1 + \beta_{p_2}\Delta\varepsilon_2 \qquad (8.4)$$

$$\left(\frac{\Delta Rs}{Rs}\right)_{\theta_2} = \alpha_{s_2}\Delta\varepsilon_1 + \beta_{s_2}\Delta\varepsilon_2 \qquad (8.5)$$

and from (2.3) $\alpha = \alpha(n,k,\theta)$

$\beta = \beta(n,k,\theta)$

then we have four equations and four unknowns and n and k could thus be found. However, it should be noted that such a method would require considerable experimentation and there must be no ageing of the film

during the course of the extensive measurements. Also a considerable amount of computation would be required to find $\Delta\varepsilon_1$, $\Delta\varepsilon_2$, n and k. We have seen in (2.3) that at oblique incidence the coefficients α and β are complex functions of the angle of incidence θ, and n and k and it is felt that in order to derive values of n and k from the experimental observables, numerical analytical techniques (such as described by Julien (1973) for the determination of n and k from (R_p/R_s) measurements)may have to be employed. It would also seem appropriate to extend the spectral range of the thermal modulation studies of gold and copper to higher photon energies, since Scouler (1967) has shown that the thermal modulation response at these photon energies is rich in structure. Temperature coefficients of optical transitions at higher energies could thus be determined. In (5.5) the structure at 3.0 eV in the thermally modulated $\Delta\varepsilon_2$ dispersion curve of gold has been tentatively assigned as a transition of the X type since we have observed a positive shift in energy with increasing temperature. Other workers (Christensen and Seraphin 1971) have indicated that it is a transition from the L symmetry point to the Fermi level. To come to more definite conclusions on the origin of this structure further work would be required. It is suggested that comparative modulation studies i.e. a thermoreflectance and a piezoreflectance measurement on the same sample would provide the necessary information to come to a more definite assignment of this transition (as well as other transitions).

Modulation spectroscopy has not previously been used to experimentally investigate the rare earth metals. In the present work, the thermoreflectance response of opaque ($\sim$ 2000Å thick) polycrystalline films of the heavy rare earth metals, gadolinium, terbium, dysprosium and erbium grown in both ordinary and ultra high vacuum environments have been studied. The $(\Delta R_p/R_p)$ response of these elements, at 315K, has been found to be rather featureless in the spectral range 1.5 to 3.0 eV. These results are in contrast with those obtained by Miller et al. (1974) who, (in a "static"

optical study), found fine structure in the optical conductivity curves of gadolinium and terbium films in the photon energy range 1.8 to 3.0 eV. The lack of structure in the present work has been explained in terms of the behaviour of the coefficients α_p and β_p relating the thermoreflectance response $\Delta Rp/Rp$ to changes in the real and imaginary parts of the dielectric constant (see equation 8.1). We have seen that in the spectral range of interest 1.5 to 3.0 eV, $|\alpha_p| >> |\beta_p|$ which implies that the thermoreflectance response will be dominated by the change in the real part of the dielectric constant, $\Delta\varepsilon_1$. Indeed, there is quite good agreement between the thermally modulated reflectance response at 97K of a gadolinium film and the change in ε_1 with temperature interpolated from Hodgson and Cleyet's (1969) results. We also noted that fine structure in the ε_1 dispersion curves obtained by Miller et al. (1974) was not so predominant as that in the $\sigma(w)$ dispersion curves.

On lowering the temperature of the films of the heavy rare earth metals to 97K the thermally modulated reflectance dispersion curves were considerably sharpened and new structure appeared. This led to the study of the thermally modulated reflectance spectra of gadolinium, terbium and dysprosium as a function of temperature. It was found that for these three elements the thermoreflectance response exhibited anomalous behaviour at the magnetic ordering temperatures. Although this anomalous behaviour of the $(\Delta Rp/Rp)$ response at the magnetic ordering temperatures of gadolinium and terbium films could be purely electrical in origin this was not the case with dysprosium. It was concluded that the anomalies in the $(\Delta Rp/Rp)$ response of dysprosium films observed at the magnetic ordering temperature were genuinely optical in origin and not caused by variations in other factors which might affect the modulated reflectance response. However, in the present work it was difficult to firmly identify a single mechanism to explain the occurrence of the thermally modulated reflectance anomalies at the Néel point of dysprosium without further

experimental and theoretical studies being undertaken. To find which mechanism is responsible for the occurrence of these anomalies it is felt that further measurements need to be made over a more extensive spectral range, down to at least 0.5 eV. This would also enable the $\Delta Rp/Rp$ response to be analyzed by the Kramers-Kronig technique, as data would then be available over a wider frequency range . Also in the present work the lowest temperature which could be attained was 90K, which meant that out of all the heavy rare earths studied terbium and gadolinium were the only metals with Curie temperatures in this range. Cooling with liquid helium would allow measurements to be taken down to at least 20K, which would allow the thermally modulated reflectance response at the Curie point of dysprosium and the Curie and Néel points of erbium to be studied. It is also suggested that if further thermal modulation studies of thin films of the rare earth metals are to be undertaken then they should be performed "in situ" in an ultra high vacuum environment owing to the reactive nature of the elements.

Throughout the present studies the only surface analytical technique at our disposal was high energy reflection electron diffraction. We have seen that the resulting patterns were often of poor visibility and it was often difficult to analyse them satisfactorily. In recent years several new techniques for surface study have been developed, the relevant new techniques being summarized below: Low energy electron diffraction (L.E.E.D.) which allows the first few layers or a surface to be studied. However, although the interpretation of the positions of the diffracted spots in L.E.E.D. patterns is fairly straight forward, the interpretation of the intensities of the spots is far more difficult, on a quantitative basis. This is essentially because the detailed theory of the interaction of electrons of low energy with solid surfaces has not been established. Auger electron spectroscopy is a technique which can be used for the non-destructive chemical analysis of surfaces. The technique depends on an energy analysis of electrons emitted from atoms by a radiationless

process resulting from the rearrangement of orbital electrons after an electron has been removed from an inner shell. With appropriately sensitive detection arrangements it is possible to identify $\sim$ 0.1 of a monolayer on a surface. To date, there appears to have been no attempt to perform "static" or "modulated" optical experiments at the same time as a detailed surface analysis of the surface is being undertaken.

In the present work one of the modulation techniques - electroabsorption has been used in the production of a totally integrated thin film optical modulator. Although the modulator overcame some of the disadvantages of conventional electro-optic modulators and modulation degrees of 10% were readily attainable for applied modulating voltages of 15V the device was found to have a low transmission, typically less than 10%. This limitation was partially overcome by suitable filter design based on a Fabry-Perot type interference filter. The filter studies were purely theoretical and in the present work no attempts were made to construct the devices. However, it is felt that the results are sufficiently good to justify attempts to fabricate devices, although the path ahead is strewn with experimental difficulties (almost exclusively concerned with the deposition of the prescribed thickness of the electro-optically active materials).

A "dry package" technique has been used in the present work to study the electromodulation of metals. However, it became clear that the electromodulation effects, as reported from electrolytic experiments, were not present in our experiments. Computer simulation studies of the metal electrolyte system then showed that the electroreflectance responses of gold, copper and silver electrolyte interfaces could be reproduced if one assumed the formation of a thin absorbing layer in the Gouy region of the electrolyte during the application of a high electric field. Although excellent agreement was obtained between the simulated and experimental electroreflectance spectra of copper and silver electrolyte interfaces, the agreement was not so good for gold. This was thought to be due to the simplicity of the model used in the present work and it is proposed that

the computational analysis be refined by considering the spatial dependence of the optical constants in the Gouy region of the electrolyte and introducing a dispersion into the induced absorption.

APPENDIX 1

The derivation of the coefficients $\gamma_{p,s}$ and $\delta_{p,s}$

In this appendix the coefficients $\gamma_{p,s}$ and $\delta_{p,s}$ in equation (2.16) Chapter II are derived. The subscripts p and s refer to the parallel and perpendicular components of polarization respectively. A modulation parameter will not only produce a change in the reflectance and transmittance of the active medium but also a change, $\Delta\psi_{p,s}$, in the phase shift, $\psi_{p,s}$, of the incident light on reflection. The modulated phase change $\Delta\psi_{p,s}$ is related to $\Delta\varepsilon_1$ and $\Delta\varepsilon_2$, the changes in the real and imaginary parts of the dielectric constant, by

$$\Delta\psi_{p,s} = (\partial\psi_{p,s}/\partial\varepsilon_1)\Delta\varepsilon_1 + (\partial\psi_{p,s}/\partial\varepsilon_2)\Delta\varepsilon_2 \qquad (A.1)$$

equation (A.1) may be written in the form

$$\Delta\psi_{p,s} = \gamma_{p,s}\Delta\varepsilon_1 + \delta_{p,s}\Delta\varepsilon_2 \qquad (A.2)$$

where

$$\gamma_{p,s} = (\partial\psi_{p,s}/\partial\varepsilon_1)$$

and

$$\delta_{p,s} = (\partial\psi_{p,s}/\partial\varepsilon_2)$$

$\psi_{p,s}$ is related to the Fresnel amplitude reflection coefficients $r_{p,s}$ by

$$\psi_{p,s} = \tan^{-1}\left(\frac{\text{Imaginary part } (r_{p,s})}{\text{real part } (r_{p,s})}\right) \qquad (A.3)$$

The Fresnel amplitude reflection coefficients $r_{p,s}$ are given below (Born and Wolf 1965)

$$r_p = \frac{n\cos\theta_1 - n_1\cos\theta_o}{n\cos\theta_1 + n_1\cos\theta_o} \qquad (A.4)$$

and

$$r_s = \frac{n\cos\theta_o - n_1\cos\theta_1}{n\cos\theta_o + n_1\cos\theta_1} \qquad (A.5)$$

where $n = (n_o - ik)$ is the complex refractive index of the medium in which the light is incident, assumed in this case to be non-absorbing i.e. $k = 0$.

$n_1 = (n' - ik)$ is the complex refractive index of the medium in which the light is transmitted.

θ_o is the angle of incidence

θ_1 is the angle of refraction.

If the medium in which the light is transmitted is absorbing then the angle of refraction θ_1 will be complex. θ_1 is related to θ_o by Snell's law, given below

$$\sin\theta_1 = n_o\sin\theta_o/(n'-ik) \qquad (A.6)$$

clearly

$$\cos\theta_1 = \left\{1 - \frac{(n_o^2\sin^2\theta_o)}{(n'-ik)^2}\right\}^{\frac{1}{2}} \qquad (A.7)$$

Substituting for $\cos\theta_1$ in terms of θ_o in equations (A.4) and (A.5) we have

$$r_p = \frac{n_o\{(n'-ik)^2 - n_o^2\sin^2\theta_o\}^{\frac{1}{2}} - (n'-ik)^2\cos\theta_o}{n_o\{(n'-ik)^2 - n_o^2\sin^2\theta_o\}^{\frac{1}{2}} + (n'-ik)^2\cos\theta_o} \qquad (A.8)$$

which may be written as

$$r_p = \frac{n_o(\varepsilon_1-i\varepsilon_2-n_o^2\sin^2\theta_o)^{\frac{1}{2}} - (\varepsilon_1-i\varepsilon_2)\cos\theta_o}{n_o(\varepsilon_1-i\varepsilon_2-n_o^2\sin^2\theta_o)^{\frac{1}{2}} + (\varepsilon_1-i\varepsilon_2)\cos\theta_o} \qquad (A.9)$$

Similarly for r_s

$$r_s = \frac{n_o\cos\theta_o - (\varepsilon_1-i\varepsilon_2-n_o^2\sin^2\theta_o)^{\frac{1}{2}}}{n_o\cos\theta_o + (\varepsilon_1-i\varepsilon_2-n_o^2\sin^2\theta_o)^{\frac{1}{2}}} \qquad (A.10)$$

From equation (A.3) we see that in order to calculate $\psi_{p,s}$ it is necessary to separate $r_{p,s}$ into real and imaginary parts. Then let

$$(t + iv) = \varepsilon_1 - n_o^2 \sin^2\theta_o - i\varepsilon_2 \tag{A.11}$$

where

$$t = \varepsilon_1 - n_o^2 \sin^2\theta_o$$

and

$$v = -\varepsilon_2$$

and let

$$(w + ix)^2 = (t + iv) \tag{A.12}$$

and

$$y = \varepsilon_1 \cos\theta_o, \qquad Z = \varepsilon_2 \cos\theta_o.$$

Substituting the above relationships into equations (A.9) and (A.10) we have

$$r_p = \frac{(n_o w - y) + i(xn_o + Z)}{(n_o w + y) + i(xn_o - Z)} \tag{A.13}$$

and

$$r_s = \frac{(n_o \cos\theta_o - w) - ix}{(n_o \cos\theta_o + w) + ix} \tag{A.14}$$

Rationalizing equations (A.13) and (A.14) gives

$$r_p = \frac{(n_o^2 w^2 - y^2) + (x^2 n_o^2 - Z^2) + 2in_o(xy + Zw)}{(n_o w + y)^2 + (xn_o - Z)^2} \tag{A.15}$$

and

$$r_s = \frac{(n_o^2 \cos^2\theta_o - w^2 - x^2) - 2ixn_o \cos\theta_o}{(n_o \cos\theta_o + w)^2 + x^2} \tag{A.16}$$

From equations (A.3) and (A.15)

$$\psi_p = \tan^{-1}\left\{\frac{2n_o(xy + Zw)}{(n_o w^2 - y^2) + (x^2 n_o^2 - Z^2)}\right\} \tag{A.17}$$

and from equations (A.3) and (A.16)

$$\psi_s = \tan^{-1}\left\{\frac{-2xn_o \cos\theta_o}{n_o^2 \cos^2\theta_o - w^2 - x^2}\right\} \tag{A.18}$$

from equation (A.12) we see , by equating real and imaginary parts, $w = v/2x$. Substituting for w in equations (A.17) and (A.18) we have

$$\psi_p = \tan^{-1}\left\{\frac{4xn_o^2(2x^2y+Zv)}{n_o^2(v^2+4x^4)-4x^2(y^2+Z^2)}\right\} \qquad (A.19)$$

and

$$\psi_s = \tan^{-1}\left\{\frac{-8x^3n_o\cos\theta_o}{4x^2n_o^2\cos^2\theta_o-b^2-4x^4}\right\} \qquad (A.20)$$

To find x in terms of ε_1 and ε_2 from equation (A.12)

$$t = w^2 - x^2 \quad \text{and} \quad v = 2wx$$

$$\text{i.e.} \quad 4x^4 + 4x^2t - v^2 = 0 \qquad (A.21)$$

Solving for x

$$x^2 = \frac{-t \pm (t^2 + v^2)^{\frac{1}{2}}}{2} \qquad (A.22)$$

since x must be a real number

$$x^2 = \frac{-t + (t^2 + v^2)^{\frac{1}{2}}}{2} \qquad (A.23)$$

Since we have the constraint that the reflectances $R_{s,p} \leq 1$ then it can be shown that

$$x = -\left\{\frac{-t + (t^2 + v^2)^{\frac{1}{2}}}{2}\right\}^{\frac{1}{2}} \qquad (A.24)$$

and so

$$x = -\left\{\frac{-(\varepsilon_1-n_o^2\sin^2\theta_o)+\left[(\varepsilon_1-n_o^2\sin^2\theta_o)^2+\varepsilon_2^2\right]^{\frac{1}{2}}}{2}\right\}^{\frac{1}{2}} \qquad (A.25)$$

For ease of manipulation let

$$r = ((\varepsilon_1 - n_o^2\sin^2\theta_o)^2 + \varepsilon_2^2)^{\frac{1}{2}} \qquad (A.26)$$

and

$$q = (r - (\varepsilon_1 - n_o^2\sin^2\theta_o)) \qquad (A.27)$$

Then from equations (A.19) and (A.20) we have

$$\psi_p = \tan^{-1}\left\{\frac{-2\sqrt{2}n_o\cos\theta_o q^{\frac{1}{2}}(\varepsilon_1 q-\varepsilon_2^2)}{(n_o^2(\varepsilon_2^2+q^2) - 2q\cos^2\theta_o(\varepsilon_1^2+\varepsilon_2^2))}\right\} \qquad (A.28)$$

and

$$\psi_s = \tan^{-1}\left\{\frac{2\sqrt{2}n_o\cos\theta_o q^{3/2}}{(q(2n_o^2\cos^2\theta_o-q)-\varepsilon_2^2)}\right\} \qquad (A.29)$$

In equation (A.28) let the numerator = c and the denominator = a then

$$\psi_p = \tan^{-1}\left(\frac{a(\varepsilon_1,\varepsilon_2)}{c(\varepsilon_1,\varepsilon_2)}\right) \qquad (A.30)$$

$$\tan\psi_p = \frac{a(\varepsilon_1,\varepsilon_2)}{c(\varepsilon_1,\varepsilon_2)} = Z \qquad (A.31)$$

$$\partial Z/\partial\psi_p = 1 + \tan^2\psi_p = 1 + Z^2 \qquad (A.32)$$

and

$$\partial\psi_p/\partial\varepsilon_1 = \partial\psi_p/\partial Z.\partial Z/\partial\varepsilon_1 = 1/1+Z^2 \ \frac{\partial}{\partial\varepsilon_1}\left\{\frac{a(\varepsilon_1,\varepsilon_2)}{c(\varepsilon_1,\varepsilon_2)}\right\} \qquad (A.33)$$

$$\partial\psi_p/\partial\varepsilon_1 = \frac{1}{a^2(\varepsilon_1,\varepsilon_2)+c^2(\varepsilon_1,\varepsilon_2)} \ \frac{\partial}{\partial\varepsilon_1}\left\{\frac{a(\varepsilon_1,\varepsilon_2)}{c(\varepsilon_1,\varepsilon_2)}\right\} \qquad (A.34)$$

Then it can be shown that

$$\partial\psi_p/\partial\varepsilon_1 = \frac{ab-cd}{(a^2+c^2)} = \gamma_p \qquad (A.35)$$

and

$$\partial\psi_p/\partial\varepsilon_2 = \frac{ae-cf}{(a^2+c^2)} = \delta_p \qquad (A.36)$$

where

$$b = \frac{\partial}{\partial\varepsilon_1}(c), \qquad d = \frac{\partial}{\partial\varepsilon_1}(a) \qquad (A.37)$$

and

$$e = \frac{\partial}{\partial\varepsilon_2}(c), \qquad f = \frac{\partial}{\partial\varepsilon_2}(a) \qquad (A.38)$$

Similarly for ψ_s, in equation (A.29) let the numerator = k and the denominator = g, then it can be shown that

$$\partial\psi_s/\partial\varepsilon_1 = \frac{gh-k\ell}{(g^2+k^2)} = \gamma_s \qquad (A.39)$$

$$\partial\psi_s/\partial\varepsilon_2 = \frac{gm-kn}{(g^2+k^2)} = \delta_s \qquad (A.40)$$

where

$$h = \frac{\partial}{\partial\varepsilon_1}(k), \qquad \ell = \frac{\partial}{\partial\varepsilon_1}(g) \qquad (A.41)$$

and

$$m = \frac{\partial}{\partial\varepsilon_2}(k), \qquad n = \frac{\partial}{\partial\varepsilon_2}(g) \qquad (A.42)$$

Performing the differentiation in equation (A.37) to (A.42) then

$$b = \frac{\sqrt{2}n_o\cos\theta_o}{r}\ (q^{3/2}(3\varepsilon_1-r) - \varepsilon_2{}^2 q^{\frac{1}{2}}). \qquad (A.43)$$

$$d = 2q/r\ (\cos^2\theta_o(\varepsilon_1{}^2+\varepsilon_2{}^2-2\varepsilon_1 r)-n_o{}^2 q) \qquad (A.44)$$

$$e = \sqrt{2}n_o\cos\theta_o/r\ (\varepsilon_2 q^{\frac{1}{2}}(4r-3\varepsilon_1)+\varepsilon_2{}^3 q^{-\frac{1}{2}}) \qquad (A.45)$$

$$f = 2/r\ (n_o{}^2 q\varepsilon_2-\varepsilon_2\cos^2\theta_o(\varepsilon_1{}^2-\varepsilon_2{}^2)+4\varepsilon_2\cos^2\theta_o(\varepsilon_1-n_o{}^2\sin^2\theta_o-r)+2\varepsilon_2 n_o{}^2 \qquad (A.46)$$

$$h = \frac{-3\sqrt{2}n_o\cos\theta_o q^{3/2}}{r} \qquad (A.47)$$

$$\ell = 2q/r\ (q - n_o{}^2\cos^2\theta_o) \qquad (A.48)$$

$$m = \frac{2\sqrt{2}\cos\theta_o q^{\frac{1}{2}}\varepsilon_2}{r} \qquad (A.49)$$

$$n = 2\varepsilon_2/r\ (n_o{}^2\cos^2\theta_o-q-r) \qquad (A.50)$$

and so the coefficients $\gamma_{p,s}$ and $\delta_{p,s}$ may be found.

Appendix 2

```
      PROGRAM KKA(INPUT,OUTPUT)
      DIMENSION RR(100),RI(100),DELR(100),EN(100),RRI(100)
     ,,RII(100)
      DIMENSION DEPSR(100),DEPSI(100),Y(100),Z(100),
     ,TITLE(2),SOURCE(5)

C---THIS PROGRAM USES THE KRAMERS-KRONIG METHOD
C---OF ANALYSIS TO CALCULATE DTHETA, THE TEMPERATURE
C---MODULATED PHASE CHANGE
C---THE COEFFICIENTS ALPHAP, BETAP,ALPHANR, BETANR,
C---ALPHAPR, BETAPR ARE CALCULATED AND THE CHANGES IN THE
C---REAL AND IMAGINARY PARTS OF THE DIELECTRIC CONSTANT
C---CALCULATED

C---NEPTS IS THE NO. OF DATA CARDS READ IN
C---NOPTS IS THE NO. OF OPTICAL CONSTANTS READ IN
C---RR(I), RI(I) ARE THE OPTICAL CONSTANTS OF THE MATERIAL
C---EN(I) IS THE PHOTON ENERGY IN E.V
C---DELR(I) IS THE EXPERIMENTAL DATA DR/R FROM THE THERMAL
C---MODULATION.
C---THETA IS THE ANGLE OF INCIDENCE IN RADIANS
C---EPS1(K) IS THE REAL PART OF THE DIELECTRIC CONSTANT
C---EPS2(K) IS THE IMAGINARY PART OF THE DIELECTRIC
C---CONSTANT
C---DEPSR(K) IS THE TEMPERATURE INDUCED CHANGE IN THE
C---REAL PART OF THE DIELECTRIC CONSTANT
C---DEPSI(K) IS THE TEMPERATURE INDUCED CHANGE IN THE
C---IMAGINARY PART OF THE DIELECTRIC CONSTANT

C---START IN THE INFRA RED
C---NCONV IS SET TO 1 WHEN WAVELENGTHS ARE TO BE READ IN

      READ 555,(TITLE(I), I=1,2)
555    FORMAT(A5,A4)
      WRITE 556,(TITLE(I), I=1,2)
556   FORMAT(*1*,5X,A5,5X,A4,5X,*OBLIQUE INCIDENCE,*
     ,* 45 DEGREES*/5X,*------*,5X,*------*)
1     FORMAT(2I2)
      READ 1,NOPTS,NCONV

C---READ AND PRINT NAME OF SOURCE OF OPTICAL CONSTANTS

2     FORMAT(5A4)
      READ 2,(SOURCE(I),I=1,5)
3     FORMAT(10X,*SOURCE OF OPTICAL CONSTANTS *,5A4)
      PRINT 3,(SOURCE(I),I=1,5)

C---READ OPTICAL CONSTANTS AND ASSOCIATED ENERGIES
C---OR WAVELENGTHS
```

```
5     FORMAT(10X,* OPTICAL CONSTANTS *,10X,* ENERGY *)
      PRINT 5
      DO 100 I=1,NOPTS
4     FORMAT(3(F6.3,2X))
      READ 4, EN(I),RR(I),RI(I)
      IF(NCONV.NE.0) EN(I) = 1.E+5/(EN(I)*8.068)
6     FORMAT(10X,2F8.3,10X,F10.2)
      PRINT 6,RR(I),RI(I),EN(I)
100   CONTINUE
23    FORMAT(I3)
      READ 23,NEPTS
31     FORMAT(20X,*NEPTS =*,I7)
      PRINT 31,NEPTS

C---READ ENERGIES BETWEEN WHICH DATA HAS BEEN TAKEN (E.V.)

7     FORMAT(2F5.3)
      READ 7,EBOT,ETOP
8     FORMAT(10X,*ENERGY RANGE OF DATA  *,F3.1,*  TO  *,
     ,F3.1)
      PRINT 8,EBOT,ETOP

C---READ ENERGY SPACING OF MEASUREMENTS

9     FORMAT(F5.3)
      READ 9,BIT
10    FORMAT(10X,*  ENERGY RESOLUTION  *,F8.3,* ELECTRON*
     ,* VOLTS*)
      PRINT 10,BIT

C---READ IN DATA FOR POINTS EQUI-SPACED IN ENERGY

      DO 200 I=1,NEPTS
11     FORMAT(F6.1)
      READ 11,DELR(I)
200   DELR(I) = DELR(I)*1.0E-6

C---PRINT DATA

12    FORMAT(10X,*ENERGY *,F4.2,*  THERMAL MODULATION  *,
     ,E10.3)
      DO 201 I=1,NEPTS
      IM1=I-1
      E=EBOT+BIT*FLOAT(IM1)
201   PRINT 12, E, DELR(I)

C---USE LINEAR INTERPOLATION TO ASSOCIATE OPTICAL
C---CONSTANTS WITH EACH EXPERIMENTAL POINT

      IL=1

      IM1=I-1
      DO 300 I=1,NEPTS
      E=EBOT+FLOAT(IM1)*BIT
      DO 301 J=IL,1000
      TEST=EN(J)-E
      IF(TEST.EQ.0.) GO TO 3004
      IF(TEST.GT.0.) GO TO 3001
      GO TO 3002
```

```
      GO TO 303
3004  K = J
3002  CONTINUE
      GO TO 305
      IF(J.GT.100) GO TO 304
301   CONTINUE
13    FORMAT(10X,* ENERGY OUTSIDE RANGE OF OPTICAL*
     ,* CONSTANTS*)
304   PRINT 13
305   IL = K-1
      STOP
      RRI(I)=RR(K)
      RII(I)=RI(K)
      GO TO 300
303   KM1 = K-1
      IL=KM1

C---LINEAR INTERPOLATION OF OPTICAL CONSTANTS

C---REFRACTIVE INDEX

      EM=(RR(KM1)-RR(K))/(EN(KM1)-EN(K))
      C=(EN(KM1)*RR(K)-EN(K)*RR(KM1))/(EN(KM1)-EN(K))
       RRI(I)=EM*E+C

C---EXTINCTION COEFFICIENT

      EM=(RI(KM1)-RI(K))/(EN(KM1)-EN(K))
      C=(EN(KM1)*RI(K)-EN(K)*RI(KM1))/(EN(KM1)-EN(K))
      RII(I)=EM*E+C
300   CONTINUE
14    FORMAT(///,10X,*   ENERGY *,10X,*  INTEPOLATED*
     ,* OPTICAL CONSTANTS*)
      PRINT 14
15    FORMAT(15X,F4.2,20X,2F7.3)
      DO 400 I=1,NEPTS
      IM1=I-1
      E=EEOT+BIT*FLOAT(IM1)
400   EN(I) = E

      PRINT 15,(EN(I),RRI(I),RII(I),I=1,NEPTS)
C---READ RANGE FOR KRAMERS-KRONIG ANALYSIS
C--- MUST COINCIDE WITH EXPERIMENTAL POINTS
16    FORMAT(2F4.2)
      READ 16,EL,EU



C---READ WIDTH OF SINGULARITY
21    FORMAT(10X,* RANGE FOR K-K ANALYSIS *,F6.2,* TO *,
     ,F6.2)
      READ 17,WTH
17    FORMAT(F10.8)
      PRINT 21,EL,EU
22    FORMAT(10X,* WIDTH OF SINGULARITY *,E10.4)
      PRINT 22,WTH

C---READ AND PRINT CONSTANTS USED IN EXTRAPOLATION
```

```
      READ 24,EXL,EXH
25    FORMAT(20X,* EXTRAPOLATION CONSTANTS *,2F8.1)
      PRINT 25,EXL,EXH
      EXL = EXL*1.0E-6
      EXH = EXH*1.0E-6

C---TABULATE FUNCTION AND INTEGRATE NUMERICALLY
C---LOCATE ENERGY AND OPTICAL CONSTANTS

      DO 502 I=1,NEPTS
      TEST=EN(I)-EL
      IF(TEST.GT.0.) GO TO 503
      GO TO 502
503   K = I-1
      PRINT 18
      GO TO 504
502   CONTINUE
505    CONTINUE
      IF(EN(K).GT.EU) GO TO 900
504   KM1 = K-1
      A=EN(K)
      B=DELR(K)

C---TABULATE FUNCTION UP TO SINGULARITY

      NDIM=0
      DO 600 I=1,KM1
      NDIM=NDIM+1
600   Y(I)=(DELR(I)-B)/(EN(I)*EN(I)-A*A)

C---PERFORM INTEGRATION

      CALL GSF(BIT,Y,Z,NDIM)
      SUM1=Z(NDIM)

C---INTEGRATE ABOVE SINGULARITY

      NDIM=0
      KP1=K+1
      DO 700 I=KP1,NEPTS
      NDIM=NDIM+1
      NL=I-K
700   Y(NL)=(DELR(I)-B)/(EN(I)*EN(I)-A*A)
      CALL GSF(BIT,Y,Z,NDIM)
      SUM2=Z(NDIM)

C---INTEGRATE STEPS EITHER SIDE OF SINGULARITY

C---LINEAR INTERPOLATION  L.H.S.

      EM=(DELR(KM1)-DELR(K))/(EN(KM1)-EN(K))
      C=(DELR(K)*EN(KM1)-DELR(KM1)*EN(K))/(EN(KM1)-EN(K))
      EBIT=EN(K)-WTH
      NSTEPS=101
      STSZ=(EBIT-EN(KM1))/100.
      DO 800 I=1,NSTEPS
      II=I-1
      X1=EN(KM1)+STSZ*FLOAT(II)
```

```
      DELRN=EM*X1+C
800   Y(I) = (DELRN-B)/(X1*X1-A*A)
      NDIM=NSTEPS
      CALL GSF(STSZ,Y,Z,NDIM)
      SUM3=Z(NDIM)

C---LINEAR INTERPOLATION  R.H.S.

      KP1=K+1
      EM=(DELR(K)-DELR(KP1))/(EN(K)-EN(KP1))
      C=(DELR(KP1)*EN(K)-DELR(K)*EN(KP1))

     1/(EN(K)-EN(KP1))
      EBIT=EN(K)+WTH
      STSZ=(EN(KP1)-EBIT)/100.
      DO 801 I=1,NSTEPS
      I1=I-1
      X1=EBIT+STSZ*FLOAT(I1)
      DELRN=EM*X1+C
801   Y(I)=(DELRN-B)/(X1*X1-A*A)
      CALL GSF(STSZ,Y,Z,NDIM)
      SUM4=Z(NDIM)

C---EXTRAPOLATION FROM ZERO TO INFINITY

      A1=EXL-DELR(K)
      A1=A1/(2.*EN(K))
      A2=(EN(K)-EBOT)/(EN(K)+EBOT)
      A2=ALOG(A2)
      A2=A2*A1
      B1=EXP-DELR(K)
      B1=B1/(2.*EN(K))
      B2=(ETOP-EN(K))/(ETOP+EN(K))
      B2=ALOG(B2)
      B2=B2*B1
      SUM5=A2-B2
      SUM6=0.0
      FACT=EN(K)/3.14159
      DTHETA=FACT*(SUM1+SUM2+SUM3+SUM4+SUM5+SUM6)

      PI = 4.*ATAN(1.)
      ANGLE = 45.
      THETA = ANGLE*PI/180.
      EPS1 = RRI(K)*RRI(K)-RII(K)*RII(K)
      EPS2 = 2.*RRI(K)*RII(K)
      C = COS(THETA)
      S = SIN(THETA)
      A = EPS1-S*S
      B = -EPS2
      Q = SQRT(A*A+EPS2*EPS2)-A
      R = SQRT(A*A+EPS2*EPS2)
      QQ = SQRT(Q*Q*Q)
      R2 = SQRT(2.)*R

      FDIFF1 = 6.*EPS1*C*QQ/R2-(2.*EPS2*EPS2*C*SQRT(Q)/R2)
     )-(4.*C*QQ/SQRT(2.))

      GDIFF1 = 2.*Q*C*C/R*(EPS1*EPS1 + EPS2*EPS2) -
     - (4.*EPS1*C*C*Q) - (2.*Q*Q*R)
```

```
      FDIFF2 = 8.*EPS2*C*SQRT(Q/2.)+(2.*EPS2*EPS2*EPS2*C/
     /(R2*SQRT(Q)))-(6.*EPS1*C*EPS2*SQRT(Q)/R2)

      GDIFF2 = 2.*EPS2+(2.*Q*EPS2/R)-(2.*EPS1*EPS1*C*C*
     **EPS2/R)+(4.*EPS2*C*C*A)-(4.*EPS2*C*C*R)-(EPS2*EPS2*
     **EPS2*C*C/R)*2.

      F12 = (EPS2*EPS2*C*4.*SQRT(Q/2.))-(4.*EPS1*C*QQ/
     /SQRT(2.))
      G12 = (EPS2*EPS2+Q*Q)-2.*C*C*Q*(EPS1*EPS1+EPS2*EPS2)

C---ALPHAP, BETAP ARE THE COEFFICIENTS OF DEPSR(K),
C---DEPSI(K) FOR DTHETA

C---CALCULATE ALPHAP

      ALPHAP = (G12*FDIFF1-F12*GDIFF1)/(G12*G12+F12*F12)

C---CALCULATE BETAP

      BETAP = (G12*FDIFF2-F12*GDIFF2)/(G12*G12+F12*F12)
      V = -SQRT(Q/2.)
      U = B/(2.*V)

C---ALPHAPR BETAPR, ALPHANR, BETANR ARE THE COEFFICIENTS
C---OF DEPSR(K), DEPSI(K) FOR DELR(K) (PARALLEL AND
C---PERPENDICULAR COMPONENTS RESPECTIVELY)

C---CALCULATE ALPHANR

      GNUM = 2.*U*C*(U*U-3.*V*V-C*C)
      PA1 = (U-C)*(U-C)
      PA2 = (U+C)*(U+C)
      DNOM = (U*U+V*V)*(PA1+V*V)*(PA2+V*V)
      ALPHANR = GNUM/DNOM

C---CALCULATE BETANR

      GNUM = -2.*V*C*(3.*U*U-V*V-C*C)
      BETANR = GNUM/DNOM

C---CALCULATE ALPHAPR

      T = SIN(THETA)*TAN(THETA)
      GNUM = 2.*U*T*(U*U-3.*V*V-T*T)
      PA1 = (U-T)*(U-T)
      PA2 = (U+T)*(U+T)
      DNOM = (U*U+V*V)*(PA1+V*V)*(PA2+V*V)
      ALPHAPR = ALPHANR+(GNUM/DNOM)

C---CALCULATE BETAPR

      GNUM = 2.*V*T*(3.*U*U-V*V-T*T)
      BETAPR = BETANR-GNUM/DNOM

C---CALCULATE DEPSI(K)---THE CHANGE IN THE IMAGINARY
C---PART OF THE DIELECTRIC CONSTANT
```

```
      DEPSI(K) = (ALPHAPR*DTHETA-ALPHAP*DELR(K))/
     /(ALPHAPR*BETAP-BETAPR*ALPHAP)

C---CALCULATE DEPSR(K) THE CHANGE IN THE REAL PART OF
C---THE DIELECTIC CONSTANT

      DEPSR(K) = (DTHETA-BETAP*DEPSI(K))/ALPHAP

18    FORMAT(6(/),13X,*RESULTS OF KRAMERS-KRONIG*
     /* TRANSFORM*)
19    FORMAT(5X,* ENERGY *,F8.2,*    REAL  *,E16.8,
     ,*  IMAGINARY  *,E16.8,* DELTHETA *,E16.8,* SUMS =*,
     ,E16.8)

      PRINT 19, EN(K),DEPSR(K),DEPSI(K),DTHETA,SUMS

      K=KP1
       GO TO 505
900   PRINT 20
20    FORMAT(//////////,50X,*  ALL DATA FINISHED  *)
      PRINT 26
26    FORMAT(58X,* END *)
      STOP
      END
```

1. ABELES F. Ann. de Physique 3, 504, 1948.

2. ABRAMOWITZ M. and STEGUN I, "Handbook of Math. Functions" Dover, 1964.

3. ALTMANN S.L. "Band Theory of Metals, the elements" Pergamon, Oxford 1970.

4. ARCHER R.J. "Manuel on Ellipsometry", Gaertner Chicago 1968.

5. ASPNES D.E. Phys. Rev. 147, 554, 1966.

6. ASPNES D.E. Phys. Rev. 153, 972, 1967.

7. ASPNES D.E. and CARDONA M. Phys. Rev. 173, 714, 1968.

8. ASPNES D.E., HANDLER P. and BLOSSEY D.F. Phys. Rev. 166, 921 1968.

9. ASPNES D.E. and FROVA A. Solid State Commun. 7, 155, 1969.

10. AVERY D.G. Proc. Phys. Soc. B65, 425, 1952.

11. BALDINI G. and NOBILE M. Solid State Commun. 8, 7, 1970.

12. BALSLEV I. Phys. Rev. 143, 636, 1966a.

13. BALSLEV I. J. Phys. Soc. Japan Supp. 21, 101, 1966b.

14. BALZAROTTI A. and GRANDOLFO M. Phys. Rev. Letts. 10, 9, 1968.

15. BATZ B. Solid State Commun. 4, 241, 1966.

16. BATZ B. Solid State Commun. 5, 985, 1967.

17. BENNET H.E. and BENNET J.M. in "Physics of Thin Films" Ed. Hass G., Thin R.E. Vol. IV, 1967, Academic New. York.

18. BERGLUND C.N. J. App. Phys. 37, 3019, 1966.

19. BIST B.M.S., KUMAR J. and SRIVASTAVA Phys. Stat. Solidi 14, 197, 1972.

20. BLODGETT A.J. and SPICER W.E. Phys. Rev. 146, 390, 1966.

21. BORN M. and WOLF E. "Principles of Optics" Pergamon Oxford 1965.

22. BOWLDEN H.J. J.O.S.A. 53, 1073, 1963.

23. BRITSYN K.I., VOLKOV B.A., MATVEEV V.V. and SMIRNOV A.A. Sov. Phys. Solid State 7, 2044, 1966.

24. BUCKMAN A.B. and BASHARA N.M. Phys. Rev. 174, 719, 1968.

25. BURDICK G.A. Phys. Rev. 129, 138, 1963.

26. CALLAWAY J. Phys. Rev. 130, 549, 1963.

27. CALLAWAY J. "Energy Band Theory" Academic N. York 1964.

28. CALLAWAY J. Phys. Rev. 134A, 998, 1964b.

29. CAMPBELL D.S. Thin Solid Films 32, 3, 1976.

30. CARDONA M., SHAKLEE K.H. and POLLAK F.H. Phys. Rev. Letts 15, 883, 1965.

31. CARDONA M. "Modulation Spectroscopy" Vol XI Solid State Phys. Ed. by Seitz F. Academic N. York 1969.

32. CHEN A.B. and SEGALL B. Solid State Commun. 18, 149, 1976.

33. CHEYSSAC P., GARRIGOS R., KOFMAN R., PENAVAIRE L., RICHARD J. and SAISSY Y. Surface Science 37, 683, 1973.

34. CHEYSSAC P. and PENAVAIRE L. Nuovo Cimento Letters 11, 369, 1974.

35 CHOPRA K.L. in "Thin Film Phenomena" McGraw Hill London 1969.

36. CHRISTENSEN N.E. and SERAPHIN B.O. Phys. Rev. B4, 3321, 1971.

37. CHUAH D.G.S. and RATNALINGHAM R. J. Low Temp. Phys. 14, 257, 1973.

38. CLARK A.E., de SAVAGE B. and BOZORTH R.M. Phys. Rev. 138, A216, 1965.

39. CLAUSSIN B.H. Proc. Phys. Soc. 77, 1100, 1961.

40. COOPER B.R. and REDDINGTON R.W. Phys. Rev. Letts. 14, 1066, 1965.

41. CURZON A.E. and CHLEBEK H.G. J. Phys. F. 3, 1, 1973.

42. DAKSS M.L., KUHN L., HEIDRICH P.F. and Scott B.A. App. Phys. Letts. 16, 53, 1970.

43. DARNELL F.J. and MOORE E.P. J. App. Phys. 34, 1337, 1963.

44. DAVIS H.L., FAULKNER J.S. and JOY H.W. Phys. Rev. 167, 601, 1968.

45 DE KLERK J. and KELLY E.F. Rev. Sci. Instrum. 36, 506, 1965.

46. EDEN R.C. and COLEMAN P.D. Proc. I.E.E.E. 51, 1776, 1963.

47. EHRENREICH H., PHILIPP H.R. and OLECHNA D.J. Phys. Rev. 131, 2469, 1963.

48. ENGELER W.E., FRITZSCHE H., GARFINKEL M. and TIEMANN J.J. Phys. Rev. Letts. 14, 1069, 1965.

49. ERSKINE J.L. and STERN E.A. Phys. Rev. B8, 1239, 1973.

50. ERSKINE J.L., BLAKE G.A. and FLATEN C.J. J.O.S.A. 64, 1332, 1974.

51. FEINLEIB J. Phys. Rev. Letts 16, 1200, 1966.

52. FISCHER J.E. and SERAPHIN B.A. Solid State Commun. 5, 973, 1967.

53. FOSTER N.F. Proc. I.E.E.E. 53, 1400, 1965.

54 FRANZ W. Z. Naturforsch. 13a, 484, 1958.

55. FRENCH B.I. I.E.E.E. J. Quantum Electronics QE4, 365, 1968.

56. FROVA A. and HANDLER P. App. Phys. Letts. 5, 11, 1964.

57. FROVA A. and BODDY B.J. Phys. Rev. 153, 606, 1967.

58. FROVA A., BODDY P.J. and CHEN Y.S. Phys. Rev. 157, 700, 1967.

59. GAHWILLER C. Hel. Phys. Acta. 39, 595, 1966.

60. GAHWILLER C. Solid State Commun. 5, 65, 1967.

61. GARFINKEL M., TIEMANN J.J. and ENGELER W.E. Phys. Rev. 148, 695, 1966.

62. GARRET C.G.B. "The Electrochemistry of Semiconductors" Ed. Holmes P.J. Academic Press N. York 1962.

63. GARRIGOS R., KOFMAN R. and CHEYSSAC P. Thin Solid Films 13, 275, 1972.

64. GARRIGOS R., KOFMAN R., JOLIVET A. and DONNADIEU A. C.R. Acad. Sc. Paris. B. 272, 1078, 1971.

65. GARRIGOS R., KOFMAN R. and CHEYSSAC P. C.R. Acad. Sc. Paris B278, 1027, 1974

66. GASGNIER M., GHYS J. and SCHIFFMACHER H. J. Less Common. Metals. 34, 131, 1974.

67. GERHARDT U. Phys. Letts. 9 117, 1964.

68. GERHARDT U., BEAGLEHOLE D. and SANDROCK R. Phys. Rev. Letts. 19, 309, 1976.

69. GERHARDT U. and MOHLER E. Phys. Status. Solidi. 18, K45, 1966.

70. GOBELI G.W. and KANE E.O. Phys. Rev. Letts 15 142, 1965.

71. GOLDFINGER P. and DROWART J. J. de Chim. Phys. 55, 721, 1958.

72. GREENWOOD D.A. Proc. Phys. Soc. A71, 585, 1958.

73. GRIFFEL M., SKOCHDOPOLE R.E. and SPEDDING F.H. J. Chem. Phys. 25, 75, 1957.

74. GROBMAN W.D. and EASTMAN D.E. Phys. Rev. Letts. 28, 1038, 1972.

75. GROVES S.H., PIDGEON C.R. and FEINLEIB J. Phys. Rev. Letts 17, 643, 1966.

76. GUTSCHE E. and LANGE H. Phys. Status Solidi 13, K131, 1966.

77. HANSEN W.N. and PROSTAK A. Phys. Rev. 160, 600, 1967.

78. HANUS J., FEINLEIB J. and SCOULER W.J. Phys. Letts. 19, 16, 1967.

79. HASE N. and ONUKI M. J. Phys. Soc. Japon 28, 965, 1966.

80. HARRICK N.J. Phys. Rev. 103, 1173, 1956.

81. HARRICK N.J. Phys. Chem. Solids 14, 60, 1960.

82. HASAN W. Ph.D. thesis 1975 London University

83. HASS G. J. Amer. Ceram. Soc. 33, 353, 1950.

84. HASS G. and Thun R.E. "Physics of Thin Films" Vol. IV Academic Press N. York 1968.

85 HEAVENS O.S. "Thin Film Physics" Methuen London 1970.

86. HENRY W.E. Phys. Rev. 98, 226, 1955.

87. HODGSON J.N. and CLEYET B. J. Phys. C. 2, 97, 1969.

88. HOLLAND L. "Vacuum deposition of thin films" Chapman and Hall London 1966.

89. HONDA M., FUJIMORI M. and NISHIMURA Y. App. Phys. Letts. 21, 587, 1972.

90. HOUSTON W.V. Phys. Rev. 57, 184, 1940.

91. HOWSON R.P., AVARITSIOTIS J. and FOX T. Thin Solid Films 30, 297, 1975.

92. IRANI G.B., HUEN J. and WOOTEN F. J.O.S.A. 61, 128, 1971.

93. ISHIBASHI Y. and STADLER H.I. J. Phys. Chem. Solids 30, 2113, 1969.

94. JACKSON C. Phys. Rev. 178, 949, 1969.

95. JACOBS R.L. J. Phys. C. 1, 1296, 1968.

96. JANAK J.F. and WILLIAMS A.R. Phys. Rev. B11, 1522, 1972

97. JOHNSON P.B. and CHRISTY R.W. Phys. Rev. B6 4370, 1972.

98. JOHNSON P.B. and CHRISTY R.W. Phys. Rev. B11, 1315, 1975.

99. JULIEN L.S. Ph.D. thesis 1973 London University.

100. JULIEN L.S. and MILLER R.F. J. Phys. D. 7, 2116, 1974.

101. KASUYA T. Progress Theoret. Phys. 14, 45, 1956.

102. KAYE G.W.C. and LABY T.H. "Tables of Physical and Chemical Constants" Longmans London 1955.

103. KEETON S.C. and LOUCKS T.L. Phys. Rev. 146, 429, 1966.

104. KEETON S.C. and LOUCKS T.L. Phys. Rev. 168, 672, 1968.

105. KELDYSH L.V. Sov. Phys. J.E.T.P. 7, 788, 1958.

106. KIREEV P.S., ORLOVA N.N., SAURIN V.N., STREL'TSOV L.N. Sov. Phys. Solid State 7, 1029, 1965.

107. KRIZEK J. Ph.D. Thesis 1973 Durham University.

108. KRIZEK J. and TAYLOR K.N.R. J. Phys. F. 5, 774, 1975.

109. KUBO R. J. Phys. Soc. Japon 12, 570, 1957.

110. KUPRATAKULN S. J. Phys. F. 3, 109, 1970.

111. LAVIN E.P. "Specular Reflection" Hilger London 1971.

112. LOUCKS T.L. "Augmented Plane Wave Method" Benjamin N. York 1967.

113. LUDEKE R. and PAUL W. "II-IV Semiconducting Compounds" Ed. Thomas D.G. Benhamin N. York 1967.

114. MACDONALD J. "Metal-Dielectric Multilayers" Hilger London 1971.

115. MEYERS H.P. J. Phys. F. 6, 141, 1976.

116. MILLER R.F. and TAYLOR A.J. J. Phys. D. 4, 1419, 1971.

117. MILLER R.F., JULIEN L.S. and TAYLOR A.J. J. Phys. D. 5, 2288, 1972.

118. MILLER R.F., JULIEN L.S. and TAYLOR A.J. J. Phys. F. 4, 2338, 1974.

119. MILLER S.E. Bell System Tech. Journal 48, 2059, 1969.

120. MISAWA K., MORILANI A. and NAKAI J. Jap. J. App. Phys. 15, 1309, 1976.

121. MIWA H. Prog. Theor. Phys. Japan 29, 477, 1963.

122. MOSS T.S. J. App. Phys. 32, 2136, 1962.

123. MOTT N. and JONES H. "Theory of properties of metals and alloys" Oxford 1936.

124. MUELLER F.M. and PHILLIPS J.C. Phys. Rev. 157, 600, 1967.

125. NEIGHBOURS J.R. and ALERS G.A. Phys. Rev. 111, 707, 1958.

126. NIKITINE S., BRAHMS S., RINGEISSEN J., DAHL J.P. and SONG K.S. "Proc. of Int. Conf. on Luminescence 1966" Ed. Szigeti G. Budapest 1968.

127. NILSSON P.O. and MUNKBY L. Phys. Kondens Materie 10, 290, 1969.

128. OLSEN C.G., PIACENTINI M. and LYNCH D.W. Phys. Rev. Letts. 33, 644, 1974.

129. PASHLEY D.W. and STOWELL M.J. Phil. Mag. 8, 1605, 1963.

130. PELLS G.P. and SHIGA M. J. Phys. C 2, 1835, 1969.

131. PEROV P.I., AVDEEVA L.A., ZHDAN A.G. and ELINSON M.H. Sov. Phys. Solid State 11, 65, 1969.

132. PÉTRAKIAN J.P. J.O.S.A. 62, 401, 1972.

133. PHILLIP H.R., and DASCH W.C. Phys. Rev. 127, 762, 1962.

134. PIDGEON C.R., GROVES S.H, and FEINLEIB J. Solid State Commun. 5, 677, 1967.

135. RAMCHANDANI M.G. J. Phys. C. 3, 1, 1970.

136. REHN V. Bull. Am. Phys. Soc. 13, 470, 1968.

137. ROBERTS R.W. Brit. J. App. Phys. 14, 537, 1963.

138. ROBERTS S. Phys. Rev. 118, 1509, 1960.

139. ROSEI R. and LYNCH D.W. Phys. Rev. B5, 3883, 1972.

140. ROSEI R., ANTONANGELI F. and GRASSANO V.M. Surface Science 37, 689, 1973.

141. RUDERMANN A. and KITTEL C. Phys. Rev. 96, 99, 1954.

142. SCHMIDT E. and KNAUSENBERGER W.H. J.O.S.A. 58, 857, 1969.

143. SCHOENBERG D. and ROAF D.J. Phil. TRANS. Roy. Soc. 255, 85, 1962.

144. SCHÜLER C. "Optical Properties and Electronic properties of metals and alloys" Ed. F. Abeles N. Holland Amsterdam 1966.

145. SCHULZ L.G. and TANGHERLINI F.R. J.O.S.A. 44, 357, 1954.

146. SCOULER W.J. Phys. Rev. Letts. 18, 445, 1967.

147. SEN GURTA P.K. Proc. Roy. Soc. Lond. A143, 438, 1934.

148. SERAPHIN B.O. "Optical Properties of Solids" Ed. F. Abeles N. Holland Amsterdam 1972.

149. SERAPHIN B.O. and HESS R.B. Phys. Rev. Letts. 14, 138, 1965.

150 SHALIMOVA K.V., ANDRUSHKO A.V. and DMITRIEV V.A. Sov. Phys. Crystallog. 8, 618, 1963.

151. SHALLCROSS F.V. Trans. Met. Soc. A.I.M.E. 236, 309, 1966.

152. SIDDALL G. Vacuum 9, 274, 1960.

153. SNAVELY B.B. Phys. Rev. 167, 730, 1968.

154. SNOW E.C. Phys. Rev. B8, 5391, 1973.

155. SOMMERS C.B. and AMAR H. Phys. Rev. 188, 1117, 1969.

156. STOKES J., SHEN Y.R., TSANG Y.W., COHEN M.L. and FONG C.Y. Phys. Letts. 38A, 347, 1972.

157 TADA K., TSOY K.S. and ZEMEL J.N. Thin Solid Films 22, 45, 1974.

158. TAYLOR H.F. J. Vac. Sci. amd Technol. 11, 150, 1974.

159. TAYLOR K.N.R. Contemp. Phys. 11, 423, 1970.

160. TAYLOR K.N.R. and DARBY M.J. "Physics of the Rare Earth Solids" Chapman and Hall London 1972.

161. THARMALINGHAM K. Phys. Rev. 130.2, 2204, 1963.

162. THEYE M.L. Phys. Rev. B2, 3060, 1970.

163. TOLANSKY S. "Multiple Beam Interferometry of surfaces and films" Dover 196

164. TOLANSKY S. "Multiple Beam interference of metals" Academic Press London 1970.

165. ULRICH R. J.O.S.A. 61, 1467, 1971.

166. WALLACE W.E. Ber. Bunsenges Phys. Chem (Germ) 76, 832, 1972.

167. WEAVER J.H., LYNCH D.W., CULP C.H. and ROSEI R. Phys. Rev. B14, 459, 1976.

168 WEITZEL I. and KEMPTER K. Extended Abstracts of Electrochem Soc. Abs. 249, 76.2, Oct. 1976.

169 WELKOWSKY M. and BRAUNSTEIN R. Solid State Commun. 9, 2139, 1971.

170. WEMPLE S.H. and DIDOMENICO M. App. Solid State Science Vol. 3. Ed. by Wolfe R. Academic Press 1972.

171. WILLIAMS G. Phys. Rev. 117, 1487, 1960.

172. WILLIAMS R.W., LOUCKS T.L. and MACKINTOSH A.R. Phys. Rev. Letts. 16, 168, 1966.

173. WINSEMIUS P. "Temperature Dependence of the optical properties of Au and Ag" Drukkerij, J.H. Pasmans S-Gravenhage.

174. WYCKOFF R.W.G. "Crystal Structures" Interscience N. York 1965.

175 YACOBY Y. Phys. Rev. 140A, 263, 1965.

176. YOSIDA K. Phys. Rev. 106, 893, 1957.

177. ZENER C. and WILLS H.H. Proc. Roy. Soc. 145, 523, 1934.